Preliminary Navigation Analysis for the Flyby Tour of ESA's JUICE mission

An investigation on the trajectory correction maneuvers design

Niccolò Gastaldello

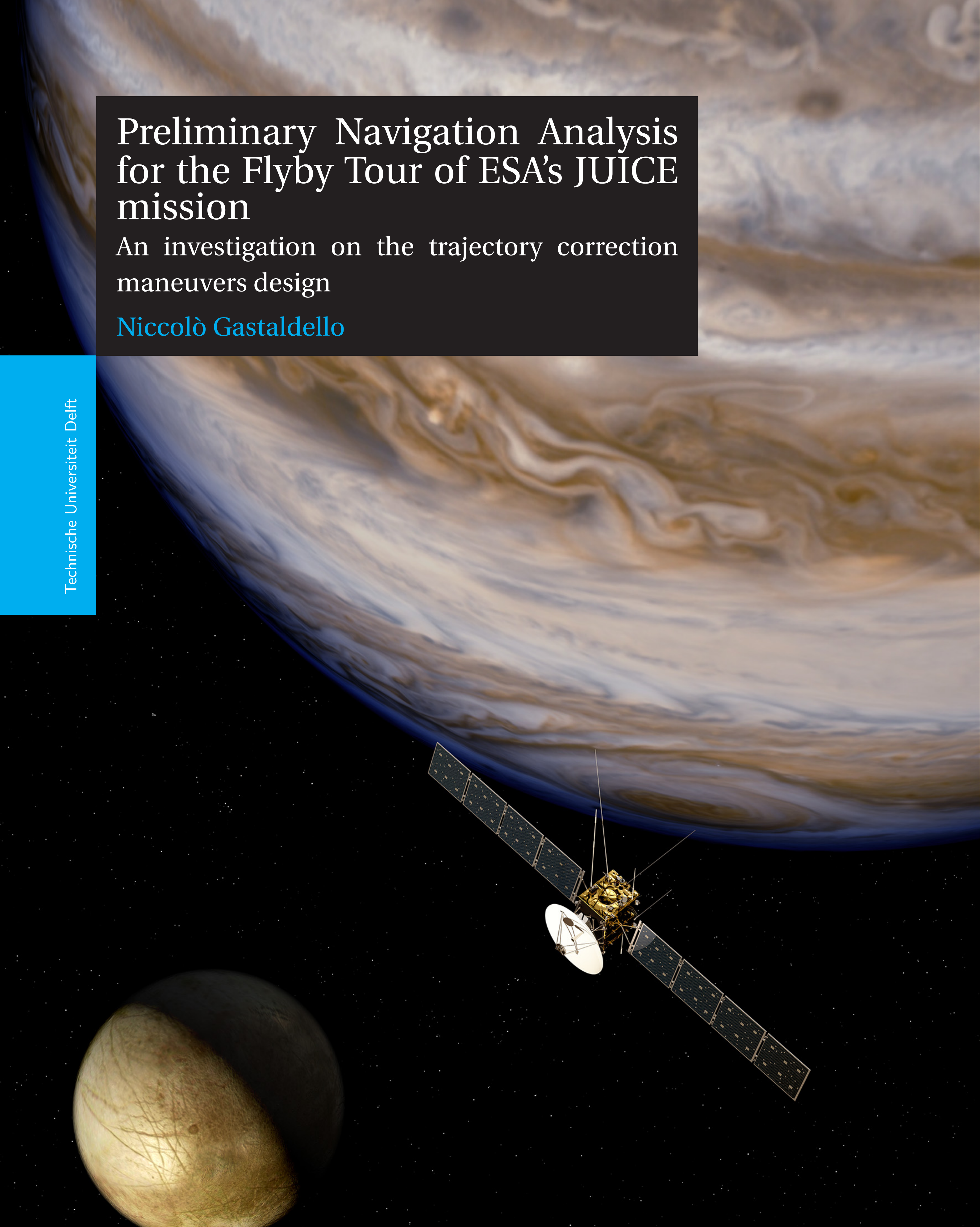

Technische Universiteit Delft

Delft University of Technology

Challenge the future

Preliminary Navigation Analysis for the Flyby Tour of ESA's JUICE mission

An investigation on the trajectory correction maneuvers design

by

Niccolò Gastaldello

in partial fulfillment of the requirements for the degree of

Master of Science
in Aerospace Engineering

at the Delft University of Technology,
to be defended publicly on Friday December 16, 2016 at 2:00 PM.

Supervisors:	Dr. ir. D. Dirkx,	TU Delft
	K.J. Cowan, MSc.,	TU Delft
Thesis committee:	Prof. dr. ir. P. N. A. M. Visser,	TU Delft
	Dr. G. Cimò,	JIVE

An electronic version of this thesis is available at `http://repository.tudelft.nl/`.
The cover image is an artistic representation of JUICE in orbit around Jupiter. The source is *http://sci.esa.int/juice/*.

Preface

This Thesis is the final project performed for the Master in Aerospace Engineering at Delft University of Technology. This research has been conducted at the Department of Astrodynamics and Space Missions.

My passion for space was born many years ago in school while discovering for the first time the wonders of our Universe and Solar System and the human endeavor to study them. This led me to study space engineering, choosing to purse a Master in Space Exploration after the Bachelor in Aerospace Engineering. This Master has been a very exciting course that taught me fundamental and advanced concepts of space flights, from the scientific motivations behind space exploration to the design of space missions. During these two years and four months I have worked hard to learn as much things as I could, participating in different activities and expanding my engineering skills. It has been a very challenging period full of new discoveries. I also had the opportunity to perform an internship in Glasgow, at the Advanced Space Concepts Laboratory, learning new things in the field of astrodynamics.

This Thesis is a research work on a topic of space exploration, in particular on the Guidance, Navigation and Control (GNC) applied to interplanetary space missions. As will be extensively described in this document, I have performed a preliminary navigation analysis for a part of the mission JUICE by the European Space Agency (ESA). This mission, that will be launched in 2022, will study Jupiter and its natural satellites. I find this mission particularly interesting due its very important scientific purposes, as the characterization of the Jovian environment and the search for possible signs of life.
My research is a study on the trajectory to be flown by the spacecraft JUICE, in particular on the trajectory control required during the execution of the Flyby Tour of the moons of Jupiter; I hope you will enjoy reading this Thesis.

This work would not have been possible without the support of my supervisor, Dr. Dominic Dirkx; I would like to thank you for the opportunity offered to me, the frequent meetings and the useful advices. I would like to thank also my second supervisor, Kevin Cowan, for the productive meetings we had during the literature study and the Thesis periods and the fruitful inputs to my work.
Special thanks also to the fellow students of the Master room on the 9^{th} floor; the time spent with you has been very pleasant. Thanks to all my old and new friends of Delft, these two years together have been really fun. A thought goes also to all my friends in Vicenza and Milano; it has been very valuable to keep your friendship for all these years. A special thanks to Lili for being always present for me.
For last, but most of all, I would like to thank my family for all the support and motivation that I received from them during my studies; without you all this would not have been possible.

Niccolò Gastaldello
Delft, November 2016

Abstract

The JUICE spacecraft is an ESA mission to the Jovian system that will be launched in 2022. It will collect scientific data about Jupiter and its Galilean moons thanks to a flyby tour of Europa, Ganymede, Callisto and a final Ganymede orbiting phase. A high number of flybys will be performed with minimum altitudes of 200 km. The tracking of the spacecraft during the flybys allows the estimation of the position of the spacecraft and the moons; in particular the knowledge of the moons positions can improve noticeably.
However, due to the uncertainties in the positions of the moons and the spacecraft itself, a robust trajectory control is required for precise flyby targeting, to ensure that the nominal mission plan is achieved with the required margins.

A preliminary navigation analysis for the mission JUICE has been developed, with the objective of the studying the influence of the spacecraft and moons positions uncertainties on the trajectory correction maneuvers (TCMs). The navigation analysis is composed of an orbit determination covariance analysis and a guidance simulator.
The covariance analysis determines the standard deviations of the parameters of interest, (spacecraft and moons initial states) from the observations computed along the trajectory of the spacecraft. Different parameters can be chosen for the covariance analysis in order to represent different mission conditions and tracking data performances.
The guidance has the purpose of computing the necessary actions to bring back the spacecraft to the desired path after the nominal one has been perturbed with the spacecraft and moons positions uncertainties; these action are the TCMs, which are represented by a ΔV due to the high thrust engine of JUICE. Three different targeting algorithms have been implemented for the guidance, with different characteristics of accuracy and speed. Two statistical maneuvers per flybys have been implemented, the pre-flyby (targeting) maneuver and the post-flyby (cleanup) maneuver.
The navigation analysis is performed using a Monte Carlo method, sampling with a normal distribution the results of the covariance analysis to obtain perturbed trajectories; statistical results are then computed. This is necessary because the results of the OD are to be interpreted in a statistical way; the real perturbed trajectory is always affected by an uncertainty.

A sensitivity analysis with respect to the tracking data types has been performed for the covariance analysis. The results show that for JUICE an uncertainty of the level of a few hundred meters can be reached, if range and VLBI data are used. However these results are just indicative since Doppler data have not been included in the simulations. The uncertainty in the positions of the Galilean moons obtained thanks to the flybys depends highly from the tracking strategy used and the data types. With the most realistic configuration (tracking interrupted before the flyby and inclusion of all the past data), the level of uncertainty can arrive to a few tens of meters, with data accuracies of 0.2 m for the range and 0.1 nrad for the VLBI. These results are for the formal errors and it is known that they are usually overly optimistic; the true error will be higher. Moreover, the importance of optical data for a further uncertainty reduction has been proven. The improvement of the Galilean moons uncertainties along the Tour as data are continuously added is also observed.
Sensitivity analysis with respect to the maneuver time and the maneuver execution errors have been performed for the Monte Carlo navigation analysis. The maneuver time has the highest influence on the size of a maneuver; each flyby presents a time for which the ΔV required to correct the trajectory is minimum. Very often this time is of 3 days before the flyby (for the targeting maneuver), as found often in literature; however many flybys have this minimum around 2 days before the flyby. The maneuver execution error has a limited impact on the total mission ΔV, but it can decrease the accuracy of the targeting, causing an higher miss distance at flyby.
The total ΔV required to perform the flyby Tour varies considerably upon the different parameters chosen; using current level accuracies (1 m for the range and 1 nrad for VLBI) and a maneuver time of 3 days before (and after) the flyby, the result is $\Delta V = 13.5$ m/s (around 0.67 m/s per flyby). This value includes the targeting and cleanup maneuvers; it is easily obtainable by the propulsion system of JUICE, concluding that it is possible to correct the trajectory for the uncertainties of JUICE and the moons with a small effort.

CONTENTS

List of Symbols

Symbol	Description	Unit
Roman		
t	time	s
m	mass	kg
r	position	m
F	force	N
c	speed of light	m/s
f	frequency	Hz
U	gravitational potential	Nm/kg
G	Gravitational constant	Nm^2/kg^2
P	Covariance matrix	-
H	Observation (information) matrix	-
$\mathbf{x}$	State vector/Position vector	[m, m/s]/[m]
$\mathbf{B}$	B-vector	m
V_∞	Hyperbolic excess velocity	m/s
J	Jacobian matrix	-
W	Weighting matrix	-
B_i	Impact radius	m
ΔV	'Delta' V (effect of a maneuver)	m/s
Greek		
Δ	Difference/Error	-/-
ϵ	Error in the observable model	-
ρ	Distance/Correlation	m/-
τ	Time delay	s
μ	Gravitational parameter	m^3/s^2
σ	Standard deviation for a parameter/Observable accuracy	-/-
ψ	Reference frame transformation matrix	-
Φ	State Transition Matrix	-
Subscripts and Superscripts		
fb	flyby	
man	maneuver	
kep	keplerian	
nom	nominal	
pert	perturbed	
prop	propagated	
obs	observable	
rss	root sum square	
avg	average	
J	JUICE	
m	moon	
IP	In Plane	
OP	Out of Plane	
r	range	
v	VLBI	
o	optical	
tca	time to closest approach	
$\bar{\ }$	A priori	

LIST OF ABBREVIATIONS

Abbreviation	Description
ESA	European Space Agency
JUICE	JUpiter ICy moons Explorer
NASA	National Aeronautics and Space Administration
JPL	Jet Propulsion Laboratory
OD	Orbit Determination
CA	Covariance Analysis
NA	Navigation Analysis
MC	Monte Carlo
VLBI	Very Long Baseline Interferometry
PRIDE	Planetary Radio Interferometer & Doppler Experiment
LSQ	Least SQuares
S/C	SpaceCraft
TCM	Trajectory Correction Maneuver
STM	State Transition Matrix
VE	Variational Equations
SOI	Sphere Of Influence
DCO	Data Cut Off
MEA	Main Engine Assembly
RCS	Reaction Control System
TUDAT	TU Delft Astrodynamics Toolbox

1
INTRODUCTION

The study of the Solar System has been part of human history for thousands of years, inspiring many astronomers in ancient civilizations as the Greeks, Egyptians and Chinese, to name a few. The Solar System is very vast and plenty of different phenomena are taking place in it. A very interesting region is the Jovian System, which consists of the biggest planet of the Solar System, Jupiter, and many natural satellites orbiting around it. The environment around Jupiter is very complex; the planet is a gas giant with a thick atmosphere and an enormous magnetic field. Jupiter is the planet with the biggest number of known natural satellites (moons) orbiting around it; the interaction of these moons with the planet is very important for the understanding of the formation and evolution of the Jovian System. This is important also for the understanding of the formation of the whole Solar System and ultimately for the emergence of life.
Life in the Solar System is known only on the Earth, but the search for it is going on continuously with robotic mission on different celestial bodies; of particular interest for this research are the biggest moons of Jupiter, the Galilean moons. These moons are Io, Europa, Ganymede and Callisto. They were discovered by Galileo Galilei in 1610 in Padova, where he performed some of the first observations of the sky with a rudimentary telescope. In some of these moons (namely Europa and Ganymede) the presence of subsurface liquid water oceans has been found; these oceans are protected from the harsh external environment by a thick layer of ice. They all have the necessary elements for the development of life as we know it; they have energy, coming from the gravitational interaction of the moons with Jupiter, they have nutrients, coming from the rocky interiors and for last time, to allow the development of life.
Space missions to investigate in detail the Galilean moons are needed; ESA is planning a major missions [1], JUICE (Jupiter ICy moons Explorer), to be launched in 2022 with scheduled arrival at Jupiter in 2030. JUICE will study extensively the Jovian System environment and the Galilean moons, flying at very low altitudes (performing flybys) over these moons while orbiting around Jupiter. Thanks to these close approaches a lot of data can be gathered by the suite of instruments of JUICE; these data will contribute enormously to improve and redefine scientific theories, possibly contributing to new exciting discoveries.

The present Thesis work is about the trajectory that the spacecraft will fly to perform these observations; this is called *flyby tour* since it will consist in a series of flybys of the Galilean moons. The (preliminary) trajectory to be flown has already been computed by ESA; however in space flight, the real trajectory always differs from the nominal one due to different phenomena which can not be accurately modeled or foreseen during the design phase. Hence the real trajectory of the spacecraft will somehow deviate from the desired one and corrective actions have to be taken. These actions are essentially maneuvers, which bring back the spacecraft to the desired location.
Among the different reasons for these trajectory deviations, an important one is the uncertainty about the knowledge of the position of the celestial bodies around which JUICE will fly. The term used to indicate the position of a celestial body is *ephemeris*. Corrective maneuvers have to be executed during the mission if the position of the moon before a flyby is different from the one used in designing the nominal trajectory, otherwise there can be the risk of an impact or a deviation from the nominal scientific operations.
The ephemerides of Jupiter and the Galilean moons come from past observations but they are not known without errors; a way to improve their accuracy is to use data from spacecraft close passages. It is thus seen the circular relationship in this dynamical process: the realization of a trajectory depends (not only) upon the

accuracy on the knowledge of the ephemerides and the ephemerides can be improved using (not only) data from the flown trajectory.
This Thesis focuses on the impact of the ephemerides knowledge on the magnitude trajectory correction maneuver, analyzing how the improvement of the ephemerides obtained as the flyby tours proceeds influences these maneuvers. This project thus does not analyze in detail the influence of all the physical phenomena that impact the design of these maneuvers, very complex task which is not possible to address in a single Master Thesis.
The main task conducted in Thesis is the implementation of a Navigation Analysis, which consist of an Orbit Determination simulator and a Guidance simulator. This is implemented specifically for the JUICE mission, but with the possibility of expanding it for other missions with some modifications.

The **research objective** of this Project is the following:

Determine the impact and mitigation of the Galilean moons ephemerides improvement obtained during the flyby tour of JUICE on the trajectory correction maneuvers.

To help the process of realizing the research objective, three **research questions** were formulated.

1) How much do the size of the TCMs decrease thanks to the ephmerides update performed during the flyby tour?

2) How do the different parameters that play a role in the orbit determination strategy influence the determination of the spacecraft position and Galilean moons ephemerides?

3) How do the different parameters that play a role in the Guidance influence the design of the TCMs?

Thesis structure
Chapter 1 is the present Introduction. Chapter 2 introduces the science case for the JUICE mission, describing the Jovian System environment and the characteristics of the mission. In Chapter 3 and 4 the theoretical basis for this work are exposed; in Chapter 3 the topic of orbit determination for interplanetary spacecrafts is described. Chapter 4 discusses the Guidance for flyby tours, presenting the targeting algorithms used in this project. These two chapters are fundamental because they represent the building blocks for the complete navigation analysis. In Chapter 5 the implementation details of the Navigation Analysis are discussed.In Chapter 6 the validation of the software written is presented. Chapter 7 and 8 present the results of this Thesis; In Chapter 7 the results from the Covariance Analysis only are presented. In Chapter 8 the results of the Navigation Analysis are presented. The Thesis is concluded with Chapter 9, where conclusions are exposed and recommendations stemming from the work performed and the results obtained are given. At the end of the Thesis two Appendices with extra information are provided.

2

THE JUICE MISSION

In this Chapter the scientific aspect of the exploration of the Jovian System is presented. Although the Thesis work is focused exclusively on the trajectory design and control, it is essential to have in mind the motivations and rationales for the mission, hence a brief introduction to the science of Jupiter and the Galilean moons has been deemed necessary.
In Section 2.1 a brief description of the Jovian environment is provided, with a particular focus on the Galilean moons. In Section 2.2 an overview over the past and future missions in the Jovian System is given. The last Section 2.3 is a summary of the main aspects of ESA's JUICE Mission.

2.1. THE JOVIAN ENVIRONMENT

2.1.1. JUPITER

Jupiter is the biggest and most massive planet of the Solar System; it is classified as a gas giant since it is composed mainly of gases, even though its interior is not any longer in gaseous form. It is the fifth planet from the Sun, located between Mars and Saturn.
The description of Jupiter interior structure, atmosphere and magnetosphere is taken mainly from [2], where plenty of information for the interested reader are available.

Interior and Atmosphere

Jupiter is an icy giant composed mainly of hydrogen and helium in hydrostatic equilibrium. A scheme of its interior structure and atmosphere is shown in Figure 2.1.

Some of the theoretical models for the internal structure of Jupiter predict a small core made of heavy elements; however, there are also models that predict no core. The existence of the core was suggested also from gravity measurements of past space missions, however it could not be constrained completely. Jupiter has an abundance of heavy elements distributed in its internal structure, so that is enriched in heavy materials with respect to the mean solar composition [2]. The core is probably composed of iron and rocks, surrounded by "ices" like H_2O, CH_4, NH_3. The mantle is probably composed of metallic hydrogen and helium, due to the high temperatures and pressure, while the outer layer is formed by molecular hydrogen and helium.

The atmosphere of Jupiter extends until a pressure of 10 bar; however, it is difficult to find its lower boundary due to the composition of Jupiter itself. Since Jupiter does not have a real solid surface, the atmosphere is defined from the point where the pressure is 10 bar [2].
Its composition was estimated through spectroscopic observations and some in situ observations, which revealed the presence of numerous gas species. The most abundant elements are H and He, which together constitute the 99% of the the atmospheric composition; the other molecules found are H_20, CH_4, NH_3, H_2S, Ar, Xr. In the atmosphere there are different phenomena, among which also the formation of clouds. Observed in visible light, Jupiter presents different interesting features like white zones, brown belts and the Great Red Spot (GRS). Through infrared observations, different temperatures for these zones were inferred; this temperature gradient creates a simple convection pattern between the belts and the zones which drives winds across the planet. The GRS and the small ovals next to it are system of giants storms; the red color of the spot is probably due to coloring agents that may contain red phosphorous or sulfur compounds.

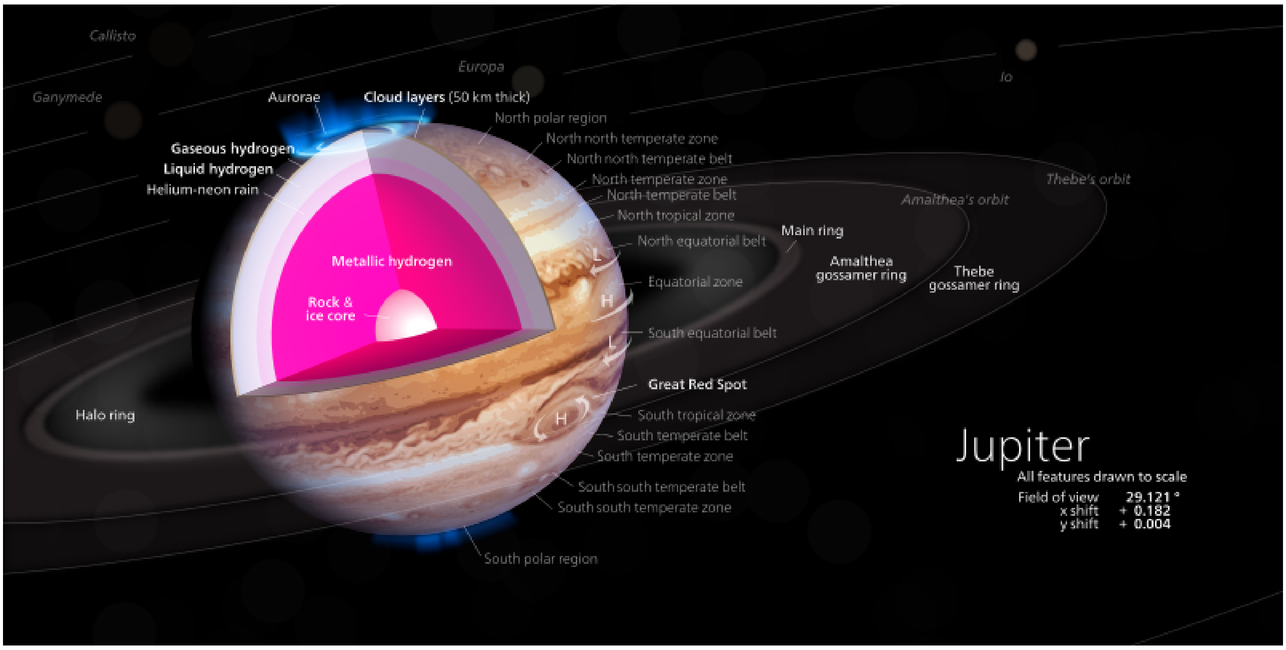

Figure 2.1: Scheme of Jupiter structure and atmosphere (from https://en.wikipedia.org/wiki/Jupiter)

Magnetosphere

Jupiter has the biggest magnetic field among the planets of the Solar System. It was studied extensively through measurements of *Galileo* with remote sensing and in situ techniques. The magnetic field is probably generated by electromagnetic currents in the metallic hydrogen layer, according to the magnetohydrodynamic dynamo theory. An interesting phenomenon, which involves the moon Io, is the interaction between the ions co-rotating with the magnetosphere and the atmosphere of Io (especially with its *neutral clouds*, made by oxygen and sulfur atoms). Due to these collisions, the clouds of Io gets ionized and these ions are accelerated to the rotational velocities of the magnetosphere. Thus, a *plasma torus* is formed that surrounds Jupiter and it is located very close to Io.

Of importance is also the interaction between the solar wind (charged particles) with Jupiter magnetosphere; this interaction is highly complex, causing different phenomena like aurorae on the poles of Jupiter.

2.1.2. The Galilean moons

Jupiter has dozens of moons (currently 67 have been counted). The most important, and target of JUICE, are the Galilean moons. Four inner moons have been detected inside the Galilean moons orbits, and the outer moons are irregular bodies much farther away from Jupiter. It is noted how the combined mass of all of these satellites is about 1/1000 of the mass of the smallest Galilean moon. A ring system has also been observed around Jupiter.

The Galilean moons are Io, Europa, Ganymede and Callisto, listed in order of distance from Jupiter; they are called Galilean because they were discovered by Galileo Galilei in 1610. They are very important from a geophysical and biological point of view; different geophysical phenomena as tidal deformations, volcanism and surface modifications take place in them. Moreover, they represent a planetary system in miniature and thus their study can enhance the comprehension of exoplanetary systems. Their main features are described here.

Io is similar to the Earth's Moon in term of mass and density; its surface is relatively young since there is an intense volcanic activity taking place on this moon. No impact craters have been seen on its surface. The volcanism is caused by the strong tidal forces exerted by Jupiter on Io; the energy of these tidal forces is dissipated through volcanic activity. Io is also rich of geological features, connected to the volcanic activity.

The tidal forces are caused by the fact that Io is locked in an eccentric orbit around Jupiter, due to the 4:2:1 resonance with Europa and Ganymede (Laplace resonance). This eccentric orbit causes variations in the tidal forces with time which generate a huge amount of heat inside Io; this heat is the source of the volcanism.

Hot spots are observed in Io, with erupting plumes arriving to hundreds of km from the surface; this plumes

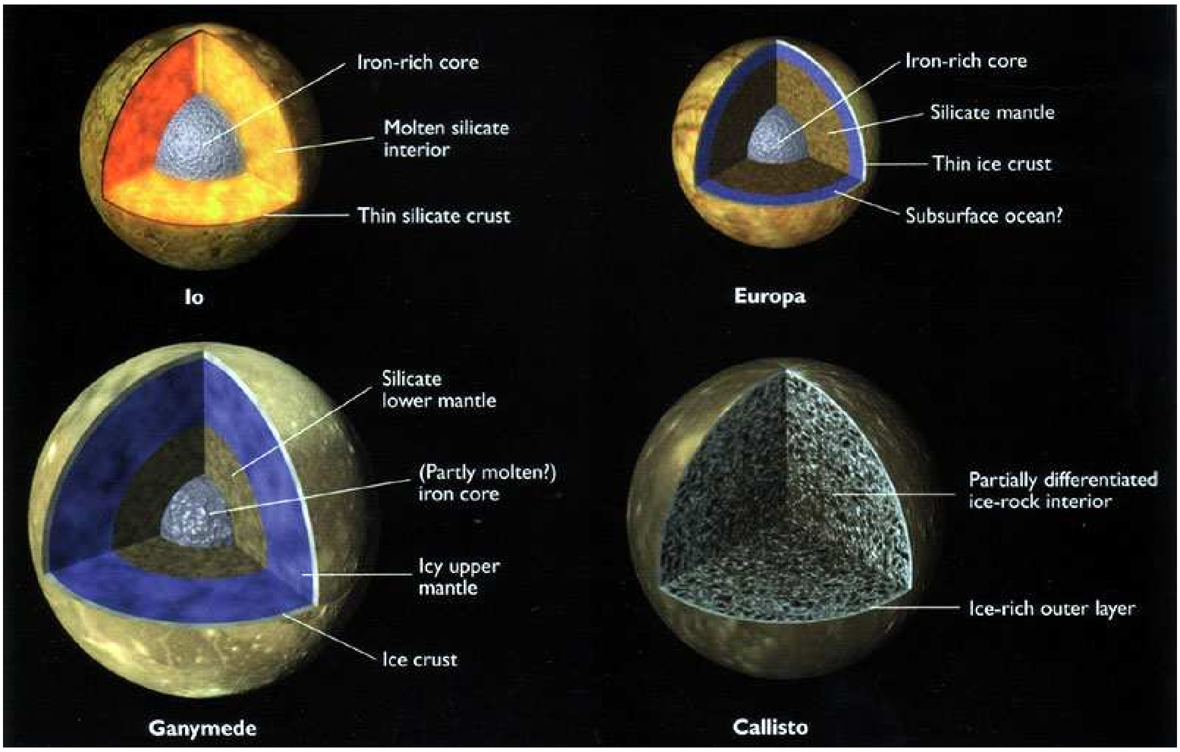

Figure 2.2: Scheme of the Galilean moons structure (Website arizona.edu)

cause the tenuous, sulfure dioxide atmosphere of Io.

Europa is smaller than Io and has spectral properties close to nearly pure water ice. Its moment of inertia and mean density imply that is a differentiated body with a rock/ice composition. The most interesting feature of Europa is the presence of water in liquid state, under its surface; this *sub-surface ocean* was detected by the Galileo spacecraft due to its signature in the induced magnetic field around Europa. This liquid ocean is in between the rocky core and the ice crust; it is probably maintained by tidal heating, although not as extreme as for Io. Europa is characterized by a lot of geological (cracks, ridges) features caused by the motion of the ice crust. It has a tenuous oxygen atmosphere, caused by the sputtering process: when water molecules are knocked off from the icy surface, they dissociate and the hydrogen atoms escape from the low gravity field, hence leaving an oxygen rich atmosphere. Another extremely interesting feature is the water jets emitted by Europa, observed by space telescopes (Hubble); their source is the internal ocean of Europa, but the physical process of their creation is still not completely understood. These jets reach an altitude of about 200 km, providing a wonderful opportunity for flyby missions like JUICE for a direct sampling of the interior oceans.

Ganymede and Callisto are different from the two inner bodies; they have a lower density, which suggest a composition of rocks and ice. The latter has also been detected in their spectra [2]. Differently from the previous two moons, they are partly covered with impact craters, indicating that geophysical processes, if taking place, are somehow slower or weaker than for the other two satellites. Ganymede (which is the largest satellite) presents a complex system of ridges and grooves that extends for hundreds of km, but only on its light areas; the dark areas are covered with craters. Of high interest is the origin of this system of geological features, which are connected to processes of tectonic resurfacing.
Another interesting fact concerning Ganymede is the detection of an intrinsic magnetic field, which must be caused by an internal liquid layer of conductive material. The theoretical models that best fit the observations of magnetic, gravity field and density data entail a liquid metallic core and a liquid water layer (at a depth of around 150 km).
Also for Callisto, from its moment of inertia estimates and magnetic field measurements, the presence of an internal salty ocean can be suspected; purpose of the JUICE mission will be to conclude on the presence of such oceans for Ganymede and Callisto [3].

Resonances among the Galilean satellites

The Galilean moons are locked in an orbital resonance, which is a precise mathematical relationships between their motion; this is strongly connected to the tidal characteristics of the system. The resonance that takes place is a *mean motion resonance*, since the mean motion of some of the Galilean moons satisfy a precise mathematical relation. The three moons which are locked in this resonance are Io, Europa and Ganymede. Io and Europa are in a $2:1$ resonance, satisfying the relations $2n_2 - n_1 - \dot{\omega}_1 = 0$ and $2n_2 - n_1 - \dot{\omega}_2 = 0$ where n is the mean motion and $\dot{\omega}$ is the mean rate of longitude of perijove of Io and Europa [4]. Europa and Ganymede are also in a $2:1$ resonance, satisfying the same relation. These resonances imply that the three satellites are aligned at very precise epochs, which are coincident with the peri and apojove of Europa. Moreover, the orbital periods of Io, Europa and Ganymede are in the ratio $1:2:4$; this particular ratio between the orbital periods is called *Laplace resonance*. The mean rates of perijove longitudes are $\dot{\omega}_1 = \dot{\omega}_2 = -0.7395°/day$ for Io and Europa [4]. A direct result of the previous two conditions is that the linear combination of the mean longitudes librates around a constant value (180°):

$$\phi = 2\lambda_3 - 3\lambda_2 + \lambda_1 \tag{2.1}$$

The mechanism that keeps in place this resonance is the following: the tidal dissipations tend to circularize the orbits, but the resonances force the eccentricity to keep a small but nonzero value. In this way the forced eccentricity cause the tidal dissipation to be a very strong source of energy. The phenomenon that brought this resonance into being is complex and is not completely understood [2]. The study of the interaction between the tidal forces and the resonances is very important for the Galilean moons (an extensive explanation is given also in [5]).

These resonances are important also for the generation of ephemerides, because they allow to relate directly the position of a moon to the position of another moon. As it will be shown in Section 3.4, in the mathematical formulation of the algorithm used to compute the positions of the moons from the observations, there are some terms that represent the indirect effect that the the displacement of a moon has on the displacement of a different moon.

2.2. Past and Future Missions

In this Section a brief overview on the past and future missions that visited and will visit the Jovian System is given.

2.2.1. Flyby Missions

The Pioneer (10 and 11) and Voyager (1 and 2) were two space missions of the 1970s by NASA to study the Outer Solar System. They were not designed to enter in orbit around Jupiter, but rather to visit different planets in the Outer Solar System performing close approaches (flybys) with them. Since all the four spacecraft were on escaping routes from the Solar System, each one of them could only perform one flyby of Jupiter. It is noted however how, just from these flybys at distances of about $40,000 - 500,000\ km$, it was possible to recover the gravity field of Jupiter [6] and a certain number of parameters describing its physical properties (including also the mass of Jupiter and its moons).

2.2.2. Galileo

The Galileo spacecraft was the only spacecraft that has been in orbit around Jupiter up to 2016; it was a NASA mission launched in 1989, which orbited Jupiter from 1995 to 2003 and gathered an enormous amount of information on Jupiter and its satellites, through an extensive series of flybys of the moons.

The Galileo mission has been very interesting from scientific and engineering points of view; from the scientific side it allowed the reconstruction of the gravity field of Jupiter and its satellites with unprecedented accuracy, it characterized the magnetosphere of the Jovian system (with attention on the induced magnetic fields in the satellites) and it found the presence of subsurface oceans at Europa and probably Callisto and Ganymede. The spacecraft encountered different problems too, as the failure of the high-gain antenna.

From the engineering point of view it was a success since its trajectory and spacecraft design were very advanced and complex. The flyby part of the mission was very complicated from the guidance-navigation point of view [7]; thanks to the experience gained with that part of the mission, different improvement have been obtained in flyby tour design and execution.

The mission ended in 2003 with a destructive entry of Galileo into Jupiter's atmosphere, to avoid any possible contamination of the satellites.

2.2.3. JUNO

NASA's Juno mission was launched in 2011 and arrived at Jupiter in July 2016. It is expected to provide a rich amount of scientific data in the next years. Like Galileo and JUICE, its objective is to contribute to improve the knowledge of the Jupiter System origin, evolution and phenomena. It will fly in a Jupiter polar orbit, collecting important data on its gravity field, magnetic field, atmosphere and plasma environment [8]. In connection with the present Thesis work, the contribution of Juno will be to provide very accurate ephemeris for Jupiter, improving considerably the current level of accuracy.

Another mission currently under development by NASA is Europa Clipper. It is envisioned to launch in the 2020s; its focus will be the exploration of Europa, one of the most interesting moons of Jupiter from geological and biological points of view, performing a high number of flybys.

2.3. ESA'S JUICE MISSION

The JUpiter ICy moons Explorer (JUICE) is a space mission by ESA, selected in 2012 as part of the Cosmic Vision Program 2015-2025, with the purpose of performing detailed investigations of Jupiter and its Galilean moons, in particular Ganymede, but with a focus also on the neighbouring moons Callisto and Europa. The study of the inter-relations between the environments of the different moons is very important because it will give a comparative picture of these moons and their potential habitability [3]. Another important scientific objective of the mission is to improve the current understanding of the formation process of the gas giants and their satellites systems; this is useful also for the study of exoplanetary systems, which are currently been searched with high interest in our galaxy.
The mission will generate an enormous amount of data that will be useful to scientists to refine the actual theories on the physical processes happening in this planetary system, for a deep comprehension of this environment and with an eye to other possible future explorations of this system.
The JUICE spacecraft is currently been built by Airbus Defence and Space, and its launch is planned for 2022.

2.3.1. SCIENTIFIC OBJECTIVES

For an extensive exposition of the science case, it is possible to read ESA's official report [1] or the related paper [3]. In this Subsection the main scientific objectives will be highlighted.
JUICE will focus on two of the four key science drivers of ESA's Cosmic Vision Program 2015-2025:

1. *Theme 1*: What are the conditions for planet formation and the emergence of life?
   These two conditions will be studied thanks to a flyby tour around the Galilean moons followed by an orbital tour around Ganymede. Different physical characteristics of these moons as composition, surface features and dynamics of subsurface oceans and icy crust will be determined thanks to the scientific instruments. These information will be fundamental for the understanding of the origin and evolution of the System and the possibility of hosting life forms.

2. *Theme 2*: How does the Solar System work?
   The focus for this theme is on the plasma and magnetic field environment of the Solar System in general, with a focus on the Jovian System. Of particular interest will be the interaction of the magnetosphere of Jupiter with the Galilean moons. Also the study of the atmosphere and internal structure of Jupiter will be studied, with a focus on the interaction of the atmosphere with the moons.

Other important scientific/engineering information that will be enhanced by JUICE are the gravity field and ephemerides of Jupiter and its Galilean moons. They are information that can be retrieved from any space mission that is tracked in the Solar System; tracking a spacecraft orbiting (or performing flyby) around a celestial body allows the reconstruction of the gravity field of such body, and the improvement of its ephemeris (see Section 3.5). These two aspects have also an engineering purpose: with such data a more precise modeling of dynamics of the Solar System is possible, which can be of use for future space missions.

2.3.2. INSTRUMENTS

JUICE will carry a powerful suite of instruments for a complete characterization of the Jovian System; ten instruments have been selected [1] plus an experiment that uses the telecommunication system of the spacecraft. The instruments can be divided in four packages, depending upon the type of measurement performed; the *remote sensing package* will measure the characteristics of the surface and atmospheres of the celestial

bodies through imaging cameras, spectrometers and spectrographs. The *geophysical package* will use laser, radiometric and radar instruments to measure the surfaces and subsurfaces, in order to obtain information on the gravity fields and compositions of the celestial bodies ([9], [10]). The *in situ package* contains electromagnetic sensors which will study the particle and plasma environment and the magnetosphere of the System. The last package is the *telecommunication* experiment, PRIDE, which will use VLBI to determine very accurately the spacecraft position (see Chapter 3).
The instruments of interest for this Thesis, the ones used for the determination of the position of JUICE are the following ([1]):

- **3GM - Gravity & Geophysics of Jupiter and Galilean Moons**: it is the radio science package, comprised of a Ka-band transponder and a ultrastable oscillator. It allows the radio tracking from Earth, moreover it will provide scientific data on the gravity fields, internal oceans and atmospheres of the moons.
- **PRIDE - Planetary Radio Interferometer & Doppler Experiment**: it is an experiment that uses the telecommunication system of JUICE to perform VLBI (Very Long Baseline Interferometry, Subsection 3.1.1), a measurement technique that allows a precise reconstruction of the spacecraft position. It will also provide scientific data about the gravity fields of Jupiter and the moons.
- **JANUS - Camera System**: it is an optical camera with scientific purposes of observing Jupiter and the moons; it can be used also for navigation since it provides also the information about the relative position JUICE-celestial body.
- **GALA - Ganymede Laser Altimeter**: although its main purposes are to characterize the shape and topology of the moons (in particular Ganymede), the laser altimeter could be used also for laser ranging, allowing for a very accurate determination of the position of JUICE. The technical feasibility is currently studied.

2.3.3. MISSION DESIGN
In this Section the Mission Profile of JUICE is presented: the trajectory, the maneuvers and the critical events will be explained. An important thing to notice is that the JUICE spacecraft is a high-thrust spacecraft, hence its trajectory is planned as consequence, with a few, high-thrust, engine impulses rather than a continuous thrusting (typical of a low-thrust engine).

A summary of the different mission phases is presented here; it has to be noticed that since it is taken from [1], it may be outdated. The baseline mission is divided in three main parts: the interplanetary cruise to arrive to Jupiter, an initial tour of Jupiter with different flybys (Flyby Tour) of the Galilean moons, and a final orbital phase around Ganymede. The end of life of the mission is also planned. The mission phases are described here in more detail.

Launch and Interplanetary Cruise
JUICE is planned to be launched in mid-2022, with a backup opportunity in August 2023. The launch will be done via an Ariane 5 rocket from Guiana Space Center.

Depending on the real launch date, the interplanetary transfer is slightly different; the baseline is to perform a cruise of 7.6-8 years with gravity assists of Earth, Venus and/or Mars to increase the orbital energy of the spacecraft, in order to arrive at Jupiter with substantial propellant savings.
The most critical part is the Jupiter Orbit Insertion (JOI) event because it has to be achieved with a very little margin of error; all the other events and maneuvers will be when JUICE is in a bounded orbit around Jupiter and hence with corrections/repetitions opportunities.
The JOI insertion maneuver will be executed at the periapsis of the spacecraft orbit around Jupiter (perijove) and will be preceded by a Ganymede gravity assist to reduce the cost of the JOI maneuver (concept of satellite-aided-capture, extensively described in [11]).

Flyby Tour
After a successful insertion in a highly elliptical orbit around Jupiter, JUICE will perform a perijove raising maneuver (PRM) at apojove, to improve the efficiency of the next gravity assists. These further gravity assist will incline the orbit to the equatorial plane of Jupiter. The 4^{th} Ganymede gravity assist will initiate the Europa phase, preceded by a Callisto flyby. Two Europa flybys will be performed during this phase.
After these flybys a highly inclined orbital phase is obtained with the aid of Callisto and Ganymede flybys;

during this phase the high latitude environment of Jupiter will be investigated. After this phase, other flybys are used to bring back the orbit to the equatorial plane in order to start the transfer to Ganymede. The flyby tour described here would take around 30 months.
The Thesis is about the navigation and guidance during this flyby tour.

Ganymede Tour
Again, other gravity assists of Callisto and Ganymede itself are used to reduce the orbital energy of the spacecraft in order to perform a Ganymede Orbit Insertion (GOI). The spacecraft will be inserted in a highly elliptical orbit around Ganymede. Due to Jupiter's perturbations, this orbit will be circularized (at the altitude of 5000 km) in around 20 days. Again due to perturbations, and without executing correction maneuvers, the orbit will get elliptical will a low periapsis (around 500 km). At this point is possible to circularize the orbit with a sequence of braking maneuvers; this orbit will be nearly polar.

End of Life
The nominal Science Mission is envisioned to end 280 days after GOI. The natural orbit evolution will cause JUICE to crash on Ganymede's surface.
During the mission phases described above, different types of observations are planned, each one optimized for the corresponding orbital phase.
The total ΔV requirement for JUICE is of $\Delta V_{req} = 1.7\ km/s$ (from JOI to EOM) and the planned capability is of $\Delta V_{plan} = 2.7\ km/s$ (from [1]). This high margin can be explained by the high uncertainties still present in the orbit design and by the necessity for an accurate orbit control.

Planetary Protection

The Planetary Protection Requirements dictate rules on the behavior of human made spacecrafts with respect to celestial bodies, in particular the ones that potentially host life forms.
For the JUICE mission, the celestial body to which the highest attention must be paid is Europa; it is in the Planetary Protection Category III which prescribes the following guidelines (from [1]):

> chemical evolution and/or origin of life interest or for which scientific opinion provides a significant chance of contamination which could jeopardise a future biological experiment.

Hence, it is required that the probability of impact with Europa shall be under 10^{-4}. This risk of collision is present only during the Europa flybys, since for the rest of the time JUICE will not come very close to Europa.
Ganymede instead is part of Category II (from [1]):

> significant interest relative to the process of chemical evolution and the origin of life, but only a remote chance that contamination by spacecraft could compromise future investigations.

Thus, calculations have to be done to guarantee that, even though a crush on Ganymede is envisioned, this event would entail a probability of any active organism reaching the subsurface ocean lower that 10^{-4}. Considering factors like sterilization from radiations, possibility of partly controlled impact and survival during transport, it can be shown that this probability is well met.

3

Fundamentals of Orbit Determination and Covariance Analysis

Orbit Determination is the procedure that allows the computation of a spacecraft orbit in space; another term that can be used is Navigation, which in a broader sense means the determination of the position of any kind of object (not necessarily in orbit).

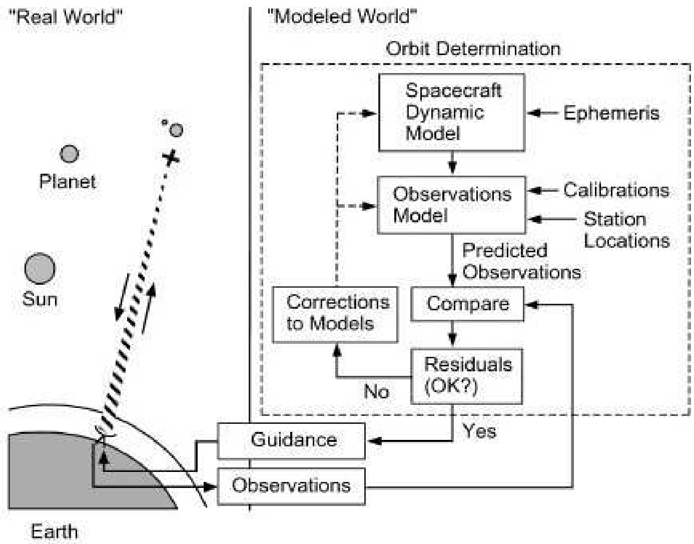

Figure 3.1: Scheme of the Navigation process [12]

The process of Navigation and its relationship with the Guidance (presented in Chapter 4) is shown in Figure 3.1. Dynamical models are used to represent the temporal evolution of the spacecraft position and velocity; using observations, it is possible to compute the state of the spacecraft that best matches these observations and the state predicted by the physical models. The process of reducing the difference between the computed observations and the real ones is the basic idea of the orbit determination procedure, that entails the use of specific algorithms. This is an iterative process that tries to correct the different errors and uncertainties that affect this procedure, to match as accurately as possible the estimated state to the observations. Physical parameters can also be estimated with this procedure.

The structure of this Chapter is the following. Firstly are exposed the most common techniques used in interplanetary spacecraft tracking, in Section 3.1. In Section 3.2 the dynamical model used in this project is described. Section 3.3 follows where the orbit determination algorithms are described; in Section 3.4 the variational equations, of fundamental importance for the orbit determination, are introduced. Concluding the

Chapter is Section 3.5 where the process of ephemerides computation for celestial bodies is described, with a focus on the Jovian System.

An important discussion should be done also for the error sources that affect the orbit determination procedure, in particular the measurements; however, since in this Thesis the effect of these errors is not considered, the treatment of this topic is not done here, but can be found in different references ([13], [14]).
A very complete and advanced reference is a technical report by Moyer [15], where the development of an OD software for JPL is illustrated.

3.1. Techniques and Observables

The main tracking techniques used in interplanetary navigation are of two types: radiometric techniques, where radio signals are used in different ways to determine directly or indirectly certain parameters related to the spacecraft position and velocity; optical techniques, where images taken by cameras are used to determine the position of a celestial body with respect to the camera, and hence the spacecraft.

3.1.1. Radiometric Techniques

Communications between ground stations and spacecrafts are commonly done using specified frequency bands of the electromagnetic spectrum, as S,X,Ka band. JUICE will make use of the X and Ka band.

In the recent years there has been a tendency to move towards higher frequency bands (as Ka-band) in order to improve the accuracy of radiometric measurements by using shorter wavelengths and to reduce the frequency dependent errors due to charged particles. This is the reason why it will be used for JUICE; the X band will be used to have a second frequency that can help to reduce or cancel the noise due to the plasma [1].
The tracking of an interplanetary spacecraft can be done with a one, two, or thee way ranging. The difference is shown in Table 3.1.

Table 3.1: Ranging Technologies

One-way	Two-way	Three-way
The signal is emitted from the spacecraft and arrives to the ground station. The emission time is determined by the spacecraft clock while the reception time by the ground station clock	The signal is emitted from the ground station and arrives to the spacecraft where is actively re-transmitted to the same ground station. The emission and reception times are determined from the ground station clock	The signal is emitted from the ground station and arrives to the spacecraft where is actively re-transmitted to the a different ground station. This is necessary if, due to Earth's rotation, the first ground station is not visible anymore. The emission and reception times are determined from the clocks of the two different ground stations

They have different implications and performances; the simplest one is the one-way ranging, since the signal propagation happens just once. The most efficient is the two-way, since the only clock used is the one of the ground station which is usually more precise than the one on-board the spacecraft. Three main radiometric techniques are used in in interplanetary navigation: range, doppler, and VLBI; each of them allows the computation of a different set of parameters related to the spacecraft state.

Range

One important information about the spacecraft trajectory is its range, which is the geometrical distance from the ground station to the spacecraft; it is determined with the *time of flight* principle: since it is known that an electromagnetic signal propagates at the speed of light (c), computing the time that it needs to travel from a source to another, is possible to obtain the distance that it has traveled with the expression

$$\rho = \tau c \tag{3.1}$$

where τ the travel time and ρ the ideal range, related to the observed range through

$$\rho_{obs} = \rho + \epsilon \tag{3.2}$$

with ϵ represent the errors that affect the measurements.
It is noted how a single range measurement is not completely useful because it does not allow for a recovery of the three dimensional position of a spacecraft; for a complete recovery are needed other range observations from different ground stations (theoretically at least other two, but practically much more to correct for the errors) or other types of data.
Typical accuracy for the range data is at 1 m level for ranging [14], with possibility of improvement to 20 cm with a technology update (which is planned for JUICE, [1]).

DOPPLER

The Doppler effect is the change of frequency of a signal due to the relative motion between the observer and the source of the signal; the mathematical expression for this effect is (as first order approximation)

$$f_R = \left(1 - \frac{\dot{\rho}}{c}\right) f_T \tag{3.3}$$

where f_T, f_R are the transmitted and received frequencies, $\dot{\rho}$ is the instantaneous range rate of the spacecraft with respect to the ground station and c is the speed of light.
The frequency received is measured through a counter, that compares the received signal with the reference transmitted signal, to extract the information of the frequency change. As demonstrated by [16] , with a single pass of Doppler data is possible to obtain information about the geocentric range rate, right ascension and declination (angular coordinates) of the spacecraft, thanks to the rotation of the Earth. This because they are geometrically related to the measured range-rate, through the relation

$$\dot{\rho}(t) = \dot{r}(t) + \omega_e r_s \cos\delta \sin(\omega t + \phi + \lambda_s - \alpha) \tag{3.4}$$

where ω_e is the Earth's rotational speed, t is the universal time, α is the right ascension, δ the declination and the other parameters are related to the geometry of the system. α and δ represent the angular position of the spacecraft. It is noted that this expression is an approximation of a more exact relationship.
The geometrical parameters of the spacecraft position (declination, δ and right ascension, α) can be extracted for a pass of a certain duration of time, analyzing the signal in equation 3.4 (in particular its amplitude and phase). With more days of Doppler data is possible to obtain also velocities normal to the line of sight and geocentric range, but these data are not as accurate as direct ranging.
Typical accuracy for the range data are at 0.1 mm/s for 60 s of integration time for Doppler [14], with possibility of improvement to 0.01 mm/s with a technology update (which is planned for JUICE, [1]).

VLBI

Although Doppler systems were the traditional way to determine angular positions of spacecrafts, the introduction and continuous improvement from the 80s of the Very Long Baseline Interferometry technique (VLBI) provided a powerful method that allows for a direct reconstruction of spacecraft right ascension and declination. A detailed historical description of the introduction of VLBI at NASA is reported in reference [17] and shows the progress of this technology; ESA [18] obtained its full VLBI capabilities in very recent years (2005).
VLBI measurements will be of fundamental importance for the JUICE mission; a dedicated VLBI experiment will be conducted with the instrument PRIDE ([19],[20],[21]). The instrument 3GM can be used for VLBI too.
The basic concepts of VLBI is to use not a single, but more ground stations, to perform differential measurements of the spacecraft and of reference radio sources (Figure 3.2).

For the determination of the angular position of the spacecraft at least two geometrically independent baselines (a baseline is the separation between two ground stations) are needed ([23],[24]). In practice more stations are used. The two stations that form a single baseline receive the signal from the spacecraft at different times; this time delay, τ, depends on the baseline geometry and on the position of the spacecraft, through the relation

$$\tau = \frac{\mathbf{B} \cdot \hat{\boldsymbol{s}}}{c} \tag{3.5}$$

where $\mathbf{B}$ is the baseline vector and $\hat{\boldsymbol{s}}$ the unit vector pointing to the spacecraft.
Conceptually speaking, it is possible to see that using two different baselines, $\mathbf{B}_1, \mathbf{B}_2$ and measuring the two

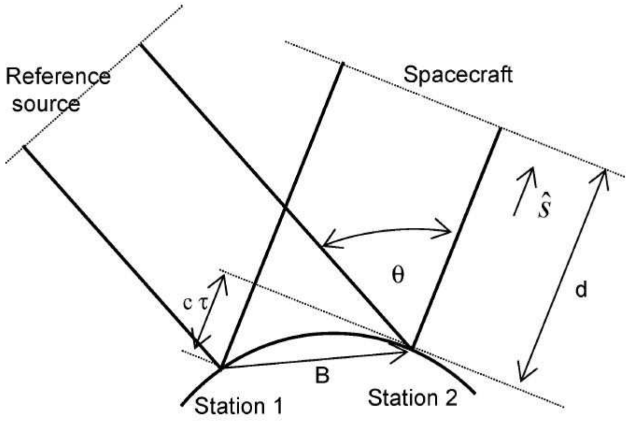

Figure 3.2: Scheme of the VLBI concept [22]

delays τ_1, τ_2, is possible to solve for the vector $\hat{s}$ (which has two components, declination and right ascension). What is done in practice is to execute another differentiation with a know radio source, which is usually a quasar (quasi-stellar radio source); it is very important to know accurately its position in the sky which, neglecting cosmological implications of the expansion of the universe, can be considered fixed in inertial space. A catalog of radio sources is available and it is continually updated; in particular, the current mission GAIA of ESA has among its objective to determine accurately the position of thousands of quasars, which could be used by the VLBI technique. Since these radio sources are very distant from Earth, their radiation is very weak; hence very big antennas are needed to obtain enough energy from their signals; NASA's Deep Space Network (DSN) uses 34 and 70 m antennas, while ESA has three 35 m Deep Space Antennas.
This radio source must be at a very small angular separation from the spacecraft, such that errors due to the path of the signal can be canceled with the differentiation process (because the two signals travel more or less through the same portion of the atmosphere). This differentiation yields the differential angles of the spacecraft-quasar direction with respect to the baselines; it is noted how the error for this differential measure is inversely proportional to the baseline length and directly proportional to the differenced time delays. From the obtained differenced angles is possible to compute the spacecraft angular position, since both the ground station and quasar positions are known (to a certain accuracy).

VLBI techniques can be divided in different categories depending upon the measurement and analysis techniques used to compute the differential delay [22]; in particular, very important is the resolution for the phase ambiguities of the signals received. Among the four possible techniques, the two operating techniques are *Delta DOR (ΔDOR)* and *VLB Array (VLBA)-phase referencing*, which are briefly exposed here.

1. ΔDOR: it is used by NASA and ESA, and was introduced by NASA's Jet Propulsion Laboratory (JPL); the name stands for Δ differential-one-way-range, which represents the differential delay between spacecraft and quasar. In this technique, standard interferometry is used to obtain the delay for the radio source, while for the spacecraft its telemetry and special tones (DOR tones) are used. The group delay of the signal is used, which is more robust than phase delay measurements. It is a proven technology that has a full operational capability.

2. VLBA-phase referencing: in this technique, the quasar and spacecraft signals are treated similarly, computing the phase delay between the two received signals. More stations are needed than ΔDOR in order to estimate accurately the spacecraft position. In this case the resolution of the phase delay is employed, thus specific DOR tones are not required from the spacecraft. Its advantage is the promising accuracy (to 0.1 nrad if Ka band is used, still to be demonstrated); its disadvantages lie in the facts that more stations are needed and that its operational capability has not yet been obtained, but only demonstrated.

The differences in terms of performances are that VLBA allows a more precise determination of the angular position since the phase of the signal is used; however it requires more ground stations for the resolution of the phase ambiguity [22]. In relation to the JUICE mission, both the techniques are envisioned to be used; in particular, the 3GM instrument will use the ΔDOR, while the PRIDE experiment will use the phase referencing technique (in [25] an extensive description of the delay measurement and processing is presented). In [26] a

sensitivity analysis is performed to describe in particular the influence of the VLBI data for JUICE.
Typical accuracy for VLBI are at 1 nrad [14], with possibility of improvement to 0.1 nrad with a technology update (which is planned for JUICE, [1]).

3.1.2. Optical Imaging

The use of onboard optical cameras is of fundamental importance for interplanetary missions, because it contributes to the relative position determination of a spacecraft with respect to a celestial body ([27], [28], [29]). If the spacecraft absolute position is known (using radio measurements) it is then possible to compute the position of the celestial body observed optically (it is possible also with radiometric data only if the spacecraft is close enough). This data type is commonly used together with radiometric data in order to increase the navigation solution accuracy (termed as *opnav*). It is especially useful when the trajectory of a spacecraft is not known to the desired accuracy and when there is an high uncertainty in the target body ephemeris, particularly for outer planets missions (Galileo, Cassini-Huygens, New Horizons). Usually cameras used for navigation are scientific cameras: their first purpose is scientific observation. Such cameras are more massive and power demanding than the ones developed specifically for opnav but are also more accurate; the trend is to move to cameras specific for navigation, making them smaller and cheaper.
JUICE camera, JANUS, is indeed a camera with primary scientific objectives, like studying the surface composition, craters distribution, atmospheric variations of the Galilean moons; the inclusion of its data in the orbit determination is part of the project, to determine how they influence the ephemerides improvement.

3.2. Dynamical Model

The equations of motion describe the motion of a body in a certain environment with respect to a reference frame. Of importance is the definition of the reference frame, the boundaries of the environment, and the magnitude of the forces acting on all the bodies. In this way it is possible to write equations that relate the accelerations of this body to its position and velocity (state), to the state of the other bodies, and to parameters and variables that may depend upon other factors (like atmospheres and solar radiation). What is obtained is a set of differential equations that is not possible to solve analytically; approximations or numerical solutions are hence necessary to obtain the temporal evolution of the spacecraft.
For JUICE, the environment in consideration is obviously the Solar System, since the spacecraft is moving in bounded orbits inside it. When it is in orbit around Jupiter, the environment can be restricted to the Jovian System, but still including the effect of the Sun.

The development of the equation of motion, whose main terms are the gravitational ones, is taken from [30]and [31]. In those references a complete derivation that includes the effects of punctual and oblate celestial bodies masses in presented; the basic formulation is reported here for the sake of conciseness. The equations are developed in a planetocentric reference frame with inertially fixed axes (that may be nonequatorial); the orientation is fixed with respect to the Ecliptic J2000 system. Avoiding a lengthy description of reference systems and frames [32], this is a quasi-inertial reference frame centered at the barycenter of the Solar System. The x axis is the mean equinox on date 1st of January 2000, the z axis points the north celestial pole, and the y axis is determined as consequence to obtain a right-handed system.

The system of differential equations to be integrated to obtain the motion of the bodies is the following (considering N bodies P_i of mass m_i)

$$\begin{cases} \ddot{\mathbf{r}}_1 = \frac{\mathbf{F}_1}{m_1} - \frac{\mathbf{F}_0}{m_0} \\ \vdots \\ \ddot{\mathbf{r}}_i = \frac{\mathbf{F}_i}{m_i} - \frac{\mathbf{F}_0}{m_0} \\ \vdots \\ \ddot{\mathbf{r}}_N = \frac{\mathbf{F}_N}{m_N} - \frac{\mathbf{F}_0}{m_0} \end{cases} \tag{3.6}$$

where $\mathbf{F}_i$ is the total external force on body i, $\ddot{\mathbf{r}}_i$ is the acceleration of body i and the index 0 is referred to the body at the center of the reference frame. The total force exerted on body P_i is

$$\mathbf{F}_i = \sum_{j=0, j\neq i}^{N} \mathbf{F}_{ij} \qquad \text{with} \qquad \mathbf{F}_{ij} = G m_i m_j \nabla_i U_{ij} \tag{3.7}$$

The force exerted on P_i by P_j is indicated as $\mathbf{F}_{ij}$ and it is expressed in Eq. 3.7 using the gravitational potential. The gravitational potential at location $\mathbf{r}_i$ deriving from body j at $\mathbf{r}_j$ is

$$U_{ij} = \frac{1}{r_{ij}} \tag{3.8}$$

with $r_{ij} = \mid \mathbf{r}_{ij} \mid = \mid \mathbf{r}_j - \mathbf{r}_i \mid$.

Computing explicitly the derivatives, the expression obtained for the acceleration of body i (considering only point masses bodies) is

$$\ddot{\mathbf{r}}_i = -\frac{G(m_0 + m_i)\mathbf{r}_i}{{r_i}^3} + \sum_{j=1, j\neq i}^{N} Gm_j \left(\frac{\mathbf{r}_j - \mathbf{r}_i}{{r_{ij}}^3} - \frac{\mathbf{r}_j}{{r_j}^3} \right) \tag{3.9}$$

The derivation for the case of oblate bodies is more complex and can be found in [30].

In the following Subsection the magnitude of the main forces that act on the spacecraft when orbiting around Jupiter are computed and a selection of the forces to be used in the simulations is performed.

3.2.1. Selection of the forces to include in the dynamical model

To select which forces to include in the simulations, a computation of the magnitude of these forces has been done, to see to what extent a force influences the dynamics of a spacecraft for this type of mission. It is noted that, since the time interval of interest is quite limited (around 24 months), the impact of a force that is at least some order of magnitude (3,4) smaller than the biggest force acting on the spacecraft is negligible; this could be not valid for different kind of problems (e.g. when studying the long term evolution of the natural bodies in the Jovian system then it is important to include more forces than in this case).

For the following computations the values of the constants are taken from [2]. The main force is the gravitational attraction on the spacecraft due to Jupiter; the magnitude of the acceleration due to this force is

$$a_J = G\frac{M_J}{r^2_{s/c-J}} \approx 0.2\ \frac{m}{s^2}$$

at a distance of 800,000 km. Comparing the other accelerations acting on the spacecraft to this value is possible to decide if to include them or not in the simulation.

Another main force that has to be used necessarily is the gravitational attraction of the Galilean moons on the spacecraft; this is not always as strong as the attraction from Jupiter itself (especially when the spacecraft is far away from a moon) but becomes the main force when the spacecraft is close to one of them (Section 4.1). The magnitude of the gravitational acceleration of JUICE during a flyby of a Galilean moon (for example Callisto) is

$$a_{moon} = G\frac{M_{moon}}{r^2_{s/c-moon}} \approx 1\ \frac{m}{s^2}$$

at a distance of 2,600 km. This value is very high due to the very small distance JUICE-moon; the acceleration due to Jupiter is smaller due to the much higher distance, even if the mass of Jupiter is higher than the mass of the moons.

The perturbing forces that could play a role for JUICE are the following

- solar radiation pressure: the acceleration of JUICE due to the solar radiation pressure is

  $$a_{SRP} = C_R\frac{WS}{cm} \approx 10^{-8}\ \frac{m}{s^2}$$

  where standard values have been used for the different parameters, related to the distance from the Sun and to the spacecraft characteristics. The solar radiation pressure can thus be neglected.

- 3rd body attraction of the Sun: in this case the ratio of the perturbing acceleration due to the Sun with respect to the main acceleration due to Jupiter can be computed. This is expressed by the formula

  $$\frac{a_{Sun}}{a_J} = \frac{M_{Sun}}{M_J}\left(\frac{r_{s/c-J}}{r_{s/c-Sun}}\right)^2 \left[\left(\frac{1}{1-\frac{r_{s/c-J}}{r_{s/c-Sun}}}\right)^2 - 1\right] \approx 10^{-6}$$

Thus

$$a_{Sun} \approx 10^{-7}\ \frac{m}{s^2}$$

This is a quite small value but it can not be completely neglected.

- 3rd body attraction of Saturn: the gravitational attraction of Saturn, that varies upon the relative position JUICE-Saturn, has the following range of values

  $$a_S = G\frac{M_S}{r^2_{s/c-S}} \approx 10^{-7} - 10^{-8}\ \frac{m}{s^2}$$

  As for the perturbation due to the Sun it can't be completely neglected.

- irregular moons gravitational attraction: Jupiter has a lot of irregular satellites. These satellites, in minimal part, also influence a spacecraft through their gravitational attraction. However, due to their very small mass, the effect is practically negligible. The acceleration due to the most massive irregular moon, Himalia, is of the order of

  $$a_{irr} = G\frac{M_{irr}}{r^2_{s/c-irr}} \approx 10^{-9}\ \frac{m}{s^2}$$

  at a distance of $700,000$ km. This value of course varies a lot depending upon the relative distance spacecraft-irregular moon, but since no close approaches are planned it is in general quite low. Thus irregular moons are not included in the simulation.

- Jupiter spherical harmonics: the maximum radial acceleration due to the spherical harmonic coefficient J_2 is expressed as

  $$a_{J_2} = 3\mu J_2\frac{R^2}{r^4}\frac{1}{m} \approx 10^{-7}\ \frac{m}{s^2}$$

  Computed at a distance of 600,000 km from Jupiter; this value can thus vary considerably.
  The magnitude is similar to the perturbation due to the Sun and Saturn, hence it can not be neglected.

- Galilean moons spherical harmonics: the same type of the previous perturbation, but due to a Galilean moon (during a close approach), has the magnitude of (for the case of a 400 km altitude flyby of Ganymede)

  $$a_{J_2} = 3\mu J_2\frac{R^2}{r^4}\frac{1}{m} \approx 10^{-7}\ \frac{m}{s^2}$$

  The magnitude of the J_2 perturbation due to Jupiter and Ganymede is similar because the smaller distance to Ganymede compensates its much lower mass than Jupiter.
  An investigation of the higher order harmonics of Jupiter and the moons is not done; anyway their effect is always smaller than the one of J_2.

The conclusion is that all these forces are different orders of magnitude smaller than the main forces acting on the spacecraft; thus, for a preliminary analysis is sufficient to include only the gravitational attraction of Jupiter and the Galilean moons on the spacecraft. However for a more precise representation of the dynamics also the perturbations due to the Sun and Saturn and the spherical harmonics of Jupiter and the Galilean moons shall be included. Simulations will be performed with and without these perturbations. It is reminded that this conclusions are valid for the preliminary analysis performed here, but they may be different for the orbit design and for more advanced navigation analysis.
A further analysis may be required to understand which forces play a role in a periodic way and which forces accumulate their effect over a long period of time; this could be done with a propagation during the whole mission period. For example, the solar radiation pressure acts continuously, hence its effect could be important over a long time span; instead, the perturbation due to the mass distribution of Jupiter is periodic (depending upon the position of JUICE with respect to Jupiter) hence its effects are different.

3.3. ALGORITHMS: LEAST SQUARES AND COVARIANCE ANALYSIS

There are two main algorithms used in the Orbit Determination procedure: the batch filter (or Least Squares Algorithm, LSQ) or the sequential filter (or Kalman filter). The LSQ accumulates an high amount of measurements, corresponding to the data arc during which the orbit determination procedure is conducted, and then solves for the spacecraft state at fixed epochs and for a set of parameters. The sequential filter instead solves for the spacecraft state at only one epoch using a single set of measurements; after the solution for an epoch the procedure continues to the next epochs. A logical consequence of this is that the batch filter is usually more computationally heavy and hence more suited for the post-processing determination of the trajectory and physical parameters, to be usually executed by Earth's control centers; the sequential filter is faster and less computationally demanding, and hence more suited for autonomous onboard orbit determination.
The use of the Least Squares Filter is envisioned in the Thesis, since the orbit determination procedure for the flyby tour of the JUICE mission will be done on ground, during the intervals between subsequent flybys; this is due to the high computational power required to solve accurately for the ephemerides, gravity fields, and other physical parameters. In particular, as described in Section 5.1, in this Thesis a full LSQ is not used but only a set of equations part of this method (Covariance Analysis).
The use of the sequential filter, even though could be interesting (to perform an analysis of the autonomous navigation of a S/C during a flyby tour) is not envisioned in this project.

Least Squares Filter

The classical formulation for the Weighted Least Squares [13] is exposed here; since the extensive treatments with all the formal derivations can be found in plenty of references are here reported just the main concepts.
A dynamical system can be described by the equations

$$\dot{\mathbf{X}} = F(\mathbf{X}), \qquad \mathbf{X}(t_0) \equiv \mathbf{X}_0 \tag{3.10}$$

$$\mathbf{Y}_i = G(\mathbf{X}_i, t_i) + \boldsymbol{\epsilon}_i, \qquad i = 1, .., l \tag{3.11}$$

where $\mathbf{X}_k \in \mathscr{R}^n$ is the state vector at time t_k, $\mathbf{Y}_i \in \mathscr{R}^p$ is the observation vector (for the times $i = 1..l$) and $\boldsymbol{\epsilon}_i$ is the related observation error vector. The function F represent the differential equations for the state and the function G relates the state to the observations. It is noted here that the vector $\mathbf{X}$ contains the spacecraft state and the parameters to be solved for (with the correspondent differential equations being equal to zero). In general $p < n$ and $m = p * l \gg n$, indicating that the total number of observations must be higher than the total number of estimated variables; this is intuitive from a mathematical point of view: to solve a system of n variables at least n equations are needed, for a unique solution. In practice, much more are needed to compute a more reliable solution. Since the relation 3.10 is, for the OD problem, nonlinear, a linearization process is needed in order to use the LSQ algorithm. A Taylor expansion of the Eq. 3.10 is used, truncated at first order; the linearization entails two main modification to the system in 3.10: the computation of the partial derivatives of the nonlinear functions with respect to the variables and the substitution of the variables and observations with their differentials. The system 3.10 is thus rewritten as

$$\dot{\mathbf{x}}(t) = A(t)\mathbf{x}(t) \tag{3.12}$$

$$\mathbf{y}_i = \tilde{H}_i \mathbf{x}_i + \boldsymbol{\epsilon}_i, \qquad i = 1, .., l \tag{3.13}$$

where

$$A(t) = \left[\frac{\partial F(t)}{\partial \mathbf{X}(t)}\right]^* \qquad \tilde{H}_i = \left[\frac{\partial G}{\partial \mathbf{X}}\right]_i^* \tag{3.14}$$

The notation $[]^*$ indicates that the partial derivatives are evaluated at the reference solution, $\mathbf{X}^*(t)$; this is an important concept in the LSQ algorithm: since it is an iterative algorithms, an initial solution must be provided, and this is the *reference* solution.
The state and observation are replaced by their respective *deviation vectors* as follows

$$\mathbf{x}(t) = \mathbf{X}(t) - \mathbf{X}^*(t) \tag{3.15}$$

$$\mathbf{y}_i = \mathbf{Y}_i - G(\mathbf{X}_i^*, t_i) \tag{3.16}$$

An important concept is the State Transition Matrix: it is the matrix that relates the change in state at a certain epoch to the change in state at a previous epoch. It is expressed as

$$\Phi(t, t_k) = \frac{\partial \mathbf{x}(t)}{\partial \mathbf{x}(t_k)} \tag{3.17}$$

relating thus the state vector deviation at different epochs in this way

$$\mathbf{x}(t) = \Phi(t, t_k)\mathbf{x}_k \tag{3.18}$$

where $\mathbf{x}_k$ is the state deviation at time k. It has a number of interesting properties, that can be found in [13], together with the description of the solution method for it (more clearly explained in [32] and in Section 3.4).
The importance of the State Transition Matrix lies in the fact that it allows to relate the observations to the state of a single epoch, solving for the state vector at a single epoch rather than at all the epochs. Considering equations 3.12 and 3.17, the relation between observations at different epochs and the state vector at one epoch is expressed as

$$\mathbf{y} = H\mathbf{x} + \boldsymbol{\epsilon} \tag{3.19}$$

where

$$\mathbf{y} = \begin{bmatrix} y_1 \\ \vdots \\ y_l \end{bmatrix}; \qquad H = \begin{bmatrix} \tilde{H}_1\Phi(t_1, t_k) \\ \vdots \\ \tilde{H}_l\Phi(t_l, t_k) \end{bmatrix}; \qquad \boldsymbol{\epsilon} = \begin{bmatrix} \epsilon_1 \\ \vdots \\ \epsilon_l \end{bmatrix};$$

where $\mathbf{y} \in \mathscr{R}^m$, with $m = p * l$ the total number of observations and $\mathbf{x} \in \mathscr{R}^n$ is the state vector to be determined at epoch t_k.
The Weighted Least Squares Filter (WLSQ) computes the best estimate of the solution minimizing the performance index

$$J(\mathbf{x}) = \frac{1}{2}\boldsymbol{\epsilon}^T W \boldsymbol{\epsilon} \tag{3.20}$$

corresponding to the sum of the squares of the observed residuals, ϵ_i, taking into account the different weights of the observations. The difference with the classical LSQ algorithm is that in the WLSQ the weights are taken into account.
The matrix W is the weighting matrix, and for uncorrelated observations errors is a diagonal matrix with the weight of each observation on the diagonal; this weight represents the inverse of the square of the precision of an observation.
The process of minimization of the performance index yields the result for the best estimate for $\mathbf{x}$:

$$\hat{\mathbf{x}}_k = \left(H^T W H + \bar{P}_k^{-1}\right)^{-1} \left(H^T W \mathbf{y} + \bar{W}_k \hat{\mathbf{x}}_k\right) \tag{3.21}$$

where the newly introduced terms $\hat{\mathbf{x}}_k$ and $\bar{P}_k^{-1}$ represent the *a priori* estimate of the state and its associated weighting matrix (also defined inverse of the a priori covariance matrix). They can come from external information, or from the estimation of the state at a previous time step and its propagation to the actual estimated epoch.
Together with the state, a very important matrix can be computed, which is the *covariance matrix* for the state; this is defined as

$$P_k = \left(H^T W H + \bar{P}_k^{-1}\right)^{-1} \tag{3.22}$$

and represents the statistical uncertainty in the determination of the state vector; in general, the higher the magnitude of its elements, the higher the uncertainty on the estimated state. The a priori weighting matrix of the state represent thus the inverse of the a priori covariance of the state.
It is noted here that the covariance matrix can be mapped at different epochs using the State Transition Matrix (equation 3.17) in the following way

$$P_j = \Phi(t_j, t_k) P_k \Phi^T(t_j, t_k) \tag{3.23}$$

This property will be useful for guidance purposes (see Subsection 4.2.1).
The solution procedure is to iterate equation 3.21, updating at each step the estimated state vector and covariance matrix, using them to compute the partial derivatives. In this way convergence should be obtained in a limited number of iterations.
This is the basic explanation for the WLSQ, but it is noticed that a lot of other things have to be taken in consideration; for example the computation of the partial derivatives in equation 3.14, which is not as straightforward as appears, especially for the dynamical parameters.

Difference LSQ-Covariance Analysis
To evaluate the performance of an estimation strategy, in particular to determine the effect of misrepresented parameters on an orbit determination solution, two ways are possible [33]. The first, more complete but also more computationally demanding, is to perform a complete simulation of the orbit determinations procedure using the LSQ. Using a nominal trajectory, including the differences between true and modeled dynamics and simulating the observations and their uncertainties, it is possible to reconstruct completely the best estimate of this trajectory in presence of model and observations uncertainties; a complete picture of the influence of different parameters on the quality of the reconstructed trajectory is possible.
The second way, which is less computationally expensive, is the *covariance analysis*, where the full simulation is not executed, but only the covariance matrix is computed; it is noted that for computing the covariance matrix (equation 3.22) only the weighting matrix and the partial derivatives of the observations with respect to the state are needed. The second matrix in particular, can depend on the state itself (upon the type of relationships between observables and state) but does not depend upon the observables themselves. In this case the state estimation is not performed, thus it is not possible to obtain the best estimation for the trajectory; the main information obtained is the uncertainty associated to it. With this method is possible to analyze the effect of parameters uncertainties in the estimated state uncertainty.

In conclusion, performing a covariance analysis consists in evaluating the matrix 3.22 (and 3.23) for a wide range of parameters that influence the orbit determination procedure, without computing the estimate of the state vector.
What is obtained are the so called *formal errors* or standard deviations, which are the square root of the diagonal of the covariance matrix. This is an useful indication about the magnitude of the uncertainties of the estimated parameters; when dealing with the formal errors however, one has to keep in mind that they can give too optimistic results, not completely realistic. In particular, in [21] it is reported that the true error could be around 2-3 times the standard deviations, for planetary ephemerides.
With the covariance analysis is not possible to obtain the *true error*, which is the difference between the estimated state and the a priori state ($\mathbf{x^{est}} - \mathbf{x^{apr}}$), since the estimation of the state is not included. The true error is usually bigger than the formal error [21]; this is indeed a limitation of the covariance analysis.
The selection of the method that will be used is exposed in Section 5.1.

3.4. Variational Equations

The Variational Equations (VE) are systems of differential equations which are important for the orbit determination procedure, especially when is needed to solve for model parameters. As exposed in Section 3.3, to solve for a state vector $\mathbf{x}$, partial derivatives of the measurements with respect to $\mathbf{x}$ are needed. A problem can arise for model parameters, if they are not explicitly appearing in the formulas for the computed observables; thus their partial derivatives can not be obtained from the equations for the computed observables, but they have to be computed in another way.
The VE are essentially a set of differential equations which have to be integrated to obtain the partial derivatives of the state with respect to the parameters; using then the chain rule and the partials of the measurements with respect to the state, it is possible to obtain the partials of the measurements with respect to the parameters. The term VE is used to indicate also differential equations for the State Transition Matrix; in this case they are used to compute the STM at an arbitrary time epoch. In this way it is possible to relate the observations at a certain time to the state at a different time, solving for only one state vector rather than for multiple state vectors. It is noticed that the VE are always integrated numerically, since in general no analytic solutions exist, given the complexity of the problem.
The numerical integration is performed with a *Runge-Kutta-Fehlberg 78* method; this is an algorithm for the integration of ordinary differential equations with a variable stepsize and error control. The initial time step-

size can be chosen; the integration error is usually increasing with the stepsize.
In the next paragraph is exposed the formulation of the VE for the STM, from [30], [32] and [34]. The formulation for the parameters is very similar.

VE for the STM
Considering the system of differential equations in the form

$$\frac{d}{dt}\mathbf{y}(t) = \mathbf{f}(t, \mathbf{y}) \tag{3.24}$$

and the STM

$$\Phi(t, t_0) = \frac{\partial \mathbf{y}(t)}{\partial \mathbf{y}(t_0)} \tag{3.25}$$

it is possible to differentiate equation 3.24 with respect to $\mathbf{y}(t_0)$

$$\frac{\partial}{\partial \mathbf{y}(t_0)} \frac{d}{dt}\mathbf{y}(t) = \frac{\partial \mathbf{f}(t, \mathbf{y})}{\partial \mathbf{y}(t_0)} = \frac{\partial \mathbf{f}(t, \mathbf{y})}{\partial \mathbf{y}(t)} \frac{\partial \mathbf{y}(t)}{\partial \mathbf{y}(t_0)} \tag{3.26}$$

Changing the order of derivatives (time with state) equation 3.26 is written as

$$\frac{d}{dt}\Phi(t, t_0) = \frac{\partial \mathbf{f}(t, \mathbf{y})}{\partial \mathbf{y}(t)}\Phi(t, t_0) \tag{3.27}$$

with initial condition $\Phi(t_0, t_0) = I$. The system of differential equations 3.27 can be solved numerically to obtain the STM at an arbitrary epoch.

In this way it is possible to solve for the initial state only rather than for the states corresponding to all the observation times, using the following relationship to modify the observation matrix (H)

$$H_{i,0} = \frac{\partial \mathbf{z}(t_i)}{\partial \mathbf{y}(t_0)} = \frac{\partial \mathbf{z}(t_i)}{\partial \mathbf{y}(t_i)}\Phi(t_i, t_0) = \frac{\partial \mathbf{z}(t_i)}{\partial \mathbf{y}(t_i)} \frac{\partial \mathbf{y}(t_i)}{\partial \mathbf{y}(t_0)} \tag{3.28}$$

It is noted that the VE have to be integrated together with the equations of motion; this is necessary because for the evaluation of the partial derivatives $\frac{\partial \mathbf{f}(t,\mathbf{y})}{\partial \mathbf{y}(t)}$ the actual state (position and velocity of satellite) is needed, but this is of course not known in general if not from a numerical integration of the equations of motion.

The effect of the Laplace resonance (see Subsection 2.1.2) is seen directly on the terms of the STM. The derivatives $\frac{\partial \mathbf{y}^i(t)}{\partial \mathbf{y}^k(t_0)}$ are very close to zero when k is Callisto and i any other moon (and also the reciprocal). Instead they have a well defined behavior when k and i are Io, Europa or Ganymede.

3.5. Ephemerides of the Jovian System

In this Section the process of generation of the ephemerides for the Jovian System is explained, together with the state of the art ephemerides of this system.

Generation of ephemerides
The generation of the ephmerides of planets and planetary satellites is based of course on the observations of direct or indirect quantities related to these celestial bodies [35].
The observational data and the dynamical models are the basis for the generation of the ephemerides.
The process of generation and update of the ephemerides can be understood with the help of Sections 3.3 and 3.4; the procedure is the following: a Least Square Filter is used to fit a model to a certain set of observations, that can span longer periods (decades or century) for long-term stable ephemeris generation [36] or short periods (weeks or months) for ephemeris update. The problem of the validity and stability of the ephemeris generated with a small set of observations is of importance, especially for flyby tours (such as JUICE), since attention has to be paid to obtain a long-term representation which is not degraded. This is addressed in particular in [36], where the fundamental aspect of how to treat the observations is discussed; the two main points are:

- observations made with more modern technologies are more accurate and thus must have higher weights than observations obtained with less accurate technologies (such as cameras of the middle of the 20th century); moreover, in situ observations (with radio technology) are usually much more accurate than remote observations (with optical technology).
- observations than span a short period of time must be de-weighted since they could yield to a solution that has a limited interval of validity: this solution represents quite well the behavior during that period of time but diverges substantially when propagates outside this interval (respect to a stable long-term solutions obtained with decades of observations). Hence, when adding short time span observations with other data to compute ephemerides updates, these observations shall be de-weighted to avoid the solution to be tailored to that particular time interval.

In the LSQ, the ephemeris of a celestial body are represented by the initial conditions of a certain set of variables, that represent the state of this celestial body; this set can be the classical cartesian coordinates set, Keplerian elements, or modified elements. The solution for the state is only at one instant in time; thus it is important the use of the state transition matrix in order to relate the observations at an arbitrary epoch to the state at the initial epoch.
The solution of the LSQ problem yields the initial state of the celestial bodies.
The data types that have the biggest influence on the ephemerides generation are range, VLBI and optical data; this because range and VLBI give the position of the spacecraft which is directly influenced by the position of a celestial body. Optical data given direct information on the position of a celestial body with respect to the camera, hence they are of high importance. Doppler data instead are very important for spacecraft tracking but less important for ephemerides generation, because Doppler data are stronger for short period effects, while range and VLBI are more important for long period effects. The ephemerides represent the position of celestial bodies over a a long period of time.

State of the Art
Before the era of spacecraft flying close to celestial bodies, the only observations available were photographic information from Earth; these are called *astrometric* observations and are obtained with telescopes. With the advent of radiometric tracking of spacecrafts a great amount of data that contribute enormously in the refinement of the Solar System ephemerides is available.
The history of the generation of the ephemerides of the bodies of the Solar System, and in particular of the Jovian system, is very long and detailed, and can be found in different references as [37] and [38]; here only a brief survey is given. They are not very accurate due to the limitations given by the semi-analytical theory.
The first modern Galilean System ephemerides were computed by Lieske [39]; in 1976 he developed a semi-analytic theory ([37]) to compute such ephemerides. His work was also based on the previous work of Sampson in 1921, where trigonometric series were developed to represent the motion of these satellites. Using Lieske's work different updates have been done, the last one being the generation of the E5 ephemerides [40] in 1998, which is based on observations up to 1995. These ephemerides use mostly astrometric observations and radiometric data from the Voyager flyby.
The most recent ephemerides of the Galilean System, that include also the radiometric tracking data of Galileo, have been developed in 2001 by Jacobson [30], in 2004 by Lainey (ephemeris of the Observatorie de Paris, [30]) and in 2010 by the JPL (called *DE* ephemeris series, [34],[41]). Also the Institute of Applied Astronomy of the Russian Academy of Sciences has developed ephemerides for the Galilean satellites (called *EPM*, [38]).
After the semi-analytical procedure of Lieske, numerical procedures have been developed to provide higher accuracy; the formalism developed by Lainey ([30]) entails a numerical integration procedure rather than a semi-analytic formulation.
Before the mission Galileo the accuracy of the Galilean moons ephemerides was of about 100-150 km [36]. After it, this accuracy improved to about 50 km, being different in radial, cross-track, along-track directions ([11]); usually the out of plane and along track components are less well determined respect to the radial component. For the Earth-centered position of Jupiter instead, the accuracy is of about 15 km in each direction.
It is expected that with flyby data the accuracy of these ephemerides will be improved noticeably at least for the time span of the mission [36]. However, the validity interval of these ephemeris would be limited in time (it is however not completely clear the length of this validity interval).

4

GUIDANCE FOR PLANETARY MOONS FLYBY TOURS

In this Chapter the guidance of a spacecraft performing a flyby tour of satellites will be addressed. The term *guidance* is used to indicate the process of determination of the actions to take in order to bring back the spacecraft to its nominal trajectory, when it is deviating from it; it is thus the process of "driving" the spacecraft along the desired path, counteracting the effects that cause these deviations.
In the classical GNC (Guidance-Navigation and Control) loop used in spacecraft trajectory control, the guidance block is placed in between the Navigation and the Control blocks; the Navigation (as shown in the previous Chapter) provides the knowledge of the current position. The Guidance uses this information to determine the corrective actions, which are sent to the Control system that realizes them. In this context, the Control system would consist in the implementation of the ΔV computed by the Guidance.
The algorithms used to compute the ΔV and the classical maneuvering scheme are presented, together with the most recent developments for satellite tours (using classical, high-thrust propulsion systems); it is noted how relatively little experience is available since just a few satellites flyby tours have been realized until now (specifically only Galileo and Cassini, NASA-led missions which visited the Jovian and Saturnian systems respectively; indicative is the fact that most of the sources found on this topic are from JPL, also for future missions, as [42], [43]).
The structure of the Chapter is the following: in the fist Section (4.1) the description of the geometry of a flyby is provided. The geometry and computation of the B-plane, an important reference plane used during flybys, is shown in Section 4.2. In the third Section (4.3) the algorithms and schemes used for the Trajectory Correction Maneuvers (TCM) are presented.

4.1. FLYBY GEOMETRY

In this Section the orbital mechanics phenomenon known as *flyby* or *close approach* is described. In the first paragraph the concept of Sphere of Influence is illustrated while in the second the effects of a flyby are described.

Sphere of Influence

The sphere of influence (SOI) of a celestial body, P_1, with respect to a celestial body, P_2, is the geometrical locus where the gravitational acceleration due to P_1 is stronger than the gravitational acceleration due to P_2, thus the motion of another body P_3 (the spacecraft) should be described with respect to P_1, considering the effect of P_2 as a perturbation.

In [44] the derivation of the geometrical shape of the SOI is exposed; comparing the gravitational accelerations of P_1 and P_2, with series expansions and analytic approximations is possible to arrive to the simplified form

$$R_{SOI} \approx \left(\frac{m_1}{m_2}\right)^{2/5} \rho \tag{4.1}$$

where ρ is the distance between P_1 and P_2 and m is the mass. Inside the SOI the motion of P_3 must be described with respect to P_1, considering P_2 as a perturbation; outside the SOI the contrary is valid. This is very important for interplanetary trajectories and flyby tours, because it allows the determination of the current main center of attraction.
In Table 4.1 is shown the radius of the sphere of influence for the Galilean moons with respect to Jupiter; it is noted how the radius of the sphere of influence is small when compared to the semi-major axis of their orbit but big when compared to their radius. Moreover, their spheres of influence lie inside the sphere of influence of Jupiter with respect to the Sun.

Table 4.1: Galilean moons SOI with respect to Jupiter

Satellite	$R_{SOI}(km)$	$R_{SOI}(a_{sat})$	$R_{SOI}(R_{sat})$
Io	7,834	0.0185	4.28
Europa	9,722	0.0145	6.22
Ganymede	32,806	0.03	12.5
Callisto	37,712	0.02	15.7

Effects of a flyby
Considering the Jovian system and the Galilean satellites here, it is briefly described what happens to a spacecraft performing a flyby tour.
The spacecraft is moving around Jupiter in a close orbit; its coordinates are described with respect to Jupiter. When the spacecraft enters the SOI of a moon, a change of coordinates for the position and the velocity can be done to compute the orbit with respect to the moon. This results in an hyperbolic orbit around the moon (if no maneuvers are executed nor atmospheric effects are taken into account); the spacecraft will enter the SOI with a certain velocity and will leave it with another velocity with respect to the moon. Neglecting dissipative effects, the magnitude of these two velocities will be the same (the *hyperbolic excess velocity*, V_∞); however, due to an effect of velocity combination, the velocity with respect to Jupiter will change. The position with respect to Jupiter instead is considered constant (at first approximation) since the flyby is quite rapid relative to an orbital period around Jupiter. The result is that the orbit around Jupiter will be different before and after the flyby. The magnitude of this effect depends upon where the spacecraft enters the SOI; selecting this position is possible to obtain a predetermined effect, such an increase or decrease of orbital energy (thus semi-major axis) or an inclination change.

The purpose of a flyby is thus twofold: firstly, it is needed in order to perform scientific observations of the moons from a close distance; secondly, it is needed to shape the trajectory of the spacecraft using a natural available resource: the orbital angular momentum of a celestial body. In this way is possible to save propellant and thus increase the dry mass of the spacecraft.
Missions to planets that have natural satellites can perform a *multiple-satellite-aided-capture*: the spacecraft performs a series of flyby before being injected into an orbit around the planet [11]; the advantage is that the energy required for the injection will be smaller, however a precise timing and a good navigation system are needed for a precise execution of such series of flybys. It is here shown briefly the effect of velocity change (from [44]), with the help of Figure 4.1. It is not an extensive treatment since the scope of the Thesis is not the design of such gravity assist maneuvers.
The entry velocity is $\mathbf{V}_{\infty t}$ and the exit velocity is $\mathbf{V}^*_{\infty t}$ (with respect to the moon). The state vector of a spacecraft when entering the SOI is specified by four scalar parameters: R_{SOI}, $V_{\infty t}$, δ, ϕ_2. All these values are known for a specified trajectory around Jupiter and hence a flyby can be completely characterized.
The velocity is bent by an angle α, that is computed with the formula

$$\sin\frac{\alpha}{2} = \frac{1}{\sqrt{1+\frac{B^2 V_{\infty t}^4}{\mu^2}}} \tag{4.2}$$

where B is the vector from the celestial body to the hyperbola asymptote. This angle is shown in Figure 4.2.
The total difference in velocity is $\Delta\mathbf{V} = \mathbf{V}_f - \mathbf{V}_i = \mathbf{V}^*_{\infty t} - \mathbf{V}_{\infty t}$ and its modulus is

$$\Delta V = 2V_{\infty t}\sin\frac{\alpha}{2} \tag{4.3}$$

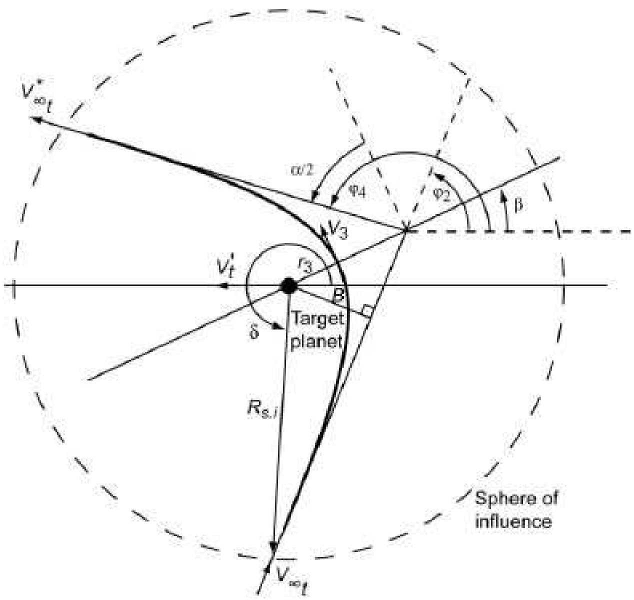

Figure 4.1: Flyby geometry [44]

This can be seen as an impulsive ΔV, as for a maneuver from an engine, with the difference that is obtained for "free", without the use of any propellant.
The energy variation of the spacecraft is

$$\Delta\varepsilon = V_t' \Delta V \cos\beta \tag{4.4}$$

where V_t' is the projection of the planet velocity on the flyby plane. From the orbital energy change the change in semi-major axis of the Jupiter-centered orbit can be computed.

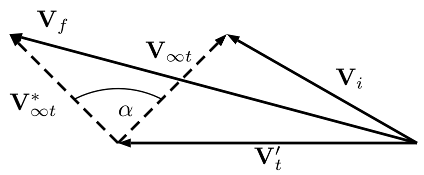

Figure 4.2: Scheme of the velocity change

From equation 4.2 is possible to see that the bending angle increases for a closer flyby, lower V_∞ and higher celestial body mass. It is noted that for a moon, since its mass is usually quite small, the effect of a flyby is not as important as in the case of a planetary gravity assist; the limit of equation 4.2 for decreasing mass is zero, meaning that in such case there is no gravity assist effect from a planetary satellite. Also the change of velocity, from equation 4.3, would be zero in such case.

4.2. B-Plane Geometry

The B-Plane is the plane that describes the geometry of a flyby in three dimensional space; it passes through the flyby target center and it is perpendicular to the hyperbola asymptote. Its importance lies in the fact that is used for flyby targeting (as will be shown in Section 4.3). In Figure 4.3 is shown a representation of the B-Plane. The unit vectors describing the B-Plane are $\hat{\mathbf{S}}, \hat{\mathbf{R}}, \hat{\mathbf{T}}$; they all pass through the celestial body center. The vector $\hat{\mathbf{S}}$ is parallel to the incoming asymptote of the hyperbolic trajectory (and thus also to $\mathbf{V}_{\infty t}$). The vector $\hat{\mathbf{T}}$ can be chosen in two ways: it can be or the cross product between the vector $\hat{\mathbf{S}}$ and the moon's orbit normal $\hat{\mathbf{N}}$; the second option is to compute it with a cross product between $\hat{\mathbf{S}}$ and a vector normal to the ecliptic plane ([11] and [45]). It is noted that in all these cases the vector $\hat{\mathbf{T}}$ will be perpendicular to $\hat{\mathbf{S}}$ and its direction varies little

depending upon the reference chosen, since in the Solar System almost all the planets and moons orbits have a very small inclination. The last unit vector, $\hat{\mathbf{R}}$ is obtained as cross product between $\hat{\mathbf{S}}$ and $\hat{\mathbf{T}}$.
The B-Plane is then defined as the plane formed by the vectors $\hat{\mathbf{T}}$ and $\hat{\mathbf{R}}$ (passing through the celestial body center); it is thus perpendicular to the incoming asymptote of the hyperbola, which pierces the B-Plane in the point defined by the vector **B**. This is the *aiming point*, which is used for the targeting of a flyby. It is not the point of closest approach, since that is the periapsis of the hyperbola (they are different due to the mass of the celestial body; for a non-massive body they are coincident and also the asymptote with the hyperbola which would not be curved).

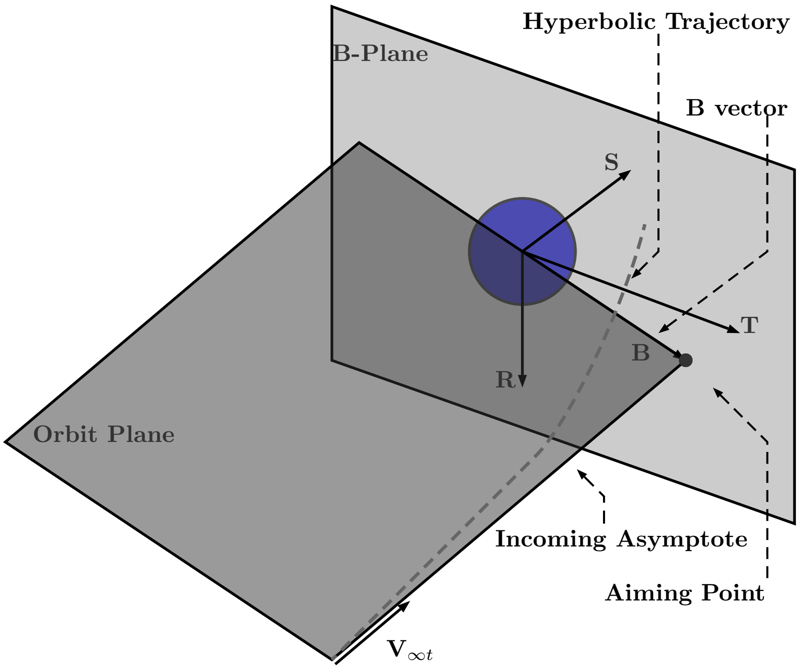

Figure 4.3: B-Plane geometry

The vector **B** is often represented in such coordinate frame

$$\mathbf{B} = B_T\hat{\mathbf{T}} + B_R\hat{\mathbf{R}} \tag{4.5}$$

It is derived using the current position and velocity as follows [46]. The first step is to compute the normal vector to the orbital plane and the eccentricity vector using the spacecraft position and velocity with respect to the moon (**r** and **v**)

$$\mathbf{n} = \frac{\mathbf{r}\times\mathbf{v}}{\|\mathbf{r}\times\mathbf{v}\|} \tag{4.6}$$

$$\mathbf{e} = \frac{1}{\mu}\left[\left(v^2 - \frac{\mu}{r}\right)\mathbf{r} - (\mathbf{r}\cdot\mathbf{v})\mathbf{v}\right] \tag{4.7}$$

The hyperbolic asymptote angle β (Figure 4.1) is then given by

$$\beta = \cos^{-1}(1/e) \tag{4.8}$$

The unit vector $\hat{\mathbf{S}}$ is then

$$\hat{\mathbf{S}} = \cos\beta\frac{\mathbf{e}}{e} + \sin\beta\frac{\mathbf{n}\times\mathbf{e}}{\|\mathbf{n}\times\mathbf{e}\|} \tag{4.9}$$

Defining so the vector $\hat{\mathbf{N}}$ as the normal to ecliptic or to the moon orbital plane, the other two unit vectors are found

$$\hat{\mathbf{T}} = \frac{\hat{\mathbf{S}} \times \hat{\mathbf{N}}}{\| \hat{\mathbf{S}} \times \hat{\mathbf{N}} \|} \tag{4.10}$$

$$\hat{\mathbf{R}} = \hat{\mathbf{S}} \times \hat{\mathbf{T}} \tag{4.11}$$

The semi-major axis and the magnitude of the B vector are found as

$$a = -\frac{\mu}{2E} = -\frac{\mu}{2\left(\frac{v^2}{2} - \frac{\mu}{r}\right)} \tag{4.12}$$

$$b = -a\sqrt{e^2 - 1} \tag{4.13}$$

The B vector is thus

$$\mathbf{B} = b\left(\hat{\mathbf{S}} \times \mathbf{n}\right) \tag{4.14}$$

Its components are

$$B_T = \mathbf{B} \cdot \hat{\mathbf{T}} \tag{4.15}$$

$$B_R = \mathbf{B} \cdot \hat{\mathbf{R}} \tag{4.16}$$

It is noted how these coordinates are not fixed in the inertial space, but depend on the actual trajectory flown by the spacecraft.
Another important parameter is the time of closest approach (T_{TCA}); this is the time needed by the spacecraft to arrive to the closest point to the celestial body (periapsis) from its current position. It is given by the following formula

$$T_{TCA} = \frac{H - e \sinh H}{\sqrt{-\mu / a^3}} \tag{4.17}$$

where H is the hyperbolic anomaly, a quantity related to the position of the spacecraft along the orbit; the current position is represented by H and the periapsis condition by $H = 0$.
A similar parameter is the linearized time of flight (L_{TOF}), which is the time until the aiming point if the spacecraft would fly in a rectilinear path along the asymptote with a speed $V_{\infty t}$.
In reference [45] a similar but different derivation of the B-Plane and B vector variables is reported. The three variables B_R, B_T, T_{TCA} are used for the targeting of flybys.

4.2.1. Mapping of the covariance matrix in the B-Plane

The covariance analysis (presented in Section 3.3) computes the uncertainties in the spacecraft and moons positions at a certain time in the reference frame that is used for the integration of the equations of motion. This is a cartesian, quasi-inertial frame centered at Jupiter. These uncertainties can be mapped into the B-Plane of the flyby moon, using different concepts of statistics. This mapping has the purpose of transforming the uncertainties of the orbit determination procedure, which are obtained in the frame in which the spacecraft position is recovered (thus Jovicentric inertial), into uncertainties in the B-Plane parameters. This has the practical usefulness of giving a very intuitive comprehension of the error of a trajectory (as miss distance from the aiming point and error in terms of time).
Considering the portion of the covariance matrix of the state of the spacecraft, P_x, this contains the information on the uncertainty of the position of the spacecraft at a certain epoch. In cartesian coordinates this is a 3×3 matrix

$$P_x = \begin{bmatrix} \sigma_x^2 & \rho_{xy} & \rho_{xz} \\ \rho_{yx} & \sigma_y^2 & \rho_{yz} \\ \rho_{zx} & \rho_{zy} & \sigma_z^2 \end{bmatrix} \tag{4.18}$$

It is noticed that the mapping is done only for the position and not for the velocity, since the information about the velocity has smaller interest (and has never been found in literature).
The first step is to map this matrix in time, to the time of passage through the B-Plane [45].

Mapping in time

This is done with the classical approach of the State Transition Matrix, (presented in Section 3.4). This is a matrix that relates the variations in state at a certain time epoch to another time epoch. THe formula fort the temporal propagation of the covariance matrix is (represented in Eq. 3.23, reported here for clarity)

$$P_j = \Phi(t_j, t_k) P_k \Phi^T(t_j, t_k)$$

where t_k represents the time of computation of the uncertainties and t_j the time of B-Plane piercing (or of closest approach, being the difference very small). This operation however implies a linearization, thus is more accurate when the time difference between the reference time and mapped time is smaller. This error depends also upon the type of dynamics; it can be considered small for the moons but not very small for JUICE, since its dynamics is more nonlinear. This will be shown in Sections 7.1 and 7.3.

Mapping in space

The mapping in space is the procedure that transforms the uncertainties in a reference frame into another reference frame. It is more complex than the mapping in time since it involves a reference frame transformation and an eigenvector problem.

The final result of this mapping is shown in Figure 4.4; this is the dispersion ellipse of the spacecraft position around the estimated aiming point, in the B-Plane. It is noted that, due to the orbit determination procedure, the estimated aiming point is in general different from the nominal aiming point.

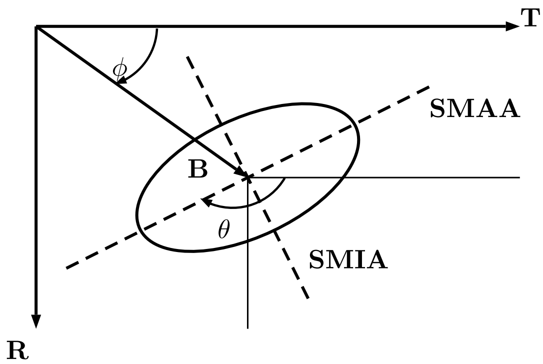

Figure 4.4: Probability (uncertainty) ellipse in the B-Plane

This ellipse represent the area where the probability of finding the spacecraft inside it is equal to a certain level. It is an ellipse and not an ellipsoid because the out of plane component is usually transformed in time error.

The mapping in space proceeds as follows; the first step is to map the covariance from the original reference frame (is assumed here to be the moon-Centered-Inertial, MCI) to the SRT reference frame (the reference frame build from the unit vectors $\hat{\mathbf{S}}, \hat{\mathbf{R}}, \hat{\mathbf{T}}$, [13])

$$\begin{aligned} P_{SRT} &= E\left[(\hat{\mathbf{x}} - \mathbf{x})(\hat{\mathbf{x}} - \mathbf{x})^T\right]_{SRT} \\ &= \psi P_{MCI} \psi^T \\ &= \psi E\left[(\hat{\mathbf{x}} - \mathbf{x})(\hat{\mathbf{x}} - \mathbf{x})^T\right]_{MCI} \psi^T \end{aligned} \tag{4.19}$$

where the matrix ψ is obtained from the MCI and SRT reference frames in this way

$$\psi = \begin{bmatrix} \hat{\mathbf{S}} \cdot \hat{\mathbf{I}} & \hat{\mathbf{S}} \cdot \hat{\mathbf{J}} & \hat{\mathbf{S}} \cdot \hat{\mathbf{K}} \\ \hat{\mathbf{R}} \cdot \hat{\mathbf{I}} & \hat{\mathbf{R}} \cdot \hat{\mathbf{J}} & \hat{\mathbf{R}} \cdot \hat{\mathbf{K}} \\ \hat{\mathbf{T}} \cdot \hat{\mathbf{I}} & \hat{\mathbf{T}} \cdot \hat{\mathbf{J}} & \hat{\mathbf{T}} \cdot \hat{\mathbf{K}} \end{bmatrix} \tag{4.20}$$

The second step is to find the dispersion ellipsoid from the covariance matrix in the SRT frame. To do this an eigenvector problem is solved [13]. The eigenvalues ($\lambda_i, i = 1,2,3$) of the matrix P_{SRT} have to be found; with them, the matrix U of normalized eigenvectors ($\mathbf{v}$) can be computed

$$U = \begin{bmatrix} \mathbf{v}_1 & \mathbf{v}_2 & \mathbf{v}_3 \end{bmatrix} \tag{4.21}$$

This matrix has the eigenvectors in its columns, ordered from the biggest to the smallest; it is used to find the direction of the principal axis (Eq. 4.23). The equation for the probability ellipsoid is

$$\frac{x'}{\lambda_1} + \frac{y'}{\lambda_2} + \frac{z'}{\lambda_3} = l^2 \tag{4.22}$$

where l correspond to different levels of confidence. The levels of confidence are $1\sigma, 2\sigma, 3\sigma$ and they represent probabilities of $20\%, 73.9\%, 97.1\%$ respectively of the state estimate to fall inside this ellipsoid, for a trivariate normal distribution (different percentages are indicated in [45], where a bivariate Gaussian density function is used instead of a trivariate). The axis of the ellipsoid are simply the square roots of the eigenvalues multiplied by the value of l, ordered from the higher value to the smaller ($Axis_i = \sqrt{\lambda_i} l$). The direction of the *principal axis*, which are the axis of the ellipsoids, is given by

$$\begin{bmatrix} x' \\ y' \\ z' \end{bmatrix} = U^T \begin{bmatrix} x \\ y \\ z \end{bmatrix} \tag{4.23}$$

where the vector $\begin{bmatrix} x & y & z \end{bmatrix}^T$ represent the axes SRT.
In this case however, since a three dimensional problem is considered, there is no guarantee that two of the principal axes will be in the RT plane; thus, the orientation angles (Euler angles) of the principal axes with respect to the original axis can be found from the eigenvector matrix U. The procedure is very simple and can be found is [13].
An alternative procedure ([45]) consists in considering, instead of a 3×3 matrix, only the submatrix (2×2) corresponding to the axis $\hat{\mathbf{R}}$ and $\hat{\mathbf{T}}$. The principal axis corresponding to the RT submatrix will necessarily lie in the RT plane (thus the B-Plane). In this way is possible to obtain the ellipse of Figure 4.4 (only the rotation angle θ has to be found). The angle theta is computed from the matrix of the eigenvectors U (ordered along the direction of decrease of the eigenvalues) as

$$\theta = \arctan\left(\frac{U_{1,0}}{U_{0,0}}\right) \tag{4.24}$$

What is usually done for the last component ($\hat{\mathbf{S}}$) is to transform its error in time of flight error; this can be computed with the linear approximation [47]

$$\sigma_{LTOF} = \frac{\sigma_S}{V_{\infty t}} \tag{4.25}$$

This is the error in the linearized time of flight, since it is computed as if the spacecraft would fly on a rectilinear path from the SOI to the aiming point.

4.3. Trajectory Correction Maneuvers (TCM)

This Section describes the models and algorithms used to design the Trajectory Correction Maneuvers (TCM); the underlying assumption is that the engine is of high-thrust type (which is the case for JUICE) since it will drive the logic of the maneuvers selection. In the first Subsection (4.3.1) the typical maneuvers scheme for a flyby tour mission is presented.
The following Subsections present the targeting algorithms implemented in this Thesis; they are needed to correct the deviations of the perturbed trajectory with respect to the nominal one. These algorithms essentially compute the $\Delta\mathbf{V}$ required to perform the maneuver. They correspond to the Guidance system for the trajectory of JUICE. The two main inputs required are the nominal trajectory and the uncertainties from the CA (Section 3.3).
Three targeting algorithms are implemented in this Thesis; they have different performances in terms of accuracy and computational complexity. Subsection (4.3.2) presents the B-Plane targeting algorithm; the following Subsection (4.3.3) presents the optimized targeting algorithm. The last type of targeting used, the approximated targeting, is presented in Subsection 4.3.4. The Section is concluded with the explanation of the model used to represent the maneuvers execution errors (4.3.5).

4.3.1. Typical Maneuvers Scheme for Flyby Tours

The classical scheme used for navigating a spacecraft in this type of missions comes essentially from the experience of the past missions *Galileo* and *Cassini-Huygens* ([48], [49], [50]). In the difference references found (mostly from NASA's JPL, as [51],[52],[53],[7]), it is envisioned to use as a baseline for the maneuvers between subsequent flybys always the same logic. Of course, depending upon the single event, variations had been done for different reasons, such as lack of time to determine the maneuver, malfunctioning of any subsystem, or simply because the spacecraft was in the correct path and hence the maneuver was not necessary.
This guideline is thus not a demonstrated rule to be always followed, but rather a good practice that comes from (relatively little) experience; it is envisioned to be used also in the NASA's Europa Clipper Mission ([42] and [43]).
It is driven by navigational and operational needs; the first are the requirements to deliver the spacecraft to the desired position and the seconds are the requirements of the ground station and spacecraft systems on the time and information needed to determine the actions to be taken.
The maneuver logic is shown in Figure 4.5.

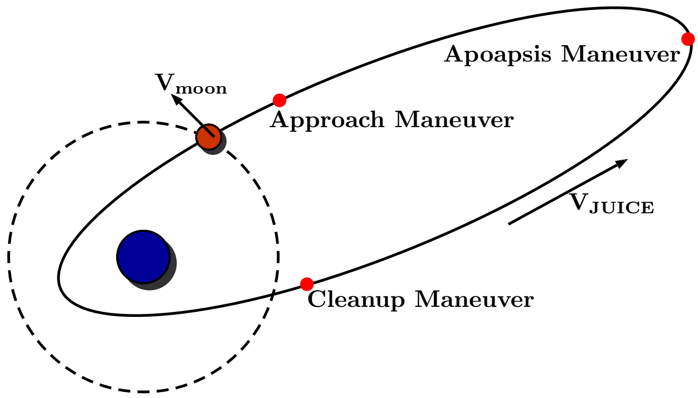

Figure 4.5: Classic TCMs strategy for a flyby tour

It is comprised by three maneuvers, ordered from the encounter i to the encounter $i+1$:

- **Cleanup (Post-flyby) Maneuver**: it is usually done about three days after the encounter i. Its purpose is to remove the navigation errors of the flyby i, due to imperfect knowledge of the ephemeris and spacecraft state.
- **Apoapsis Maneuver**: it is usually done around apoapsis and is a shaping maneuver; this means that it is planned in order to meet the science criteria of the next flyby $(i+1)$.
- **Approach (Targeting, Pre-flyby) Maneuver**: it is usually done about three days prior to the next encounter $i+1$. Its purpose is to fine-tune the next flyby $(i+1)$. The targeting algorithms described in the next Section are used for it.

The maneuvers considered in this work are the first and the third; their implementation details will be discussed in Section 5.3. The order of magnitude of these maneuvers depends upon different factors, as mass of the moons, orbit characteristics, accuracy of the dynamical modeling of the spacecraft; they are usually of the order of magnitude of cm/s to a tens of m/s ([53], [42]). An important consideration to do is regarding the available time for these operations: since the orbital period of a spacecraft in such a flyby tour is usually quite small (for example for a part of the Cassini mission the time between two consequent flybys was of 16 days), there is not much time for the orbit determination procedures. For this reason the maneuvers are scheduled as soon as possible after a flyby (but still taking into account the time for gathering the measurements). In the Cassini mission there were five days from the Cleanup Maneuver to the Apoapsis Maneuver, which were sufficient for two tracking periods (needed to reduce the uncertainty) of the spacecraft; the same for the period from the Apoapsis Maneuver to the Approach Maneuver.
Another important concept is the Data Cut Off (DCO); this is the time until when data are taken for an OD arc. For example, the tracking of JUICE can be interrupted a few days before a maneuver in order to provide enough time for its design.

In [53] are given indications on which maneuver to remove if needed: this is the apoapsis maneuver because it has a smaller effect on the rest of the trajectory. Removing the other two maneuvers instead can cause higher errors and can be damaging for the mission.

A difference has to be explained between *deterministic* and *statistical* maneuvers; the first are determined by the mission designer and are part of the nominal trajectory. They have to be executed in order to follow the nominal trajectory. The latter are not part of the nominal trajectory, but they are computed by the navigation analyst (in a pre-mission simulation and then during the real mission) considering the results of the orbit determination. It is sometimes unclear in which category a maneuver falls; in [42] for example is indicated that the Cleanup and the Apoapsis Maneuvers are deterministic, as they are optimized to reduce ΔV.

4.3.2. B-Plane Targeting Algorithm

To target the desired aiming point in the B-Plane a guidance algorithm is needed. This algorithm shall compute the actions to take (essentially the ΔV of the correction maneuver to execute) from the input data of the desired (nominal) and real (perturbed) trajectory of the spacecraft. There is a fundamental assumption [54] in this algorithm: the direction of the B-Plane axis is considered fixed; this is justified from the fact that the asymptotic line angle varies of a very small amount for initial velocity changes.
The most used algorithm comes from [54],[55] and is termed B-Plane targeting algorithm since it uses the B-Plane parameters (4.2) to design the maneuver. From the references found, it appears to be the algorithm used to navigate the spacecraft during a flyby. In [46] this algorithm is improved and also a new algorithm is constructed. It is noted however that no sources reporting the use of these two new approaches in real missions have been found.
Only the classic version of this algorithm is envisioned to be used in this Thesis; it is discussed here, while the other two are only briefly described.

B-Plane Targeting with numerical derivatives

This is the classical approach that uses the two B-Plane components, B_R and B_T, and the time of closest approach (T_{TCA}) as variables to target. A Taylor series expansion is written for the vector $\mathbf{B} = \begin{bmatrix} B_R & B_T & T_{TCA} \end{bmatrix}^T$, ignoring the higher order terms

$$\mathbf{B} = \mathbf{B}^* + \frac{\partial \mathbf{B}}{\partial \mathbf{V}} \left(\mathbf{V} - \mathbf{V}^* \right) \tag{4.26}$$

where the * indicates the nominal conditions (thus $\mathbf{B}^*$ represents the desired values and $\mathbf{B}$ the perturbed, real values). Rewriting equation 4.26 as

$$\mathbf{\Delta B} = \frac{\partial \mathbf{B}}{\partial \mathbf{V}} \mathbf{\Delta V} \tag{4.27}$$

where $\mathbf{\Delta B} = \mathbf{B}^* - \mathbf{B}$ and $\mathbf{\Delta V} = \mathbf{V}^* - \mathbf{V}$. This linear system of equations can be solved

$$\boldsymbol{\Delta V} = \Omega^{-1} \boldsymbol{\Delta B} \tag{4.28}$$

The matrix Φ is the Jacobian and its complete expression is

$$\Omega = \frac{\partial \boldsymbol{B}}{\partial \mathbf{V}} = \begin{bmatrix} \frac{\partial B_R}{\partial \Delta V_x} & \frac{\partial B_R}{\partial \Delta V_y} & \frac{\partial B_R}{\partial \Delta V_z} \\ \frac{\partial B_T}{\partial \Delta V_x} & \frac{\partial B_T}{\partial \Delta V_y} & \frac{\partial B_T}{\partial \Delta V_z} \\ \frac{\partial T_{TCA}}{\partial \Delta V_x} & \frac{\partial T_{TCA}}{\partial \Delta V_y} & \frac{\partial T_{TCA}}{\partial \Delta V_z} \end{bmatrix} \tag{4.29}$$

In this version of the algorithm the Jacobian matrix is computed numerically by giving a small variation to the velocity and computing the change in B-Plane parameters (finite differences), as follows

$$\Omega = \lim_{\boldsymbol{\delta V} \to 0} \frac{\boldsymbol{B}(\boldsymbol{V} + \boldsymbol{\delta V}) - \boldsymbol{B}(\boldsymbol{V})}{\boldsymbol{\delta V}} \tag{4.30}$$

A forward difference scheme is accurate enough since this derivatives are quite well-behaved [46], as will be shown in Section 6.3.
With equation 4.28 the $\boldsymbol{\Delta V}$ is obtained and the maneuver can so be executed to correct the deviations in the B-Plane parameters.

The weaknesses of this method are two: first of all, it is based on a linearization and hence is not completely correct; the second is the numerical computation of the derivatives, that requires a careful selection of the perturbation $\delta\mathbf{V}$ for a precise computation.

The first problem can be addressed by using an iterative scheme to reduce the truncation error: after computing $\boldsymbol{\Delta V}$, the velocity is updated as

$$\boldsymbol{V}^{i+1} = \boldsymbol{V}^{i} + \boldsymbol{\Delta V}^{i} \tag{4.31}$$

and the new, intermediate, B-Plane parameters are computed. The deviation from the nominal one is computed again and the procedure is repeated until a tolerance on the B-Plane parameters is satisfied. The total $\boldsymbol{\Delta V}$ is then the sum of all the precedent $\boldsymbol{\Delta V}^{i}$. The second problem can be addressed by using higher order derivative schemes, but this would add complexity and computational cost, and by selecting an appropriate value of the perturbation for computing the partials.
As shown in Figure 4.6, the interval of linearity is quite wide; errors are only at the extremes due to numerical problems or decrease of linearity. It is anyway important to check the behavior of the numerical derivatives to ensure an accurate computation. This will be done in Section 6.3.

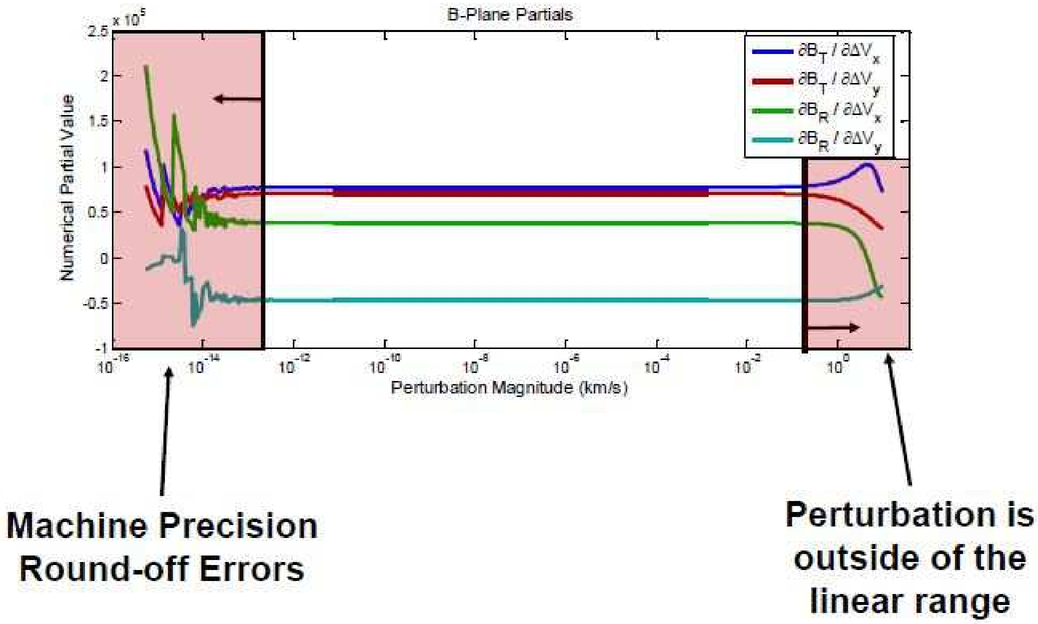

Figure 4.6: Partial derivatives for the B-Plane parameters (slides of University of Colorado)

B-Plane Targeting with analytical derivatives
This is the first modified approach presented in [46]; the only difference with the previous algorithm is the computation of the derivatives, which is performed analytically. Exact analytic expressions substitute thus the numerical approximations.
It is noted that iterations are still needed, because also in this approach a Taylor series expansion with a truncation takes place; moreover, from [46] it appears that the results obtained are identical to the previous method, with the same number of iterations. The only advantage thus appears to be the simplest computation of partials and the small decrease in computational time. This algorithm is used only in Section 8.3.1 for a particular investigation; its usage was otherwise not necessary.

B vector and eccentricity targeting (for periapsis or T_{TCA})
The second approach presented in [46] is different from the previous two. In particular, an analytic solution for the maneuver ($\boldsymbol{\Delta V}$) is found, deleting thus the need of iterations. In this approach, the B vector and the eccentricity are targeted, differently from the previous case. The targeting of a particular eccentricity can be directly related to the periapsis radius or to the time of closest approach. The ΔV is obtained directly with a

formula using the current and desired position at flyby. In the reference of above this approach is verified by comparison with the classical approach: also in this case the results obtained are practically identical. The advantage are the elegance of its formulation, the absence of mathematical approximations and the absence of iterations. This algorithm is not used in this work.

4.3.3. Optimized Targeting Algorithm

The optimized targeting algorithm is a different targeting algorithm than the B-Plane targeting that can overcome the limitations of the latter; as will be discussed in the Section 6.3.1, it is necessary to improve the trajectory correction maneuver design obtained with the B-Plane targeting since its results are not always accurate. These results are valid only under certain assumption (in particular concerning the distance of the spacecraft from the flyby); the optimized targeting instead provides valid results under (almost) every circumstance.
This improvement (that can be considered a simple *optimization*) is based on the observation that a ΔV at a certain time has a direct effect on the position of the spacecraft at a later time; there are not any analytical direct formulas that can relate this two parameters, but a numerical propagation has to be performed to see these effects. The concept is that a certain ΔV will modify the position of the spacecraft at the time of flyby in a predetermined way, thus allowing to compute the one required to obtain the desired position after a certain time; this can be done only in an iterative way.
With these observations it was straightforward to implement a simple optimizer, using a Newton-Raphson scheme. The function to drive to zero is

$$\mathbf{f}(\mathbf{y}) = \mathbf{x}^{fb}_{corr}(\Delta\mathbf{V}^{man}) - \mathbf{x}^{fb}_{nom} \equiv \Delta\mathbf{x}^{fb}(\Delta\mathbf{V}^{man}) \tag{4.32}$$

where $\mathbf{x}_{corr}$ and $\mathbf{x}_{nom}$ are the spacecraft position vectors for the nominal and the corrected trajectory, respectively. The nominal trajectory is the one desired while the corrected one is the real trajectory after the application of the necessary $\Delta\mathbf{V}$ (at the moment still unknown). The apex *fb* stands for flyby time and $\Delta\mathbf{V}^{man}$ is the maneuver. The notation $\mathbf{x}^{fb}_{corr}(\Delta\mathbf{V}^{man})$ indicates that the state at flyby is a function of the correction ($\Delta\mathbf{V}^{man}$) applied at maneuver time. The state at the time of flyby is obtained with a full numerical propagation

$$(\mathbf{x}^{man}_{pert}, \Delta\mathbf{V}^{man}) \quad \xrightarrow[t_{man}\rightarrow t_{fb}]{propagation} \quad \mathbf{x}^{fb}_{corr} \tag{4.33}$$

To simplify the notation, the apexes *fb* and *man* will not be included in the next passages.
The objective function represents the miss distance of the corrected trajectory with respect to the nominal trajectory; intuitively, for a precise targeting, this has to be zero.
The objective function is expanded in Taylor series (neglecting higher order terms due to the almost linear relationship) and set equal to zero

$$\Delta\mathbf{x} \approx \Delta\mathbf{x}_0 + \frac{\partial\Delta\mathbf{x}}{\partial\Delta\mathbf{V}}(\Delta\mathbf{V} - \Delta\mathbf{V}_0) = \mathbf{0} \tag{4.34}$$

With some manipulation the expression for the desired ΔV is obtained.

$$\frac{\partial\Delta\mathbf{x}}{\partial\Delta\mathbf{V}}(\Delta\mathbf{V} - \Delta\mathbf{V}_0) = -\Delta\mathbf{x}_0$$
$$\Delta\mathbf{V} - \Delta\mathbf{V}_0 = -\frac{\partial\Delta\mathbf{x}}{\partial\Delta\mathbf{V}}^{-1}\Delta\mathbf{x}_0$$
$$\Delta\mathbf{V} = \Delta\mathbf{V}_0 - \frac{\partial\Delta\mathbf{x}}{\partial\Delta\mathbf{V}}^{-1}\Delta\mathbf{x}_0$$

From this equation an iterative scheme is readily implemented

$$\Delta\mathbf{V}_{i+1} = \Delta\mathbf{V}_i - J_i^{-1}\Delta\mathbf{x}_i \tag{4.35}$$

In this equation the index i refers to the number of the iteration. The matrix J is the jacobian matrix of the miss distance at flyby with respect to the ΔV:

$$J = \frac{\partial\Delta\mathbf{x}}{\partial\Delta\mathbf{V}} = \begin{bmatrix} \frac{\partial\Delta x}{\partial\Delta V_x} & \frac{\partial\Delta x}{\partial\Delta V_y} & \frac{\partial\Delta x}{\partial\Delta V_z} \\ \frac{\partial\Delta y}{\partial\Delta V_x} & \frac{\partial\Delta y}{\partial\Delta V_y} & \frac{\partial\Delta y}{\partial\Delta V_z} \\ \frac{\partial\Delta z}{\partial\Delta V_x} & \frac{\partial\Delta z}{\partial\Delta V_y} & \frac{\partial\Delta z}{\partial\Delta V_z} \end{bmatrix} \tag{4.36}$$

This matrix is computed with a simple finite difference scheme: the corrected trajectory at step i is perturbed three times, each time with an independent perturbation of the three components of the velocity. Then is propagated until flyby; with the flyby state is possible to approximate the derivative with a simple finite difference scheme. For example, the derivative of the state with respect to a ΔV in the x direction only is approximated as

$$\frac{\partial \Delta \mathbf{x}}{\partial \Delta V_x} = \lim_{\delta V_x \to 0} \frac{\Delta \mathbf{x}(\Delta V_x + \delta V_x) - \Delta \mathbf{x}(\Delta V_x)}{\delta V_x} \tag{4.37}$$

This partial onstitutes the first column of matrix 4.36. This is conceptually simple but computationally expensive, because three independent propagations are needed to compute these partials.
The fundamental advantage of this method, as will be shown in Chapter 6, is that the real position of the spacecraft at flyby time is corrected precisely; the main disadvantage is that it is computationally expensive since it requires the numerical propagation of the trajectory to obtain the spacecraft state vectors at the desired time. For each iteration of the optimizer, four different propagation have to be executed (one for the computation of the current state and three for the computation of the Jacobian matrix).
The connection between the B-Plane targeting algorithm and the Newton-Raphson optimizer is the following: the $\Delta\mathbf{V}$ computed with the B-Plane targeting is the initial guess for the optimizer, thus $\Delta\mathbf{V}_0$. The optimizer then performs a series of iterations (a maximum number is fixed) until convergence; convergence is reached when the corrected position differs from the nominal position by less than the tolerance (tol)

$$\| \mathbf{x}^{fb}_{corr} - \mathbf{x}^{fb}_{nom} \| = \| \Delta \mathbf{x}^{fb} \| < tol \tag{4.38}$$

The tolerance chosen is of 10 km for the simulations, since it appears a reasonable value compared to the flybys minimum altitudes (200 km); this value has been chosen also because is quite easy to obtain hence requiring fewer iterations of the optimizer (see 6.3.2). Similar optimization strategies have been found also in different references, as in [56], [57] and [51]. In the first two references similar concepts are proposed, while in the third a more complex strategy is implemented.

4.3.4. Approximated Targeting Algorithm

Despite the improvement given by the optimizer, another factor has to be considered: the computational cost. The usage of the optimizer implies four different propagations per iteration; moreover, a small time step has to be used in order to have accurate results. A faster way to compute the ΔV is implemented in the approximated targeting; as the name suggests, the ΔV computed in this way is not as accurate as the one computed with the optimized targeting. However it has to be accurate enough to provide ΔV estimates close to their real values (obtained with the optimized algorithm). This error shall be limited to a few percent otherwise the approximation is useless; the analysis of the goodness of the approximation is presented in Subsection 6.3.3.
The approximated targeting is implemented from the observation of the almost linear behavior of the ΔV respect to the perturbation applied. In this approximation the ΔV is computed with the use of a Jacobian matrix, with the following expression

$$\Delta \mathbf{V} \approx \frac{\partial \Delta \mathbf{V}}{\partial \boldsymbol{\sigma}_r} \boldsymbol{\sigma}_r \tag{4.39}$$

where the Jacobian matrix is

$$J = \frac{\partial \Delta \mathbf{V}}{\partial \boldsymbol{\sigma}_r} = \begin{bmatrix} \frac{\partial \Delta V_x}{\partial \Delta \sigma_x} & \frac{\partial \Delta V_x}{\partial \Delta \sigma_y} & \frac{\partial \Delta V_x}{\partial \Delta \sigma_z} \\ \frac{\partial \Delta V_y}{\partial \Delta \sigma_x} & \frac{\partial \Delta V_y}{\partial \Delta \sigma_y} & \frac{\partial \Delta V_y}{\partial \Delta \sigma_z} \\ \frac{\partial \Delta V_z}{\partial \Delta \sigma_x} & \frac{\partial \Delta V_z}{\partial \Delta \sigma_y} & \frac{\partial \Delta V_z}{\partial \Delta \sigma_z} \end{bmatrix} \tag{4.40}$$

The term $\boldsymbol{\sigma}_r$ represents the perturbation on the position vector at the time of maneuver (it is thus a vector); this is essentially the result of the covariance analysis.
The Jacobian matrix in equation 4.40 represents the sensitivity of the required ΔV to the initial position perturbation; it depends on the flyby in consideration, on the maneuver time and on the dynamical model used. It can be computed with a central difference scheme:

$$\frac{\partial \Delta \mathbf{V}}{\partial \sigma_r} = \frac{\Delta \mathbf{V}(\sigma_{r0} + \Delta \sigma_r) - \Delta \mathbf{V}(\sigma_{r0} - \Delta \sigma_r)}{2 \Delta \sigma_r} \tag{4.41}$$

where this computation has to be done independently for each component of the perturbation vector. In this way is possible to decouple the covariance analysis from the guidance: the jacobian matrices have to be generated once for each flyby (for all the desired maneuver times and dynamical models) and then stored. When performing a navigation analysis, it is sufficient to compute $\boldsymbol{\sigma}_r$ at the desired time and then perform the multiplication of 4.39 to get the ΔV. The Jacobian matrix is computed with the optimized algorithm, so that the approximation is referred to the improved correction. In this way all the process of using the B-Plane targeting algorithm and subsequently the optimizer is substituted with a single multiplication; no propagation is performed. The computational saving given by this procedure is really important, since a more numerical propagations are substituted with a single matrix multiplication. The validation of this procedure is presented in Subsection 6.3.3 where the error introduced by this approximation is quantified.

In the Thesis all these three algorithms are used; in particular, the B-Plane targeting is used only to provide the initial guess for the optimizer. Instead, when the the approximated targeting is used there is no need for the B-Plane targeting.

4.3.5. TCM Execution Error Model

The maneuver execution error model found in literature is quite a simple one, but has been used throughout the years for plenty of missions. It is called the Gates' maneuver execution model, from C.R. Gates of JPL, and it dates back to 1963; the original document from Gates could not be found, hence the model presented comes from other references ([11], [52], [51]). This model assumes that the error of the execution of a maneuver is due to two factors: the magnitude of the maneuver itself and the pointing of the engine during the maneuver. Since it is not possible to control the propellant flow and the pointing with absolute precision, there will be an error with respect to the nominal conditions. For each of these two variables, the error is divided in two components: a fixed amount, which is constant, and a variable amount, which is proportional to the magnitude of the maneuver. This is a simplified, but realistic model, since it takes into account eventual systematic errors in the design and/or mounting of the engine and eventual random errors that can be amplified from the flow of propellant.
In Table 4.2 is shown this model for the Cassini-Huygens spacecraft (from [52]); this model was prepared before launch and was then updated with inflight data.

Table 4.2: Maneuver Execution Error Model for Cassini-Huygens [52]

		MEA	RCS
Err on Magnitude	Proportional (%)	0.2	2.0
	Fixed (mm/s)	10.0	3.5
Err on Pointing	Proportional ($mrad$)	3.5	12
	Fixed (mm/s)	17.5	3.5

The values are presented for the two engines, the Main Engine Assembly (MEA) and the Reaction Control System (RCS). The fixed values are in mm/s, while the proportional are in percentages (for the pointing error can also be in radians). These values represent the 1σ standard deviation of a Gaussian distribution with zero mean; in a simulation thus these errors must be added accordingly. The final error on the ΔV is then computed with a Root Sum Square on the single errors, as follows [58].

The error for the magnitude is

$$\Delta\mathbf{V}_{err-mag} = rand \cdot \sqrt{\sigma^2_{fixed-m} + \left(\sigma_{prop-m} \cdot \Delta V\right)^2}\,\Delta\hat{\mathbf{V}} \tag{4.42}$$

where $rand$ is a random number computed with a normal distribution with mean zero and standard deviation one. σ_{fixed} is the fixed error and σ_{prop} is the proportional error (as from Table 4.2). This error is a vector with the same direction of the nominal $\Delta\mathbf{V}$ ($\Delta\hat{\mathbf{V}}$).
The error for the pointing is

$$\Delta\mathbf{V}_{err-point} = rand \cdot \sqrt{\sigma^2_{fixed-p} + \left(\sigma_{prop-p} \cdot \Delta V\right)^2}\,\Delta\hat{\mathbf{V}}_{norm} \tag{4.43}$$

where

$$\Delta\hat{\mathbf{V}}_{norm} = \Delta\hat{\mathbf{V}} \times \hat{\mathbf{z}} \tag{4.44}$$

and $\hat{\mathbf{z}}$ is the unit vector in the z direction of the ECLIPTIC J2000 frame. This error is considered along one direction only for simplicity. The final error is just the sum of the previous two

$$\Delta\mathbf{V}_{err-tot} = \Delta\mathbf{V}_{err-mag} + \Delta\mathbf{V}_{err-point} \tag{4.45}$$

This error can thus be in any direction, depending upon the magnitude of the random numbers; the real maneuver can thus be smaller or bigger than the nominal one (if the vector $\Delta\mathbf{V}_{err-tot}$ is parallel or anti-parallel to $\Delta\hat{\mathbf{V}}$).

5

Implementation and Software Architecture

In this Chapter the implementation of the Navigation Analysis (NA) is described; the Navigation (or Maneuver) Analysis is a method to assess the feasibility of a space mission, from the point of view of the ΔV needed to keep the spacecraft on the desired trajectory, correcting the uncertainties affecting its orbit. The NA implemented is composed by the Covariance Analysis (Chapter 3) and by the Guidance for Flyby Tours (Chapter 4). It is implemented specifically for the mission JUICE (Chapter 2), but it can be easily adapted to any similar type of mission.

Software implementation: Tudat

The NA has been implemented in the TU Delft Astrodynamics Toolbox (Tudat, [59]); a brief description of the toolbox is given here. This is a C++ toolbox written and maintained by the Department of Astrodynamics & Space Missions of TU Delft. This toolbox contains different well-structured routines for astrodynamics simulations, such as conversion of orbital elements, orbit propagation and optimization.
It contains also a great number of test cases which have a twofold purpose: validate the written routines and allow new users to rapidly understand how to use these routines in their programs. A description of the history and all the details of the project can be found in the above mentioned reference and in the website of Tudat (http://tudat.tudelft.nl).

A modified version of Tudat has been used for the project [60]. This version includes all the necessary algorithms for performing the orbit determination of a spacecraft, which are not yet available in the base version of the Tudat toolbox.
In this version of Tudat are available all the features described in Chapter 3; in particular, the LSQ algorithm and all the related functionalities are implemented. Thus, a good part of the code needed for the project was already available in the toolbox; however, an extensive programming activity has been done, for mainly two reasons. The first one is that since the toolbox is written in a general way, in order to be used for a lot of different projects, a great effort is needed in order to create a simulator for a specific need (e.g. as could be the orbit determination of a geostationary satellite, of a LEO satellite, of an interplanetary mission). This entails mainly the creation of a lot of auxiliary functions, and in some rare cases, even the modification of the base toolbox (as for example in the eventuality of some incompatibilities that were not foreseen before). The second reason is that the necessary algorithms for the second part of the project (the flyby tour guidance) were not available, thus they had to be written, verified and linked to the rest of the code.

The NA is useful also for identifying potential areas of risk and improvements for a mission, as the risk of impacts into the moons, the operational schedule of the mission (how much time is available for the orbit determination and data processing between flybys) and ΔV reduction (for deterministic and statistical maneuvers). This Chapter has the following structure: in the first Section (5.1), the choice of the Covariance Analysis as orbit determination method is justified. Follows a description of the implementation of the CA in Section 5.2. The integration of the Covariance Analysis with the Guidance for Flyby Tours into a Navigation Analysis is then described in Section 5.3. The last Section (5.4) describes the implementation of the Monte Carlo method; this method is used to transform the Navigation Analysis in a statistical analysis.

5.1. The choice of the Covariance Analysis

The method of the Covariance Analysis has been chosen over a full Least Squares (see Section 3.3, where the difference is explained) simulation for different reasons. This choice has been done at the start of the project, hence the following developments had to comply with such choice. The reasons for this choice are listed below.

1. *low computational cost and time required*: as shown in Section 3.3, the CA is less computationally expensive and time-consuming than the LSQ. In the LSQ more iterations have to be performed, while in the CA just one iteration is done. Since the time increases roughly linearly with the number of iterations, it is clear that running the same number of simulations using a LSQ instead than a CA would require much more time. Considering that one of the objectives of the work is to analyze an high amount of combinations of parameters the CA was the most suitable choice from this point of view.

2. *the analysis executed is a preliminary analysis*: the navigation analysis executed in the framework of this Thesis is a preliminary one, meaning that orbit determination process and the maneuvers design are modeled with a good accuracy but still with the use of some assumptions. The implementation of a completely realistic navigation analysis that models all the aspect of such complex mission is outside the scope of a Thesis.

3. *the information available about the mission were not complete*: as explained in Chapter 6, not all the information necessary for an exact analysis were available. In particular, it was impossible to reproduce the nominal trajectory of JUICE with a numerical integration; hence, the execution of an LSQ would be somehow flawed. In particular, the state vector computed from the LSQ would not be completely exact; this because when propagating the trajectory not all the forces that were considered when creating it are included, and also the maneuvers are not included. Due to this inconsistency, the advantages of the LSQ with respect to the CA could not be fully exploited.

4. *it is has often been used for navigation analysis*: the usage of a covariance analysis instead of a LSQ has been found in different sources ([49] and [56]) for similar missions (e.g. Cassini and the envisioned NASA's Europa Multiple-Flyby Mission).

For these reasons the Covariance Analysis was deemed suitable to perform a preliminary navigation analysis for the JUICE mission, analyzing the influence of JUICE and the moons positions uncertainties on the navigability of the trajectory. There is however an important conceptual difference between using a LSQ or a CA as orbit determination method in a navigation analysis; this is explained in the following paragraph.

Limitations of the Covariance Analysis

To design a TCM (Section 4.3) it is necessary to simulate a deviation from the nominal trajectory. With the LSQ the "real" trajectory is directly obtained as result of the algorithm (see Eq. 3.21), and can be used to design the maneuvers, because this will be generally different from the "nominal" trajectory. It is obtained because the algorithm produces the best estimate of the trajectory, starting from a dynamical model, initial conditions and observations (see Chapter 3.3). If the observations are corrupted with some noise or if the dynamical model used in the procedure is different from the dynamical model used to generate the nominal trajectory, then the result of the LSQ ("real" trajectory) will be different from the nominal trajectory. In this way the real process of interplanetary orbit determination is completely simulated because this is exactly what happens in the real world: the observations are not completely accurate and the dynamics is always an approximation of reality. Hence with a LSQ is possible to analyze, independently or concurrently, the effects of uncertainties in the dynamical model or errors in the observations. However, with the CA the perturbed trajectory is not obtained directly since no state estimation is performed; this perturbed trajectory is obtained by modifying the nominal one with the uncertainties of the estimation only. These uncertainties are contained in the covariance matrix of the state and are the main results of the CA (see Eq. 3.22). The perturbed state is obtained in the following way. The covariance matrix of the spacecraft and moon positions is

$$P = \begin{bmatrix} \sigma_{Jx}^2 & & & & & \\ & \sigma_{Jy}^2 & & & \ddots & \\ & & \sigma_{Jz}^2 & & & \\ & & & \sigma_{mx}^2 & & \\ & \ddots & & & \sigma_{my}^2 & \\ & & & & & \sigma_{mz}^2 \end{bmatrix}$$

This matrix represents the squares of the uncertainties of the positions at a certain time epoch (which correspond to the initial epoch of the estimation interval). The indexes x, y, z represent the three different Cartesian axes of the reference frame ECLIPTIC J2000, while the indexes J, m stand for JUICE and moon. The off-diagonal elements, not represented, are the correlation between the diagonal elements. The standard deviations of the state of the spacecraft and the moon are the square root of the diagonal elements. The perturbed state for the spacecraft and the moons are computed then as (neglecting the correlations)

$$\begin{cases} x_J^{pert} = x_J^{nom} + rand \cdot \sigma_{Jx} \\ y_J^{pert} = y_J^{nom} + rand \cdot \sigma_{Jy} \\ z_J^{pert} = z_J^{nom} + rand \cdot \sigma_{Jz} \\ x_m^{pert} = x_m^{nom} + rand \cdot \sigma_{mx} \\ y_m^{pert} = y_m^{nom} + rand \cdot \sigma_{my} \\ z_m^{pert} = z_m^{nom} + rand \cdot \sigma_{mz} \end{cases}$$

where σ are the standard deviations and $rand$ is a random number generated with a Gaussian distribution (explained in Section 5.4). In this way the perturbed trajectory represents only the uncertainty in the positions of the spacecraft and the moons (Figure 5.1) as determined by the orbit determination algorithm. This varies a lot depending upon the tracking schedule used, the data weights, and other factors.

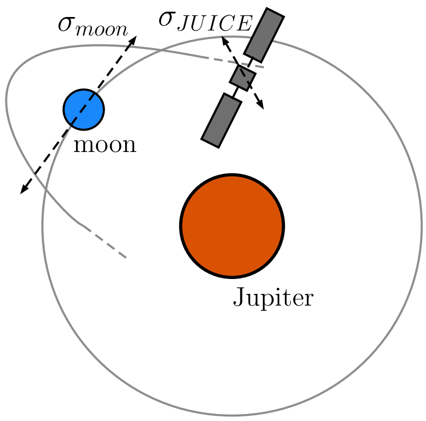

Figure 5.1: Scheme of orbit uncertainty from the Covariance Analysis

Thus, the maneuvers designed in this way will not be completely representative of the real mission, because a lot of different phenomena that cause the deviation of the trajectory are neglected, as gravitational perturbations from other celestial bodies, solar radiation pressure and other forces. These maneuvers represent only the ΔV required to correct for the uncertainties in the positions of the Galilean moons (ephemerides) and the spacecraft. The consequence is that the ΔV is not always close to the real one; for example, if the accuracy obtained is very high (around tens or hundreds of meters) then the maneuver will be really small, even if in reality the spacecraft could be off by hundreds of km or more from the nominal position due to different perturbations. If instead the accuracy is quite low (around tens of kilometers) then the ΔV obtained is a good approximation, because the other effects are possibly smaller than the ephemerides errors.

5.2. Implementation of the Covariance Analysis

The details about the implementation of the CA (see Section 3.3) are discussed here. A conceptual scheme of the implementation is shown in Figure 5.2, with the different building blocks of the analysis. Some of these blocks were already available in Tudat, while some others had to be written.

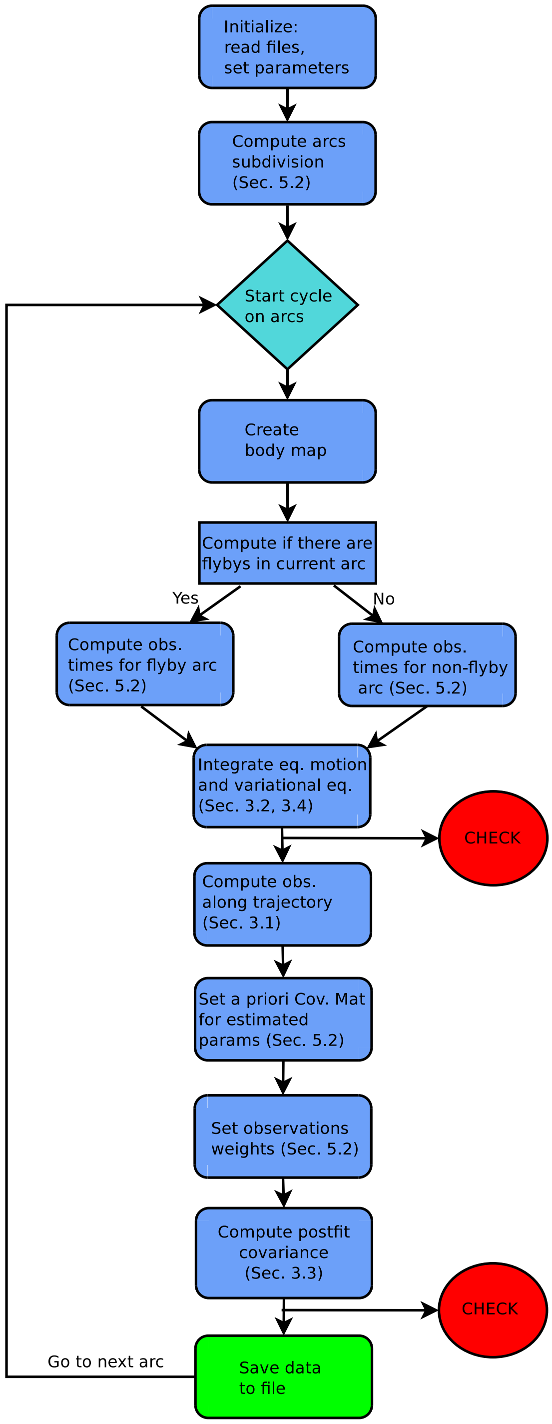

Figure 5.2: Conceptual scheme of the Covariance Analysis

In Figure two checks can be seen, after the integration of the equations of motion and the computation of the post-fit covariance matrix; they are explained in Subsection 5.3.4 and 6.2.1. Are here discussed the details of the main blocks implemented, following the order of the Figure. These are:

- computation of the arcs subdivision;
- computation of the observation times (for both flyby and non-flyby arcs);
- setting of the a priori covariance matrix for the parameters and the observations weights.

The rest of the blocks were already available in Tudat and required only minor modifications for the project.

The logic of the arcs subdivision is shown in Figure 5.3; an arc is a period during which the orbit determination takes place. This subdivision is required in order to design the TCM in different arcs. Three parameters rule this subdivision: the *nominal arc duration* (t_{nom}), the *minimum arc duration* (t_{min}), and the *flyby arc duration* (t_{fb}).

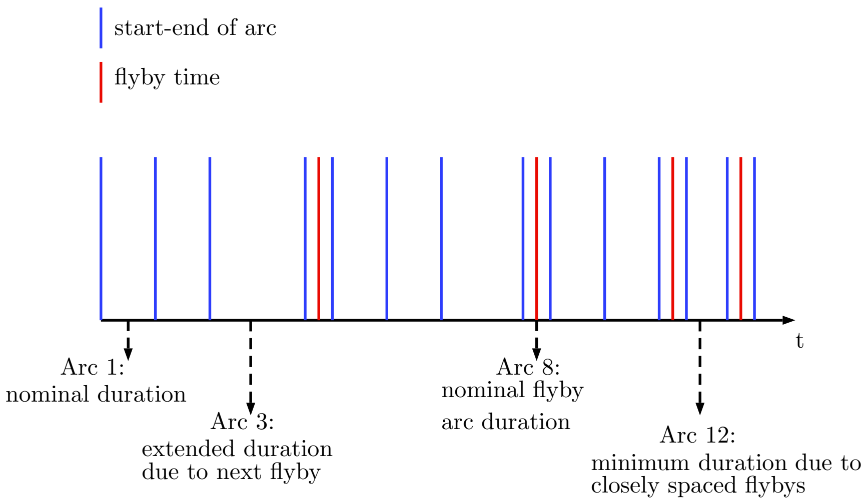

Figure 5.3: Scheme of time subdivision

Indicating with t_i^0 the initial time of arc i and with t_i^f the final time of arc i, the procedure used to create the arcs is the following. Arcs of nominal duration are created until a flyby is encountered

$$\begin{aligned} t_i^f &= t_i^0 + t_{nom} \quad \text{until flyby} \\ t_{i+1}^0 &= t_i^f \end{aligned}$$

When a flyby is found an arc of duration t_{fb} centered around the flyby time is created. It is checked that the size of the arc preceding the flyby is not smaller than the minimum arc duration, otherwise there is risk of not convergence of the CA. If that happens, that arc is joined with the one before, yielding a single arc of extended duration. Indicating with i the flyby arc and with $i-1$ the arc before, the procedure is

$$\text{if} \quad t_i^0 - t_{i-1}^0 < t_{min} \quad \rightarrow \text{join arc i-1 with arc i-2}$$

Special care must be taken during the central part of the flyby tour, when the flybys of Callisto are very close in time (around 15-20 days). In that case the three values described above have to be chosen carefully in order to avoid the creation of an arc with two flybys, feature not possible. The typical duration of these arc is of a few days; in particular, the arcs around a flyby are usually of 6-8 days (from [56]).

The logic of the selection of the observation times is shown in Figure 5.4, for both the flyby and non-flyby arcs. For the non-flyby arcs, the two parameters that rule this selection are the amount of hours per day and the frequency of the observations. These are valid for range, Doppler and optical data, while for VLBI there is an extra feature to add: the number of days per week during which observations are gathered. This is due to the very expensive cost of performing VLBI measurements (Section 3.1.1), hence this is done at a lower rate with respect to the other measurements.

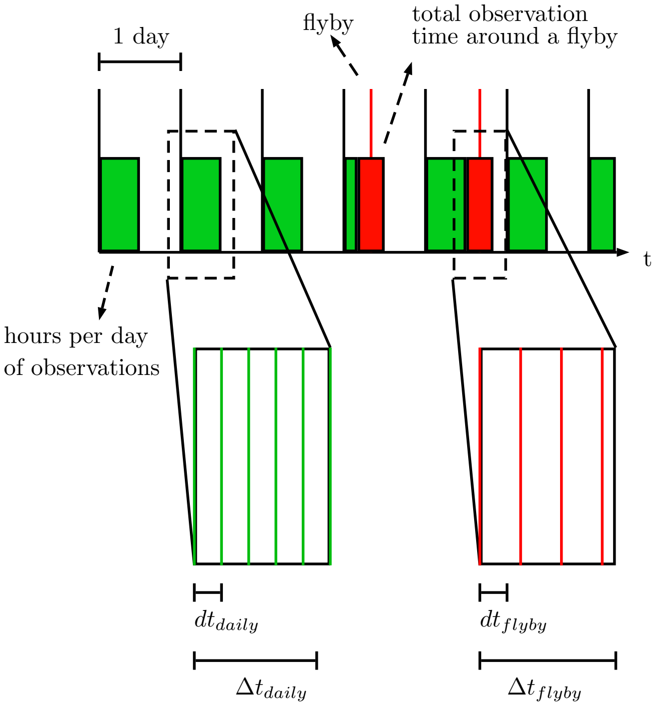

Figure 5.4: Scheme of observations gathering

When a flyby is reached the observation schedule is applied in the arc that contains the flyby and eventual data that should come from the daily observation schedule are neglected. The observation schedule around a flyby is created from two parameters: the range of time around the flyby and the frequency of the observations.

During a flyby an interruption of the tracking data due to instruments pointing requirements[42] could be needed; to simulate this it is sufficient to set the frequency of the observables to zero or equal to the inverse of the flyby arc duration, such that observations are taken only at the beginning and end of the arc.

It has to be noticed that optical data are never taken during a flyby, because of the inaccuracy of the center-finding algorithm when very close to a celestial body [28]; moreover for the optical data it is possible to set a parameter that indicates the interruption of the measurements a fixed amount of time before (or after) a flyby.

The data types used in this project are *range, VLBI* and *optical. Doppler* data, although of primary importance for interplanetary spacecraft tracking, are excluded for the following reasons

- a software issue limited the capability of generating Doppler measurements;
- when simulating Doppler data, it is necessary to include different features (as propagation errors, integration time) to have a realistic representation. Moreover a very accurate dynamic representation of the spacecraft is required. This is due to the fact that the angular position that can be retrieved with Doppler data (see 3.1.1) is just a weak signature of the signal, it is not provided directly by the Doppler data. Since these two modeling were outside the scope of the Thesis, Doppler data would not have provided very accurate results;
- Doppler data have less influence than range and VLBI in ephemerides estimation due to their different information content ([16]). Since range and VLBI allow a direct determination of the spacecraft position and there gravitational acceleration depends upon the position, with these two techniques the influence of a celestial body can be determined more clearly;

- as explained in [12], an alternative to Doppler for spacecraft tracking is to use just range and VLBI. This is explained also by the fact that for low spacecraft declination, Doppler data are inaccurate. Moreover, if only range and Doppler are used, there is the risk to obtain a wrong orbit solution since the weakly observed angular position with Doppler is highly sensitive to dynamical model inaccuracies. The consequence is that the effects of these inaccuracies are "confused" by the estimator as a wrong angular position. A detail explanation is provided in the reference cited above.

Due to these reasons the estimation is performed with range and VLBI data only, which can considered a valid alternative of using Doppler data. However, since Doppler is still used in real orbit determination, the estimation on of JUICE has to be considered only indicative and not correspondent to the real mission performance.

The setting of the a priori values of the covariance matrix is done by creating a diagonal matrix with the inverse of the uncertainties (the *weights*). This procedure is quite straightforward; only for the uncertainties of the Galilean moons position a more complex procedure that involves a reference frame transformation has to be done. This because the uncertainties for the moons are commonly provided in the *radial, along-track, cross-track (r-a-c)* components of their orbits with respect to Jupiter; however the estimation is performed with respect to a quasi inertial Cartesian reference frame (Ecliptic J2000), requiring thus a reference frame transformation to obtain the uncertainties in the latter reference frame. This transformation is performed by computing the rotation matrix $R^{xyz/rac}$ at the time correspondent to the estimation of the moon position. The transformation is then

$$\begin{bmatrix} \sigma_x \\ \sigma_y \\ \sigma_z \end{bmatrix} = R^{xyz/rac} \begin{bmatrix} \sigma_r \\ \sigma_a \\ \sigma_c \end{bmatrix}$$

where the input vector represents the uncertainties in the *r-a-c* frame and the output vector in the Ecliptic J2000 frame.
The procedure of setting the observations weights is the following; the weight of an observation is

$$w_{obs} = \frac{1}{\sigma_{obs}^2} \tag{5.1}$$

where σ_{obs} is the accuracy of that data type. It is assumed that all the observables have the same Gaussian standard deviations, although this is not very realistic since their accuracy depends upon a multitude of factors like geometry, atmosphere and ground station characteristics. The different observables are also assumed uncorrelated. These are simplifying assumptions that are good for a preliminary analysis. The consequences of these simplifications are that the results between different parts of the mission will be quite similar, since the weights of the observations is the same; effects like degradation of the signal due to an alignment Earth-Sun-spacecraft are not considered. This will happen is some parts of the mission, depending upon the relative position Earth-Jupiter with respect to the Sun. Moreover neglecting the correlations can give more optimistic results since for example eventual systematic errors would be not considered in the final computation.

Single arc and data accumulation estimations
Two different versions of the covariance analysis have been implemented, the *single arc data* estimation and the *multi arc, data accumulation* estimation. Their difference is described below.

- *single arc data*: in this case the states of JUICE and the moons are estimated independently in each arc containing (or preceding) a flyby. The CA is always divided in arcs, but the estimation in each arc is independent from the estimation in other arcs (from this the name *single arc data*). For the estimation only the observations gathered during that arc are used. The number of moons estimated can be selected, but it is a convenient choice to estimate only the flyby moon (in Section 7.1 the influence of the number of estimated bodies is analyzed).
  This case has been used because is quite realistic and easy to handle. However, it has also some downsides; the main one is that just a limited amount of data is used to estimate the uncertainty in the positions of JUICE and the moon. This means that for planning a TCM, along with the current nominal position and a priori values for the uncertainties, only a few days of observations are used. In this way there is a kind of waste of data available, because all the observations of the past are not used anymore

for the current flyby. This version is representative of the case that the tracking during the previous flybys has failed and hence those data are lost; thus the current estimation can only include the data from the current flyby.
In Figures 5.5 and 5.6 are shown the two different configurations of the single arc estimation; in the first the estimation is performed in the arc before the flyby, while in the second it is performed during the flyby arc. The first case represents the interruption of the spacecraft tracking due to pointing requirements during the flyby that do not allow the pointing of the antenna to Earth.

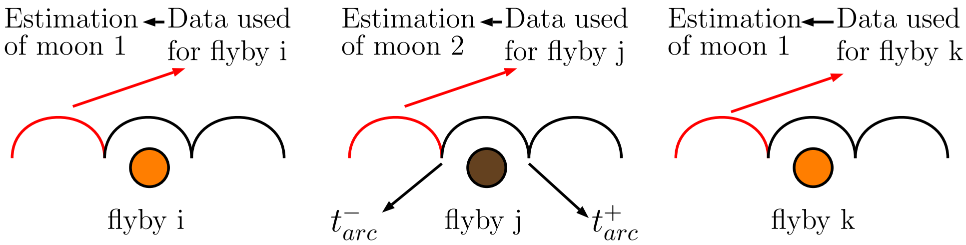

Figure 5.5: Scheme of single arc estimation during pre-flyby arcs

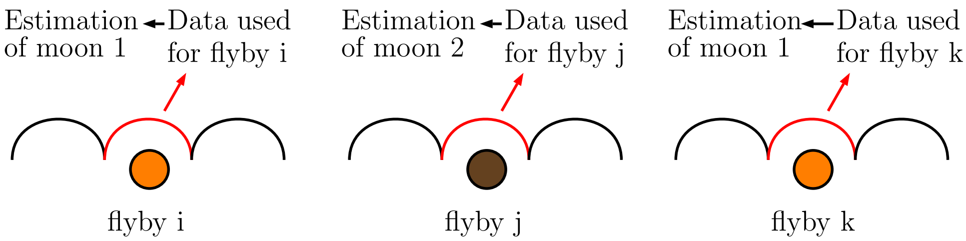

Figure 5.6: Scheme of single arc estimation during flyby arcs

- *multi arc, data accumulation*: in this case JUICE and all the four Galilean moons are estimated during an arc preceding a flyby or during a flyby arc. The estimation however includes also observations from previous arcs, to exploit the information content of all the previous flybys.
  In this version data from the past are accumulated together to perform the estimation for the moons; for JUICE instead, only current data are used. This because for the spacecraft the current position is already determined with a good accuracy with data from a single arc, hence there is no need to use also past data. Another reason why JUICE is not included in this data accumulation procedure is that due to non-conservative forces the dynamics of JUICE is very non-linear, hence the STM (section 3.4) that shall be used would not be very accurate. For the moons instead this is fundamental to improve their accuracy and it can be done because their dynamics is more predictable.
  In particular, for the estimation at the i^{th} flyby (with $i > 1$), the data used come from all the preceding flybys. It is noticed that for each flyby, the state estimated is always the state at the beginning of the *first* flyby arc (t_0). To do so, the information matrix H has to be modified at each estimation (for the meaning of the matrix H see Section 3.3); in particular it has to be increased of size according to the new observations. After the first flyby, the matrix H has the size $[m_1 \times n]$, where m_1 is the number of observations during the 1st flyby arc and n is the number of estimated states (in this case $n = 24$ because there are four moons are for each of them the Cartesian state is estimated). The matrix is then increased in the following way

$$H^j_{tot} = \begin{bmatrix} H^i_{tot} \\ H_j \end{bmatrix}$$

  where H_j is the matrix that contains the partial derivatives of the observations with respect to the state vector (information matrix), for the arc j only; it has size $[m_j \times n]$. The matrix H^i_{tot} instead is the global information matrix at arc i, which corresponds to the first flyby before j (but not usually during the previous arc, so generally $j - 1 \neq i$); it contains all the previous information matrices of the flyby arcs. They are stored increasing the number of rows but keeping the number of columns fixed; the total size of H^i_{tot} is thus

$$[(m_1 + m_2 + .. + m_i) \times n]$$

Since the estimated state is always the same (at a fixed time instant), the matrix H_j has to be referred to that time instant; as seen in Section 3.4 this is done using the state transition matrix. Defining H'_j as the information matrix at time t_j and H_j the information matrix at time t_0, their relation is

$$H_j(t_0) = H'_j(t_j)\Phi\left(t_j, t_0\right) = \frac{\partial h(t_j)}{\partial x(t_j)}\frac{\partial x(t_j)}{\partial x(t_0)} = \frac{\partial h(t_j)}{\partial x(t_0)}$$

This is the matrix that will increase the "global" information matrix. The weighting matrix has to be increased too, by adding the weights for the new observations included.
This version of the Covariance Analysis is thus better suited to simulate the ephemerides improvement obtained along the flyby tour. In Figures 5.7 and 5.8 are shown the schemes of the data accumulation estimation; in the first the data from pre-flyby arcs only are used, while in the second data from flyby arcs only are used.

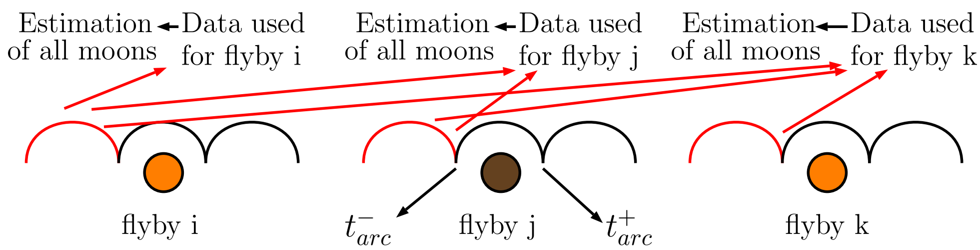

Figure 5.7: Scheme of data accumulation estimation during pre-flyby arcs

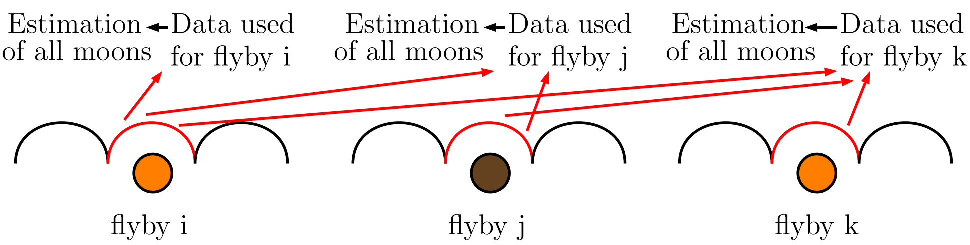

Figure 5.8: Scheme of data accumulation estimation during flyby arcs

In Table 5.1 are reported the main parameters that rule the covariance analysis implemented. They are divided for category; some of them are just binary parameters, used to select if to use a feature of not.

Table 5.1: Parameters that influence the Covariance Analysis

Name	Symbol	Unit or range	Description
Observations			
Use VLBI	[-]	[0-1]	Use VLBI observations
Use optical	[-]	[0-1]	Use optical observations
Range accuracy	σ_R	[m]	Accuracy of the range observations
VLBI accuracy	σ_V	[rad]	Accuracy of the VLBI observations
Optical accuracy	σ_O	[rad]	Accuracy of the optical observations
Dynamical model			
Use Jupiter SH	[-]	[0-1]	Use the spherical harmonics of Jupiter
Use Galilean moons SH	[-]	[0-1]	Use the spherical harmonics of the Galilean moons
Use Sun perturbation	[-]	[0-1]	Use the Sun perturbation
Use Saturn perturbation	[-]	[0-1]	Use the Saturn perturbation
Time			
Initial time	t_0	[d-m-y]	Initial time of simulation
Final time	t_f	[d-m-y]	Final time of simulation
Duration of simulation	ΔT	[d]	Duration of the simulation (alternative to the final time)
Time step	Δt	[s]	Time step of the simulation
Flyby arc start time	t^-_{flyby}	[d before flyby]	Start time of a flyby arc (in days before the flyby)
Flyby arc end time	t^+_{flyby}	[d before flyby]	End time of a non flyby arc (in days after the flyby)
Nominal arc duration	t^{nom}_{arc}	[d]	Nominal duration of an arc
Minimum arc duration	t^{min}_{arc}	[d]	Minimum duration of an arc
Observations schedule			
Flyby data frequency	Δt_{flyby}	[s]	Frequency of data during flyby, for range, VLBI, Doppler
Flyby data interval	ΔT_{flyby}	[s]	Interval of data gathering during flyby, for range, VLBI, Doppler
Non-flyby data frequency	$\Delta t_{non-flyby}$	[s]	Frequency of data during non-flyby, for range, VLBI, Doppler and optical
Non-flyby data interval	$\Delta T_{non-flyby}$	[hrs/day]	Hours per day of data gathering during non-flyby, for range, VLBI, Doppler and Optical
Optical data interruption	d^{opt}_{int}	[d]	Interruption of optical data gathering before or after a flyby (in days)
Days per week of VLBI data	d^{VLBI}_{week}	[d/w]	Days per week of gathering of VLBI data
A priori data			
A priori σ on Gal. moons position	σ^{moon}_r	[m]	A priori uncertainty on the Galilean moons position
A priori σ on Gal. moons velocity	σ^{moon}_v	[m]	A priori uncertainty on the Galilean moons velocity
A priori σ on JUICE position	σ^{JUICE}_r	[m]	A priori uncertainty on JUICE position
A priori σ on JUICE velocity	σ^{JUICE}_v	[m]	A priori uncertainty on JUICE velocity

5.3. Implementation of the Navigation Analysis

A navigation analysis includes a maneuver placement scheme (4.3.1), a targeting strategy (4.3.2, 4.3.3, 4.3.4), an execution error model (4.3.5) and OD strategy (3.3). This scheme is found in different references ([52], [51], [56], [11]).

The starting point for the navigation analysis implemented is the covariance analysis. In the CA, spacecraft and moons position uncertainties are generated from their a priori uncertainties and the observations along the trajectory. With these results is then possible to compute the displacement from the nominal trajectory and thus the TCM (see Section 5.1). Figure 5.9 represents the generic scheme of the guidance that is integrated with the covariance analysis to obtain a full navigation analysis. This scheme is referred to a single perturbed trajectory; however as it will be seen in Section 5.4 the navigation analysis will be performed in a Monte Carlo way, to extract statistical information about the distribution of the perturbed trajectories that correspond to a single nominal trajectory.

This guidance is inserted between the last two blocks of Figure 5.2, *compute postfit covariance* and *save data to file*, before passing to the next arc.

This scheme is referred in particular to the targeting maneuver and to the B-Plane and optimized targeting. This is slightly different for the approximated targeting, where a single operation is done instead of the different ones required for the optimized case. It is noticed that if one of the targeting algorithm fails the navigation analysis is considered failed (it is interrupted and considered not successful); different parameters shall then be tried to obtain a successful simulation. This however happened very rarely, indicating that the algorithms are robust (4.3).

In the next Subsections the different logic for the maneuver design are explained (Subsections 5.3.1, 5.3.2, 5.3.3). The main differences between these schemes are in the selection of the arc where to perform the estimation (the computation and propagation of the covariance matrix) and which data to include to design a certain maneuver.

The parameters that rule the guidance are listed in Table 5.2.

Table 5.2: Parameters that influence the guidance

Name	Symbol	Unit or range	Description
Maximum number of iterations	max_{iter}	[1-∞]	Maximum number of iterations of the B-Plane targeting
Tolerance on B_R, B_T	tol_B	[m]	Tolerance on the B_R, B_T for the B-Plane targeting
Tolerance on t_{TCA}	tol_{TCA}	[s]	Tolerance on the t_{TCA} for the B-Plane targeting
Magnitude of perturbation	[-]	[m/s]	Magnitude of perturbation for the computation of the Jacobian matrix $\frac{\partial \mathbf{B}}{\partial \mathbf{V}}$
Pre-flyby TCM time	$t^{TCM}_{pre-flyby}$	[hrs]	Time of the pre-flyby TCM, in hours before the flyby
Post-flyby TCM time	$t^{TCM}_{post-flyby}$	[hrs]	Time of the post-flyby TCM, in hours after the flyby
Ephemerides improvement	[-]	[0-1]	Use the improvement of the ephemerides from OD when designing the TCMs
Add maneuver error	[-]	[0-1]	Add the maneuver execution error to the simulations
Optimize targeting	[-]	[0-1]	Apply the optimizer to the TCM design (6.3.1)
Tolerance on flyby miss distance	tol^{flyby}	[m]	Tolerance on the flyby miss-distance for the optimizer

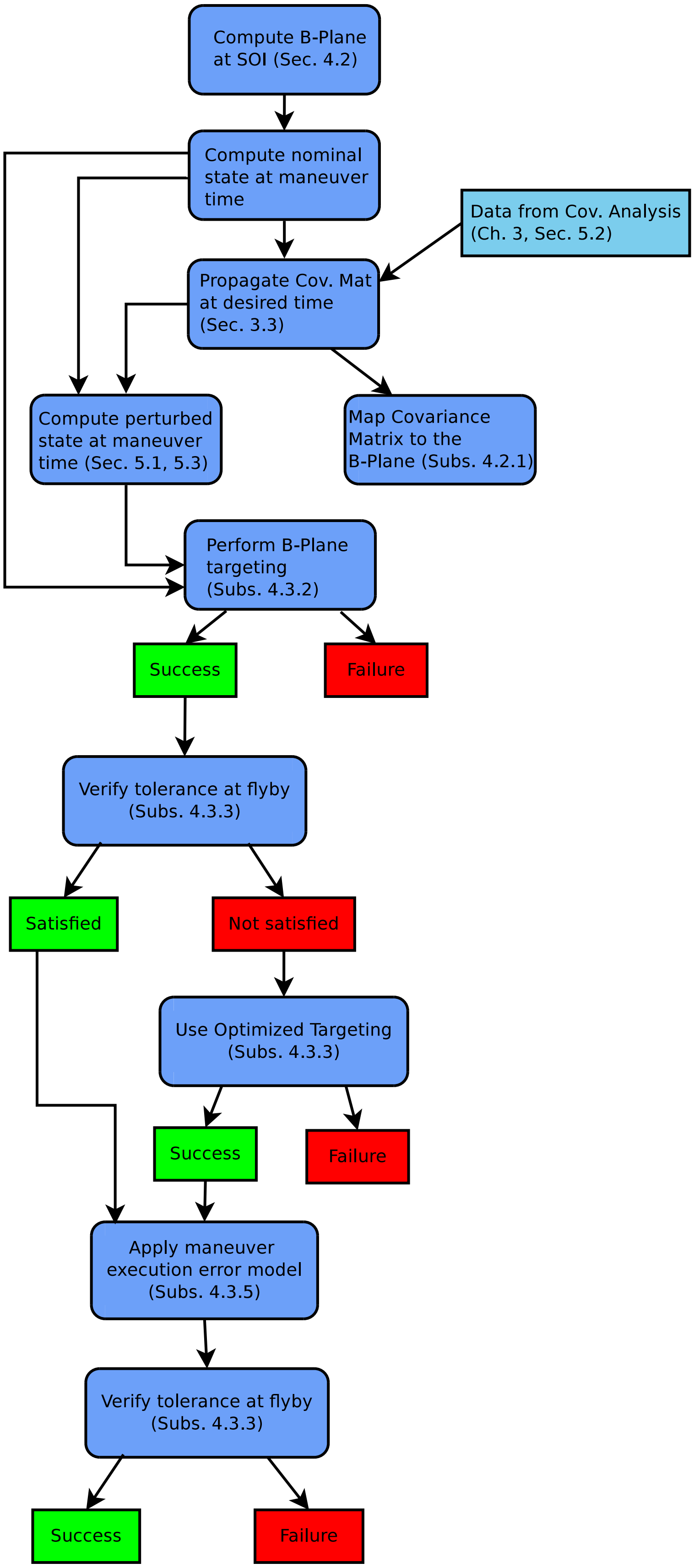

Figure 5.9: Conceptual scheme of the guidance logic for the targeting maneuver

5.3.1. DESIGN OF TARGETING AND CLEANUP MANEUVERS USING FLYBY, SINGLE-ARC DATA

Targeting maneuver

In this case the approach maneuver is designed using data from the last flyby for that moon only, in particular during the flyby arc of the spacecraft. This is schematically represented in Figure 5.10. The *single arc data* version of the CA is used.

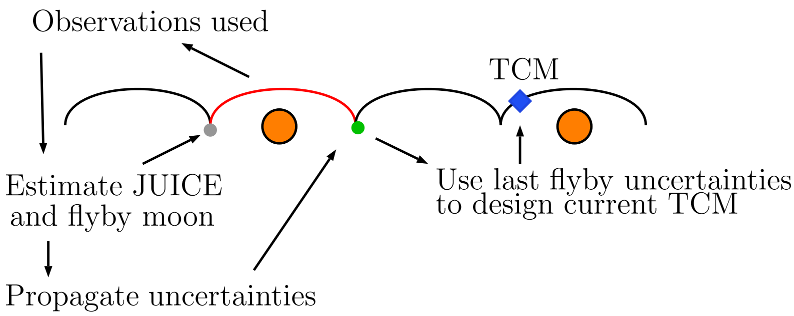

Figure 5.10: Scheme of pre-flyby TCM design using only flyby, single-arc data

For each moon before their first flyby there are no data available yet since no estimation has been performed; thus the a priori uncertainties are used for the first flybys. For the subsequent flybys the uncertainty determined during the previous flyby (of that moon) is used. For JUICE instead the uncertainty used in the one determined just before the flyby. The assumption used for this design is that the tracking during one (or more) of the previous flybys has failed and thus it is not possible to use the data accumulation in the moons estimation.

The covariance matrix that is used to compute the perturbed trajectory with respect to the nominal comes from the flyby arc estimation. This case represent the possibility of tracking the spacecraft during a flyby, which is not always possible due to mission requirements that could forbid the pointing of the antenna to Earth. Moreover, since JUICE is estimated just before the flyby, it is assumed that there is enough time available for mission control to receive the tracking data, perform the OD and determine the maneuver; this could not be realistic if the maneuver has to be done very close to the data cut off time (DCO). A problem of this scheme is that, due to the lack of the state transition matrix for the next arcs, the uncertainty can be propagated only to the end of the arc and not to the exact maneuver time; this propagation would not be anyway very stable since it would be done outside the estimation arc. Hence the covariance used is the one propagated at the end of the last flyby. This introduces a small error since the the propagated uncertainty has usually a periodic behavior; however the influence is really small and in the Monte Carlo simulations there is anyway a random sampling of the uncertainties.

All the three targeting algorithms implemented (see Section 4.3) can be used for this maneuver.

Cleanup maneuver

The cleanup (or post-flyby) maneuver is the maneuver executed to correct for the errors of an imperfect flyby; it can be considered roughly symmetrical to the approach maneuver with respect to the flyby, because it is also executed from a few hours up to 3 days after the flyby. To design it, the same B-Plane targeting algorithm used for the approach maneuver is used; the B-Plane used for the targeting is the one of the flyby that has just been executed. The data used to design it come from the flyby arc, as seen in Figure 5.11. It is thus assumed that the tracking during the flyby can be performed.

The rationale of this choice is the following. The purpose of the cleanup maneuver is to remove the errors due to the flyby, bringing back the trajectory to the nominal one if the flyby is not performed perfectly. Since a keplerian hyperbola is symmetrical with respect to the focus, a correction computed with the B-Plane targeting gives a state vector that, if propagated backwards, yields the nominal flyby state. This means that a propagation forward of the nominal state (under the assumption of keplerian orbit) would give that corrected nominal state at a certain time. The problem with this logic is that of course the orbit is not keplerian; hence the optimized targeting should be applied (6.3.2) to obtain the exact correction (but targeting the future flyby and not the current). This can not done because there are no data available for a reliable propagation (as will be explained in Subsections 6.1.2 and 6.1.3). It is not possible to use the targeting (optimized and B-Plane) algorithm across a very long time span because the results would not be realistic due to propagation errors only. Thus is not even

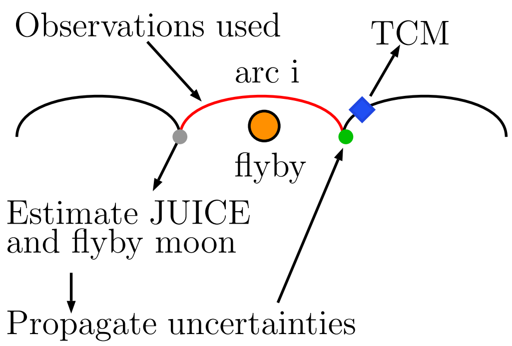

Figure 5.11: Scheme of post-flyby TCM design using only flyby, single-arc data

possible to check if the maneuver is correct or not; a further propagation up to the next flyby would be needed, to see if the errors of the previous flyby have really been corrected or not. With the current data available this can not be done (see Section 6.1). Thus a rough estimation of the cleanup maneuver is simply obtained with the B-Plane targeting algorithm.

5.3.2. Design of targeting and cleanup maneuvers using flyby, multi-arc data

This version of the algorithm is schematically shown in Figure 5.12. It uses the *data accumulation* version of the CA, specifically using observations from the flyby arcs. The assumptions used is that is possible to track the spacecraft during the flybys.
For the first flyby of the Tour the a priori uncertainties of the moons are used; for the following flybys instead the uncertainties coming from the data accumulation estimation are used. Since the targeting maneuver takes place before the flyby, it is clear that is not possible to use the results of the current estimation to design such maneuver, because it would be designed using data from the future; hence only data from the past flybys are used. The uncertainty used for JUICE comes always from the arc preceding the flyby.

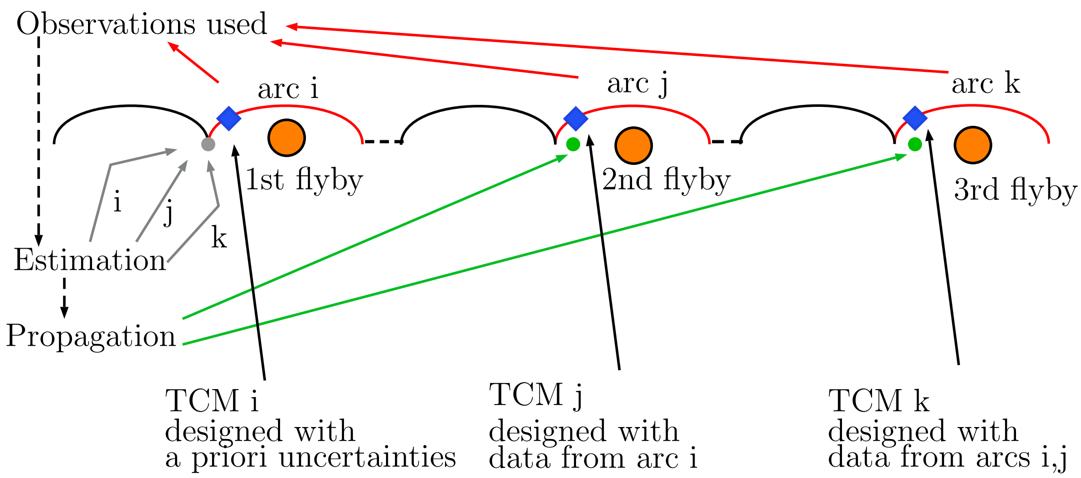

Figure 5.12: Scheme of pre-flyby TCM design using only flyby, multi-arc data

The computation of the covariance matrix is referred to the state at t_0 (the first epoch of estimation); however, since the maneuver is executed at a time different from this, the standard deviations have to be referred to the maneuver time. This is done using the covariance propagation law

$$P(t_{man}) = \Phi(t_{man}, t_0)\, P(t_0)\, \Phi^T(t_{man}, t_0)$$

In this way the standard deviations at the maneuver time t_{man} come from the information from all the previous encounters, exploiting so all the potentialities of the flyby tour rather than just a single flyby. The state transition matrix needed for this propagation can be computed a priori and then stored, since it depends only upon the dynamics of the Galilean moons; it is important to compute it respect to the right initial time

t_0. This propagation is done only for the moons uncertainty; for JUICE the uncertainty computed in the pre-flyby arc is used. Contrarily to Subsection 5.3.1, in this case the propagation is done because the global STM is available due to the data accumulation algorithm and because it is more stable since more data are used to compute the covariance matrix.
The cleanup maneuver is designed by propagating the uncertainties of the moons to its maneuver time.

5.3.3. Design of targeting and cleanup maneuvers using pre-flyby, multi-arc data

This version of the algorithm is schematically shown in Figure 5.13. It uses the *data accumulation* version of the CA, specifically using observations from the arcs before the flybys. The assumptions used is that, due to pointing requirements, is not possible to track the spacecraft during the flybys, but the tracking has to be interrupted some time before it.
For the first flyby of the Tour the a priori uncertainties are used; for the following flybys instead the uncertainties coming from the data accumulation estimation are used. However to design the targeting maneuver for the current flyby data from the past only (and not from the current estimation) are used, as in the previous case. This because the tracking can be interrupted at any time before a flyby (also a few hours before), hence it is not realistic to use those data for the current maneuver (a certain time is necessary to mission control to receive the data, perform the OD, design the maneuver and uplink it to the spacecraft). The uncertainty used for JUICE comes always from the arc preceding the flyby.
The process of propagation of the covariance matrix of the moons to the time of maneuver is the same exposed in the previous Subsection.

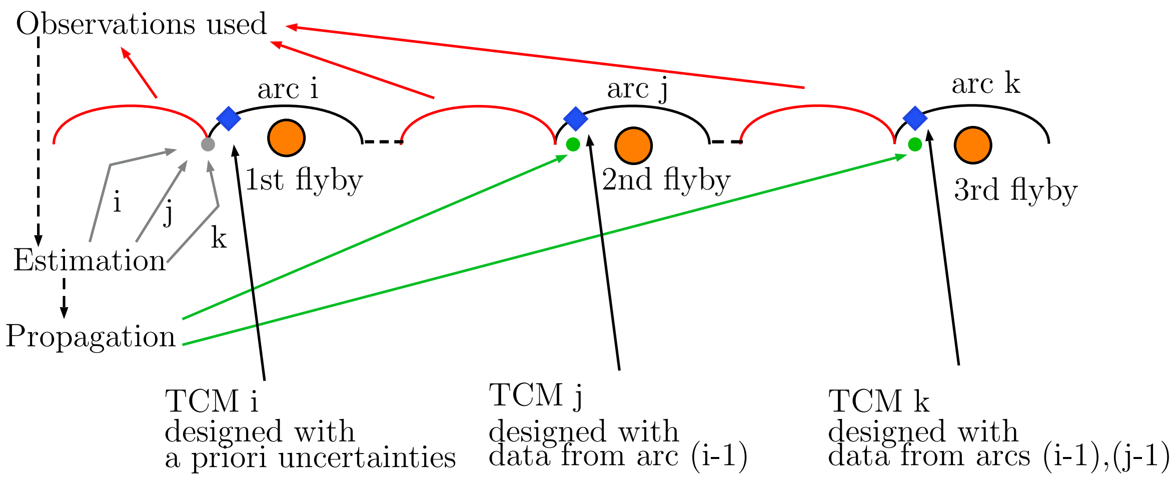

Figure 5.13: Scheme of pre-flyby TCM design using only pre-flyby, multi-arc data

5.3.4. Feasibility Control for the Navigation Analysis

A number of different checks are done in order to avoid the algorithm to crash or to provide wrong/unfeasible results that could create problems in the further step of results analysis in Matlab. These checks are the following, in order of execution in the code:

1. *check of crashing into a Galilean moon during propagation*: this can happen only when the spherical harmonics of the Galilean moons are used in the dynamical model, since in this case the Galilean moons are represented as celestial bodies with a finite radius and not as point masses.
   Since this event causes the interruption of the simulation, an exception is thrown if this happen and a file is saved, to indicate the crashing. It is noted that nothing can be done to avoid the crash on runtime, hence a simulation with a crashing is considered failed.

2. *complex values for initial standard deviations*: in some cases, the initial values for the standard deviations can be complex, which means that the results of the simulations are not valid. This is a mathematical representation of a physical problem that will be treated in Section 6.2.1. If for any of the arc of the simulation the initial standard deviations are complex values, then the simulation is interrupted and considered failed.

3. *high values for condition number*: the condition number of the normalized covariance matrix is computed for every arc of a simulation and compared to a fixed threshold value. If any condition number exceeds the threshold, then a warning is showed and a file is saved. The simulation is considered successful but the results are however considered to be inaccurate. In Section 6.2.1 this problem is explained and analyzed in more detail.

4. *failure of the guidance targeting algorithms*: as explained in Section 4.3.2, the B-Plane targeting algorithm is implemented in a cycle which ends when the tolerance on the B-Plane parameters is satisfied. It could happen in some situations that this algorithm fails (for example if the perturbation is too high and the tolerance required is too small) and hence a TCM can not be computed.
If this happens the simulation is considered failed and a flag is saved; it has to be noticed however that this almost never happened, since the algorithm is quite robust and the perturbations are never huge.

5. *optimization of the targeting maneuver*: the optimization of the B-Plane targeting algorithm can be successful or can fail. Since the optimization consists of a cycle that ends when the tolerance on the flyby position is satisfied, it can happen that this tolerance is not satisfied. In this case the simulation is still considered successful but a warning is issued, to indicate that the maneuver computed could not be optimized (it is just the one from the B-Plane targeting). Also in this case the optimization procedure showed a very good robustness.

5.4. Statistical Monte Carlo Analysis

Since the TCMs are statistical maneuvers (at least those considered in this work), they have to be simulated by means of statistical analysis; in the real mission the exact maneuver will be determined in real time from the results of the orbit determination.
The Monte Carlo (MC) method can be used to perform such analysis, from which statistical results on the ΔV will be obtained. In the Monte Carlo method, a high number of simulations is performed using different random values for the input variables of the problem. A Gaussian distribution is often used to generate the values of these variables ([56], [57], [42]) and it is used in this work.
The Monte Carlo simulation implemented has the following characteristics: a single MC simulation has fixed settings for the CA (a priori uncertainties of state, tracking data schedule) and fixed maneuver scheme (number and location). The results of the CA (the uncertainties of the spacecraft and moons positions) are sampled with a Gaussian distribution. This means that the standard deviations extracted from the covariance matrix (at each arc and independently between arcs) are randomized for a certain number of times (the number of samples of the MC, n_{MC}). Each standard deviation is randomized independently from the others, to avoid correlations; then, from the nominal trajectory, n_{MC} different perturbed trajectories are generated by applying the randomized standard deviations to the nominal trajectory. With the perturbed trajectory and the nominal one it is then possible to compute the maneuvers. In this way the CA is executed only once; what is repeated is the targeting algorithm, which has to be applied separately for every perturbed trajectory.
Similar methods have been found in literature; in [56] for example, each simulation consisted of 1000 perturbed trajectories (each perturbed trajectory is computed by sampling the covariance matrix: the variance of the state is used to generate 1000 perturbed trajectories from a nominal one). The results, for each flyby and for each perturbed trajectory, are then saved. At the end statistical information are extracted from these data. The statistical information computed are the mean, the standard deviation and the 95 % percentile for the following quantities:

- ΔV for each flyby;
- total ΔV (for the flyby tour);
- σ_R, σ_T, σ_{TCA} for each flyby. These are the orbit determination uncertainties projected in the B-Plane (and on the time of closest approach).

The 95 % percentile is computed with the *Nearest Rank Method*. This statistical indicator has the meaning that for around 95% of the cases the value of that variable will be smaller than the value of the 95^{th} percentile. The value of 95 has been chosen because it is has been found quite often in papers reporting similar analysis; it is an indicator of the worst case scenario, thus a conservative estimation of the ΔV.

6

VALIDATION

In this Chapter the process of validation of the software written and the data available (essentially the trajectory of JUICE) is presented.
In Section 6.1 a brief analysis of the data provided by ESA is shown, together with a discussion of some problems and the ways to overcome them. In Section 6.2 the validation of the covariance analysis algorithms (3.3 and 5.2) is discussed. In the Section 6.3 the validation of the guidance algorithms is discussed, together with the explanation of the procedure that brought to the improvement of the B-Plane Targeting (see 4.3 and 5.3). In the last Section (6.4) the validation of the Monte Carlo method is presented (described in Section 5.4).

6.1. ANALYSIS OF THE JUICE TRAJECTORY PROVIDED BY ESA

The nominal trajectory of JUICE together with the ephemerides of the celestial bodies used to generate it (as of March 2016) were provided by ESA. The trajectory was provided as a time history of the cartesian state of JUICE (position and velocity) with respect to the reference system Ecliptic J2000 centered at Jupiter. The ephemerides of the Galilean moons are also referred to this reference frame, while the ephmerides of the other celestial bodies are referred to the Solar System Barycenter (SSB).

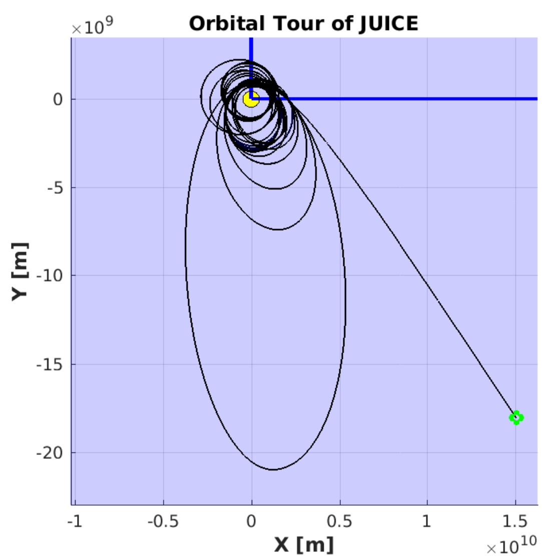

(a) [01/09/2029-02/06/2033] - Complete mission

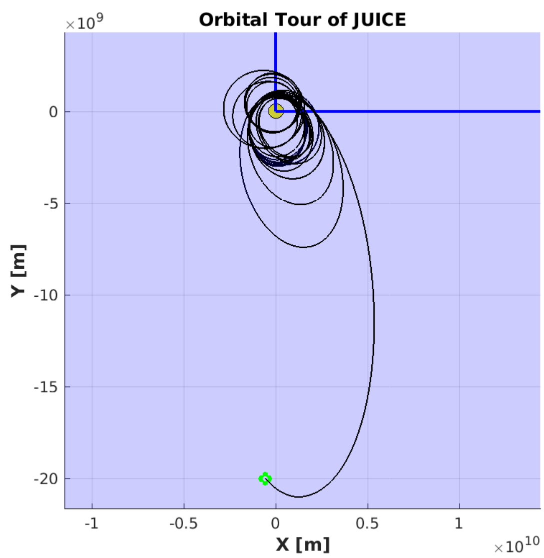

(b) [01/01/2030-01/06/2032] - Flyby Tour

Figure 6.1: Trajectory of JUICE

The time interval of the mission can be found in [1]; the different phases of the mission are the following:

the Jupiter orbit insertion is planned for 01/2030, which is also the start date for the Galilean moons tour. This tour last until the 09/2032, date of the Ganymede orbit insertion. The end of the nominal mission is planned for 06/2033. It has to be considered that the aforementioned document dates back to September 2014, while the trajectory has been received on April 2016; since the mission is still in the developments phase, it is possible that the trajectory received was different from the one described in the document. The time interval selected for the analysis is 01/2030 - 06/2032; the complete flyby tour is included and the Ganymede orbital phase is excluded. Before the Jupiter orbit insertion JUICE is in an hyperbolic orbit about Jupiter; this is shown in Figure 6.1a, where the complete orbit of JUICE that has been received is plotted in the reference frame Ecliptic J2000 (z-axis view). The arrival trajectory is a straight line, hence an hyperbolic trajectory. After the approach there is the first Ganymede flyby (G1) and then the JOI (Jupiter Orbital Insertion) maneuver, after which the orbit of JUICE becomes bounded around Jupiter, as visible from Figure 6.1b.

6.1.1. THE SEARCH FOR FLYBYS

In the official ESA document of the JUICE mission [1] a list of the flybys is not reported, but only a description of the flyby sequence; it was necessary to locate them manually from the trajectory and the ephemerides given. Figure 6.2 shows all the flybys that have been found in the time interval of the flyby tour and the relative distance JUICE-moons (from their center of mass). The threshold used for the computation of the flybys was set arbitrarily to 20,000 km (this distance represents a compromise between the sizes of the biggest and smallest spheres of influence of the Galilean moons as shown in Section 4.1).

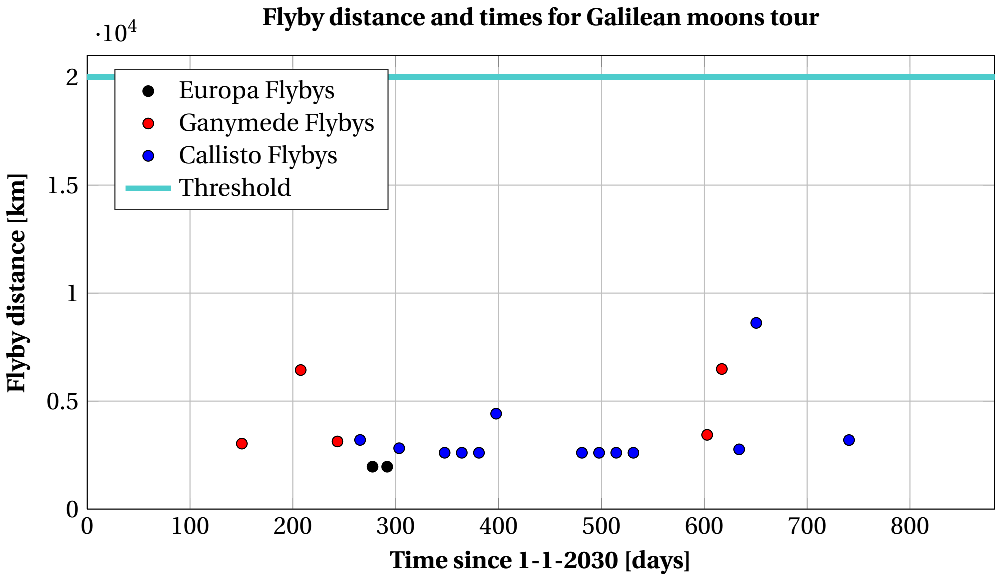

Figure 6.2: Galilean moons flybys time and distance

From a comparison of Figure 6.2 with reference [1] it is concluded that the general flyby tour is found correctly, a part for minor differences that do not spoil the navigation analysis, considering also that the mission is in the design phase.

The exact geometry of the single flybys has been verified for the first two Europa flybys, the only shown in reference [1]. In Figures 6.3 and 6.4 the geometry of the first Europa flyby is visible; the 3 planes that are shown are the Ecliptic J2000 plane, the trajectory plane and the B-Plane. Also the hperbolic orbit is plotted. The trajectory found is visually identical to the one in the reference. This can be considered a verification of the computation of the hyperbola and the B-Plane for the JUICE mission; a complete validation for the algorithms related to the B-Plane is given in 6.3.

In Table 6.1 are reported the main information for each flyby: these are the time, the distance, the altitude, the hyperbolic excess velocity and the time to closest approach (t_{TCA}, see Section 4.2) computed from the real JUICE trajectory and from the Keplerian hyperbola approximation with the formula 4.17. This time is computed from the piercing of the sphere of influence by the spacecraft until the flyby time. It is thus indicative of the duration of a flyby (which can be roughly considered the double of this time).

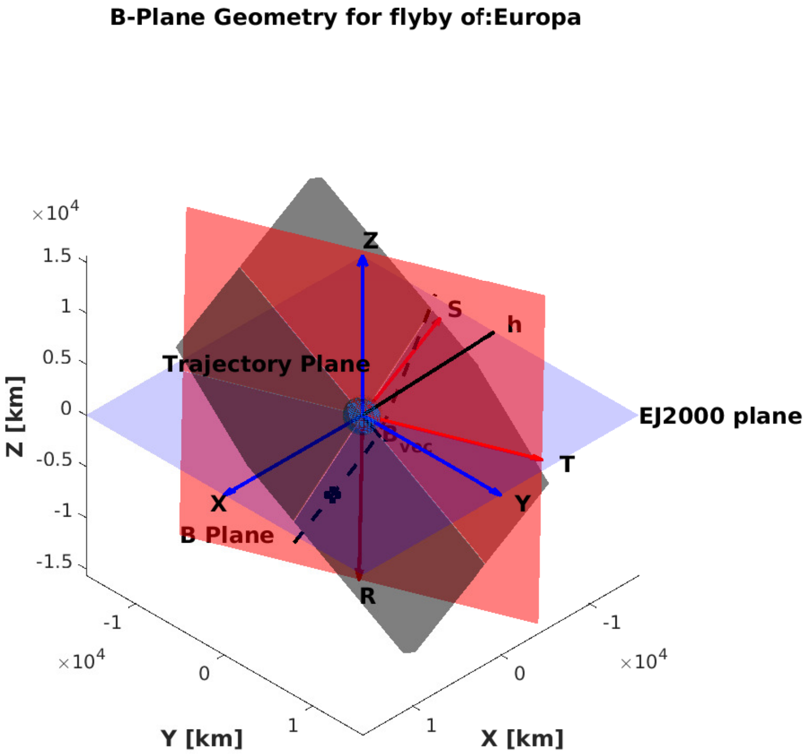

Figure 6.3: Flyby geometry, 3D view - E1 flyby

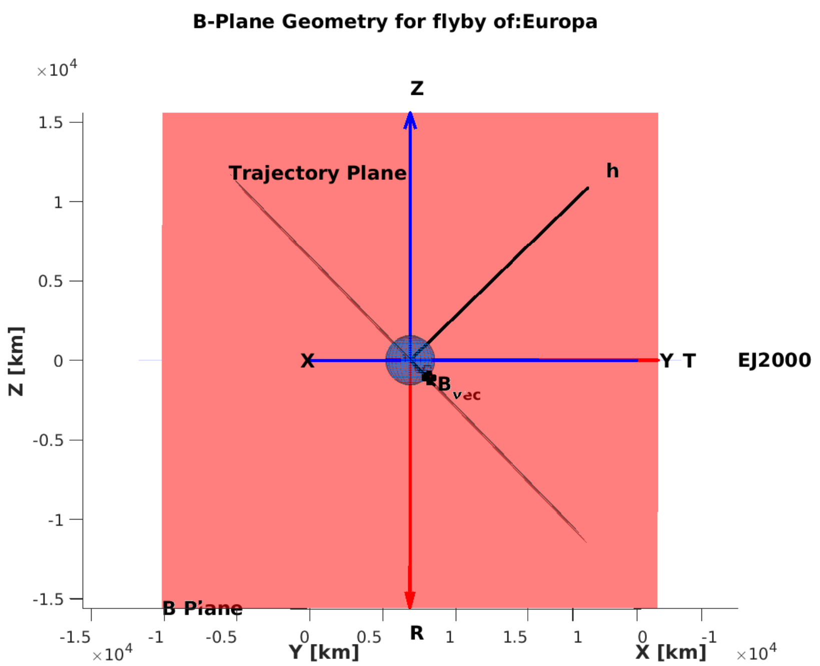

Figure 6.4: Flyby geometry, B-Plane frontal view - E1 flyby

It is possible to notice that the t_{TCA} is in general quite small; it ranges from around 40 minutes (for Europa, the smallest Galilean moon) to a maximum of 4.5 hours for Callisto (the second biggest moon after Ganymede). A single flyby of a natural satellite is thus very rapid, in contrast to the flyby of a planet which can last days. This is due to the very small sphere of influence of a natural satellite (with respect to its planet) and to the very high energetic hyperbolic orbit flown around it. This property, as will be shown in Sections 6.1.2 and 6.3.2, has to be taken in consideration for a careful analysis of the targeting algorithms; the usage of the standard algorithms has to be tailored to this characteristic of the flyby tour.

Table 6.1: Flybys parameters

Flyby	Date	Distance	Altitude	V_∞	t_{TCA} real	t_{TCA} kepler	Δt_{TCA}
-	$d-m-y$	km	km	km/s	hrs	hrs	s
E1	05/10/2030	1963	402	3.67	0.700	0.698	-4.2
E2	19/10/2030	1962	402	3.64	0.708	0.708	-1.8
G1	31/05/2030	3031	400	5.42	1.642	1.638	-11.3
G2	27/07/2030	6437	3806	5.50	1.608	1.605	-10.9
G3	01/09/2030	3131	500	5.50	1.625	1.620	-16.0
G4	26/08/2031	3437	806	3.74	2.325	2.322	-9.5
G5	10/09/2031	6486	3855	3.73	2.342	2.331	-38.4
C1	23/09/2030	3201	791	5.17	1.991	1.990	-4.5
C2	31/10/2030	2818	408	5.04	2.041	2.041	-3.2
C3	14/12/2030	2608	198	5.09	2.025	2.023	-4.2
C4	31/12/2030	2608	198	5.09	2.025	2.024	-3.2
C5	16/01/2031	2607	197	5.09	2.025	2.023	-6.0
C6	02/02/2031	4417	2007	5.11	2.008	2.006	-8.1
C7	27/04/2031	2607	197	5.09	2.025	2.022	-10.4
C8	13/05/2031	2607	197	5.11	2.016	2.015	-4.7
C9	30/05/2031	2609	199	5.11	2.008	2.008	-2.7
C10	16/06/2031	2607	197	5.13	2.008	2.007	-6.6
C11	26/09/2031	2765	355	2.17	4.425	4.417	-26.4
C12	13/10/2031	8619	6209	2.16	4.491	4.477	-51.4
C13	11/01/2032	3195	785	2.18	4.433	4.418	-52.0

Another consideration is about the approximation of the trajectory, when very close to the flyby moon, to a Keplerian hyperbola; computing the difference (Δt_{TCA}) in time to closest approach between the real one and the one calculated with the Keplerian approximation, it is possible to see that this is always quite small, ranging from -2 s to a maximum of -50 s. This means that the approximation holds quite well when inside the sphere of influence. It is interesting to notice two things: the first is that this difference is always negative, meaning that the nominal time is always an underestimation of the real time. The second is that this difference increases when the value of t_{TCA} increases; this can be justified by the fact that the nonlinearities have more time to introduce their effects. These observations will be useful in 6.3.1.

6.1.2. THE PROBLEM OF THE DYNAMICAL MODEL

The dynamical model used to design the trajectory was not available; this was a problem because in this work JUICE and the moons have to be numerically propagated for the following reasons

- to perform the CA the trajectory has to be integrated, in particular to compute the observations and the state transition matrix (see Sections 3.3 and 3.4 and Eqs. 3.14 and 3.27).
- to perform the optimized targeting (see Subsection4.3.3).

Without the right dynamical model the propagation introduces errors with respect to the nominal trajectory (the one provided by ESA); for the CA this implies that the matrices obtained will not be completely correct. For the optimization this imply that at the time of flyby there would always be some errors which are just a numerical problem. These errors can partly influence the performance of the Covariance-Navigation analysis and thus they must be quantified and possibly reduced. A procedure to search for the exact dynamical model through a trial and error integration process could be implemented, but this was not done because it would have been time demanding and because the navigation analysis can still be performed correctly, with certain assumptions. It is important that the propagated trajectory does not diverge too much from the nominal one in order to guarantee that the covariance analysis is performed on the real JUICE mission and not on a different trajectory (especially around a flyby). However, it is not necessary to reproduce the nominal trajectory with a huge accuracy (i.e. to less than 1 km); a deviation of a few tens of km is considered acceptable since the flyby will be represented quite realistically.

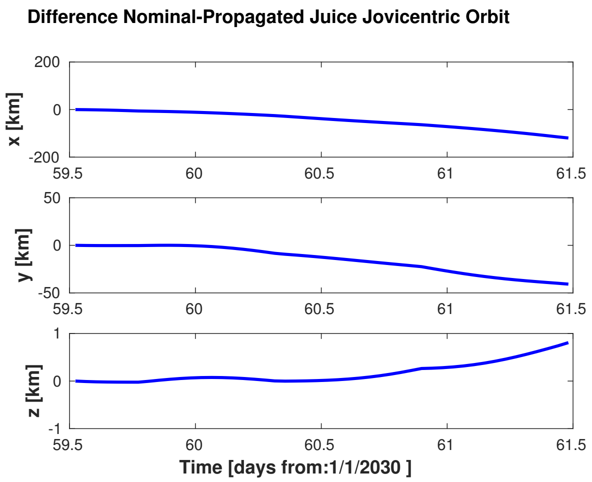

(a) Time: 2 days

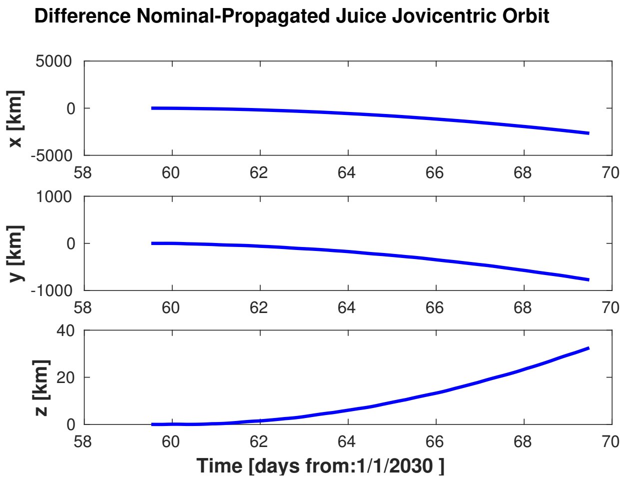

(b) Time: 10 days

Figure 6.5: JUICE Propagation - Simple dyn. model, no flyby included

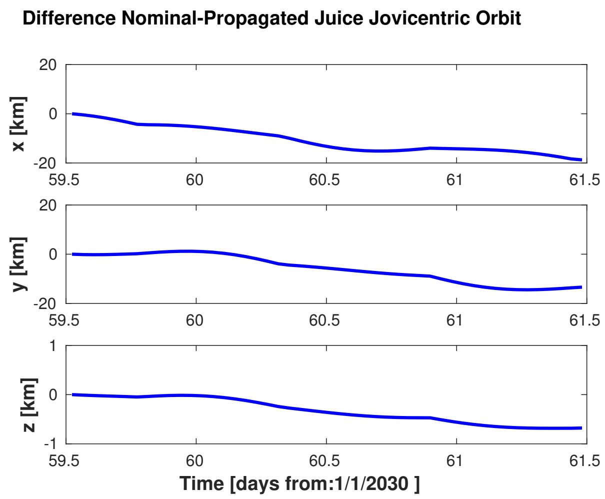

(a) Time: 2 days

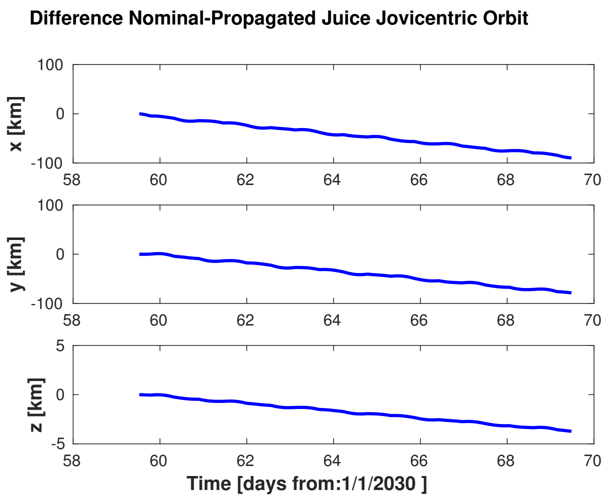

(b) Time: 10 days

Figure 6.6: JUICE Propagation - Complex dyn. model, no flyby included

To verify these assumptions, the propagation of JUICE has been compared with the nominal trajectory for a wide range of time intervals, time steps and dynamical model configurations.

In Figure 6.5 the propagation of JUICE for 2 and 10 days, with a simple dynamical model and without including any flyby is shown. The simple dynamical model includes only the point mass attractions of Jupiter and the Galilean moons; the spherical harmonics of Jupiter and the Galilean moons are not included, as well as the Sun and Saturn perturbations. The complex dynamical model includes the aforementioned perturbations; the spherical harmonics of Jupiter are included up to degree and order 4, while the ones for the moons up to 2.

The propagation with the complex dynamical model is shown in Figure 6.6.
Comparing the four plots it is possible to make the following observations: the errors increase with propagation time and for the case of simple dynamical model. This is expected because the error accumulates with time (rounding errors and truncation) and because a simple dynamical model neglects a lot of forces that play an important role. It can be seen that when a simple dynamical model is used, already after two days of propagation the error is bigger than 100 km in the x component only. After 10 days this is bigger than 3000 km in the x direction only. With the complex dynamical model these errors are more limited, to 20 and 100 km respectively. These two integrations have been done with a time step of one hour; this step can be acceptable when the spacecraft is far away from a flyby, but this is not the case anymore when approaching a Galilean moon, because the dynamic becomes really fast (as shown in Table 6.1).

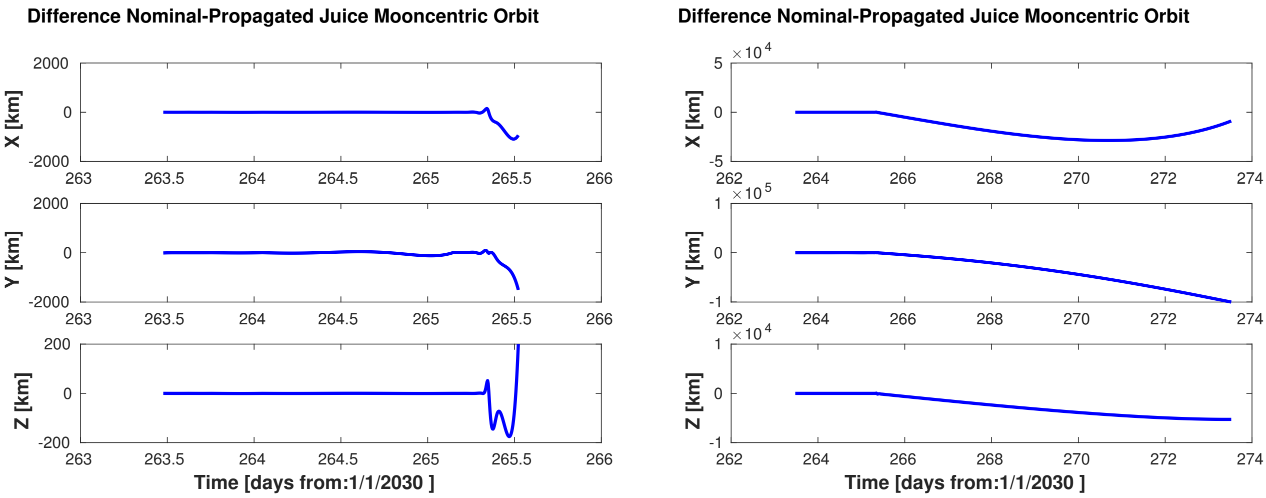

(a) Time: 2 days

(b) Time: 10 days

Figure 6.7: JUICE Propagation - Complex dyn. model, Callisto flyby included, time step 3600 s

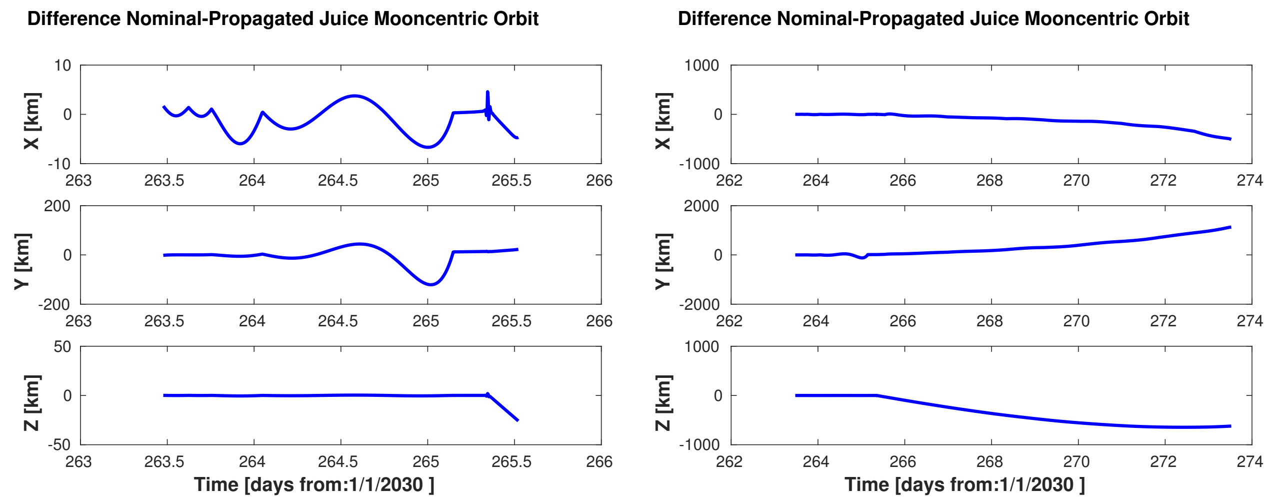

(a) Time: 2 days

(b) Time: 10 days

Figure 6.8: JUICE Propagation - Complex dyn. model, Callisto flyby included, time step 600 s

Figure 6.7 shows the propagation around a flyby (of Callisto). It is clearly visible the effect introduced by the flyby: the trajectory diverges of thousands of km after it. Two actions have been taken to correct for this error: the reduction of the arc duration around a flyby and the reduction of the time step. A suitable time step around a flyby is of maximum 1200 s, but preferably of 600 s. A smaller time step causes an excessive computational overload, while a bigger time step still cannot represent faithfully the dynamics. In Figure 6.8 is shown the same propagation of Figure 6.7 but with a time step of 600 s. It can be seen that the improvement is net: with a time step of 3600 s the maximum deviation is of ~ 1000 km while with a time step of 600 s the maximum deviation is of ~ 50 km, for a propagation time of two days. For a propagation of 10 days these deviations increase to 10,000 km and 1,000 km respectively. Although is not possible to represent exactly the nominal trajectory a lot of days after a flyby even with a small time step, until a few days after it the deviation is limited and before it is really small. Hence in the multiarc analysis an arc must be chosen of a few days (e.g. 6, 8) around a flyby (Section 5.2) to limit this effect. Figure 6.9 is a visualization of the orbit of JUICE with respect to Callisto for a propagation time of 10 days, with time steps of 600 s and 3600 s. From this plot is clearly visible the net improvement coming from a smaller time step.

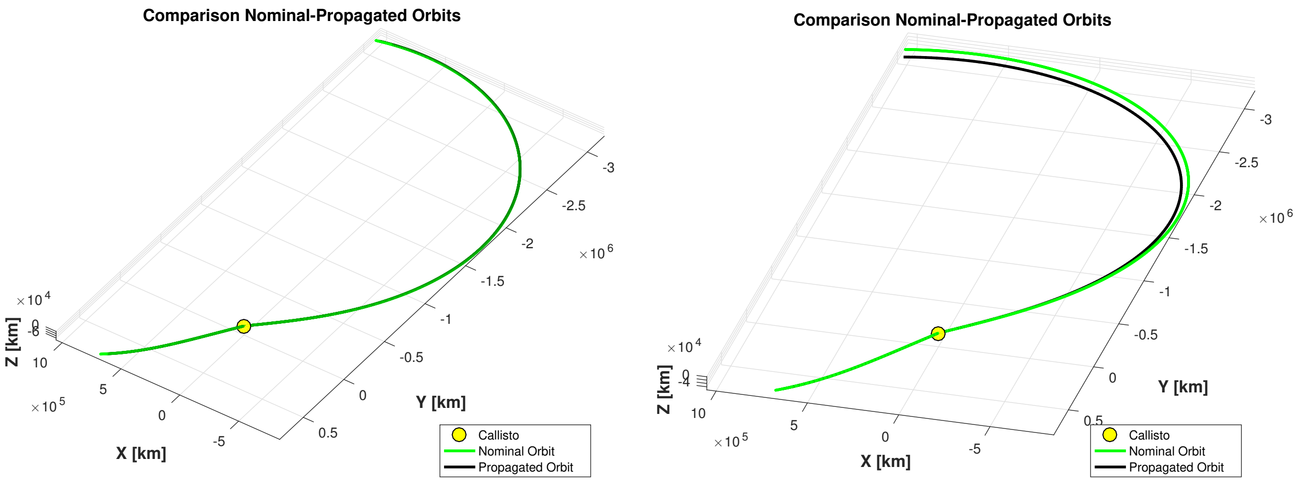

(a) Time step: 600 s

(b) Time step: 3600 s

Figure 6.9: JUICE Propagation - Complex dyn model, Callisto flyby included, time: 10 days

Moreover, the use of a small step size is mandatory when using a complex dynamical model for another reason; when representing the Galilean moons with spherical harmonics, they are considered as celestial bodies with a finite radius. Hence during the propagation of JUICE it is possible that the spacecraft impacts the flyby moon if the integration error becomes bigger than the flyby altitude (in the direction of the moon). If this happens the simulation crashes; to minimize this risk a small time step must be used to decrease the propagation errors at flyby.
It has been demonstrated that using a complex dynamical model with a small time step gives the best reproduction of the trajectory; however this is also more computationally expensive than using a simple model with a bigger time step. Most of the simulations will be run with a simple model using a small time step (600-1800 s), to reduce the computational time, since a high number of simulations has to be performed.

6.1.3. THE PROBLEM OF THE MANEUVERS

The data on the maneuvers performed by JUICE (times and magnitudes) were not available. For the same reasons of the dynamical model, they should also be included in the propagation of JUICE. It was not possible to overcome this limitation, but the only thing that could be done was to search for them and understand their influence on the process.

Using the cartesian state history of the JUICE with respect to Jupiter and knowing that the maneuvers are impulsive (due to the high-thrust engine), the only possible way to try to locate the maneuvers was to inspect the plot of the velocity with respect to time. Two plots were used, the magnitude of the velocity with respect

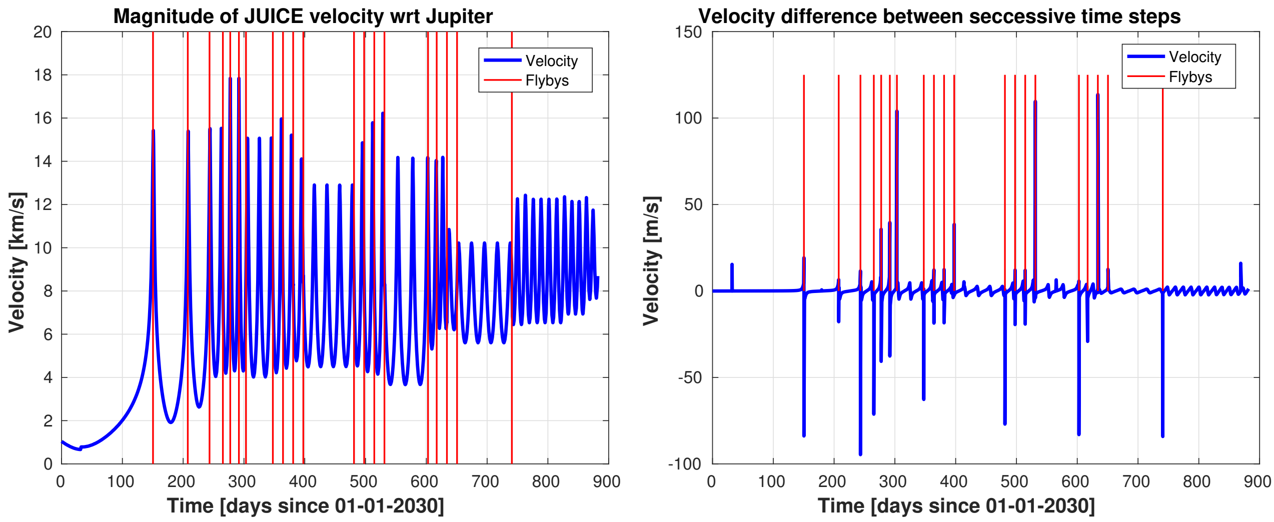

(a) Velocity magnitude

(b) Velocity differences

Figure 6.10: Velocity plots for the maneuvers search

to time and the difference between the velocity at one time step and the preceding one. The plot were visually inspected in search for anomalous peaks since it was not possible to set a criteria to discriminate a "natural" ΔV (due to the natural evolution of the orbit) from an artificial ΔV.
In Figure 6.10a is shown the magnitude of the velocity of JUICE; the flyby times are also plotted (red lines) since the velocity has a rapid change due to the gravity assist effect (it is necessary to discriminate the effect of a gravity assist from an impulsive maneuvers, since they can be quite similar). In this plot not all the local maximum correspond to flyby; most of them are just pericenter passages of JUICE, where the velocity is maximum.
In Figure 6.10b is shown the difference of the magnitude of the velocity between subsequent time steps; on the left of the plot, at around 32 days after the beginning of the flyby tour, is clearly visible a maneuver that is practically instantaneous. The maneuvers found are reported in Table 6.2.

Table 6.2: Maneuvers found

Days since 01/01/20130	Magnitude [m/s]
32.15	15
179.50	0.7
413.65	5.5
565.50	6
869.00	16
Total	43.2

The total ΔV found is 43.2 m/s during the flyby tour (as selected by fixing the initial and final date). This is comparable with what found in [1] but not completely correspondent; there is indicated that the ΔV from G2 to GOI (Ganymede Orbital Insertion) is of around ~ 150 m/s. The two reasons of this difference are that the GOI maneuver is excluded from the search and that this method could have failed (especially if a maneuver is not really impulsive but with a finite duration then it is difficult to find it).

Regarding the maneuvers found in Table 6.2, they are all quite far away from flybys (around 15-20 days minimum), hence it can be assumed that they do not create problems when analyzing an arc close to a flyby since they are excluded from the propagation interval. The effect of a maneuver on the integration of JUICE is show in Figure 6.11 where the nominal cartesian state of JUICE is compared to the propagated cartesian state of JUICE, selecting a time interval that includes a maneuver (but without including this maneuver in the propagation). It is clearly visible the effect of the maneuver: the difference propagated-nominal orbits is practically negligible (or at least smaller than 10^4 km) until the maneuver time and it increases very rapidly

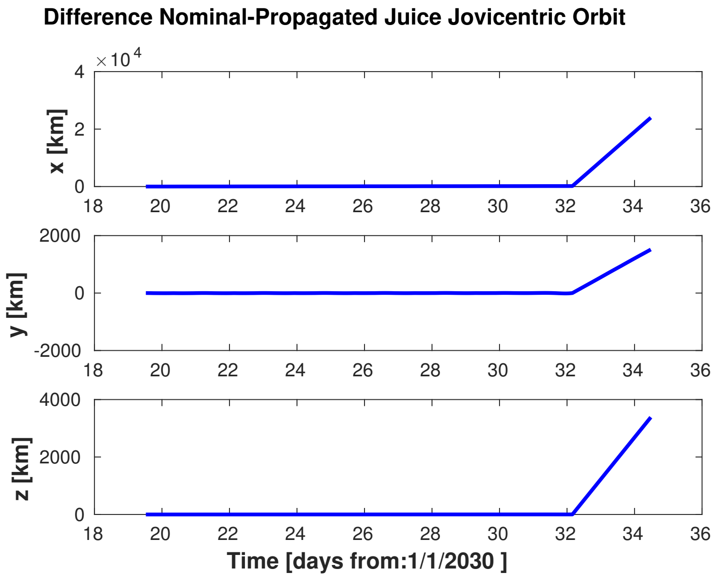

Figure 6.11: Effect of neglecting the maneuvers in the propagation

just after it. The trajectory of JUICE diverges completely from the nominal one after the maneuver and this divergence increases with time.

6.2. Covariance Analysis algorithms

Regarding the validation for the Covariance Analysis (see 3.3 and 5.2), this was not strictly necessary because the main algorithms used were already available in Tudat, hence they are already validated. However it was necessary to validate the new functions written for the CA. The process of validation is described below for each new function that was written.

1. computation of arcs subdivision: the validation of this algorithm consisted essentially in reproducing Figure 5.3. Since there are twenty flybys, the division is not done manually but with an algorithm that uses three different parameters (nominal arc duration, flyby arc duration, minimum arc duration). This algorithm has been tested in TUDAT to verify that the arc subdivision that it computed was in agreement with the chosen parameters. A plot is generated with the start and end times of the arcs; it is then inspected to verify the subdivision. In Figure 6.12 is shown a zoom of one of these plot, where the green lines represents the start and end times of the arc and the dots represent the flyby moon. The inspection of these plots revealed very often a feasible arc subdivision.

2. generation of observation times: for the validation of the algorithm that generates the observation times (represented in Figure 5.4) a simple computation in Matlab was executed with the parameters that rule the generation of the observation times vector (frequency of observations, total hours per day, days per week for VLBI and days of interruption before a flyby for optical data). The total number of observations was computed from these parameters, for the interval of interest. In Tudat the number of observations is shown; these two numbers were compared to check if the algorithm that generates the observation times works in accordance to the specifications. It has to be noticed that in Tudat this algorithm works with a cycle that uses tolerances on time, because of the modifications on the tracking schedule introduced by the flybys. Hence the results were not expected to be identical to Matlab, where no tolerances were used, but exact formulas. The results confirmed that the algorithm that generates the observation times works well, both for the flyby and non-flyby arcs.

3. setting of the a priori covariance matrix: the validation of this function consisted simply in inspecting the a priori covariance matrix for each arc (saved in a file) and check if the values correspond to the one specified. This simple validation gave positive results, guaranteeing that the a priori covariance matrix loaded in Tudat is exactly the one desired. An identical procedure is done for the weighting matrix.

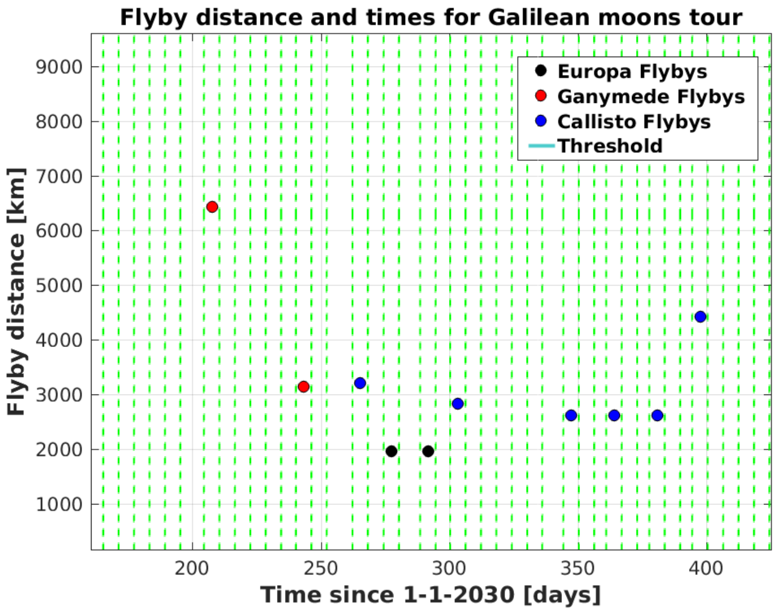

Figure 6.12: Validation of arcs subdivision algorithm

For the validation of the results of the CA, it is not really possible to have a complete validation of them, because there are not examples completely reproducible. This because is not known a reference where all the parameters and assumptions used to generate certain results are reported; hence is not possible to reproduce exactly a certain CA.

Thus to validate the CA results have been generated for similar configurations of CA found in literature; the reference taken is [26], where extensive covariance analysis are conducted. It is noted however how in that case the simulations include only the estimation of the Galilean moons and not JUICE, contrarily to what done here; moreover, the Ganymede phase of the JUICE mission is also included. Another difference is that in [26] the moons are directly observed with radio tracking and the uncertainty about the orbit of JUICE is added to the data weights; in this Thesis instead only JUICE is directly observed. Due to these and other differences it is not expected to obtain the exact same results, even if using the same weights for the measurements and a priori uncertainties. The results obtained (uncertainties of the moons and their behavior with respect to data types and accuracies) are of the same order of magnitude to the ones of the paper; some behaviors are not the same, due to the different CA configurations.

All the results of the Covariance Analysis will be extensively analyzed in Chapter 7; the conclusion for the validation is that the software written shows overall a quite realistic behavior of the true orbit determination for interplanetary mission, even with the necessary approximations and limits (Section 5.1). However, as it will be seen in 7.2, the results obtained are often optimistic.

6.2.1. Feasibility control for the Covariance Analysis

The CA depends upon a great number of parameters, as it is shown in Table 5.1; they have an influence on the results in different ways. A problem that can be encountered is that the simulation does not converge (as stated in Subsection 5.3.4); this means that the results are not valid, hence the particular set of parameters used for that simulation (for example tracking schedule of measurements, data weights) is not feasible. The two indicators of the validity of a simulation are

- the numerical type of the estimated standard deviations (extracted from the estimated covariance matrix) which can be real or complex. The problem is when there is at least one standard deviation (corresponding to a parameter) that is complex. This is a mathematical issue of the algorithm that indicates an ill-posed problem;

- condition number of the (normalized) estimated covariance matrix.
  The condition number of a matrix A is defined as

$$k(A) = \frac{\sigma_{max}(A)}{\sigma_{min}(A)}$$

where $\sigma(A)$ are the singular values of the matrix A.

The meaning of the first indicator is the following. Since the covariance matrix has in the diagonal the standard deviation squared of the estimated parameters, these values have to be positive quantities in order to give real standard deviations. In case of negative diagonal elements, the standard deviations would be complex values, hence losing of physical meaning (since they represent the errors of the estimated parameters). However, from a mathematical point of view, this matrix can have negative elements on its diagonal due to its computation process (Eq. 3.22). The inverse of the a priori covariance is selected by the user and hence it satisfies the condition of non-negative diagonal elements. But due to the other terms there is no guarantee that the computed covariance matrix will have positive diagonal elements.
For simple applications of the Covariance Analysis, with few parameters to be estimated and few observations processed, the algorithm is very stable and performs correctly; this is not the case for the current application, where is common to have from hundreds to thousands of observations (to simulate the continuous tracking of a deep space mission) and where plenty of parameters are estimated, some of them not measured directly.
This has been observed to happen in particular when the schedule of the tracking data is too dense and/or their accuracies are also very high (for the case of concurrent estimation of JUICE and the moons). The effect can be interpreted as a too optimistic estimation of the standard deviations: due to this great amount of data the errors on the positions are constrained to very low levels (even cm or mm). When approaching zero (meaning no uncertainty on the position) the final effect can be that the standard deviations become complex, thus indicating overly optimistic errors estimations.
The second indicator, the condition number, is representative of the different orders of magnitude of the elements of the covariance matrix. It is important to notice that this operator is applied to the normalized covariance matrix, since the absolute magnitude of the standard deviations depend on the type of parameter and its measurement unit, and it would be meaningless to compare different type of parameters (e.g. an error of 10 km on the position of a planet has not the same importance of an error of 10 km/s on the velocity of a spacecraft).
It is desired to have a condition number as low as possible, which represent a reliable estimation of the standard deviations of the different parameters. A very high condition number indicates that the solution is not defined with a good quality, with the given set of measurements ([32]); the problem posed is not well defined (it is difficult to estimated the required parameters with that number and accuracy of the observations). The consequence is that the values obtained may have significant numerical errors (since the condition number plays a role in the process of matrix inversion) and are not representative of the true uncertainties.
In literature ([26], [36]) it is found that high condition numbers (up to $10^{14} - 10^{16}$) are typical in spacecraft and planetary estimation problems, especially if a Cartesian representation of the state is used. This is the case in Tudat, where the integration and estimation is done in Cartesian coordinates. The value of 10^{16} has be chosen as threshold to consider a simulation successful.
Another reason for high condition number is the ill-posed problem represented by the orbit determination of a spacecraft around another planet during short arcs ([61]); this is due to the particular geometrical configuration of the problem.
There are however some actions that is possible to take to counteract this problem; the two most effective remedies, as found in literature ([36]), are to reduce the weights for the radiometric measurements, use optical data and modify the a priori covariance matrix of the parameters. These actions should in general stabilize the solution, giving more often feasible results (real standard deviations) and lower condition numbers.

The two issues happen in different ways depending upon the different versions of the CA (see Section 5.2). For example, when estimating only JUICE these problems were rarely encounter; the condition number is very often under 10^6, indicating a good accuracy.
Instead when estimating together JUICE and one or more moons (as done in this Thesis) these problems are more common; in particular the estimation of a single moon together with JUICE does not cause very high condition number (around 10^{10}). The estimation of all the four moons causes higher condition number (around 10^{14}). Another element that influences the convergence is the estimation arc (see Fig. 5.5 and 5.6): it is more difficult to obtain convergence during a flyby arc rather than during the arc preceding a flyby. The length of the estimation arc influences too the convergence of the estimation. Some examples are given in Section 7.2.

It was not guaranteed thus that every combination of data weights, schedule and arc durations would provide feasible results; hence a grid search has been performed to find feasible combinations of parameters. The intervals used for search of feasible sets of parameters come from literature. The results presented in this Thesis use combinations of parameters that satisfy the convergence criteria.

6.3. Guidance algorithms

In this Section the validation and verification for the guidance algorithms is presented. Firstly, the computation of the B-Plane parameters (see 4.2) from a cartesian trajectory has to be validated, followed by the validation of the B-Plane Targeting algorithm (see 4.3.2). Theey are exposed in Subsection 6.3.1. This algorithm is initially validated for a Keplerian trajectory, but since it will be applied to a non-Keplerian trajectory (the one of JUICE) it has to be validated also for this case. This process will result in the optimization targeting presented in Subsection 4.3.3. The validation of this optimizer is described in Subsection 6.3.2. The last Subsection 6.3.3 presents the validation of the approximated targeting algorithm (see 4.3.4).

6.3.1. Validation of the B-Plane targeting algorithm

The initial verification of these algorithms has been done with the results found in the paper [46]; this was the only reference found with quantitative values of the Kepler elements used to compute the B-Plane, the B-Plane targeting algorithm and the associated results. They are reported in Table 6.3.

Table 6.3: Nominal Kepler elements used for the B-Plane algorithms verification

Parameter	Symbol	Unit	Value	
Gravitational parameter	μ	km^3/s^2	4903	
Periapsis altitude	h_p	km	1000	
Eccentricity	e	$-$	1.1	
Inclination	i	$^\circ$	45	
Longitude of ascending node	Ω	$^\circ$	30	
Argument of perigee	ω	$^\circ$	90	
True anomaly	θ	$^\circ$	-146.09038	
Results				
			Paper	Obtained
B vector (T comp)	B_T	km	11578	11578.407
B vector (R comp)	B_R	km	-4824	-4823.539
Time to close approach	t_{TCA}	s	92558	92558.204

The results of the implemented B-Plane computation algorithm are in complete agreement with the results in literature, with negligible differences due to the different values of the Moon radius (used to compute the semi-major axis of the orbit from the periapsis altitude, which was not specified in the paper). The implementation of the algorithm is thus considered correct.
Before proceeding with the verification of the B-plane targeting, the verification of the computation of the Jacobian matrix for this algorithm has to be done; the only reference found is the plot of Figure 4.6, which shows the linearity interval for the partial derivatives of the B-Plane parameters with respect to the velocity perturbation used to compute the partials. Similar plots have been reproduced and are shown in Figure 6.13.

These plot are of course different from the ones in Figure 4.6, because they are computed with different reference orbits. However they have the same behavior, thus confirming the hypothesis of well behaved partial derivatives for certain values of velocity perturbations. This range of linearity of the partial derivatives is found for velocity perturbations of $\delta V = \left[10^{-14} - 10^{-2}\right]$ km/s. Thus to obtain accurate partial derivatives, a velocity perturbation inside this interval has to be used; the value selected is of 10^{-10} km/s.

For the verification of the B-Plane targeting algorithm, it is not possible to obtain the same values of the reference [46] because a random perturbation is applied to the original cartesian state to compute the targeting; although the perturbed B-Plane parameters are reported, they cannot be obtained without the knowledge of the perturbed cartesian state used to generate them, and this was not available. But the order of magnitude of the perturbation is reported: 200 km (1 σ) error on the position and a 10% error on the velocity. It is thus possible to apply a similar perturbation and verify if the results are of the same order of magnitude of

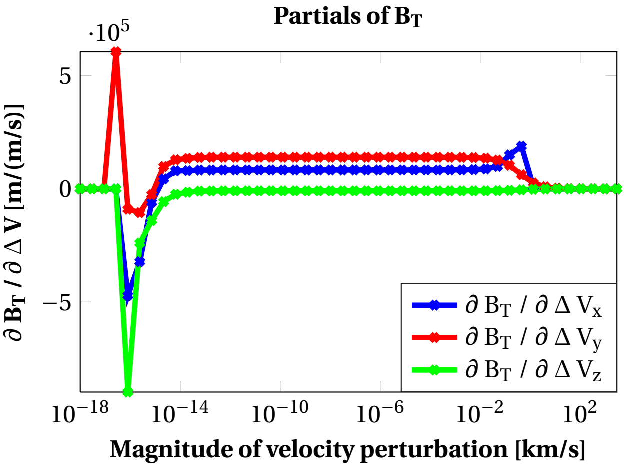

(a) B_T

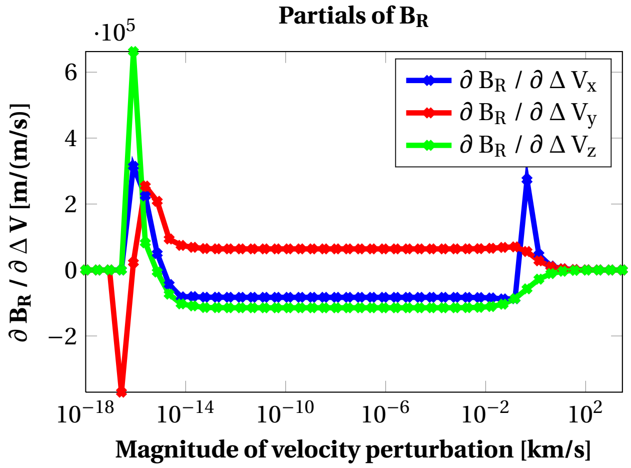

(b) B_R

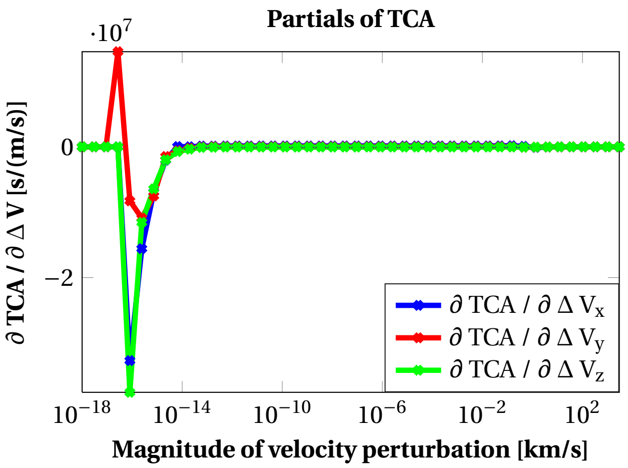

(c) TCA

Figure 6.13: Partials for B_T, B_R and TCA

the ones in the reference; moreover, to verify the effectiveness of the targeting, the B-Plane parameters can be recomputed using the corrected cartesian state (obtained applying the results of the targeting algorithm). If the recomputed parameters are identical to the nominal ones then the targeting has been successful.
In the reference the computed correction is of $\Delta V = 0.107$ km/s, obtained after 5 iterations (the tolerance used is not indicated). Executing the targeting for 10 times, each time with a different initial condition, gives a mean ΔV of 0.058 km/s with a median number of iterations of 3 and a standard deviations of 0.02 km/s. The perturbed state corrected with this ΔV (with the correspondent vectorial one) gives the correct nominal B-Plane parameters, satisfying the tolerance set (of 1 m and 1 s). The implementation of the targeting algorithm is thus considered verified.

The verification of the algorithm for a Keplerian orbit was straightforward; however, since the orbit of JUICE is highly non-Keplerian, the application of the B-Plane targeting algorithm in this case can be problematic. An analysis to understand under which conditions is possible to use this algorithm for the strongly perturbed orbit of JUICE has been performed. The result of this analysis is that the B-Plane targeting is not good enough and the optimized targeting algorithm (see 4.3.3) must be used.

Comparison of nominal orbit with Keplerian hyperbola
A comparison between the nominal trajectory at flyby and the Keplerian hyperbolic orbit computed at flyby can be done to see how much these two trajectories deviate from each other. The nominal trajectory is the real trajectory of JUICE as obtained by the files, while the Keplerian hyperbolic orbit is computed with the state of JUICE at SOI.

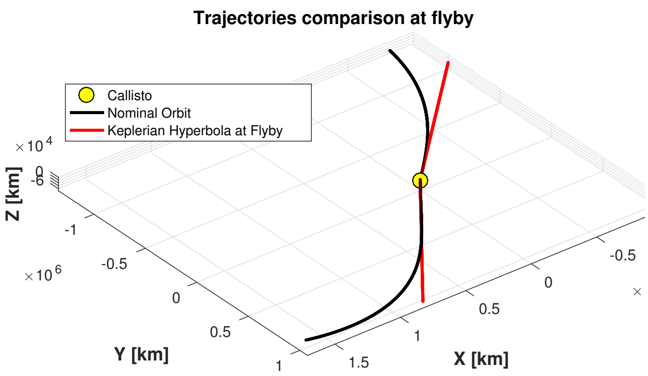

(a) Plot of orbit

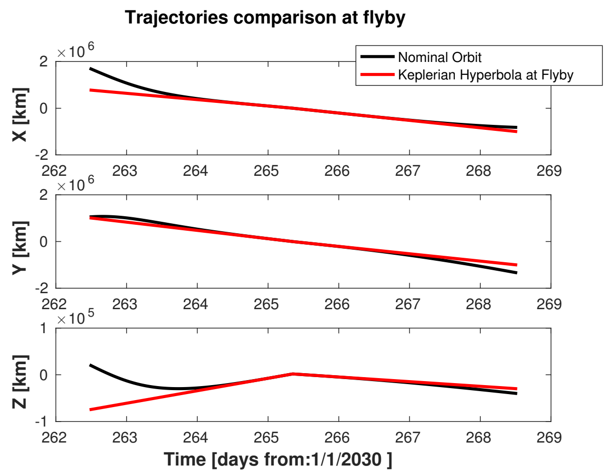

(b) Cartesian components of position

Figure 6.14: Comparison of nominal trajectory of JUICE with Keplerian hyperbola at flyby

From Figure 6.14 is possible to see that the Keplerian hyperbola deviates substantially from the real trajectory, as expected. In particular, the two trajectories are very similar around the flyby time (265.34 days from 01/01/2030), roughly for half a day before and after the flyby time. Outside this time they deviate considerably; this is normal considering that the sphere of influence of the Galilean moons is really small, hence the hyperbolic approximation is valid only for a limited interval.

Comparison of state transition matrix
Another comparison that can be done between the nominal trajectory and the Keplerian hyperbola is on the state transition matrix (STM), in particular on the portion that includes the partial derivatives of the position with respect to the velocity. The state transition matrix is computed from the maneuver time until the flyby time; the sensitivity of the position to the velocity is computed as (for the x component)

$$\frac{\partial x}{\partial V}_{rss} = \sqrt{\frac{\partial x}{\partial \dot{x}}^2 + \frac{\partial x}{\partial \dot{y}}^2 + \frac{\partial x}{\partial \dot{z}}^2}$$

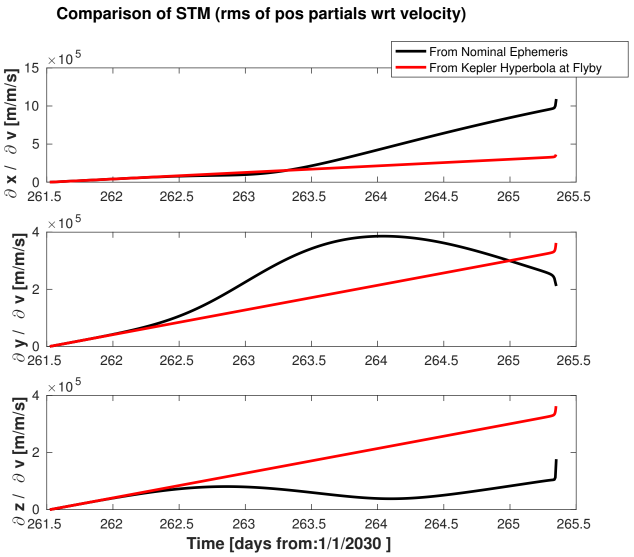

(a) Time from flyby: 4 days

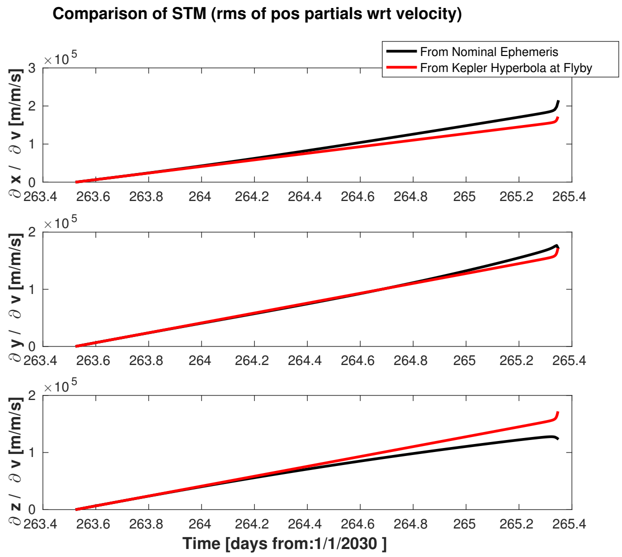

(b) Time from flyby: 2 days

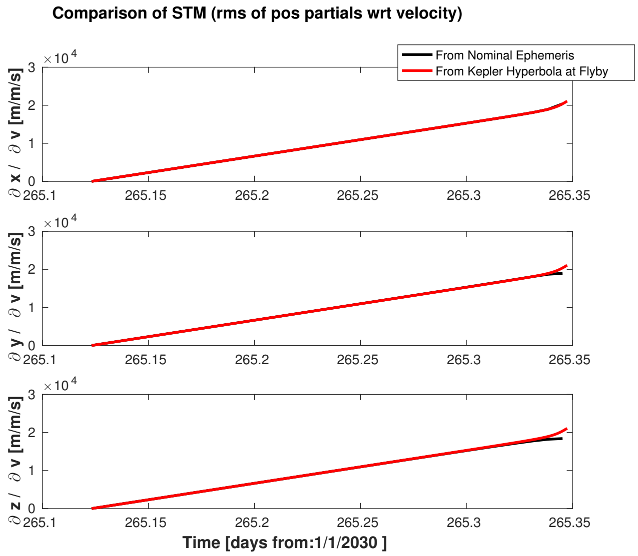

(c) Time from flyby: 4 hours

Figure 6.15: State Transition Matrix comparison

From Figures 6.15 is possible to see that the STM are quite different when far away from the flyby, diverging completely after some days of propagation (3-4). Until 2 days from before a flyby the difference is still quite low and up to a few hours before a flyby the two portions of the matrices are practically identical.

This is a first confirmation that the B-Plane targeting algorithm can be used with no problems for a non-Keplerian trajectory until a few hours before a flyby (ideally inside the SOI), but there can be problems for its application outside the SOI. Considering that the typical pre-flyby maneuver time is of 3 days [42], it is essential to perform a deeper investigation on the usage of this algorithm to ensure its effectiveness.

Comparison of B-Plane targeting applied to Keplerian and Non-Keplerian trajectories

The last comparison to be done is on the application of the B-Plane targeting algorithm to the nominal and Keplerian orbits when both are perturbed by the same perturbation. In this way is possible to compare the performance of the B-Plane targeting for the two different orbits, perturbed exactly in the same way.
The procedure is the following: at the time of maneuver (t_{man}) the nominal and keplerian state are perturbed with an identical perturbation ($\boldsymbol{\sigma}$)

$$\mathbf{x}^*_{nom} = \mathbf{x}_{nom} + \boldsymbol{\sigma} \tag{6.1}$$
$$\mathbf{x}^*_{kep} = \mathbf{x}_{kep} + \boldsymbol{\sigma} \tag{6.2}$$

The B-Plane parameters for the nominal (non-Keplerian) and keplerian trajectories (both perturbed and unperturbed) are computed and their difference is evaluated

$$\delta\mathbf{B}_{nom} = \mathbf{B}^*_{nom} - \mathbf{B}_{nom} \tag{6.3}$$
$$\delta\mathbf{B}_{kep} = \mathbf{B}^*_{kep} - \mathbf{B}_{kep} \tag{6.4}$$

The $\Delta\mathbf{V}$ is then computed for both the trajectories using the B-Plane targeting algorithm (4.3.2)

$$\Delta\mathbf{V}_{nom} = \Delta\mathbf{V}(\mathbf{x}^*_{nom}, \mathbf{x}_{nom}) \tag{6.5}$$
$$\Delta\mathbf{V}_{kep} = \Delta\mathbf{V}(\mathbf{x}^*_{kep}, \mathbf{x}_{kep}) \tag{6.6}$$

This procedure has been tried for different flybys and the results have been compared. In Table 6.4 are shown the results for two flybys, when varying the maneuver time (indicated in hours from the flyby); only two are shown since the trend is always very similar.

It is possible to see that the perturbations in the B-Plane parameters are very similar when the perturbation is applied until around 10 hours before the flyby time; also the ΔV for the nominal and keplerian orbits is practically identical until this time. Instead, when going more far away from the flyby time the differences start to increase, showing the different effect of an identical perturbation applied to the two different orbits (in complete accordance with what seen in the previous paragraph). This is another confirmation of the fact that is reliable to use the B-Plane targeting when close to a flyby but its usage outside the SOI is not completely correct for non-keplerian trajectories. However, it is difficult (and not required) to find the exact time until when this use is allowed; there is not a clear limit, the transition is quite smooth.
An observation has to be made: when computing the B-Plane parameters for the Keplerian and non-Keplerian orbits, their values are quite similar only inside the SOI but they diverge completely outside the SOI, arriving to differences of more than 500 % (for example two days before the flyby). So, even if the deviations $\delta\mathbf{B}$ are similar for the keplerian and non-keplerian orbits, the nominal values to which they refer may be very different. Hence, when computing the targeting for a non-keplerian trajectory well outside the SOI, the B-Plane parameters that are targeted are not the real ones of the actual flyby, because their computation is not accurate.

To understand the real effect of the B-Plane targeting on a non-keplerian trajectory, the integration of the equations of motion of JUICE under all the forces taken into account is done. The procedure is the following: at the time of maneuver (t_{man}) the corrected trajectory is computed with the B-Plane targeting (see Subsection 4.3.2, Eq. 4.31) from the nominal (non-Keplerian) and perturbed trajectories. Then all the three trajectories are propagated until the flyby time and compared.

$$\mathbf{x}_{nom}(t_{man}) \longrightarrow \mathbf{x}_{nom}(t_{flyby}) \tag{6.7}$$
$$\mathbf{x}_{pert}(t_{man}) \longrightarrow \mathbf{x}_{pert}(t_{flyby}) \tag{6.8}$$
$$\mathbf{x}_{corr}(t_{man}) \longrightarrow \mathbf{x}_{corr}(t_{flyby}) \tag{6.9}$$

It is noticed that $\mathbf{x}_{nom}(t_{flyby})$ is the state at flyby obtained by the propagation of the nominal state at the time of maneuver, but is different from the nominal state taken at flyby time (the state that can be retrieved from files). It is chosen to use as the nominal state the result of the propagation in order to rule out the spurious effects introduced by the propagation with an inaccurate dynamics (Subsection 6.1.2); in this way the

Table 6.4: Comparison of B-Plane targeting applied to keplerian and non-keplerian trajectories

Trajectory type	t_{man} [hrs from t_{flyby}]	δB_T m	δB_R m	δt_{TCA} s	ΔV m/s
First flyby (Europa)					
non-kep	1	-36.5	236.6	-0.3	0.336
kep	1	-38.7	236.8	-0.3	0.336
non-kep	2	-109.0	251.0	-0.3	0.179
kep	2	-115.0	252.0	-0.3	0.180
non-kep	4	-227.0	291.0	-0.4	0.098
kep	4	-264.0	293.0	-0.4	0.100
non-kep	10	-130.0	405.0	-0.5	0.057
kep	10	-137.0	442.0	-0.5	0.053
non-kep	24	-322.0	612.0	-0.2	0.047
kep	24	-738.0	890.0	-0.7	0.037
non-kep	36	-1567.0	856.0	-0.1	0.044
kep	36	-2621.0	1271.0	-0.9	0.033
non-kep	48	-2464.0	1030.0	-0.03	0.044
kep	48	-3504.0	1632.0	-1.1	0.033
Second flyby (Europa)					
non-kep	1	544.0	247.0	-0.5	0.880
kep	1	542.0	248.0	-0.5	0.880
non-kep	2	452.0	-230.0	-0.6	0.470
kep	2	442.0	-234.0	-0.6	0.470
non-kep	4	316.0	-196.0	-0.6	0.251
kep	4	246.0	-209.0	-0.6	0.249
non-kep	10	-4.0	-51.0	-0.6	0.119
kep	10	-201.0	-122.0	-0.7	0.113
non-kep	24	-1001.0	421.0	-0.6	0.072
kep	24	-1310.0	134.0	-0.9	0.062
non-kep	36	-2380.0	849.0	-0.4	0.061
kep	36	-2259.0	375.0	-1.1	0.050
non-kep	48	-3944.0	1257.0	-0.1	0.058
kep	48	-3208.0	612.0	-1.3	0.045

comparison of the three states at flyby will show only the effects of the correction given by the B-Plane targeting and not the errors introduced by the propagation.

The criteria to consider successful the algorithm is the following. Defining the errors at flyby as

$$\delta_{pert} = ||\mathbf{x}_{pert}(t_{flyby}) - \mathbf{x}_{nom}(t_{flyby})|| \tag{6.10}$$

$$\delta_{corr} = ||\mathbf{x}_{corr}(t_{flyby}) - \mathbf{x}_{nom}(t_{flyby})|| \tag{6.11}$$

then the criteria for success is

$$\begin{cases} \delta_{corr} < \delta_{pert} \rightarrow \text{ success} \\ \delta_{corr} \geq \delta_{pert} \rightarrow \text{ failure} \end{cases}$$

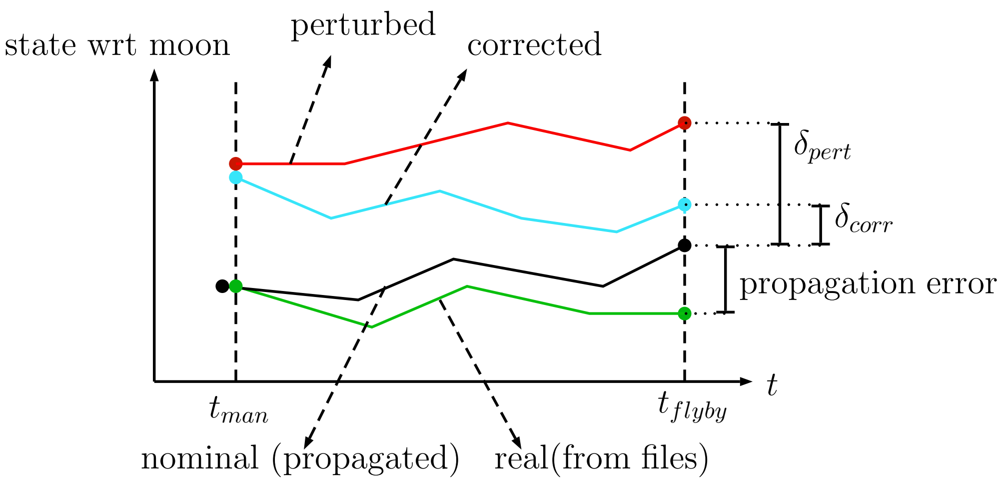

Figure 6.16: Scheme of trajectory correction

The logic of this criteria is that if the corrected state at flyby is an improvement of the perturbed state, then the algorithm was successful; this is shown schematically in Figure 6.16. However, this does not say anything on the magnitude of the deviation. If the deviation of the perturbed state at flyby is of 10 km and the deviation of the corrected state is of 5 km it seems logical to consider the algorithm successful; but it the former is of 1,000 km and the latter of 800 km then it is unclear if to consider the algorithm successful. This is the reason why an improved targeting algorithm is needed.

In Figure 6.17 the plots of the propagation described are shown; the plots show the differences of the perturbed (red line) and corrected (blue line) trajectories with the nominal (propagated) trajectory for different maneuvers times.
When the maneuver is executed 2 hours (inside the SOI) or 10 hours (outside the SOI) before the flyby, the results are quite good: the correction at the flyby is always an improvement of the perturbed trajectory and it matches to the nominal orbit within 1 km. The situation becomes much worst when applying the maneuvers 48 and 72 hours before the flyby. In the case of 48 hours before the improvement with respect to the perturbed trajectory is really small, if not negligible. Moreover this improvement is only for the x and y axes, while for the z axis there is no improvement. The corrected trajectory is anyway quite far away from the nominal (around 50 km). For the case of maneuver 72 hours before the flyby, the situation is even worst: in this case the correction fails, since the corrected trajectory is always worst than the perturbed.
Although this behavior is not always identical for all the flybys and for all the magnitude of the perturbations (in some cases the correction is effective also at 3 days before flyby), a few cases are enough to say that this algorithm is not robust when applied to non-Keplerian trajectories.
Considering that the typical maneuver time for the pre-flyby (targeting) maneuver is around 3 days before flyby, it is necessary to improve this algorithm in order to get accurate results.
The improvement is performed with the optimized algorithm (see 4.3.3), validated in the next Subsection.

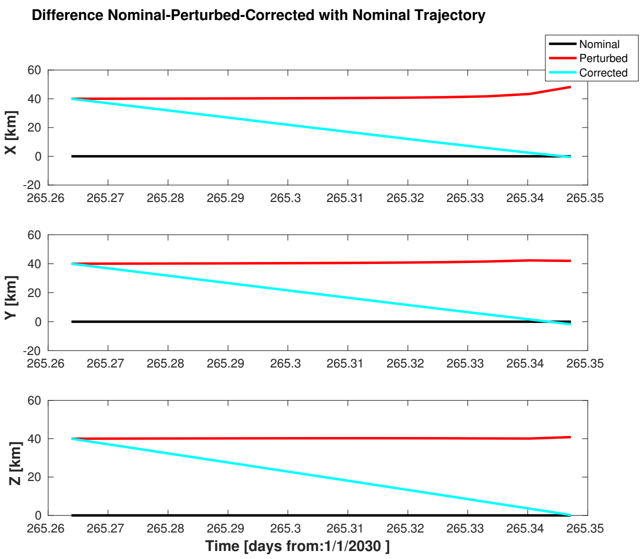

(a) time: 2 hours before flyby

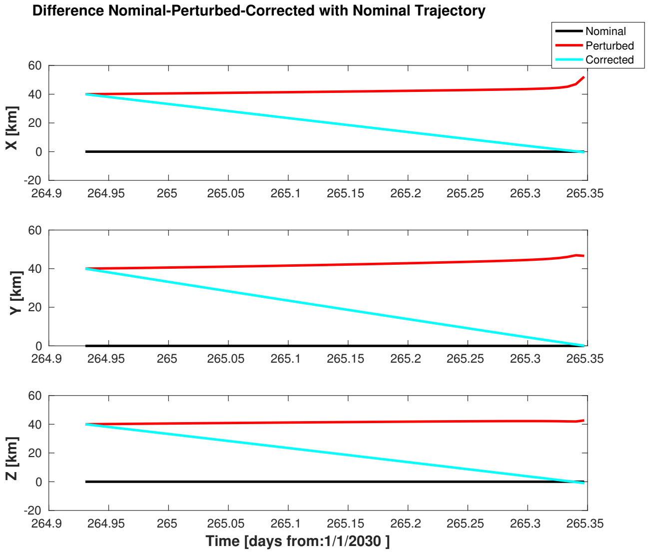

(b) time: 10 hours before flyby

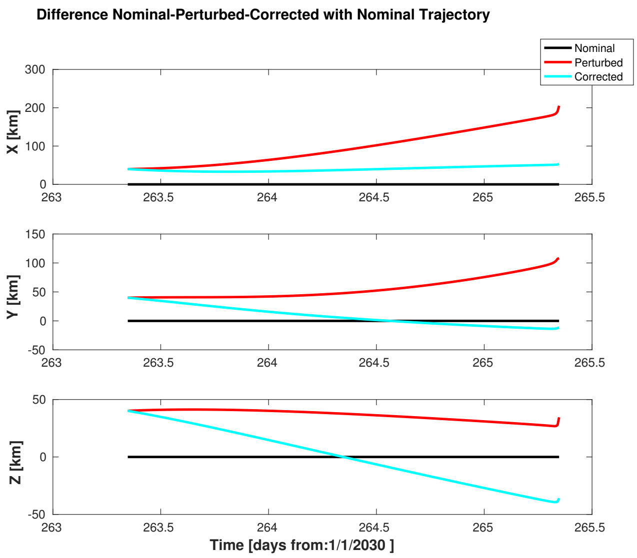

(c) time: 48 hours before flyby

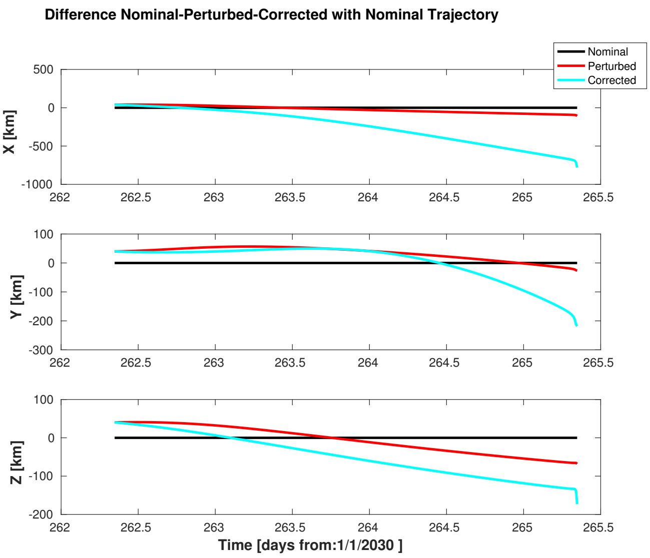

(d) time: 72 hours before flyby

Figure 6.17: Propagation from maneuver time to flyby time with B-Plane ΔV - 2,10,48,72 hrs

6.3.2. VALIDATION OF THE OPTIMIZED TARGETING ALGORITHM

To validate the optimizer different runs have been performed varying the maneuver time and the perturbation magnitude.
In Figure 6.18 some results of the validation process are shown; the optimization is considered successful if the corrected trajectory is always converging to the nominal trajectory at the time of flyby (within a tolerance of 10 km). Only the plots for the maneuver times of 48 and 72 hours before flyby are shown because very often for the maneuver times of 2 and 10 hours an optimization is not needed, since the B-Plane targeting is accurate enough to satisfy the tolerance. The tolerance set for these simulations is of 10 km; when performing the TCM quite close to a flyby this tolerance is satisfied already by the B-Plane targeting algorithm, hence the optimizer does not do any iteration. For the other cases the number of iterations is anyway quite limited (around 1-3).

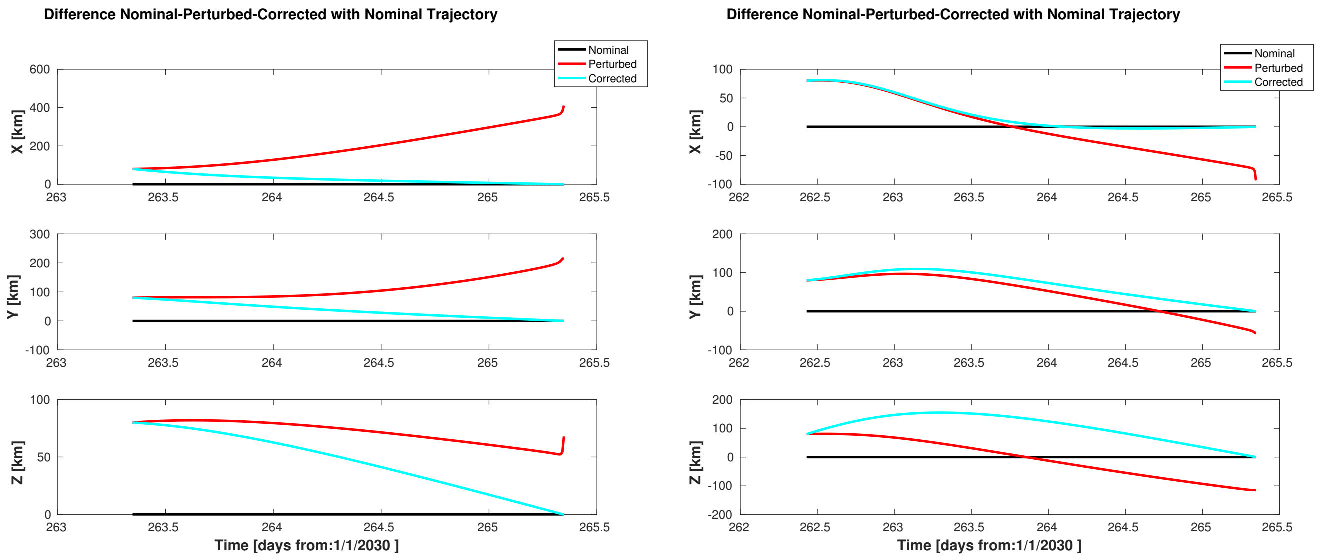

(a) time: 48 hours from flyby

(b) time: 72 hours from flyby

Figure 6.18: Propagation from maneuver time to flyby time with optimized ΔV - 48 and 72 hrs

From a comparison of Figures 6.17 and 6.18 the improvement is visible: the corrected (optimized) trajectory is always within the selected tolerance at flyby, contrary to the perturbed trajectory.
Regarding the ΔV differences between the B-Plane targeting and the optimized results, they are usually relatively small, on the order of a few mm/s or cm/s; this is in accordance to the fact that just a few iterations are required, meaning that the starting point is already a good candidate. This difference can become to be up to 30-40 % for the whole tour, being smaller for each single flyby.
The improvement has been verified for all the flybys of the tour and for different maneuvers times (from 1 hour to 72 hours before the time of flyby); convergence is obtained also for different levels of perturbation and tolerances. The percentage of success of the optimizer is quite high, indicating the robustness of the algorithm.
The conclusion is that to obtain reliable and accurate TCMs before a flyby, the usage of the optimizer is essential when the spacecraft is outside the sphere of influence of a Galilean moon.

6.3.3. VALIDATION OF THE APPROXIMATED TARGETING ALGORITHM

The approximated targeting algorithm (see 4.3.4) has to be verified in order to determine the errors introduced by it and decide if its usage is possible in this project.
A comparison of the results provided by the approximation with respect to the results provided by the optimized targeting has been done for different maneuvers time and for different perturbations magnitude (100 m, 1 km, 10 km, 100 km). For each combination three quantities are reported to evaluate the goodness of the approximation.
The first is the percentage difference of the total flyby tour ΔV

$$\delta_{tot} = \left| \frac{\Delta V^{tot}_{approx} - \Delta V^{tot}_{real}}{\Delta V^{tot}_{real}} \right| \times 100 \tag{6.12}$$

The total flyby tour ΔV is simply the sum of the the ΔV for all the flybys:

$$\Delta V^{tot} = \sum_{i=1}^{N} \Delta V^{i}$$

where N is the total number of flybys.

The second is the maximum difference of ΔV during the flyby tour (so it is referred to a single flyby only). This index is

$$\delta_{max} = max\left(\left| \frac{\Delta V^{i}_{approx} - \Delta V^{i}_{real}}{\Delta V^{i}_{real}} \right| \right) \times 100 \quad \text{for i=1..N} \tag{6.13}$$

The third is the mean of this difference for all the 20 flybys

$$\delta_{mean} = mean\left(\left| \frac{\Delta V^{i}_{approx} - \Delta V^{i}_{real}}{\Delta V^{i}_{real}} \right| \right) \times 100 \quad \text{for i=1..N} \tag{6.14}$$

In Table 6.5 are shown the results of this comparison. This Table shows the best results obtained in term of deviation with respect to the optimized targeting; different combinations of σ_{r0} and $\Delta\sigma_r$ have been tested. The combinations with $\sigma_{r0} \neq 0$ are not considered since conceptually not correct; among the six values of $\Delta\sigma_r$ used (200 m, 600 m, 1 km, 10 km, 20 km, 50 km), the one shown in the Table gives the results with the lowest errors.

Table 6.5: Comparison between real-approximated ΔV [$\sigma_{r0} = 0$ **km,** $\Delta\sigma_r = 600$ **m**] **- Percentages**

t_{man}	Perturbation [km]											
[hr from t_{fb}]	0.1			1			10			100		
	δ_{tot}	δ_{max}	δ_{mean}	δ_{tot}	δ_{max}	δ_{mean}	δ_{tot}	δ_{max}	δ_{mean}	δ_{tot}	δ_{max}	δ_{mean}
1	0.1	12.2	2.3	0.2	5.2	2.3	0.1	5.4	2.1	0.2	5.6	2.2
2	0.1	7.4	1.0	0.2	5.1	1.1	0.1	5.1	2.2	0.2	5.1	2.3
4	0.3	7.2	0.3	0.2	2.2	0.3	0.1	0.4	1.1	0.2	0.1	1.2
10	0.1	4.2	0.4	1.2	12.2	1.1	2.1	12.2	2.1	2.2	12.1	2.2
24	5.1	16.1	1.3	0.2	8.2	3.3	0.1	8.4	3.1	0.2	8.3	3.2
48	1.1	18.2	1.0	0.1	5.0	0.3	0.1	4.2	0.1	0.3	4.1	0.2
72	0.1	2.0	1.4	0.2	1.2	0.3	0.1	1.4	0.1	0.2	1.1	0.2

A first thing to notice is that the results seem to become more accurate when the perturbation applied becomes close to $\Delta\sigma_r$; this makes sense since the derivative computed with a finite difference scheme is just a local approximation of the behavior of the derivative. This is just a consequence of the numerical approximation.

It was decided to compute the derivative around the nominal state ($\sigma_{r0} = 0$ km) since it appeared mathematically more correct. Special care must be taken in this case, because if only a small deviation $\Delta\sigma_r$ is used, the perturbed state would be always very close to the nominal one, hence the B-Plane targeting algorithm could be enough to satisfy the tolerance. If one wants to avoid the use of the B-Plane targeting algorithm only, the tolerance on the final flyby miss-distance has to be lowered considerably (up to 50-100 m) such that the use of the optimizer is needed. This requires some more iterations and computational time but gives more accurate results; however, it was not possible to guarantee that for every flyby of each combination the optimized algorithm is used. In some cases the B-Plane targeting was enough even when selecting a small tolerance; it was not kept track of these cases.

Different values of $\Delta\sigma_r$ have been used to compute this derivative and comparisons between the approximation and the real ΔV have been done. The conclusion is that a quite small $\Delta\sigma_r$ has to be used, together with a small tolerance on the flyby miss-distance, otherwise the computation of the Jacobian will not be accurate. In particular, when using values around 5-10 km for the computation of the Jacobian, the validation gave quite

bad results when using perturbations smaller than 5-10 km. This means that the partial derivatives were not accurate when computed with such big perturbations (for example with a perturbation of 20 km the errors arrived to more than 100 % for the total ΔV).
After different cycles of Jacobian computation and comparisons real-approximated values, a good compromise has been found by using $\Delta\sigma_r = 600$ m and a tolerance on the flyby of 100 m (this is quite a small value but it is not completely unrealistic). For this case the maximum value of the index δ_{tot} is just of 5 %, only one time. Very often it is just equal or smaller than 1 %. The same holds for the index δ_{mean} that describe the average of the errors for all the flybys. The index δ_{max} instead shows generally higher values, with maximum of 18 % but usually around 5 %. This is expected since it can be that for certain flybys (due to the geometry, the altitude, etc.) the approximation is not very good.
To strengthen the validation for this approximation, the results of Table 6.5 have been further analyzed. In particular, outliers have been searched among the different flybys; a value is considered an outlier if it is closer to the index δ_{max} rather than to δ_{mean}. It is noticed that this comparison is done only in a qualitative way. In general it has been observed that the number of outliers is quite small, from 1-3 per combination. This is a good sign, indicating that in general the approximation is reliable, but sometimes is worst (it could be for a more complicated geometry, or for a more rapid flyby, ecc.). However, in one case the situation is worst: this is the case $t_{man} = 24$ hrs from flyby, for a perturbation of 100 m. This is the same case that has the highest index δ_{tot}, considerably higher than the other cases; for this one the number of outliers is 7. Also for higher perturbation magnitudes the number of outliers is a bigger than the other cases (other maneuver times), being 4 and 5 for perturbation of 10 and 100 km.
Unluckily it was not possible to find an explanation for this, since the maneuver time of 24 hours before the flyby has apparently nothing particular or different with respect to the other cases. More cases could not be tried due to time constraints. This phenomena is anyway quite limited in magnitude, hence was not considered a major problem that could forbid the usage of the approximation. The reason could be a particular geometry of the trajectory at that time (more on this is in Section 8.3.1).
The conclusion is that is not possible to use the approximated targeting algorithm when computing the ΔV for a single trajectory since the errors would be quite important. However for a statistical analysis it is acceptable, since the perturbations are applied both in excess and in deficiency, hence the approximated ΔV will also be sometimes in excess and sometimes in deficiency with respect to the real one. If a high number of samples is used then these two effects compensate each other. Moreover, even if the ΔV for each flyby is not very accurate, the total ΔV is accurate enough as seen from Table 6.5.
Thus, taking these considerations into account and considering the computational saving (a single multiplication rather than an optimization process), this approximation will be used, at least for parts of the simulations.
A last justification, of computational nature, for the use of this approximation comes from the paper [62], where a similar kind of analysis is done; in particular what is done is a planetary protection analysis for the mission Juno. In the paper is indicated that, when performing Monte Carlo analysis with large number of samples for trajectories propagation for 150 years (much more than the time span considered in this Thesis), the JPL supercomputers had been used for the computations; it is clear how these simulations require a great computational power, hence time. Thus, at this level and with the limited resources available, results with simplified and faster code are a good compromise.

Finally, Figure 6.19 presents a trade-off between the three targeting algorithms.

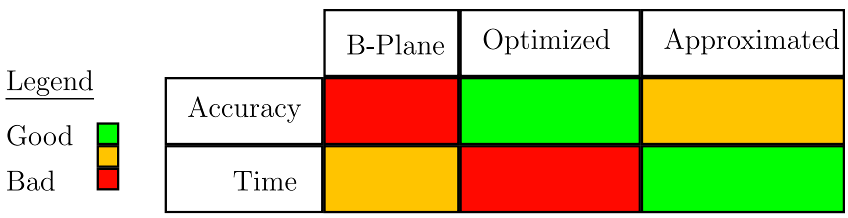

Figure 6.19: Targeting algorithms trade-off

6.4. MONTE CARLO METHOD

A brief validation has been done also for the Monte Carlo method (explained in Section 5.4). The validation consisted essentially in the determination of a good number of samples to be used for the simulations.
The following strategy has been used: for the same CA configuration, different MC runs have been executed with different numbers of samples, in the range [100-25,000]; this has been done for the version of the code that uses the approximated targeting, because it would have been prohibitively expensive for the optimized targeting. The results of all of these runs have been analyzed to see the differences between them; if two runs with different numbers of samples give the same results (or very similar, since it is impossible to obtain exactly the same results) it means that those number of samples are sufficient for reliable results. But trying only two cases is not enough, more are needed to see if there is a change of trend. The minimum number of samples necessary for a reliable statistical analysis can then be selected.
Table 6.6 presents the results of the total ΔV statistics for each Monte Carlo run with a different number of samples; the plots on the single ΔV per flyby have also been analyzed but are not reported here for conciseness.

Table 6.6: Validation of the Monte Carlo Analysis

$N°$ samples	Total ΔV statistics		
	Mean	$1-\sigma$	95%
	m/s	m/s	m/s
100	7.30	0.74	8.64
500	7.34	0.68	8.46
1000	7.33	0.71	8.54
2000	7.31	0.72	8.50
4000	7.31	0.72	8.54
7000	7.29	0.73	8.52
10000	7.31	0.72	8.52
15000	7.32	0.73	8.53
20000	7.31	0.72	8.50
25000	7.30	0.72	8.52

From the Table and the plots it was concluded that a suitable number of samples can be considered $N = 1000$, since from that value onwards the results are very similar. The values of the statistical indicators are more similar after $N > 1000$, while they deviate more for $N < 1000$. This means that to represent with sufficient fidelity the dispersion of the perturbed trajectories around the nominal one a value of samples high enough to explore the uncertainty space must be used.
It is noted that when using the approximated targeting the difference in term of computational time between running a MC simulation with 100 and 5000 samples is practically negligible, hence an higher value of samples can be used without any overload. Instead, when using the optimized targeting, the computational overload increases proportionally with the number of samples, requiring thus the use of a smaller number.
In the Monte Carlo simulations performed (Sections 8.1 and 8.2) the number of samples is set to 2000 (when the approximated targeting is used).
Finally, it is noticed how similar number of samples are found also in literature, for example in [56].

7

Covariance Analysis Results

This Chapter presents the results of the Covariance Analysis conducted for flyby tour of the mission JUICE; as stated in Chapter 5 this is the starting point for a full Navigation Analysis, since it provides the uncertainties of the states of JUICE and the moons, needed to design the maneuvers.
The structure of the Chapter is the following; in Section 7.1 the influence of the number of bodies to be estimated on the convergence and quality of the results is analyzed. Section 7.2 presents the results of the sensitivity analysis performed for 3 different configurations of the CA with respect to the data types, weights and tracking schedule. The last Section (7.3) presents some considerations about the ephemerides improvement that can be obtained thanks to the mission. In Appendix A the influence of other parameters on the CA results is analyzed.

The results presented here originate from the implementation of the CA (Section 5.2) using the theory exposed in Chapter 3. Different versions of the CA are used, to analyze the influence of the different assumptions of the CA strategies on the results. The research question addressed is the second; the purpose of this Chapter is to assess how the different parameters and assumptions that play a role in the orbit determination strategy influence the determination of the spacecraft and the Galilean moons positions uncertainties.

7.1. Influence of the number of estimated bodies on CA convergence

In this Section the influence of the inclusion of different bodies (where a body is the spacecraft or a celestial body) in the estimation process is analyzed, showing in particular the effects on the condition number.
The number of bodies estimated has a strong influence on the overall behavior of the filter (as explained in Subsection 6.2.1); three different configurations are tried

- estimation of JUICE only;
- concurrent estimation of JUICE and the flyby moon (with *single arc data*);
- concurrent estimation of JUICE and all the four Galilean moons (with *data accumulation*).

7.1.1. Estimation of JUICE only

In this case it is relatively easy to obtain real standard deviations and reasonable values for the condition numbers, because only JUICE (which is directly observed) is included in the estimation. In Table 7.1 are shown the results for some simulations for different time intervals (with a fixed observation schedule and data weights). The column "CN" represents the order of magnitude of the condition number, the column $\sigma(t_0)$ the type of the initial standard deviation and the column $\sigma(t)$ the type of the standard deviation propagated with time.

This results are obtained using range and VLBI data; they are just indicative of the worsening of the condition number when increasing the arc length; it has to be kept in mind that due to the absence of Doppler data the estimation of JUICE is not the primary focus of the Thesis (see 5.2). Moreover, the results for longer durations suffer also from the problem of the divergence of the numerical propagation (see 6.1) hence the trajectory observed after a long period of time is different from the real one.

Table 7.1: Condition numbers and standard deviation types for the estimation of JUICE only

Days	Flyby moon(s)	CN	$\sigma(t_0)$	$\sigma(t)$
2	-	$\sim 10^6$	Real	Real
5	G	$\sim 10^6$	Real	Real
10	G	$\sim 10^6$	Real	Real
20	G-G	$\sim 10^9$	Real	Real
40	G-G-C	$\sim 10^9$	Real	Complex
80	G-G-C-C	$\sim 10^{12}$	Real	Real
120	G-G-C-C	$\sim 10^{15}$	Real	Real
160	G-G-C-C-C	$\sim 10^{15}$	Complex	Complex

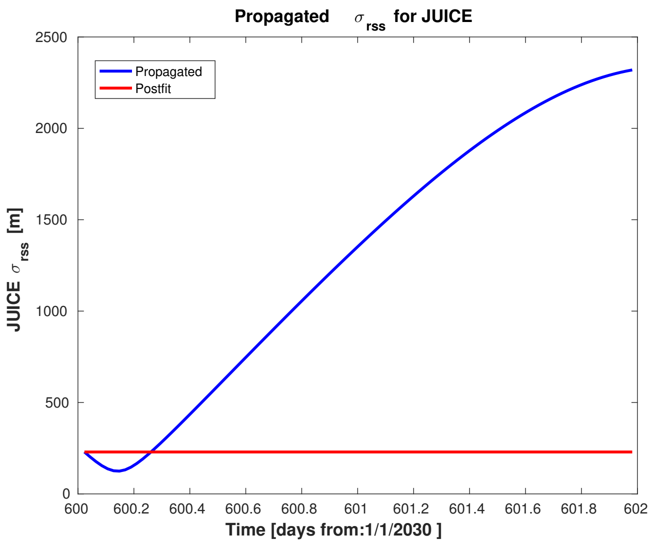

(a) 2 days

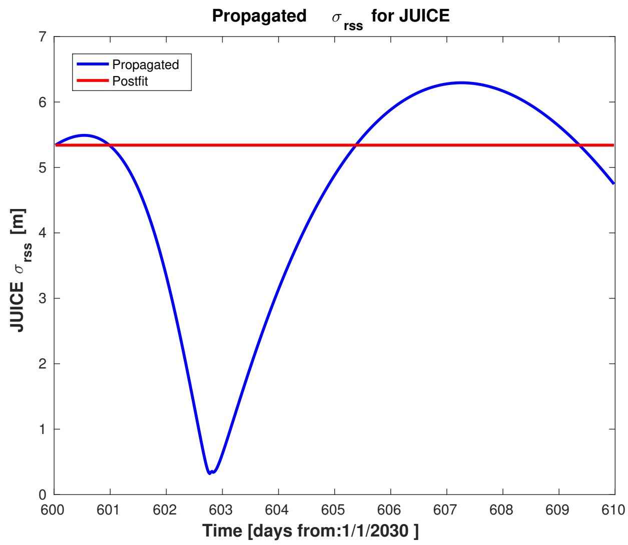

(b) 10 days

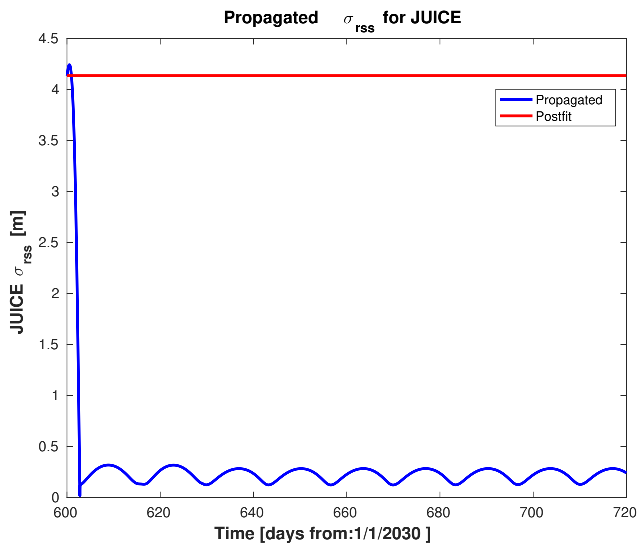

(c) 120 days

Figure 7.1: Propagation of JUICE standard deviation

It is is noticed how especially for short time intervals the simulations are well behaved; the condition numbers are quite low and the standard deviations are almost always real. This is also due to the fact that VLBI data are used, which provide a direct observation of the out-of-plane position (see 3.1); if range (and Doppler) data are used then the condition number would be much higher since the determination of a spacecraft around another planet using only those data is an ill-posed problem for short arcs lengths ([61]). When increasing the time interval to high values (40 days) some problems arise; this means that when estimating the position of the spacecraft using data that span a very long time interval the algorithm has difficulties in processing all the data to give a feasible solution. A different observation schedule can improve the results.
Since in the multi arc analysis, for what seen in Chapters 5 and 6, the use of such long time intervals is not envisioned, it is not necessary to investigate further the behavior of the estimation of the spacecraft for long time intervals. It is enough to find the intervals of time during which the estimation process is accurate and reliable; in this way it is possible to generate arcs with proper duration for the multi-arc analysis. Figure 7.1 shows the standard deviation of the three dimensional position (σ_{rss}, which stands for *root sum square*) for JUICE. This is defined as

$$\sigma_{rss} = \sqrt{\sigma_x^2 + \sigma_y^2 + \sigma_z^2}$$

In the plots the term *post-fit* indicates the standard deviation of JUICE at the beginning of the arc (the one computed by the algorithm with Eq. 3.22), while the term *propagated* indicates the standard deviation propagated along the arc with Eq. 3.23. A standard observation schedule (as in Table 7.5) has been applied. The first observation is that increasing the amount of data (when increasing the arc length) the standard deviation decreases; this is expected, however after a certain amount of data the improvement is limited. The improvement from 2 days to 10 days of observations is noticeable, while the improvement from 10 days to 120 is very small. This means that with the selected values of weights for the measurements it is not possible to go beyond a certain uncertainty. The second observation is on the propagation of the formal error. For a very brief interval, the standard deviation increases in an almost linear way; for longer intervals it shows a periodic effect. In the plot 7.1b is possible to see a minimum: this correspond to a flyby; this means that the state transition matrix for JUICE is strongly influenced by the flyby. In the plot 7.1c is seen the behavior for a long period; this is however not reliable because in this case the condition number is quite high and because the state transition matrix comes from a linearization, hence for such a long interval is not representative of the true dynamics. It is concluded that an appropriate arc length for the estimation is between 3-15 days.

7.1.2. Concurrent estimation of JUICE and the Galilean moons

The coupled estimation of the state of JUICE and the Galilean moons is the case where the two problems of non-convergence described in 6.2.1 are encountered more often. This is however the most realistic case because it represents accurately the real procedure of orbit determination. They are briefly discussed here.

Estimation of the flyby moon only

This is the first version of the concurrent estimation that has been implemented; it has shown good convergence properties but sometimes it can fail, giving complex standard deviations. This depends especially from the arc selection: if the estimation is performed during the flyby arc then there is a great reduction of the uncertainty for the moon position at flyby time, while if the estimation is performed in the arc preceding the flyby then there is not an evident minimum. This has the consequence that sometimes the minimum can become a complex standard deviation, giving an unrealistic result. The condition number is also higher for this case. Instead, when estimating before a flyby this rarely happens.
This is represented in Figures 7.2a and 7.2b, where Ganymede is estimated respectively during the flyby arc and in the arc preceding the flyby.

Figure 7.3 shows the condition numbers for all the arcs, for the case of estimation during the flyby arc. It is possible to see 20 peaks which correspond to the flybys; in those arcs the estimation is more difficult, presenting condition numbers from 10^{10} to 10^{16}. This is the effect of including the estimation of a moon; in the other arcs, where only JUICE is estimated, the condition number is always below 10^9. This happens since the addition of one body to be estimated adds complexity to the problem and the matrix to be inverted become worst conditioned; the physical reason is that some of the coordinates to be estimated for the moons are not related (or are weakly related) to the spacecraft state, thus producing an information matrix that is bad conditioned. This depends also upon the length of the estimation arc, since if the geometry Earth-spacecraft-moon varies more the matrix would be better conditioned ([61]).

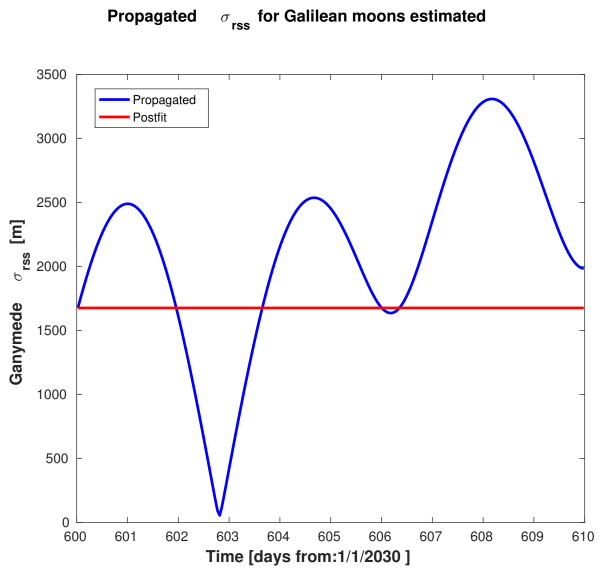

(a) During flyby of Ganymede (at 602.8 days)

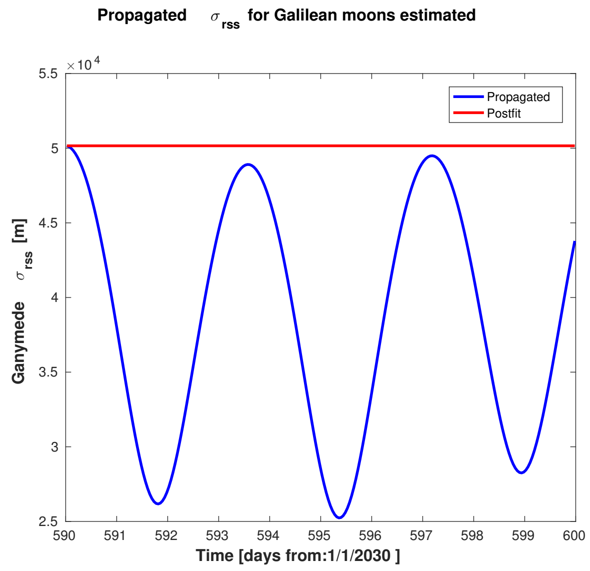

(b) Before flyby of Ganymede

Figure 7.2: Standard deviations for the estimation of Ganymede

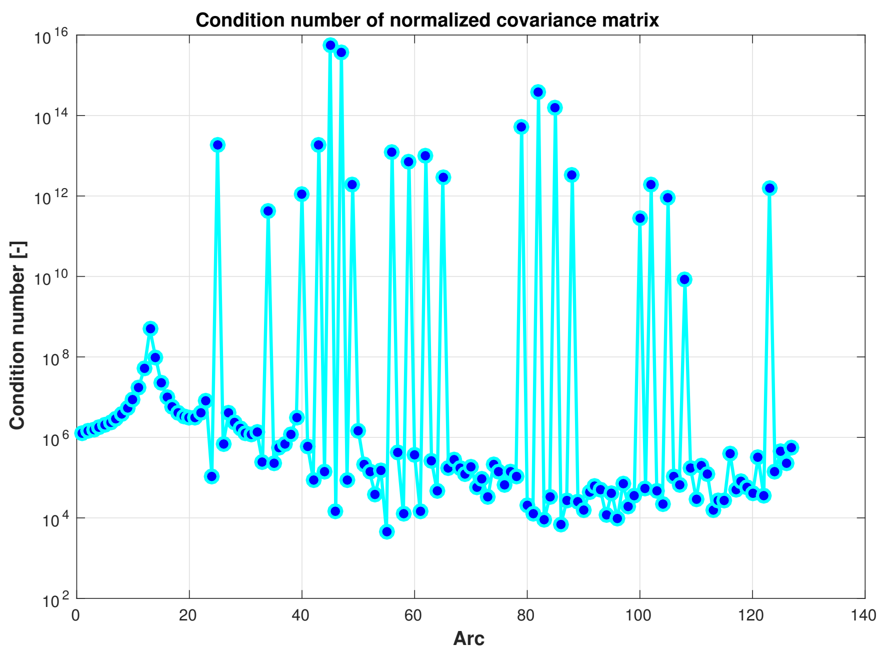

Figure 7.3: Condition number for the estimation of the flyby moon only

Estimation of all the Galilean moons
In this version all the four moons are included in the estimation; this is necessary for the *data accumulation* estimation (see Section 5.2). This is possible especially due to the Laplace resonance (see 2.1.2), that relates the dynamics of a moon to the dynamics of another moon; hence during a flyby of a single moon also the other three can be estimated ([36]). This influence is lower for Callisto because it is not in resonance with Io, Europa and Ganymede, however due to the high amount of flybys to Callisto this does not cause a problem.

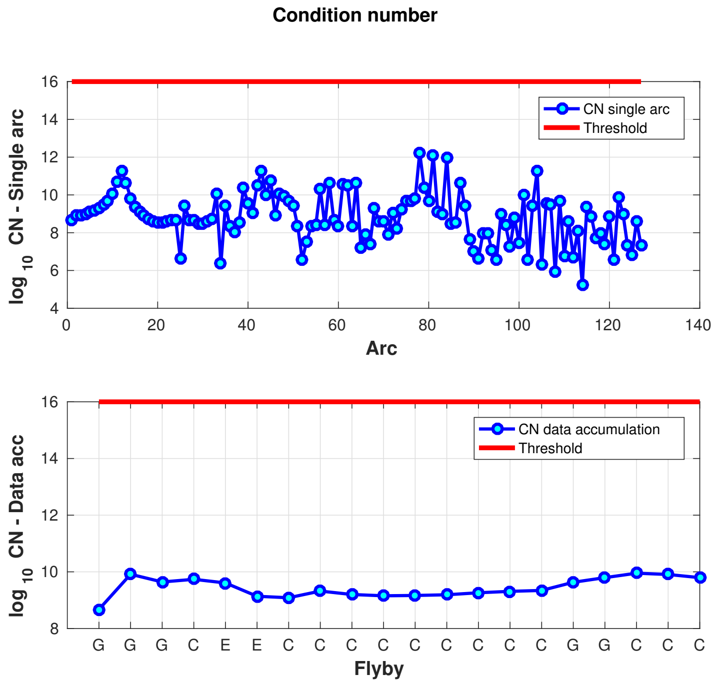

Figure 7.4: Condition number for the estimation of the four moons

Figure 7.4 shows a plot of the condition numbers for the estimation of the four moons. In the upper plot is shown the condition number for the covariance matrix computed using only the observations from one arc; in the lower plot is shown the condition number for the covariance matrix computed with the data accumulation (this is computed only for the flybys). It is noticed that all these condition numbers are below the threshold (set to 10^{16}) hence meaning that the estimation is accurate. In particular, while for the single-arc case the condition number are often close to $10^{12} - 10^{14}$, for the data accumulation case they are alway under 10^{10}. This means that when adding data from the past in the estimation of the moons the results obtained are more accurate rather then estimating the moons with data from a single flyby. The data accumulation algorithm has also the effect of stabilizing the inversion. This plot is for the estimation of the moons in the pre-flyby arcs; the estimation of all the moons during a flyby arc gives worst results (as seen in the previous paragraph), with condition number more often close to 10^{16} also for the data accumulation case.

7.2. Sensitivity analysis for the Covariance Analysis

A sensitivity analysis has been performed to investigate the behavior of the uncertainties of JUICE and the moons, computed from the CA, with respect to the tracking data types, accuracies and schedule. In Appendix A the influence of the multi-arc division, the a priori standard deviations for JUICE and the moons and of the dynamical model are analyzed too. Of particular importance is the selection of the multi-arc division (see 5.2). This Section is divided as follows: in Subsection 7.2.1 the results for the single arc estimation performed during the flyby arcs are presented (see Section 5.2 and Figure 5.6). This strategy represents the case of failure of the spacecraft tracking during one (or more) of the previous flybys; thus for each flyby data from that flyby are used only, and not from past flybys. In Subsection 7.2.2 the results for the data accumulation estimation performed during the flyby arcs are presented (see Section 5.2 and Figure 5.8). This strategy represents the case of tracking of the spacecraft possible during the flyby arc and for all the flybys. In Subsection 7.2.3 the results for the data

accumulation estimation performed during the pre-flyby arcs (see Section 5.2 and Figure 5.7) are presented. This strategy represents the case of tracking of the spacecraft not possible during the flyby arcs due to other spacecraft requirements; thus the tracking is interrupted just before a flyby. The results for JUICE are presented only in Subsection 7.2.3 since they are independent upon the moons estimation strategy.
The settings used for these analysis are presented in the respective Subsections. The accuracies used for the tracking data are in the following intervals (see Subsection 3.1 for the data types explanation)

$$\begin{aligned}
&\text{range:} \quad \sigma_r \in [0.2-10] \quad m\\
&\text{VLBI:} \quad \sigma_v \in [0.1-10] \quad nrad\\
&\text{optical:} \quad \sigma_v \in [1-50] \quad \mu rad
\end{aligned}$$

Regarding the optical data, they are taken up to 2-3 days before a flyby; since their accuracy is specified in angular form, if they are used at a small distance then the linear accuracy obtained would be very high ([28]). For the usual distances of the spacecraft at 2-3 days before the flybys (on the order of 10^5 km) the linear accuracy obtained for the best angular accuracy ($\sigma_o = 1\mu\, rad$) is of around 5 km; for the worst case is of around 250 km. The current linear accuracy of optical data is around 10-20 km. The dynamical model chosen is the simple one (see 3.2.1) since it is computationally less demanding than the complex one. The time step used for the integration of the equations of motion is of 1800 s, to reduce the effects of divergence due to the numerical propagation (as explained in 6.1.2).
The tracking data schedules used (shown in the next Subsections in Tables 7.2 and 7.5) are representative of the real tracking capabilities. However they are modified to reduce the amount of data collected with respect to the current operational capabilities; these correspond to collect a radio observation each 5 minutes for 8 hours per day ([26] and [14]). This is done because sometimes the CA can give overly optimistic results (see Section 3.3), thus decreasing the total amount of data this effect is reduced. Moreover, the selection of the tracking schedule depends also upon the convergence of the CA (see 6.2.1).

7.2.1. Strategy 1: single arc estimation during flyby arcs

In this strategy the flyby moon is estimated during the flyby arc (see Fig 5.6) using data from that flyby only. In Table 7.2 the settings used for this case (and also for the next Subsection 7.2.2) are presented. The duration of the flyby arc is of 6 days, centered around the flyby. Due to convergence issues (see 6.2.1 and 7.1.2) the tracking schedule used is not optimal; in the real mission a more frequent tracking is possible.

In Table 7.3 the results obtained for the different data types and accuracies used are shown; the results are expressed as average of the in-plane (σ_{IP}) and out-of-plane (σ_{OP}) standard deviations for each moon

$$\sigma_{IP} = \sqrt{\sigma_x^2 + \sigma_y^2} \qquad \sigma_{OP} = \sigma_z$$

The average is computed for each moon using its respective estimation data; the average for Europa is over 2 flybys, for Ganymede over 5 and for Callisto over 13. Io is never estimated since there are no flybys for it.
The reduction of the uncertainty (the a priori is of 80 km per axis) is always present for every moon; in particular it is observed that the improvement is better for Europa and Ganymede and worst for Callisto. In Figure 7.5 (correspondent to the last case of the Table) the rss of the uncertainties for each flyby are shown; it is visible that for Callisto they are in general higher. It has been noticed that in general, if the same amount of data is used for every flyby, the estimation of Callisto is more difficult than the estimation of Europa and Ganymede; this could depend upon the length of the estimation arc (as explained in 7.3). Since the orbital period of Callisto is higher than the ones of the other two moons a longer observation arc could be needed.

The improvement is more consistent in general for the in-plane component with respect to the out-of-plane; this is expected since with range data the determination of the out-of-plane position is more problematic. From the Table is clear that there is an improvement when using more types of data and better accuracies. In particular, when adding VLBI data the decrease of the out-of-plane component is quite significant, as expected from this type of data (see 3.1.1). The contribution of VLBI is also for the in-plane component, since this measurement provides information also in a in-plane direction. When adding optical data the improvement is noticeable for both the components too. It is noted however that tracking data are interrupted 2 days before the flyby, hence just one day of optical data is used here.
The uncertainty reduction is overall significant with respect to the a priori but is not very high; the level is

Table 7.2: Covariance Analysis settings for Strategy 1-2

Symbol	Name	Value	Unit
-	Dynamical model	Simple	-
t_0	Start time	1-1-2030	-
t_f	End time	10-2-2032	-
Δt	Time step for num. integration	1800	s
ΔT_{flyby}	Flyby arc length	6	days
ΔT_{nom}	Nominal arc length	6	days
ΔT_{min}	Minimum arc length	4	days
σ_{moon}	A priori uncertainty of Galilean moons	80	km
σ_{JUICE}	A priori uncertainty of JUICE	600	km
Δt_f^R	Range data step (flyby)	1200	s
Δt_f^V	VLBI data step (flyby)	1800	s
ΔT_f^R	Range data interval (flyby)	2	hrs
ΔT_f^V	VLBI data interval (flyby)	2	hrs
Δt_{nf}^R	Range data step (non-flyby)	3600	s
Δt_{nf}^V	VLBI data step (non-flyby)	3600	s
Δt_{nf}^O	Optical data step (non-flyby)	1800	s
ΔT_{nf}^R	Range data interval (non-flyby)	4	hrs/day
ΔT_{nf}^V	VLBI data interval (non-flyby)	4	hrs/day
ΔT_{nf}^O	Optical data interval (non-flyby)	6	hrs/day
-	VLBI amount per week	1	day/week
-	Optical interruption around flyby	2	days

Table 7.3: Sensitivity analysis results for the Galilean moons - Singe arc, tracking during flyby

Variables			Results					
Data accuracies			Europa		Ganymede		Callisto	
σ_R	σ_V	σ_O	σ_{IP}^{avg}	σ_{OP}^{avg}	σ_{IP}^{avg}	σ_{OP}^{avg}	σ_{IP}^{avg}	σ_{OP}^{avg}
m	$nrad$	μrad	km	km	km	km	km	km
0.2	-	-	0.57	4.21	3.01	4.78	3.42	11.83
1	-	-	2.78	19.48	9.38	18.68	10.26	33.65
10	-	-	14.73	55.10	27.11	48.22	20.27	67.29
1	0.1	-	1.16	11.35	4.52	3.64	5.47	10.91
1	1	-	2.14	8.98	8.44	8.12	8.88	23.49
1	10	-	2.94	10.76	9.19	9.24	9.47	27.09
1	0.1	1	0.30	0.69	0.75	0.59	1.11	1.47
1	0.1	10	1.60	5.11	2.71	3.87	3.01	7.68

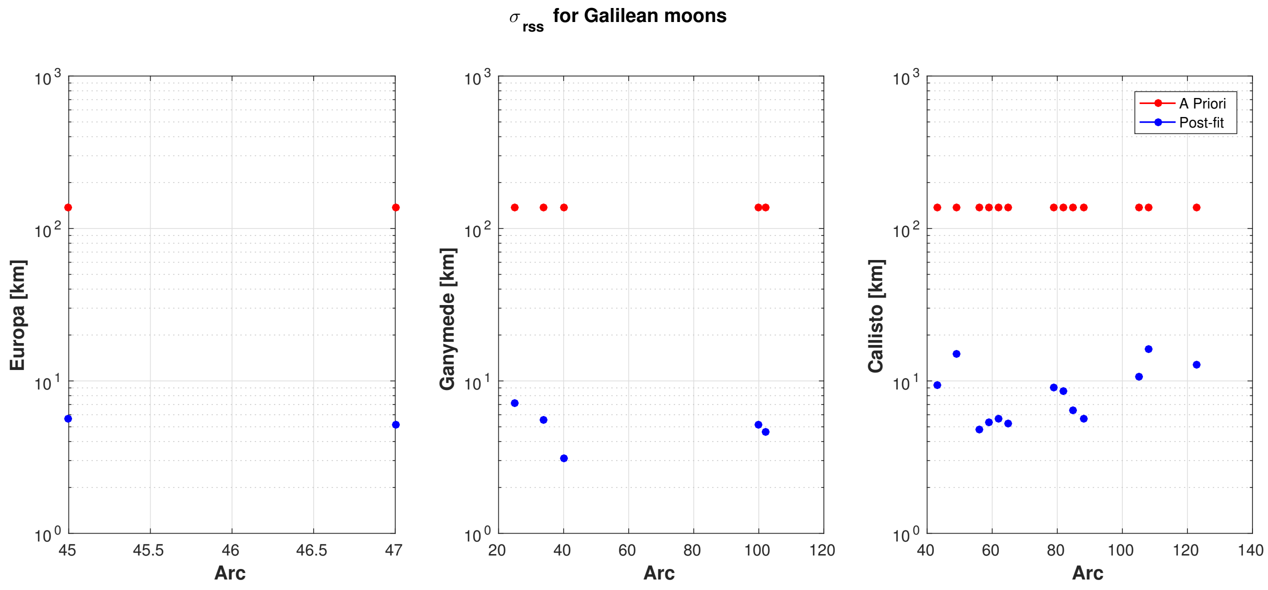

Figure 7.5: Single-arc estimation results for the Galilean moons

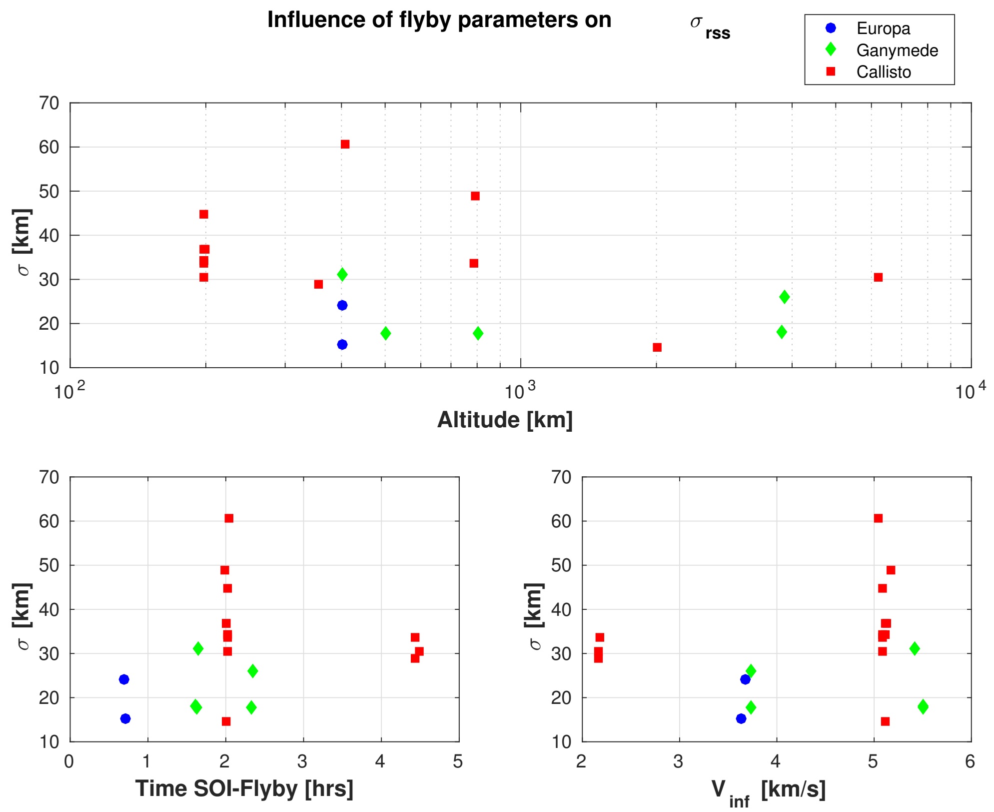

Figure 7.6: Correlations for single-arc estimation of the Galilean moons

always from a few km to tens of km. Only for Europa and Ganymede, for the case of best data accuracies, it reaches a few hundred meters. This depends by the fact that a very small amount of data are used; in the next Subsections it will be seen how a further improvement is obtained with the data accumulation.
In Figure 7.6 possible correlations between the results of the CA and the characteristics of the flybys (from Table 6.1) are searched for. The Figure is referred to the second combination of Table 7.3. It is visible again that generally the uncertainties for Callisto are higher than for Europa and Ganymede. While in general no apparent correlations are present, for Callisto it is observed that the worst uncertainties are observed for the medium altitude flybys, with a low flyby duration and a high hyperbolic excess velocity. However in correspondence of those characteristics also low uncertainties are found. Regarding the altitude of the flybys, not necessarily a low altitude flyby gives better accuracies; this can be due to the fact that the altitude differences are anyway quite limited. For example the uncertainties for the 6000 km and 200 km flybys of Callisto give very similar uncertainties. It is concluded that, even if correlations could exist, there are not enough flybys to individuate them clearly.

7.2.2. STRATEGY 2: ESTIMATION DURING FLYBY ARCS WITH DATA ACCUMULATION

In this strategy all the four moons are estimated during the flyby arc (see Fig 5.8) using data from all the previous flybys performed. The settings used are in Table 7.2. It is noted that due to convergence issues, worst data accuracies with respect to the current capabilities (3.1.1) have to be used to obtain feasible results; this is also justified by the fact that during a flyby it may not be possible to point the High-Gain-Antenna to Earth but only the Medium-Gain-Antenna to Earth, with a decrease of the signal power and hence of the accuracy of the radio observables.

Table 7.4: Sensitivity analysis results for the Galilean moons - Data accumulation, tracking during flyby

Variables			Results											
Data acc.			Io			Europa			Ganymede			Callisto		
σ_R	σ_V	σ_O	σ_{IP}	σ_{OP}	σ_{avg}	σ_{IP}	σ_{OP}	σ_{avg}	σ_{IP}	σ_{OP}	σ_{avg}	σ_{IP}	σ_{OP}	σ_{avg}
m	$nrad$	μrad	km	km	km	km	km	km	km	km	km	km	km	km
Range, VLBI, optical (flyby moon)														
5	-	-	0.05	0.10	0.11	0.06	0.01	0.05	0.0001	0.001	0.002	0.0001	0.0001	0.0002
10	-	-	0.10	0.20	0.23	0.12	0.03	0.10	0.0002	0.002	0.005	0.0002	0.0003	0.0004
10	0.2	-	0.09	0.20	0.22	0.11	0.02	0.09	0.0002	0.002	0.005	0.0002	0.0003	0.0004
10	5	-	0.10	0.20	0.23	0.12	0.03	0.10	0.0002	0.002	0.005	0.0002	0.0003	0.0004
10	0.2	10	0.09	0.19	0.22	0.11	0.02	0.09	0.0002	0.002	0.005	0.0002	0.0003	0.0004
10	0.2	1	0.09	0.19	0.21	0.11	0.02	0.09	0.0002	0.002	0.005	0.0002	0.0003	0.0004
20	-	-	0.29	0.65	0.73	0.38	0.12	0.32	0.0007	0.008	0.02	0.0008	0.001	0.001
20	1	-	0.29	0.64	0.71	0.37	0.11	0.30	0.0007	0.007	0.01	0.0008	0.001	0.001

In Table 7.4 the results are shown; the values in the Table represent the initial in-plane and out-of-plane standard deviations (computed at the end of the mission, thus using all the flybys) and the average of the propagated standard deviation, computed as follows

$$\sigma_{avg} = \frac{\sum_{i=1}^{n} \sigma_{rss}^{i}}{n}$$

where σ_{rss}^{i} is the three dimensional standard deviation for a moon at the time instant t_i and n is the total number of epochs, coming from the time discretization in the computation of the state transition matrix. Since the propagated standard deviations (computed with Eq. 3.23) show a periodic behavior, the average is computed to have a more representative index that takes into account the behavior of the uncertainty with time. The uncertainties are lowest for Callisto, followed by Ganymede, Europa and Io. This correspond to the decreasing sequence of number of flybys (13 for Callisto, 5 for Ganymede and 3 for Europa). Even though the tracking data accuracies used (especially for the range) are not the best possible the results show a decrease on the level of the m for Callisto and Ganymede and hundreds of m for Europa and Io. For Callisto at the end of the tour the total uncertainty is at the level of 0.3 m, comparable with the one of JUICE; this is unrealistic, since such an accuracy for a celestial body is definitively too high. It is noted that in these simulations the condition numbers were always around $10^{15} - 10^{16}$, indicating that probably the results are not completely valid (they

have quite big errors). They give an idea of the improvement attainable during the flyby tour; to obtain more realistic results different a priori values shall be used for the moons. This is not done here but only briefly addressed in Appendix A. Another element that plays a role is the dynamical model: a more complex dynamical model gives worst results (see A) hence representing possibly more realistic uncertainties for this case.
Regarding the data types, it is seen that improving the accuracies of the range data the uncertainties decrease; the influence of VLBI is however quite limited and is noticed only for very good VLBI accuracies, being almost null for worst accuracies. This can be explained by the fact that the improvement given by the range is already so good that the VLBI do not have a strong influence. It has to be remembered however that just one day of VLBI observations is scheduled per week; this means that the amount of VLBI data is much lower than the range data. The influence of the optical data is also quite small; this is explained by the fact that optical data are interrupted 2 days before the flyby and the arc starts just 3 days before, giving just a very small amount of them.

Figure 7.7 presents the improvement of the ephemerides uncertainties for the case σ_r = 10 m and σ_v = 5 nrad); the plot is in a logarithmic scale in the y-axis to appreciate the decrease of different orders of magnitude of the uncertainty from the a priori value (in red).
The green line represents the estimation of the four moons using only the data from the correspondent flyby, while the blue line represents the estimation of the four moons using all the past flybys data. For all the moons the single-arc estimation does not improve noticeably the uncertainty (the green line is very often close to the red line); the decrease is of a few kilometers per moon, similarly to the previous Subsection (7.2.1). The improvement is noticeable for the single-arc only during the correspondent flyby arc; these minima are clearly visible for Europa, Ganymede and Callisto. The higher improvement for Callisto due to the data accumulation is observed. This starts only after its first flyby; during the first three flybys there is no improvement. This can be explained by the fact that Callisto is not part of the Laplace resonance (see 2.1.2). During the central series of flybys of Callisto the improvement is of about one order of magnitude, from 10 m to 1 m.

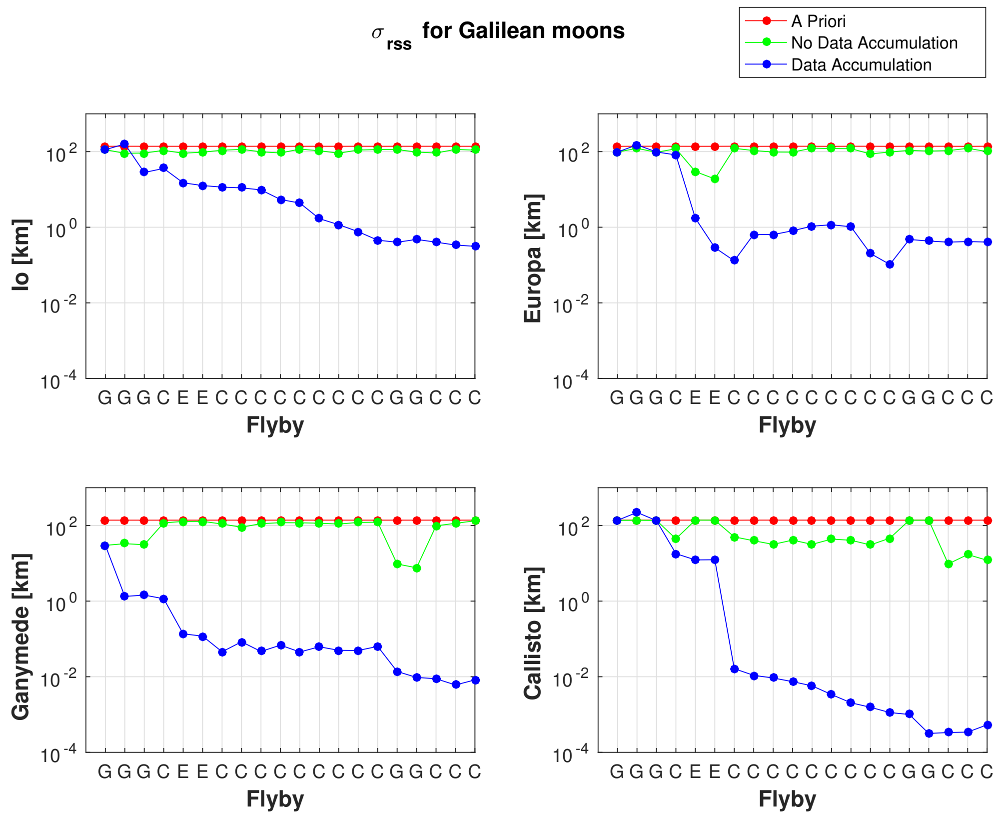

Figure 7.7: σ_{rss} for the Galilean moons during the Tour - Data accumulation, flyby arc estimation

It is concluded that this case is a good representation of using the tracking data during all the flybys; however their use gives somehow too optimistic results. This is also a mathematical problem that comes from the

structure of the matrices; other alternatives can be implemented to see if the same set of observations would give more realistic standard deviations with a different orbit determination solution algorithm (see 3.3).
In [36] it is indicated that using very good data for a short interval of time can give results tailored to that time interval; this means that the results obtained show that during a flyby the position of a moon is know with very high accuracy. This is expected since the spacecraft is very close to the moon hence the gravitation influence is really high. Thus this knowledge of the moons position can be so accurate only for brief periods, when a spacecraft is orbiting close to them, but does not represent a long-term accuracy (see Section 7.3).

7.2.3. Strategy 3: estimation during pre-flyby arcs with data accumulation

In this strategy all the four moons are estimated during the pre-flyby arc (see Fig 5.7) using data from all the previous flybys performed. The settings used are in Table 7.5. Two different tracking schedules are used. Only two different schedules are tried because in theory the effect of increasing the amount of observations and increasing the accuracy of the observations should be similar.

Table 7.5: Covariance Analysis settings for Strategy 3

Symbol	Name	Value	Unit	Value	Unit
-	Dynamical model	Simple	-	Simple	-
t_0	Start time	1-1-2030	-	1-1-2030	-
t_f	End time	10-2-2032	-	10-2-2032	-
Δt	Time step for num. integration	1800	s	1800	s
ΔT_{flyby}	Flyby arc length	6	hours	6	hours
ΔT_{nom}	Nominal arc length	10	days	10	days
ΔT_{min}	Minimum arc length	6	days	6	days
σ_{moon}	A priori uncertainty of Galilean moons	50	km	50	km
σ_{JUICE}	A priori uncertainty of JUICE	400	km	400	km
		Tracking schedule A		Tracking schedule B	
Δt_f^R	Range data step (flyby)	1200	s	1200	s
Δt_f^V	VLBI data step (flyby)	1200	s	1200	s
ΔT_f^R	Range data interval (flyby)	6	hrs	2	hrs
ΔT_f^V	VLBI data interval (flyby)	6	hrs	2	hrs
Δt_{nf}^R	Range data step (non-flyby)	1200	s	1200	s
Δt_{nf}^V	VLBI data step (non-flyby)	1200	s	1200	s
Δt_{nf}^O	Optical data step (non-flyby)	1800	s	1800	s
ΔT_{nf}^R	Range data interval (non-flyby)	6	hrs/day	2	hrs
ΔT_{nf}^V	VLBI data interval (non-flyby)	6	hrs/day	2	hrs
ΔT_{nf}^O	Optical data interval (non-flyby)	6	hrs/day	2	hrs
-	VLBI amount per week	1	day/week	1	day/week
-	Optical interruption around flyby	2	days	2	days

Estimation of JUICE

Regarding the estimation of JUICE (performed arc by arc), the different plots of Figure 7.8 show its standard deviation determined in each arc for different data types and weights.

The comparison between the cases of only range data show that the improvement using an accuracy of 0.2 m respect to 1 m is noticeable but not enormous; in the first case the σ_{rss} are in the range [1 m - 10 km], concentrated especially in the interval [100 m - 5 km], while in the second case they are in the interval [5 m - 50 km], concentrated especially in the interval [500 m - 50 km]. The minima are in correspondence of the flyby arcs; this is due to the higher amount of data used during a flyby (6 hours of data are collected around a flyby, while in non flyby arcs only 6 hours of data per day are collected).
When using the VLBI data the situation improves considerably; in the most optimistic configuration (accuracy of 0.2 m for range and 0.1 nrad for VLBI) the uncertainty of JUICE is of [1 m - 100 m], with minima as low as 1 m during flybys. When using worst weights (1 m for range and 1 nrad for VLBI) the uncertainty is concentrated in the interval [10 m - 500 m]. The results for different weights, not shown here, show a similar behavior: when

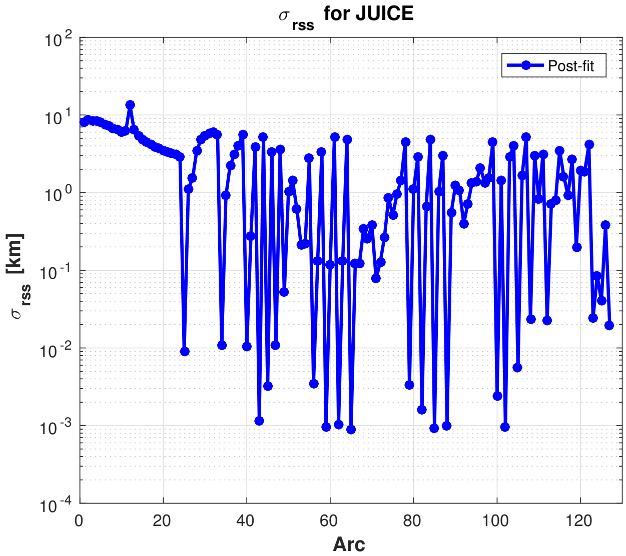

(a) Range only - $\sigma_r = 0.2$ m

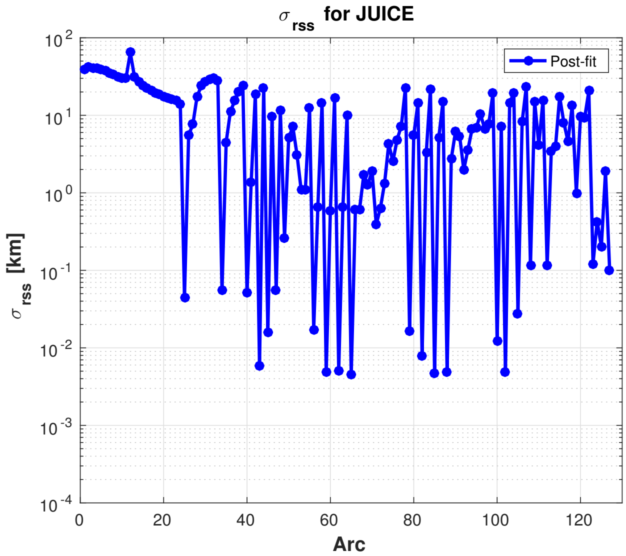

(b) Range only - $\sigma_r = 1$ m

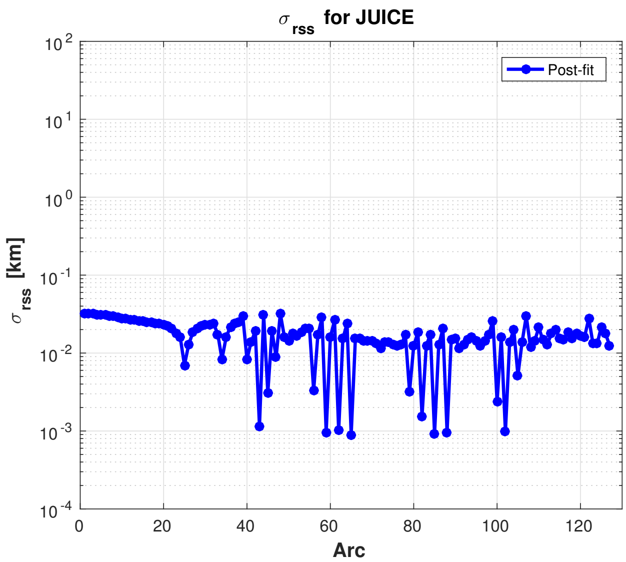

(c) Range and VLBI - $\sigma_r = 0.2$ m, $\sigma_v = 0.1$ nrad

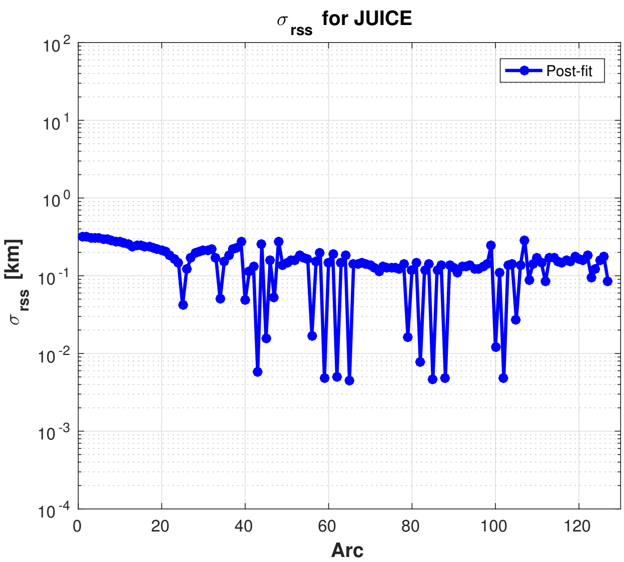

(d) Range and VLBI - $\sigma_r = 1$ m, $\sigma_v = 1$ nrad

Figure 7.8: JUICE standard deviation for each arc

using only range data with an accuracy of 10 m, the uncertainty on the position of JUICE increases to levels of up to 200 km, quite close to the initial a priori standard deviation (400 km per axis).

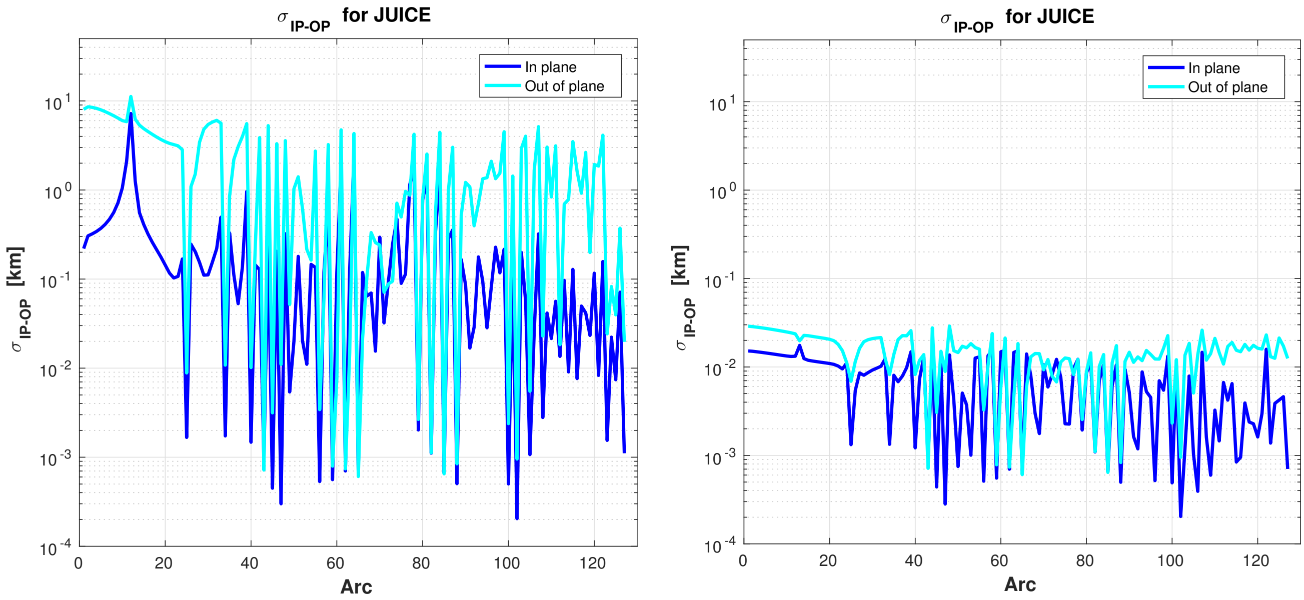

(a) Only $\sigma_r = 0.2$ m

(b) $\sigma_r = 0.2$ m, $\sigma_v = 0.1$ nrad

Figure 7.9: JUICE in plane and out of plane standard deviations for each arc

In Figure 7.9 are shown the standard deviation for the in-plane and out-of-plane components of the standard deviations for JUICE. It is interesting to notice that, although both the IP and OP components improve when using VLBI data, the improvement is better for the OP component; in Figure 7.9a the difference between the IP and OP components is often of 1 order of magnitude or more, while in Figure 7.9b this difference is smaller. As expected, VLBI data are fundamental for the determination of the out of plane position of the spacecraft. The results when using range only show quite high values (and also worst condition numbers) since due to the geometry of the problem, the tracking of a spacecraft around another planet from Earth is not well determined, at least for short arcs ([61]). It is necessary to add other information other than range to constrain the out-of-plane position. Regarding the tracking schedule, using the tracking schedule B (with less frequent measurements) degrades the accuracy on JUICE but in a limited amount. For example, for the case of tracking with range and VLBI with nominal accuracies, the reduction is from 100 m to 300 m (average for all the values of JUICE). This indicates that, even for a reduced tracking schedule, the performance for JUICE are sufficiently good.

The conclusion is that, if data with the current level accuracy are used (see 3.1) together with a nominal tracking schedule, an accuracy of around 100 m can be guaranteed for the spacecraft, with tracking arcs of a few days and including VLBI data; it is clear that is not possible to use range data alone. This is in accordance with [26]. Moreover, an improvement of the quality of the tracking technology to 0.2 m (as planned for the tracking system of JUICE, 3GM) for range and 0.1 nrad for VLBI (realizable if Ka-band transponder are used) is very beneficial for the determination of the position of JUICE.

It has to be kept in mind that due to the absence of Doppler (see 5.2) data and dynamical model inaccuracies, the results obtained for JUICE are just indicative and they do not represent the definitive accuracies that can be obtained. Using Doppler data, together with VLBI, would allow a even more accurate determination of the out-of-plane component of the position; however, if the VLBI schedule is reduced since Doppler is used, the results could be worst since the accuracy of VLBI for the angular position is higher than the accuracy of Doppler.

Estimation of the Galilean moons

The results of the sensitivity analysis for the Galilean moons are shown in Table 7.6, for the two different tracking schedule.

Table 7.6: Sensitivity analysis results for the Galilean moons - Data accumulation, tracking during pre-flyby

Variables			Results											
Data accuracies			Io			Europa			Ganymede			Callisto		
σ_R	σ_V	σ_O	σ_{IP}	σ_{OP}	σ_{avg}	σ_{IP}	σ_{OP}	σ_{avg}	σ_{IP}	σ_{OP}	σ_{avg}	σ_{IP}	σ_{OP}	σ_{avg}
m	$nrad$	μrad	km	km	km	km	km	km	km	km	km	km	km	km
Schedule A														
Range only														
0.2	-	-	0.02	0.07	0.06	0.006	0.07	0.05	0.007	0.05	0.03	0.01	0.02	0.03
1	-	-	0.09	0.39	0.30	0.03	0.39	0.25	0.03	0.25	0.17	0.07	0.10	0.17
10	-	-	0.32	3.90	3.01	0.33	3.92	2.54	0.36	2.54	1.71	0.74	1.03	1.73
Range and VLBI only														
0.2	0.1	-	0.02	0.07	0.06	0.006	0.07	0.05	0.007	0.05	0.03	0.01	0.02	0.03
0.2	1	-	0.02	0.07	0.06	0.006	0.07	0.05	0.007	0.05	0.03	0.01	0.02	0.03
0.2	10	-	0.02	0.07	0.06	0.006	0.07	0.05	0.007	0.05	0.03	0.01	0.02	0.03
1	0.1	-	0.09	0.39	0.30	0.03	0.39	0.25	0.03	0.25	0.17	0.07	0.08	0.16
1	1	-	0.09	0.39	0.30	0.03	0.39	0.25	0.03	0.25	0.17	0.07	0.10	0.17
1	10	-	0.10	0.39	0.30	0.03	0.39	0.25	0.03	0.25	0.17	0.07	0.10	0.17
10	0.1	-	0.31	3.53	2.68	0.31	2.82	1.83	0.35	1.77	1.20	0.71	0.30	1.42
10	1	-	0.32	3.89	3.00	0.33	3.90	2.52	0.36	2.52	1.70	0.73	0.89	1.66
10	10	-	0.34	3.90	3.01	0.33	3.92	2.54	0.36	2.54	1.71	0.74	1.02	1.73
Optical data for: Io,Europa														
0.2	0.1	1	0.003	0.05	0.04	0.004	0.04	0.03	0.007	0.04	0.03	0.01	0.02	0.03
0.2	0.1	10	0.008	0.07	0.06	0.006	0.07	0.05	0.007	0.05	0.03	0.01	0.02	0.03
1	1	10	0.02	0.33	0.26	0.03	0.31	0.20	0.03	0.25	0.17	0.07	0.10	0.17
1	10	1	0.005	0.06	0.06	0.009	0.05	0.03	0.03	0.16	0.11	0.07	0.10	0.16
1	10	50	0.05	0.36	0.30	0.03	0.38	0.25	0.03	0.25	0.17	0.07	0.10	0.17
10	1	10	0.08	0.64	0.63	0.09	0.51	0.34	0.32	1.60	1.10	0.70	1.02	1.67
Optical data for: flyby moon														
0.2	0.1	1	0.02	0.07	0.06	0.006	0.07	0.05	0.007	0.05	0.02	0.01	0.02	0.02
0.2	0.1	10	0.02	0.07	0.06	0.006	0.07	0.05	0.007	0.05	0.03	0.01	0.02	0.03
1	1	10	0.09	0.39	0.30	0.03	0.39	0.25	0.03	0.25	0.16	0.07	0.10	0.16
1	10	1	0.09	0.37	0.27	0.03	0.22	0.15	0.03	0.16	0.11	0.06	0.05	0.07
1	10	50	0.09	0.39	0.30	0.03	0.39	0.25	0.03	0.25	0.17	0.07	0.10	0.17
10	1	10	0.31	3.78	2.68	0.29	2.28	1.50	0.34	1.59	1.10	0.65	0.52	0.71
Schedule B														
Range, VLBI and optical (flyby moon)														
0.2	0.1	-	0.06	0.13	0.11	0.01	0.14	0.09	0.01	0.12	0.08	0.02	0.04	0.07
0.2	0.1	1	0.06	0.13	0.11	0.01	0.14	0.09	0.01	0.11	0.07	0.02	0.03	0.06
1	-	-	0.31	0.69	0.56	0.06	0.73	0.47	0.06	0.60	0.40	0.14	0.20	0.39
1	0.1	-	0.31	0.69	0.56	0.06	0.72	0.47	0.06	0.59	0.40	0.13	0.18	0.38
1	1	10	0.13	0.69	0.56	0.06	0.72	0.46	0.06	0.59	0.39	0.14	0.20	0.36

For almost all the simulations performed, the moon that is better estimated is Callisto, followed immediately after by Ganymede, then Europa and finally Io (for the indicator σ_{avg}). Considering that for these simulations the tracking is performed until 3 hours before the flyby, this is expected since the flyby data are exploited almost until the flyby time. This means that the 13 flybys of Callisto allow a better determination of this moon with respect to the other three; it is noticed that the average standard deviation is computed as a mean of the propagated standard deviation along the tour (Eq. 3.23), hence is catches the effect of all the flybys.

However for the in-plane component, this is not always determined better for Callisto, but very often for Ganymede and Europa. Instead, the out-of-plane component is always better determined for Callisto. This can be explained with the Laplace resonance, which involves Io, Europa and Ganymede but not Callisto and relates their in-plane positions. Moreover, as seen from the single-arc estimation (see 7.2.1) the estimation of Callisto is often more problematic than for the other moons. For the case of range data only, a strong improvement is observed when using an higher accuracy; the position is determined with an accuracy of a few tens of meters for the four moons using $\sigma_r = 0.2$ m. The in plane component is always better resolved than the out of plane component. The uncertainty scales almost linearly with the range weight, at least for the cases of 0.2 m and 1 m, while for the case of 10 m it deviates from a linear relationship.

When including VLBI data there is not always a net improvement such as for JUICE. In particular, the improvement is very limited or absent when very precise range data are used. The improvement is higher in correspondence of worst range accuracies. When using $\sigma_r = 1$ m and $\sigma_v = 0.1$ nrad this improvement becomes of 6.2 % for Callisto (about 10 m on 170 m). When using VLBI data with lower accuracies instead the improvement is zero (for example for $\sigma_v = 10$ nrad) or at least not visible at the level of tens of m (the improvement at the level of the meter is here neglected). Moreover is observed that the influence of VLBI data is mostly on the out of plane component of the position.
This means that when using already a lot of range data with good quality, the influence of VLBI data on the determination of the Galilean moons is limited (being however of fundamental importance for JUICE); instead, if less range data are available or with a worst accuracy, the use of VLBI is very important for a good estimation.

For the inclusion of optical data, two different strategies are analyzed, the observation of only Io and Europa and the observation of the Galilean moon target of a flyby.
For the first strategy, the observation of Io and Europa, the inclusion of optical data is not always beneficial for all the moons, but almost always only for Io and Europa. When very accurate range and VLBI data are collected, the inclusion of medium quality-bad ($\sigma_o = 10\ \mu rad$) optical data improves in a small amount the accuracy for Io and Europa (and not for Ganymede and Callisto). The inclusion of good quality ($\sigma_o = 1\ \mu rad$) optical data improves more the accuracy (for Io and Europa). Both the in-plane and out-of-plane components are improved. For the cases of worst accuracies for range and VLBI, the improvement for Io and Europa is relatively higher, unless bad quality optical data are used ($\sigma_o = 50\ \mu rad$).
For the second strategy of optical data, the observation of the flyby moon only, the improvement is more noticeable for Callisto. The same considerations on the weights as before are still valid. In this case all the 13 flybys of Callisto are fully exploited because every time Callisto is observed optically, reducing its uncertainty to 20 m for the case of best weights (an improvement of 33 %). Also in this case the inclusion of low quality optical data has little or no influence for Callisto and the other moons. It is noticed that the uncertainties increase for Io respect to the case of no optical data. The inclusion of optical data sometimes worsen the solution for a certain moon while improving the solution for another moon; this is an effect of the algorithm, that gives more weight to the moon that is observed optically, decreasing it for the other moons.
The conclusion is that, if the optical data are of too low quality (5 orders of magnitude worst than VLBI) then their inclusion is not crucial, especially if high quality radio tracking is available. Instead, if optical data are available with good quality their inclusion is essential for a further improvement of the ephemerides.
When using the degraded tracking schedule, the retrieved uncertainties are higher, as for JUICE. However the effect, at least for the tracking schedule B, is not very detrimental since the magnitude of the uncertainties increases just of a few hundred meters. Thus even a reduced tracking capability would allow a reliable estimation of the moons but with worst accuracies.

These results are for the uncertainties computed at the end of the tour, after all the flybys, but they do not show how the uncertainties vary along the tour. This is shown in Figure 7.10 where the evolution of the standard deviations along the tour for all the moons is shown (for the case of $\sigma_r = 1$ m and $\sigma_v = 0.1$ nrad). The improvement obtained with the single arc estimation is always limited, as expected because only data from one arc are used, while the improvement for the data accumulation is noticeable (as in the previous Subsection). For Io and Callisto the improvement is quite regular as the number of flybys increases; in particular for Callisto the central series of flybys decrease the uncertainty continuously, but in a limited amount. For Europa instead the improvement is not very regular (there are more oscillations). The greatest initial improvement is for Ganymede, as expected since the first three flybys are of this moon; for Callisto the improvement starts after its first flyby and becomes quite important in the central sequence of flybys. At the end of the tour there is a certain stabilization; the standard deviations evolution becomes almost flat for Io, indicating that new flyby would not bring a substantial improvement (however this can not be proven). For Europa and Callisto instead the behavior is still quite oscillating, meaning that a good improvement would still be possible with other flybys. This general behavior is however dependent upon the configuration under exam.

Concluding this Subsection, a comparison between the standard deviation for JUICE and the moons is done. Generally, the uncertainty for JUICE is determined with an higher accuracy than for the moons, because the spacecraft is tracked directly. The accuracy of JUICE is usually around two orders of magnitude better then the accuracy for the moons, for good data weights. However, when using low accuracies and the data accumulation version of the CA then the order of magnitude of the moons uncertainties becomes comparable with the one of the uncertainties of JUICE.

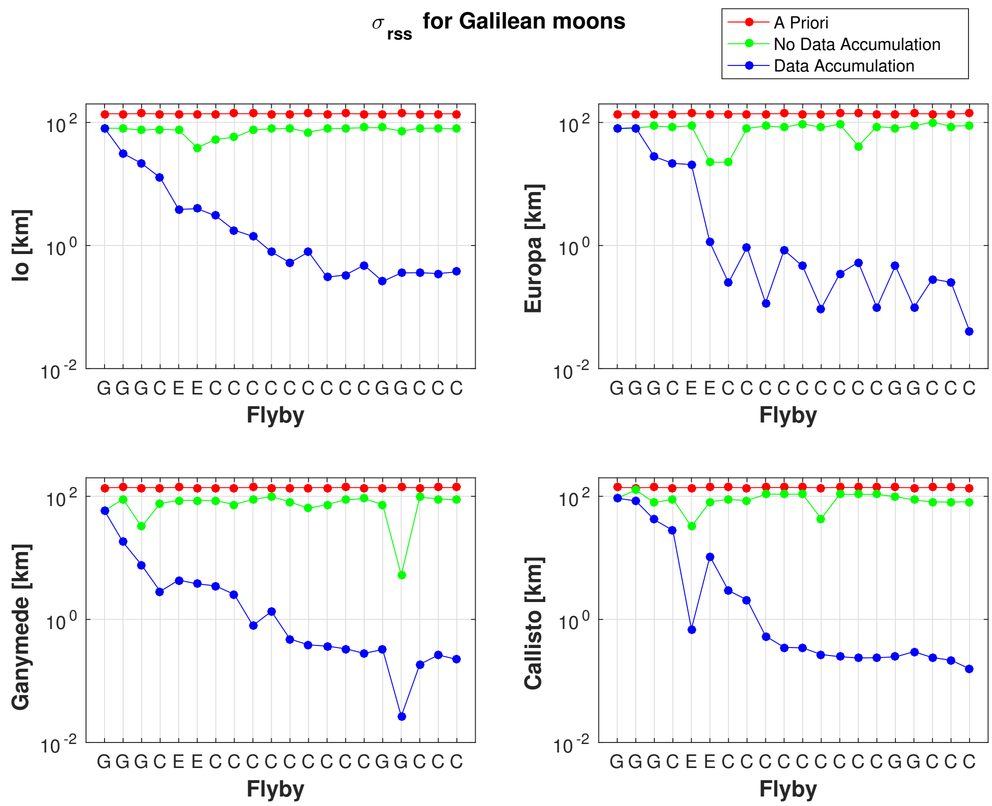

Figure 7.10: σ_{rss} for the Galilean moons during the Tour - Data accumulation, pre-flyby arc estimation

Comparison between the three strategies

The first observation to be done is that the results for all the three strategies appear to bee slightly too optimistic; especially for the case 2 where uncertainties of 0.2 m for the moons are obtained, which do not have a meaning for a planetary bodies. It is known in literature that the real accuracy is worse than the formal errors. In [35] sub-meter standard deviation for the semi-major axis of the inner planets are found too, although processing different types of data. One of the reason for these very optimistic uncertainties is due to the inaccurate modeling of the observables and the absence of measurements errors. In [12] a complete summary of these errors is presented; they can sum up to the meter level, thus prohibiting the use of the best accuracies ($\sigma_r = 0.2$ m, $\sigma_v = 0.1$ nrad). Moreover the computation of the observables has been assumed regular and with no interruptions; this is not the case for the real mission, where communications could be interrupted (due to solar events or the spacecraft eclipsed by Jupiter). The consequence of these assumptions is that, as seen in Figure 7.2a, the propagated uncertainty of a moon at the time of flyby goes towards zero. This happens also because probably some terms of the STM depend upon the relative distance spacecraft-moon, thus at the exact flyby time this distance is much smaller than at different times. However, due to the increased gravitational signature on the spacecraft during a flyby it is true that the relative distance can be determined much better, because the gravitational attraction of the celestial body is higher than any external perturbation. Thus such a

good knowledge appear partly possible, but only at the exact flyby time and not for long periods (see 7.3).
Comparing the three Strategies, it is concluded that the expected overall behavior is confirmed; the best uncertainties are for the Strategy 2, followed by Strategy 3 and finally by Strategy 1. Strategy 2 and 3 use more data for each flyby (see 5.2) than Strategy 1; strategy 2 uses data from exactly the flyby arcs rather then interrupting the tracking before it, as in Strategy 3.
The most realistic results are for the Strategy 3, since it is expected that data can be gathered for all the flybys (contrary to the assumptions of Strategy 1) and that the tracking is interrupted just before the flyby (which can happen in real missions). It is noted how estimating a moon with single-flyby data only but during the whole flyby can sometimes give better results than estimating a moon with using past data but interrupting the tracking a few hours before the flyby. The moon for which the difference between the strategies 2 and 3 is smaller is Io because its estimation is always indirect; when better data accuracies are used in Strategy 3 its estimation is better than in Strategy 2 for worse data. This does not happen for Callisto and Ganymede where the estimation is always better in Strategy 2, even for worse data. The potentiality of a complete flyby allows a far better estimation of the initial position. With respect to real mission operations these results show for each moon only the first flyby is quite risky, since the exact location of the moon is quite uncertain; after it, the position will be known much better for that moon decreasing considerably potential risks of impacts (see Section 8.4).
The results obtained for the moons are comparable with literature, especially for the most realistic case considered here (Strategy 3); in [49] similar uncertainties (from tens of meters to a few kilometers) are obtained for a similar mission (Cassini), which performed a flyby tour of the moons of Saturn. This is a confirmation that this Strategy gives the most realistic results, as already concluded. In the same reference, for some of the flybys of Titan (a moon of Saturn) uncertainties to the levels of 0.02 km are found too, showing that these results, even though unrealistic, can be obtained in this kind of simulations.
The research question number 2 can be considered answered since the effects of the different assumptions (strategies) and different parameters (especially the data types) on the results have been characterized.

7.3. On the improvement of the Galilean moons ephemerides

In this Section the contribution to the improvement of the ephemerides of the Galilean moons resulting from the flyby tour is discussed. The improvement is divided in short-term (for time intervals up to the mission duration) and long-term (for time intervals longer than the mission duration). This Section addresses the second research question, concerning the ephemerides improvement obtained with the Tour; in particular, the validity of this improvement over different time scales is studied.

Short term improvement

The propagation of the uncertainties is done using Eq. 3.23; the covariance matrix at an arbitrary time instant is computed with the initial covariance matrix and the state transition matrix. The STM is computed for every $t_j \in [t_0, t_{end}]$ (where the interval can be an arc or the total mission) with a time step Δt.

In Figure 7.11 the propagation of the uncertainties for two different arcs of the multi-arc covariance analysis is shown (for the configuration $\sigma_r = 1$ m, $\sigma_v = 0.1$ nrad of Strategy 3). In these and other plots the behavior is quite similar; depending on the length of the arc (spanning from a minimum of 4 days up to 10 days), there can be a periodic behavior only or a secular variation of the uncertainty. In particular, for Io there is always a periodic behavior while for Callisto there is often an increase without any periodicity. For Europa and Ganymede instead, there is periodic behavior for the cases of longer arcs (7.11a), while there is not for the cases of short arcs (7.11b). This difference can be explained considering the orbital periods of the Galilean moons (see Table 7.7).

Table 7.7: Galilean moons orbital periods around Jupiter

T_{orbit} $[days]$			
Io	Europa	Ganymede	Callisto
1.769	3.551	7.155	16.69

If an arc is longer then the orbital period of a moon, then the propagation will show a periodic structure due to the periodicity of the orbit; instead, if the arc is smaller than the orbital period, then it is more difficult to catch this behavior and the periodicity is lost.

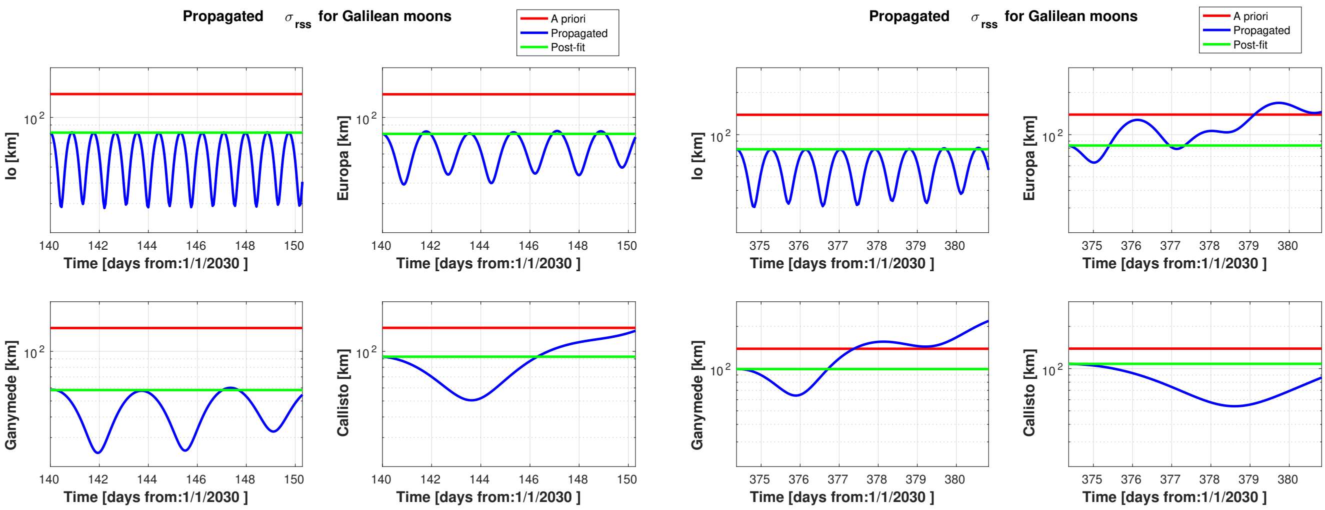

(a) 1^{th} flyby of Ganymede - Arc length: 10 days **(b) 5^{th} flyby of Callisto - Arc length: 6 days**

Figure 7.11: Propagation of the Galilean moons uncertainties during a single arc

This explains why in the plot 7.11a, where the arc is around 10 days, the periodic structure is captured for Europa and Ganymede, while in the plot 7.11b, where the arc is around 6 days, the periodic structure is partly captured for Europa but not for Ganymede. The propagation for such short arcs is thus not completely stable. A confirmation of this behavior comes from the structure of the propagated covariance matrix, in accordance with [36]. The covariance matrix at t_0 is

$$P_0 = \begin{bmatrix} \sigma_{x_0}^2 & & \ddots \\ & \sigma_{y_0}^2 & \\ \ddots & & \sigma_{z_0}^2 \end{bmatrix} \tag{7.1}$$

where for simplicity it has been reduced to to three standard deviations of the Cartesian position, neglecting the off-diagonal elements (while the full covariance matrix has 24 elements on the diagonal). The correspondent state transition matrix is

$$\Phi(t_j, t_0) = \begin{bmatrix} \frac{\partial x}{\partial x_0} & \frac{\partial x}{\partial y_0} & \frac{\partial x}{\partial z_0} \\ \frac{\partial y}{\partial x_0} & \frac{\partial y}{\partial y_0} & \frac{\partial y}{\partial z_0} \\ \frac{\partial z}{\partial x_0} & \frac{\partial z}{\partial y_0} & \frac{\partial z}{\partial z_0} \end{bmatrix}_j \tag{7.2}$$

The structure of the propagated covariance is

$$P_j = \begin{bmatrix} \sigma_{x_j}^2 & & \ddots \\ & \sigma_{y_j}^2 & \\ \ddots & & \sigma_{z_j}^2 \end{bmatrix} \tag{7.3}$$

where the standard deviations are (in a simplified form, neglecting the off-diagonal elements)

$$\sigma_{x_j} = \sqrt{\sigma_{x_0}^2 \cdot \left(\frac{\partial x}{\partial x_0}\right)^2 + \sigma_{y_0}^2 \cdot \left(\frac{\partial x}{\partial y_0}\right)^2 + \sigma_{z_0}^2 \cdot \left(\frac{\partial x}{\partial z_0}\right)^2}$$

$$\sigma_{y_j} = \sqrt{\sigma_{x_0}^2 \cdot \left(\frac{\partial y}{\partial x_0}\right)^2 + \sigma_{y_0}^2 \cdot \left(\frac{\partial y}{\partial y_0}\right)^2 + \sigma_{z_0}^2 \cdot \left(\frac{\partial y}{\partial z_0}\right)^2} \tag{7.4}$$

$$\sigma_{z_j} = \sqrt{\sigma_{x_0}^2 \cdot \left(\frac{\partial z}{\partial x_0}\right)^2 + \sigma_{y_0}^2 \cdot \left(\frac{\partial z}{\partial y_0}\right)^2 + \sigma_{z_0}^2 \cdot \left(\frac{\partial z}{\partial z_0}\right)^2}$$

Inspecting the state transition matrix it is possible to see that for each Galilean moon the terms are periodic with time, with a period equal to the orbital period of the moon. Although an analytic formula for the state transition matrix in cartesian coordinates does not exist, in [32] analytic partials for the cartesian elements with respect to the Keplerian elements are computed. These partials show that some of the terms of the matrix depend from the true anomaly, which is of course periodic along the orbit. Another term that appear is the mean motion multiplied by time, which is the cause of the divergence effect. As reported in [61] the STM in orbital mechanics has always coefficients that grow at least linearly with time. The overall behavior of the propagation that is visible at longer scales (periodic or divergent) depends upon the magnitude of the coefficients multiplying the periodic terms and the linear terms. These coefficients come from the covariance matrix at initial time (eq. 7.1).

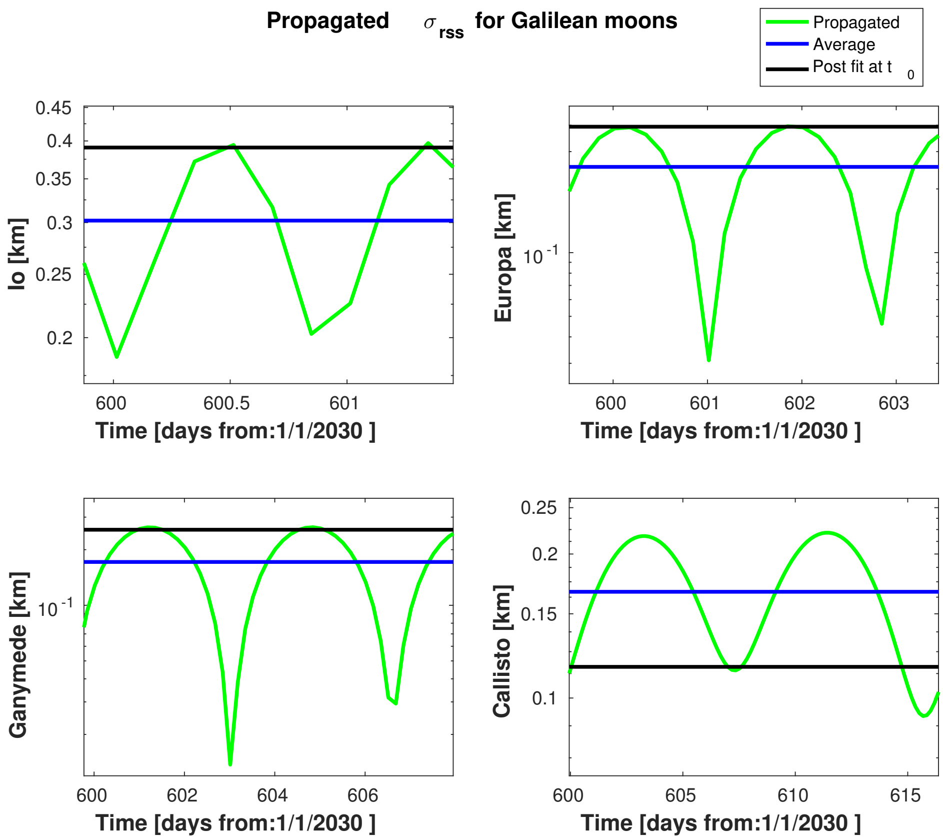

Figure 7.12: Periodic behavior of the propagated covariance

The structure of the propagated standard deviations is thus also periodic with a period equal to

$$T_{prop} = \frac{T_{orbit}}{2}$$

since the squaring in equations 7.4 has the effect of doubling the frequency of the oscillations. This structure is clearly observable in Figure 7.12, where is shown a zoom of the covariance propagation during the complete flyby tour duration (the plots are not smooth due to the time discretization which is quite coarse). It is possible to see that the period of the oscillations is around half of the orbital period for each moon (it is not exactly half because the STM is computed numerically and the orbits are not Keplerian).

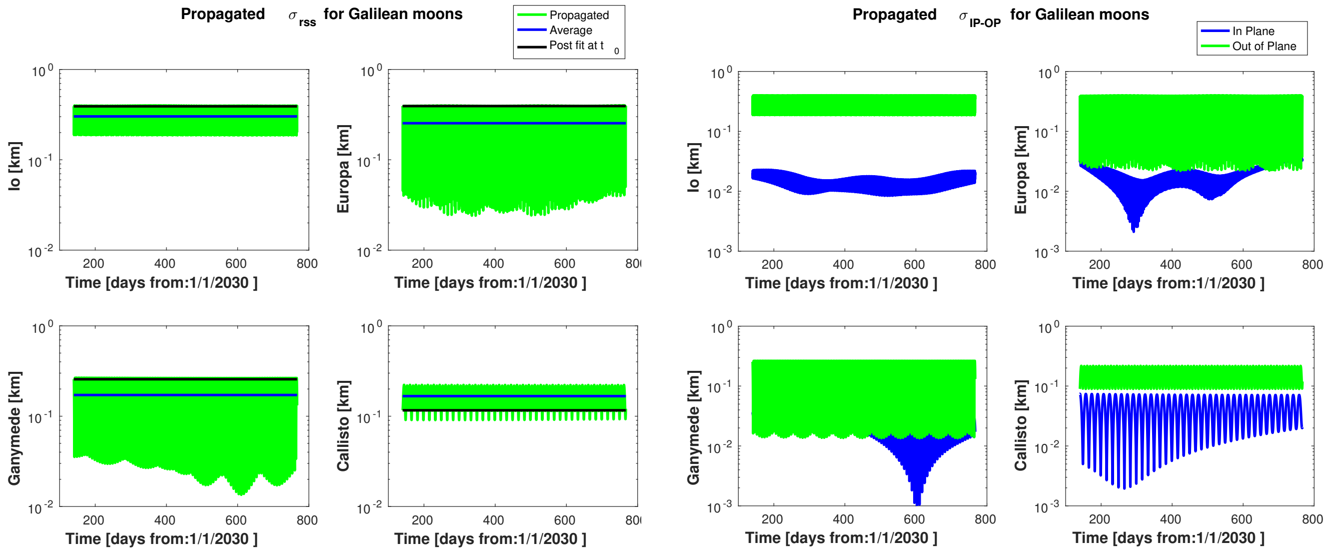

(a) Three dimensional standard deviation

(b) In-plane and out-of-plane standard deviations

Figure 7.13: Propagation of the Galilean moons uncertainties during the flyby tour time

Figure 7.13 shows the propagation of the covariance for the entire duration of the flyby tour, divided in three dimensional (7.13a) and in-plane and out-of-plane (7.13b); the case in consideration is for $\sigma_r = 1$ m, $\sigma_v = 0.1$ nrad and no optical data (of Strategy 3). The propagation is performed for the covariance matrix at $t_0 = 21-05-2030$ (corresponding to the first pre-flyby arc) computed at the end of the mission, using all the data; it is expected to be stable ([36]).

The propagation inside the interval of the mission is stable for all the Galilean moons, meaning that the uncertainty of the ephemerides is bounded between the minimum and maximum values of the oscillations. This means that the terms that increase linearly are negligible in magnitude with respect to the periodic terms; this can be due to the fact that the propagation is performed in a period of time during which observations are taken regularly, and the moons are estimated quite often (20 times), giving information well distributed in time. The average uncertainty during this interval is of around 0.5 km for Io and Europa and of 0.2 km for Ganymede and Callisto. These levels are in accordance with [49], where similar plots are provided for the uncertainties of the satellites of Saturn, as retrieved by Cassini data.

Long term improvement

The results of the long term propagation for the covariance matrix are shown in Figure 7.14, where the covariance matrix has been propagated for the time of 4 years, so outside the end of the mission. It is clearly visible a divergence for Io, Europa and Ganymede that starts at around 760 days after 1-1-2030, corresponding to the end date of the flyby tour. The divergence is most evident for Europa and less for Io and Ganymede. For Callisto instead there is not a divergence but only a small increase of the propagated standard deviations at the end of the interval. The periodic behavior remains for all the four moons, but for Io, Europa and Ganymede it is superimposed to a secular variation. For what explained before, it can be concluded that over such long period of time the linear increasing terms of the state transition matrix take over the periodic terms. The difference between Callisto and the other 3 moons can be explained by the high number of flybys of Callisto: the stability of this improvement is higher for Callisto.

In [36] it is indicated that the mapping of the covariance necessitates a stable system; the results obtained here indicate that the system is stable only during the interval of the mission, but not outside the fit interval, where the secular terms increase. The divergence could be partly due to the linearization process and the big time step used to generate the state transition matrix for 4 years (of 10 hours). The current results are obtained with data from 20 flybys only; the inclusion of past observations was not possible in the scope of the project. An interesting investigation would be to see the effect of adding the flyby data of JUICE to the existent data used to compute Jovian System ephemerides and analyze their impact. As explained in Section 3.5, the ephemerides of celestial bodies are computed using a huge amount of data from a very long time span (especially astrometric observations from Earth). Flybys are important data to improve the quality of the ephemerides, due to the vicinity of the spacecraft to the celestial body and the higher accuracy of radio tracking, but alone they are not enough for a complete description of the system dynamics for a long time span. As reported in [36], to represent faithfully the evolution of the uncertainties over a certain period of time, observations that cover all that period are needed. If the future uncertainty wants to be estimated instead, past data that cover a long time span have to be used to constrain the dynamical evolution over a longer period of time. In that way the estimation would not tailor the system to the flyby data only, which can not catch the long time dynamical effects.

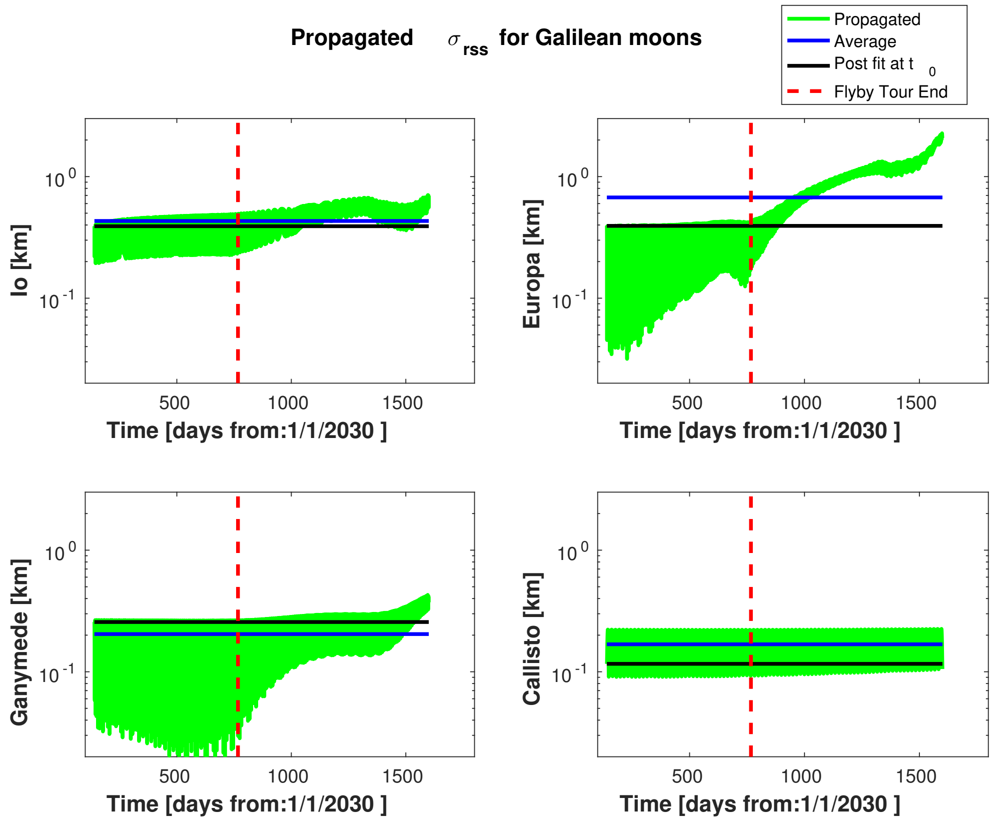

Figure 7.14: Propagation of the Galilean moons uncertainties for 4 years

8 NAVIGATION ANALYSIS RESULTS

In this Chapter the results of the Monte Carlo Navigation Analysis are presented (for the theory see Chapter 4, for the implementation see Section 5.3 and 5.4 and for the validation see Section 6.3). The Chapter is structured in the following way. In Section 8.1 the total Tour ΔV is presented for different configurations of the CA (see Chapter 7) and of the guidance. Section 8.2 presents the ΔV for all the flybys, for one of the configurations of the preceding Section, in order to analyze the contribution of each flyby to the total ΔV budget. In Section 8.3 a detailed sensitivity analysis of the ΔV with respect to the maneuver time is performed, since this parameters has the highest influence on the results. An analysis on the influence of the maneuver error (see Subsection 4.3.5) is performed too. The last Section 8.4 presents the results of the impact analysis performed, which helps to further understand the influence of the covariance analysis results on the flybys performances. This analysis is performed to give a feeling of the risk of impacts for JUICE when performing the flyby tour. It is anyway a limited analysis due to the different assumptions adopted.

The simulations presented in this Chapter use the approximated targeting algorithm (see 4.3.4) where not specified differently; this because it has a sufficient accuracy but a much greater computational speed with respect to the B-Plane and optimized targeting (see Subsection 6.3.3 and Figure 6.19). The difference in the computational cost between the approximated and the optimized Monte Carlo simulations is very significant; for one Monte Carlo run with 500 samples the approximated version needs only about 10 s, while the optimized version needs about 60-120 minutes (depending upon the time of maneuver and hence the length of the propagations). As shown in the validation of the Monte Carlo (Section 6.4), a minimum of 1000-2000 samples is required to have good statistical indicators; this would imply a prohibitive cost for the optimized targeting, since different sensitivity analysis have to be performed. Moreover for the simulations the server of the department of Space Engineering of TU Delft has been used; due to resources constraints a reduced number of samples had to be used when using the optimized targeting. The conclusion is that, for a preliminary statistical analysis the use of the approximated algorithm is sufficient; however in real mission operations the use of an optimized targeting is necessary. In Appendix B some results with the optimized algorithm are presented.
Where not specified, the simulations are performed with the simple dynamical model; just a few simulations have been performed with the complex dynamical model (the difference is explained in Subsection 3.2.1). The rationale is that the simple dynamical model required a smaller computational time and the differences are relatively small.

The research questions addressed by this Chapter are the first and the third; the first purpose of this Chapter is to quantify the reduction of the ΔV coming from the TCM required to correct for the moons and spacecraft uncertainties when the knowledge of the moons ephemerides improves (Question 1). This is addressed in Sections 8.1 and 8.2. It is highlighted again that the results obtained here analyze only the influence of the spacecraft and moons uncertainties on the maneuvers and not other uncertainties or displacements from the nominal trajectory (see 5.1).
The second purpose is to determine the influence of the different parameters of the guidance on the TCMs (Question 2); in particular, two main parameters have been analyzed (in Section 8.3), the maneuver time and the maneuver execution error.

8.1. MONTE CARLO SIMULATIONS RESULTS FOR TOTAL TOUR ΔV

In this Section the results of the Monte Carlo simulations for the total Tour ΔV are presented for the following configurations

- baseline case: the a priori standard deviations for the moons are used for all the flybys, to simulate no ephemerides improvement (the knowledge on the moons position does not improve);
- influence of JUICE position uncertainties only: the ΔV required to correct for the uncertainties in the position of JUICE (after the orbit determination) is computed;
- Strategy 1 of the CA (see Subsection 5.3.1 for the explanation and 7.2.1 for the results of the correspondent CA); this configuration assumes that the tracking is performed during the flyby arcs but the uncertainty computation is performed using a single flyby only and not the previous ones;
- Strategy 3 of the CA (see Subsection 5.3.3 for the explanation 7.2.3 for the results of the correspondent CA); this configuration assumes that the tracking is performed during the pre-flyby arcs and the uncertainty computation is performed using all the data from the previous flybys;

As explained in Section 5.3, to respect the causality principle, a certain pre-flyby maneuver is designed using data from the past only; for Strategy 1 this means that a maneuver is designed using the moon uncertainty determined at the previous flyby of that moon. For the first flyby of each moon, the a priori value is used. For Strategy 3 this means that a maneuver is designed using all the data from the previous flybys (of all the moons) but not the data from the current one. This could be possible since the tracking is performed before the flyby and not during; however a certain time is needed to perform the OD and compute the maneuver, hence it is operationally impossible. Only with an autonomous navigation system it could be possible. The post-flyby maneuver instead is designed using also the current flyby data, to simulate the further improvement obtained with the current flyby; this is realistic for maneuvers placed at least 48 hours after the flyby, in order to allow the time for the OD and maneuver design.
Strategy 2 of the CA (exposed in Subsection 5.3.2 and 7.2.2) is not used here since it would give too optimistic results as seen from the results in Section 7.2; Strategy 1 and 3 give a good overview of the results obtainable under different mission operations assumptions. The maneuvers computed with Strategy 1 and 3 are the pre and post flyby maneuvers (see 4.3.1 and 5.3). In Sections 8.1.3 and 8.1.4 the results are presented for different values of the observables types and weights and of the maneuver time. The maneuver times investigated are in the interval

$$\text{maneuver time:} \quad t_{man} \in [1-72] \quad \text{hours before (after) flyby}$$

This interval is selected since from literature ([56], [42]) the common TCM execution time for similar flybys tours is 3 days before (or after) the flyby. The smaller maneuver times are used to analyze what happens in case of failure of the first planned TCM (for the pre-flyby maneuver).
For the two different Strategies, the correspondent CA configurations in Section 7.2 are used (see Tables 7.2 and 7.5). However, to reduce the amount of data presented, a reduced number of configurations with respect to 7.2 is used. Only one tracking data schedule is used. The a priori uncertainty for the moons is always set to 80 km per axis.
The fixed settings for the Monte Carlo analysis are the following: the samples used are 2000 and the confidence level used is equal to three (see Subsection 4.2.1); this means that the ΔV results provided are with a confidence of 97.1 % (for a trivariate Gaussian distribution). This level has been chosen since it allows a more realistic representation of the possible distribution of the perturbed trajectories with respect to the nominal.

8.1.1. BASELINE CASE: NO EPHEMERIDES IMPROVEMENTS

In this case the a priori uncertainty of the moons positions is used for all the flybys, simulating thus no ephemerides improvement. The consequence is that the measurements have influence on the uncertainty of JUICE only and not of the Galilean moons; but since the level of the uncertainty of JUICE is much lower than the a priori uncertainty of the moons (under the assumption that sufficient data weights are used, for example $\sigma_r < 5$ m and $\sigma_v < 5$ nrad, see 7.2.3 for the results of JUICE), in this case the uncertainty of JUICE can be neglected. Thus the influence of the different data weights is not analyzed, but only the influence of the maneuver time.

In Table 8.1 the mean, standard deviation and 95 % percentile are shown for each simulation. The results are for the pre-flyby maneuver only; for the post-flyby maneuver they are quite similar since the same perturbation is applied.

Table 8.1: Monte Carlo Analysis results - Baseline case

N	ΔV - mean	$\Delta V - 1\sigma$	$\Delta V - 95\%$	t_{man}
	m/s	m/s	m/s	$hrs(flyby)$
1	2128.95	209.81	2478.64	1
2	1063.75	104.91	1237.97	2
3	532.41	52.37	621.50	4
4	217.10	21.37	253.61	10
5	90.16	9.33	106.17	24
6	47.36	6.76	59.07	48
7	79.98	13.69	102.99	72

The magnitude of the ΔV (for all the three statistical indicators) decreases when moving the time of the maneuver far away form the flyby time until the time of 48 hours. However, between 48 and 72 hours from flyby there is an inversion of the ΔV behavior: it increases instead of decreasing; this behavior will be analyzed in detail in Subsection 8.3.1; in the next Sections less maneuvers times are used to reduce the size of the Tables. An interesting thing to notice is that from 1 hour before the flyby to 48 hours, the reduction of the ΔV is very close to be directly proportional to the time of the maneuver.
In order to bring back the spacecraft to the nominal trajectory after a perturbation is applied, a certain time is required. This because, even if the TCM is modeled as instantaneous, its effect on the position is not: only the velocity of the spacecraft changes instantaneously; the effect on the position are seen only after some time has passed. Intuitively, if there is a lot of time available before an event (in this case the flyby) a small and precise action has a lot of time available to produce the required results (the change in position). It is immediate to understand that, if a big perturbation needs to be corrected just 1 hour before the flyby, not a lot of time is available to correct the future position of the spacecraft, hence a lot of energy is required.
The ΔV required for the cases of 1 to 4 hours are prohibitive for the total ΔV budget for JUICE, since they are closer to the deterministic maneuvers to be performed (see 6.1). This shows that a reduction of the moons positions uncertainties is necessary.
For last it is noted how the 95 % percentile is always higher than the sum of the mean with the standard deviation. Moreover, the standard deviations is never bigger than the mean value, showing reliable statistical results.

8.1.2. Results for the uncertainties of JUICE only

In Table 8.2 is shown the total ΔV required to correct for the uncertainty on the position of JUICE (after the orbit determination). It is noticed again that this uncertainty is applied around the nominal position at the time of maneuver since a CA is performed only and not a LSQ (see Section 5.1).
It is clearly visible that for both the cases of current data accuracies (results from 5 to 8) and for improved data accuracies (planned for JUICE, results from 1 to 4) the ΔV required is really small and practically negligible with respect to other error sources. Instead, in case of a bad tracking (results from 9 to 13) the ΔV required would be much higher; in this case moreover the maneuver is much more risky since the knowledge of the position would be quite inaccurate hence with a higher risk of impact on the moon.

8.1.3. Results for Strategy 1

In Strategy 1 the maneuvers are designed using data from a flyby only (for the pre-flyby maneuver the previous flyby of that moon if available, if not the a priori uncertainty is used; for the post-flyby maneuver the current flyby is used).

In Table 8.3 the results obtained are shown; first of all it is possible to see a general decrease in the ΔV with respect to the case of no ephemerides improvement (Table 8.1). In all the cases presented there is a decrease in ΔV (for the same maneuver time); the cases with the smallest improvements are the ones with the worst data accuracies (numbers 17-20). As highlighted in Subsection 8.1.2, when using bad tracking data the uncertainty

Table 8.2: Monte Carlo Analysis results - JUICE uncertainties only

N	ΔV - mean	$\Delta V - 1\sigma$	$\Delta V - 95\%$	t_{man}
	m/s	m/s	m/s	$hrs(flyby)$
$\sigma_r = 0.1$ m, $\sigma_v = 0.2$ nrad				
1	0.07	0.01	0.09	4
2	0.01	0.002	0.01	24
3	0.01	0.002	0.01	48
4	0.01	0.003	0.02	72
$\sigma_r = 1$ m, $\sigma_v = 1$ nrad				
5	0.55	0.08	0.69	4
6	0.08	0.01	0.10	24
7	0.03	0.00	0.04	48
8	0.09	0.02	0.13	72
$\sigma_r = 10$ m				
9	252.62	51.58	341.56	4
10	37.76	7.87	51.41	24
11	12.52	2.78	17.39	48
12	33.94	9.97	51.02	72

of JUICE is not anymore negligible with respect to the moons uncertainties. Thus the positive effect of the (limited) ephemerides improvement obtained is partly canceled by the high uncertainty for JUICE.
The decrease in ΔV is high in absolute value when moving the maneuver time towards the flyby time; for example, when using very high accuracy for range and VLBI (0.2 m for range and 0.1 nrad for VLBI) there is a reduction of 434 m/s (81 %) and 66 m/s (82 %) for the maneuver times of 4 and 72 hours (for the pre-flyby maneuver). For the post-flyby maneuver the reduction is of 513 m/s (96 %) and 77 m/s (96 %) for the two maneuver times. This decrease is higher in absolute value but very similar in relative value. This behavior appears to be logical because when the spacecraft is close to flyby the ΔV is higher hence there is a big margin for improvement if the error in position is reduced. Instead, when far away, a difference in 10-20 km in error does not impact a lot the ΔV required for the maneuver.

The behavior with respect to the tracking data accuracies is the one expected: there is a decrease in ΔV when the quality of the data improves. This was expected due to the results of the CA (Section 7.2) and the almost linear relationship perturbation-ΔV (see 4.3.4). For example, for the case of range data only, the improvement obtained when using an accuracy of 0.2 m instead of 1 m is around 45 % for the pre-flyby maneuver and 65 % for the post-flyby maneuver.
When adding VLBI data the decrease is also noticeable, however more limited than the case of improvement of range data (for example, the ΔV for combinations 1-4 are lower than for combinations 13-16), indicating that an improvement of the range data impacts more than adding VLBI data but keeping a bad accuracy.

The comments about the ΔV are relative to the average values; in the Monte Carlo analysis also the standard deviation (1σ) and the 95% percentile are computed.
The standard deviation scales with the ΔV magnitude; it is almost directly proportional to the average. This is expected, since an higher value of average ΔV implies that around it there are more values possible; it would be strange to observe standard deviations higher than the average ΔV or standard deviations infinitesimally smaller than the average.
This means that for the cases of high ΔV, the real maneuver required could be more expensive than the estimated, thus demanding more propellant. To avoid the spacecraft to deplete its propellant before expected, the propellant budget is computed using the 95 % (or 99%) percentile, that represents the worst-case scenario. As observed from the Tables, this value is considerably higher than the average; usually is higher than the average plus the standard deviation.

When optical data are included (where the flyby moon is observed) there is a further decrease in ΔV; it has to be noticed however that these improvement may bee too optimistic because the distance JUICE-moon may be too small to obtain accurate information. Since the flyby arc starts 3 days before the flyby, the optical data

Table 8.3: Monte Carlo Analysis results - Strategy 1

	Pre-flyby			Post-flyby			
N	ΔV - mean	$\Delta V - 1\sigma$	$\Delta V - 95\%$	ΔV - mean	$\Delta V - 1\sigma$	$\Delta V - 95\%$	t_{man}
	m/s	m/s	m/s	m/s	m/s	m/s	$hrs(flyby)$
$\sigma_r = 0.2$ m							
1	117.64	20.54	152.57	37.47	6.66	49.29	4
2	19.57	3.77	26.21	7.90	1.32	10.26	24
3	9.17	2.58	13.83	5.22	0.92	6.84	48
4	17.34	5.06	26.87	5.48	1.05	7.36	72
$\sigma_r = 1$ m							
5	205.08	26.86	250.45	119.76	16.55	148.51	4
6	32.92	4.54	40.69	25.93	3.50	31.99	24
7	14.53	2.82	19.56	16.94	2.33	20.98	48
8	31.58	6.76	43.65	17.90	2.81	22.88	72
$\sigma_r = 0.2$ m, $\sigma_v = 0.1$ nrad							
9	98.01	19.79	132.03	18.95	3.46	25.15	4
10	16.60	3.68	23.20	3.96	0.68	5.15	24
11	8.21	2.57	12.96	2.65	0.47	3.48	48
12	13.93	4.77	22.71	2.93	0.63	4.05	72
$\sigma_r = 1$ m, $\sigma_v = 1$ nrad							
13	152.25	22.62	191.46	75.99	11.68	96.51	4
14	25.61	4.09	32.68	15.70	2.25	19.48	24
15	12.13	2.72	17.02	10.36	1.51	13.05	48
16	24.43	5.80	35.27	10.74	1.79	13.90	72
$\sigma_r = 10$ m, $\sigma_v = 10$ nrad							
17	248.80	29.38	299.21	187.78	22.69	224.95	4
18	41.71	5.22	50.74	39.56	4.69	47.58	24
19	18.92	3.16	24.45	27.95	3.37	33.82	48
20	43.90	9.21	60.10	30.17	4.79	38.86	72
$\sigma_r = 1$ m, $\sigma_v = 1$ nrad, $\sigma_o = 1$ μrad							
21	86.52	19.57	120.20	6.99	1.13	8.95	4
22	14.69	3.65	21.20	1.48	0.22	1.85	24
23	7.55	2.57	12.27	1.01	0.16	1.29	48
24	11.45	4.68	20.38	1.04	0.16	1.31	72
$\sigma_r = 1$ m, $\sigma_v = 1$ nrad, $\sigma_o = 10$ μrad							
25	110.52	20.07	144.61	31.49	4.75	39.79	4
26	18.61	3.73	25.39	6.97	1.03	8.78	24
27	9.24	2.59	13.89	4.74	0.71	6.00	48
28	14.59	4.76	23.57	5.12	0.86	6.65	72

interruption has been set to two days in order to allow their inclusion. In reality this could not be possible from such a small distance and a different strategy shall be investigated.
The ΔV reduction for the pre-flyby maneuver is of 27 % and 40 % for the the case of $\sigma_o = 10\mu$ rad, for the maneuver times of 4 and 72 hours; when improving the optical data accuracy to 1μ rad the decrease is of 43 % and 53 %, for the same two cases. For the post-flyby maneuver these reductions are higher, of 58 % and 48 % for the worst accuracy and 90 % for the best accuracy. This improvement is really high, thus indicating that the usage of optical data is fundamental for a efficient navigation during the flyby tour.
From the simulations it has been noticed that in the presence of optical data the influence of VLBI data quality on the final ΔV is reduced; this means for for a fixed configuration of range and optical data the results will be almost independent upon the VLBI data. This because the optical data are of higher importance for the ephemerides rather than the VLBI data.
The conclusion is that optical data are important for a more accurate estimation of the state of the moons, but is necessary to use them in combination with good quality radiometric observations. Moreover, it is noted that in the real mission it could not be always possible to observe the target moon before the flyby due to pointing requirements.
The results show a difference between the size of the pre-flyby (targeting) and post-flyby (cleanup) maneuvers. This is due to two reasons: first of all the cleanup maneuver is designed using data from the current flyby, so there are no cases where the a priori uncertainty has to be used (as for the targeting). The second reason is that the targeting algorithms used is different, being the B-Plane targeting. For what exposed in Subsection 5.3.1, due to some limitations and assumptions, it was not possible to design an accurate cleanup maneuver, hence the one computed is not fully indicative of the real maneuver required. Moreover the B-Plane targeting algorithm is often in error when used outside the SOI (6.3.1).
The ΔV for the cleanup maneuver is almost always smaller due to the first reasons, that the current flyby uncertainties are used; it is thus noticed that to correct for a wrong flyby execution a relatively small ΔV is required, but comparable to the one required to target the flyby.
In the Table, the results for the maneuver time of 4 hours after the flyby are unrealistic because there would not be the time to perform an OD of the spacecraft, analyze the results and design the maneuver. In [42] is indicated that, based on the Cassini experience, is is acceptable to use one Orbit Determination track after a flyby to design the cleanup maneuver. Since this track has to be of at least one day to allow a good determination, it appears that the minimum time required for this maneuver is of two days after the flyby.

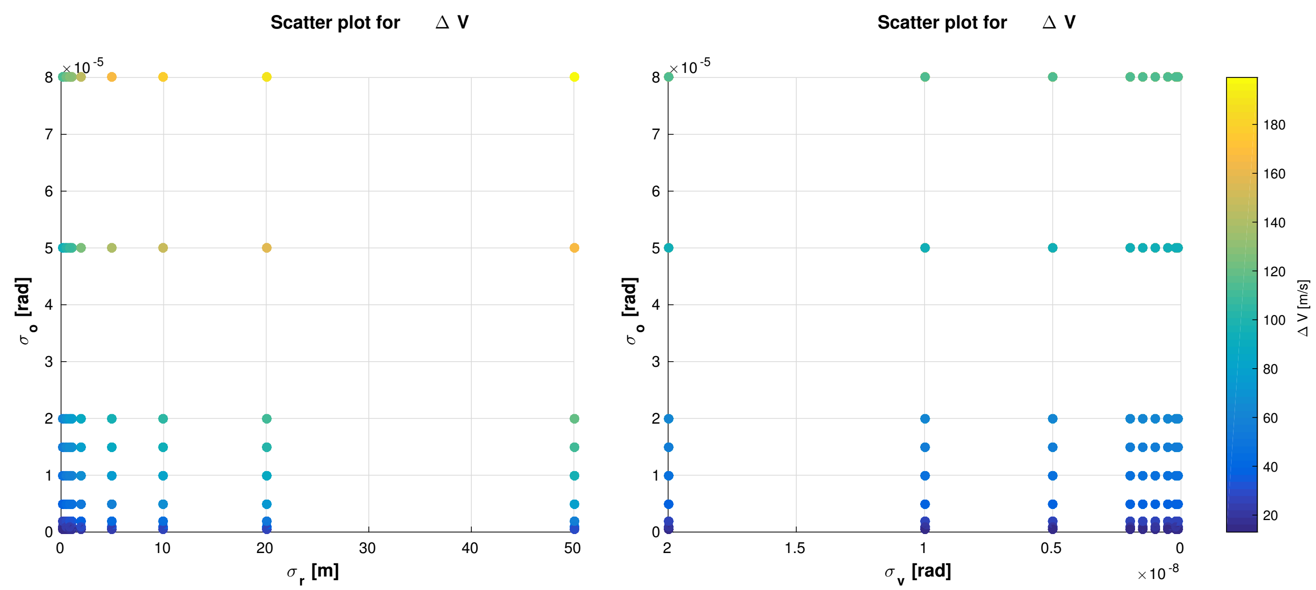

(a) ΔV Sensitivity respect to optical and range weights

(b) ΔV Sensitivity respect to optical and VLBI weights

Figure 8.1: ΔV sensitivity with respect to data weights

In Figure 8.1 the sensitivity of the ΔV respect to the data weights is shown; this Figure shows in a graphical way what described before; this plots are obtained from 729 Monte Carlo simulations (9 different data weights per type have been tried, giving $9^3 = 729$ combinations). It is clearly visible that, as observed from the Tables, the greatest influence is from the optical data, then from the range and finally from VLBI. This because the variations in the σ_o and σ_r directions have a greater gradient than in the σ_v direction.

8.1.4. Results for Strategy 3

In Strategy 3 the maneuvers are designed using all the data from the past flybys for the moons, but performing the tracking during the arc just before the flyby (for the pre-flyby maneuver the data from the current pre-flyby arc are not included while for the cleanup maneuver they are). These arc have a duration between 10 and 6 days, depending on the distance between the flybys (for example during the central sequence of flybys of Callisto the length is reduced to 6 days). The tracking is interrupted 3 hours before the flyby.

Table 8.4: Monte Carlo Analysis results - Strategy 3

	Pre-flyby			Post-flyby			
N	ΔV - mean	$\Delta V - 1\sigma$	$\Delta V - 95\%$	ΔV - mean	$\Delta V - 1\sigma$	$\Delta V - 95\%$	t_{man}
	m/s	m/s	m/s	m/s	m/s	m/s	$hrs(flyby)$
$\sigma_r = 0.2$ m							
1	48.13	13.75	72.46	16.23	6.60	28.67	4
2	7.56	2.18	11.45	3.48	1.18	5.67	24
3	3.39	1.03	5.24	2.89	1.07	4.83	48
4	3.75	1.00	5.54	3.47	1.24	5.71	72
$\sigma_r = 1$ m							
5	79.05	16.37	108.28	30.91	8.34	46.46	4
6	12.14	2.49	16.53	7.08	1.73	9.99	24
7	4.74	1.12	6.71	5.71	1.53	8.49	48
8	9.29	2.98	14.95	6.67	1.81	9.89	72
$\sigma_r = 0.2$ m, $\sigma_v = 0.1$ nrad							
9	43.04	13.74	67.78	14.71	6.18	26.17	4
10	6.81	2.19	10.73	3.08	1.02	4.89	24
11	3.01	1.00	4.77	2.53	0.93	4.25	48
12	3.20	0.92	4.86	2.77	0.98	4.52	72
$\sigma_r = 1$ m, $\sigma_v = 1$ nrad							
13	62.21	15.25	89.01	29.38	8.17	44.47	4
14	9.51	2.35	13.91	6.79	1.65	9.73	24
15	3.81	1.07	5.68	5.36	1.41	7.97	48
16	7.48	2.59	12.19	5.97	1.62	8.89	72
$\sigma_r = 10$ m, $\sigma_v = 10$ nrad							
17	141.12	24.73	182.79	101.95	19.08	135.13	4
18	21.49	3.68	27.81	25.94	5.41	35.42	24
19	7.99	1.57	10.71	20.15	4.39	27.88	48
20	24.06	7.07	36.58	21.76	5.08	30.55	72
$\sigma_r = 1$ m, $\sigma_v = 1$ nrad, $\sigma_o = 1$ μrad							
21	37.05	12.52	58.87	1.60	0.28	2.11	4
22	5.79	2.01	9.41	0.39	0.06	0.50	24
23	2.45	0.90	4.09	0.32	0.06	0.44	48
24	4.47	2.17	8.60	0.37	0.07	0.50	72
$\sigma_r = 1$ m, $\sigma_v = 1$ nrad, $\sigma_o = 10$ μrad							
25	48.81	13.28	71.78	7.41	1.30	9.71	4
26	7.71	2.10	11.48	1.83	0.32	2.38	24
27	3.12	0.92	4.75	1.50	0.29	2.01	48
28	6.17	2.58	11.15	1.70	0.39	2.39	72

The results obtained are shown in Table 8.4. The same observations of the previous Subsection apply also here. The ΔV is always reduced with respect to the case of no ephemerides improvement. This reduction is higher for the cleanup maneuver than for the targeting maneuver, since more data are used for it. It is interesting to notice however that sometimes, for a same configuration, the cleanup manuever is higher than the targeting maneuver (for examples for the cases 7, 15, 19). This can be due to the inaccuracy of the B-Plane targeting or to the fact that the covariance determined at the time of the cleanup maneuver is higher than the one at the time of the targeting maneuver. This happens mostly around the time of 48 hours. The ΔV is reduced if better tracking data accuracies are used, with a great influence coming from the use of optical data. The behavior of the ΔV with respect to the time of maneuver is similar to the one observed in the previous Subsection, with a decrease until 48 hours but an increase from 48 hours to 72 hours.

In this version of the algorithm it is possible to see that the contribution of the uncertainties of JUICE and the Galilean moons on the ΔV required to perform the tour can become really low if good data weights are used and if the maneuver time is chosen properly. For example, for the case of best accuracies (σ_r = 0.2 m, σ_r = 0.1 nrad) and maneuver performed two days before the flyby, the total cost of the tour is of 9.02 m/s, just 45 cm/s per flyby. With current level accuracies (σ_r = 1 m, σ_r = 1 nrad) the total cost of the tour is of 13.65 m/s, around 68 cm/s per flyby. It has to be remembered that this represent only the *relative* contribution of the JUICE-moons uncertainties on the total statistical ΔV, thus the real ΔV will be higher.

Comparison between the two strategies

A comparison between the two different strategies with respect to the baseline case is performed here. First of all, it is noted that both the strategies always reduce the ΔV required with respect to the baseline case, no ephemerides improvement (for the configurations of parameters used). Despite this is somehow a trivial result, since it was expected that reducing the uncertainty in the position the maneuver required to correct for that uncertainty would decrease, this reduction has now been quantified for a wide range of parameters. Thus the data obtained can give a useful indication for the ΔV (and thus propellant) budget for JUICE in order to perform its mission correctly.

The comparison between the two strategies reveals that the lower ΔV are obtained with the Strategy 3, for almost all the cases. However there are some cases for which the results are better with Strategy 1 rather than with Strategy 3. These cases are 11-12, but only for the cleanup maneuver and for the 95 % percentile. This can be explained by the fact that, with such combination of data accuracies, the reduction of the uncertainties obtained with the data accumulation CA arrives at very low value and can not decrease more. This level is very similar to the reduction obtained with the single arc estimation, but during the flyby arc; since the 95 % percentile is referred to a precise perturbed trajectory, generated with a random number, it can be that the random number for Strategy 3 was higher than the one for Strategy 1, giving so an higher overall ΔV.

For all the other cases instead the ΔV from the maneuver designed with all the past data, even if from before the flyby (Strategy 3), is lower than the ΔV from the maneuver designed with last flyby data only (Strategy 1). This means that using the data from the previous flybys along the Tour allows a more precise maneuver execution; this could be partly expected from what seen in Section 7.2, where the CA results for these two strategies are compared and the best results of Strategy 3 were already observed. Moreover, the results from Strategy 3 are more realistic for two reasons: first of all, it is not realistic to track the spacecraft during each flyby due to pointing requirements of the spacecraft instruments (for example in [42] is written that the tracking is interrupted 24 hours before the flyby). Secondly, if the flybys are successful, it is logical to include the data from all the flybys in the position determination of the moons at future times, to improve thus their estimation. The reduction obtained with Strategy 3 is usually around 40-60 % better than Strategy 1.

It has to be noted however that the amount of data used for Strategy 3 is slightly higher than for Strategy 1; this can be seen from Tables 7.2 and 7.5. In particular, the VLBI frequency for Strategy 1 is lower and the tracking arc is always of 6 days, while for Strategy 3 it varies between 6 and 10 days.

Regarding the optical data, in Strategy 3 more optical data are simulated with respect to Strategy 1 (from the start of the arc up to 2 days before the flyby). However the relative improvement is not higher than for Strategy 1. The reduction of the ΔV in the presence of optical data can arrive to 45 % for both the strategies. This can be explained by the fact that the uncertainties are already very low without optical data, hence their inclusion can improve the estimation but can not go beyond a certain threshold. Moreover, since the accuracy is expressed in radians, the linear accuracy of the optical data depends upon the distance spacecraft-moon; if the spacecraft is at a distance of hundreds of thousands of km from the moon than the linear accuracy is of around hundreds of km. Since the radius of the moons is around 1,500-2,000 km that accuracy is quite bad and thus the optical data will not have a great influence.

The results obtained are quite similar to the ones found in literature for similar mission (e.g. [42], where a Europa Tour is studied) for the targeting maneuver but more different for the cleanup. For the targeting an

average value of [0.2 - 0.6] m/s per flyby has been found here (with current level and improved accuracies and maneuver performed 3 days before flyby). The targeting maneuvers found in the reference of above are of around [0.05 - 0.5] m/s per flyby. Instead, the values for the cleanup maneuver show an higher difference: the average found here are of [0.2 - 0.4] m/s per flyby while in the reference higher values ([0.5 - 7] m/s per flyby) are computed. This difference can be explained due to the necessary restrictive assumptions required in this project (5.3) for the computation of the cleanup maneuvers.
From the ΔV obtained it can be stated that the flyby tour is navigable (under the assumptions adopted in this Thesis), since they are feasible values for the propulsion system of JUICE.
The conclusion from this Section with respect to the research questions 1 is that, as expected, the flyby tour yields to the ephemerides improvement and thus a reduction of the statistical ΔV required. This reduction has been quantified for a wide number of cases.

8.2. MONTE CARLO SIMULATIONS RESULTS FOR SINGLE FLYBYS

In this Section the results of the Monte Carlo analysis for a single configuration among the ones presented in the previous Section are presented; the results are analyzed for each flyby, showing their individual contribution to the total ΔV budget. The main results presented here are the formal errors of JUICE and the Galilean moons mapped at the time of flyby (t_{flyby} or t_{fb} in brief) in the B-Plane (see 4.2.1) and the ΔV required for the TCMs (for the pre-flyby and post-flyby maneuver). The first results are in reality results from the covariance analysis but the mapping on the B-Plane is performed only during the navigation analysis.
Possible correlations between the ΔV obtained and the characteristics of the flyby as altitude, velocity and duration are searched for.
The simulations presented in this Section are for the Strategy 1 and 3; the configuration used is the following. Range and VLBI data only are used with accuracies of $\sigma_r = 1$ m and $\sigma_v = 1$ nrad; the time of maneuver is of 3 days before and after the time of flyby. This configuration has been chosen because it represent the current accuracy of the tracking data and a commonly used maneuver time.

8.2.1. RESULTS FOR STRATEGY 1

The results for the Strategy 1 are presented here. The ΔV and the correspondent uncertainty (the sum of the 3 dimensional uncertainties of JUICE and the flyby moon) at the time of maneuver are shown in Figure 8.2.
The ΔV required is around between [0.5 - 8] m/s per flyby for the pre-flyby maneuver and [0.2 - 1.7] m/s per flyby for the post-flyby maneuver. In Figure 8.2a is interesting to notice that the highest ΔV are for the first flyby of Ganymede, Callisto and Europa. This is expected since, as visible from the lower part of the Figure, the uncertainty used for the first flybys is the a priori one, since no flybys of that moon have been performed yet. It is noted how for these three flybys the one that contributes the most to the ΔV budget is the one of Callisto, which requires almost 4 times more ΔV than the first flybys of Europa and Ganymede. This can be due to the different mass of the moons; it is however strange because Callisto has a mass intermediate between Europa and Ganymede. However also the following flybys of Callisto show a higher ΔV than for the other moons, for a similar level of uncertainty. For the post-flyby maneuvers, the ΔV peaks are due to the higher uncertainty for those maneuvers; the higher uncertainties come from the covariance analysis and from the covariance propagation. For both the maneuvers, it is possible to see that the blue plot follows quite good the red plot, indicating that the magnitude of the maneuver is always dependent upon the magnitude of the uncertainty (as already seen in 4.3.4).

In Figure 8.3 the uncertainties mapped in the B-Plane at the time of flyby are shown. The uncertainty in the R-axis of the B-Plane are very often bigger than the uncertainties in the T-axis; it is reminded that, due to the B-Plane geometry (see 4.2), the R-axis is directed more or less along the Z-axis of the reference frame, while the T-axis is parallel the XY-plane. In some cases however σ_T is bigger than σ_R. This can be explained by the fact that VLBI data are used here, hence the out-of-plane component is improved much more than for the case of range data only. The reduction of the a priori uncertainty of the moons (80 km per axis) is always quite significant, due to the fact that tracking is performed during the flyby. The uncertainties in the linearized time of flight (σ_{TCA}) are quite small, being in 17/20 cases smaller than 5 s and in the other three cases (corresponding to the first flybys) around 15 s.

Figure 8.4 shows the plot of all the statistical indicators for the pre-flyby ΔV; it is noticed how the 95 % percentile is always higher than the sum of the average ΔV with the 1σ standard deviation. It is seen also how the standard deviations are proportional to the ΔV magnitude.

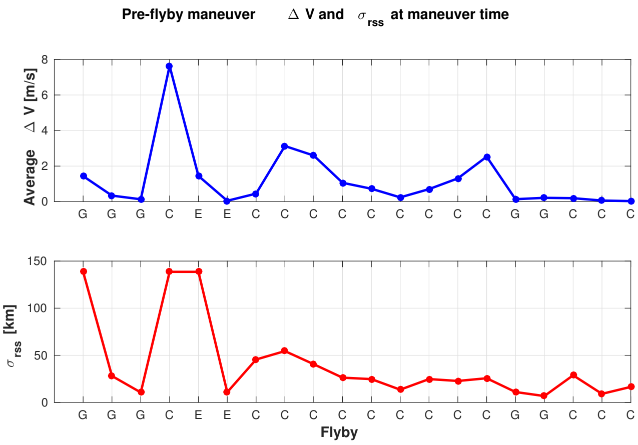

(a) Pre-flyby maneuver

(b) Post-flyby maneuver

Figure 8.2: Uncertainties at maneuver time and ΔV - Strategy 1

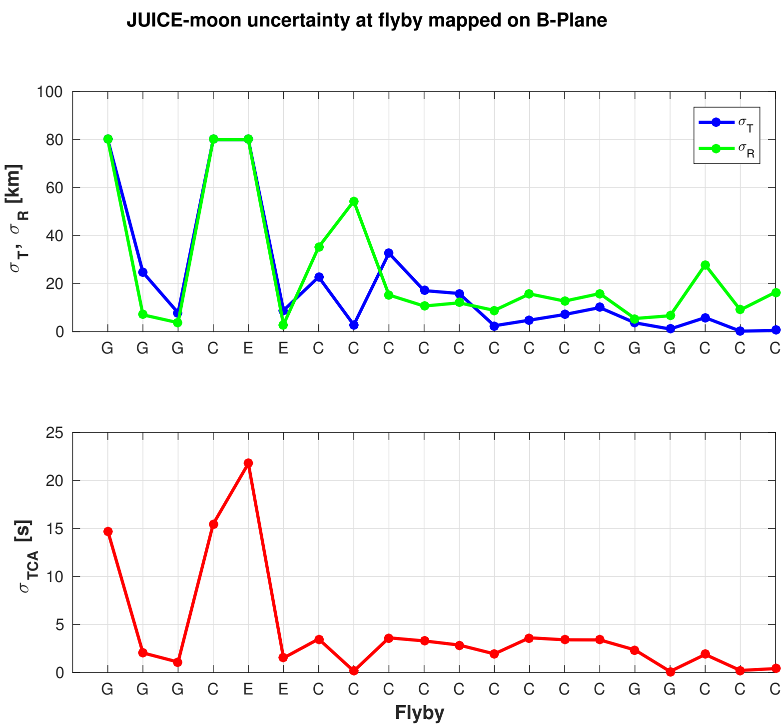

Figure 8.3: Uncertainties mapped in the B-Plane - Strategy 1

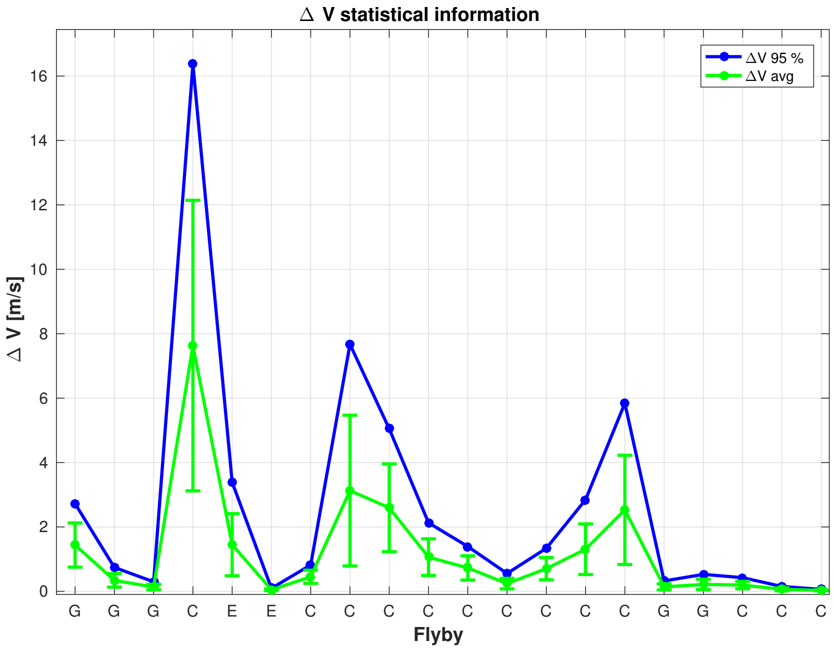

Figure 8.4: Pre-flyby ΔV statistics for every flyby - Strategy 1

In the following some plots of the uncertainty ellipses (see 4.2.1) in the B-Plane for different flybys are presented. These plots are essentially the 2D representation of the uncertainties of Figure 8.3 and they are used to analyze the size of the uncertainties with respect to the celestial body dimension.

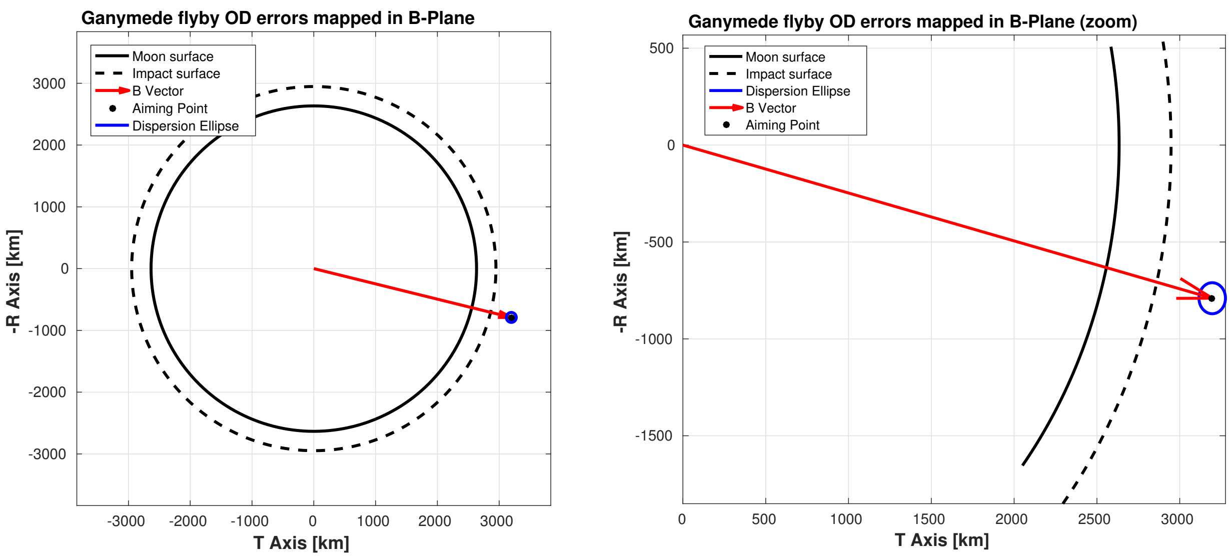

(a) Global view

(b) Zoom

Figure 8.5: Uncertainty ellipse in the B-Plane - 1st flyby

The plots for the 1st flyby of Ganymede are shown in Figure 8.5, with the complete surface of the moons to the left (8.5a) and with a zoom on the uncertainty ellipse to the right (8.5b). The impact surface represents the minimum distance from the center of the moon that is required for the B-vector in order to avoid impact (in

Section 8.4 an explanation is given). In the Figure it is visible also the nominal B-vector, that is directed towards the aiming point. The uncertainty ellipse is centered around the nominal point, since only a covariance analysis and not a full least square estimation is performed; when a full estimation is performed the uncertainty ellipse is centered around the best estimate of the aiming point.
From 8.5a is possible to see that the uncertainty is very small compared to the size of the moon, and also that the first flyby has a quite low altitude. In Figure 8.5b the ellipse is clearly visible; the difference in semi-major and semi-minor axis is close to zero since the a priori uncertainty is used for this case. It is noticed that the semi-major and semi-minor axis are in general different from σ_R and σ_T; they are computed in Subsection 4.2.1. In some particular cases they are almost coincident.
The effect of the improvement given by the optical data on the mapped uncertainty is shown in Figure 8.6. The uncertainty ellipse shrinks considerably and changes its orientation; using only range and VLBI data it is almost a circle, while when adding optical (with an accuracy of $\sigma_o = 10\mu$ rad) it becomes more elliptical and with the semi-major axis oriented almost along the T-axis. This means that the uncertainty in the R-axis is reduced more than the one in the T-axis.

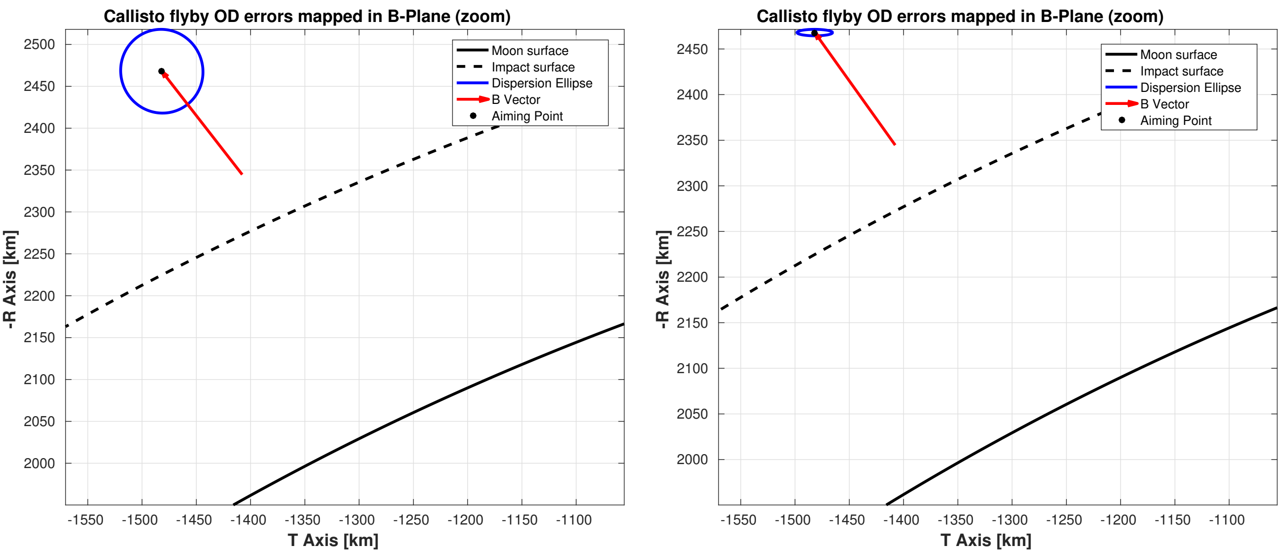

(a) Range and VLBI data

(b) Range, VLBI and optical data

Figure 8.6: Reduction of uncertainty ellipse due to optical data

Figure 8.7 shows four different parameters that characterize a flyby (distance, altitude, time from SOI to flyby and V_∞); these parameters were already presented in Table 6.1.
A comparison between these four parameters and the ΔV obtained for each flyby is shown in Figure 8.8; the ΔV is computed with the baseline case, in order to use the same perturbation for every flyby. Figure 8.8a shows these plots for all the 3 moons while Figure 8.8b shows these plots for Callisto only; this is necessary because possible correlations could depend upon the gravitational parameter of the flyby moon, which is different for the three moons. From these plots, and in particular from 8.8b, is noted that the flybys that require the highest ΔV (for Callisto) are also at very low altitude (around 200 km), but this does not imply that all the very low altitudes flyby require a high ΔV. For example one of the low altitude flybys of Callisto requires the same ΔV of the 6000 km altitude flyby. Regarding the other two parameters investigated, the duration of the flyby and the hyperbolic excess velocity, it can be stated that also for them no evident correlations are found (as for the same type of plots for the covariance analysis, see Figure 7.6). The highest ΔV are in correspondence of low flyby durations and high hyperbolic excess velocities; this however does not imply that in correspondence of this factors the ΔV has to be necessarily high, since it is not confirmed by the plot. Instead, for long flyby durations and low excess velocities the ΔV are the smallest; there are however just a few flybys with these characteristics (3/13 for Callisto), thus is not possible to conclude that this is a general rule. These 3 flybys are the last three of the Tour; they have a low hyperbolic excess velocity, thus the velocity of the spacecraft with respect to the

moon during the flyby is low. A maneuver has the effect of rotating and modifying the size of the velocity vector; when the magnitude of this vector is higher it can be more difficult to do this (as for a plane change maneuver in a circular orbit). Instead, when the magnitude is small it could be easier to modify this vector.

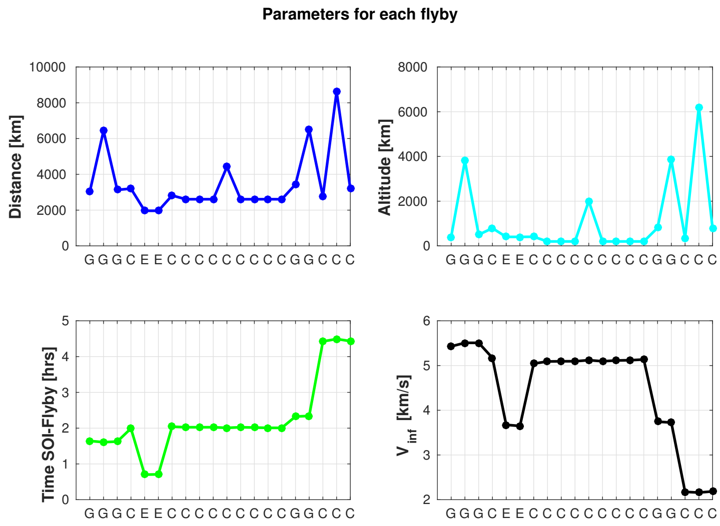

Figure 8.7: Flybys parameters

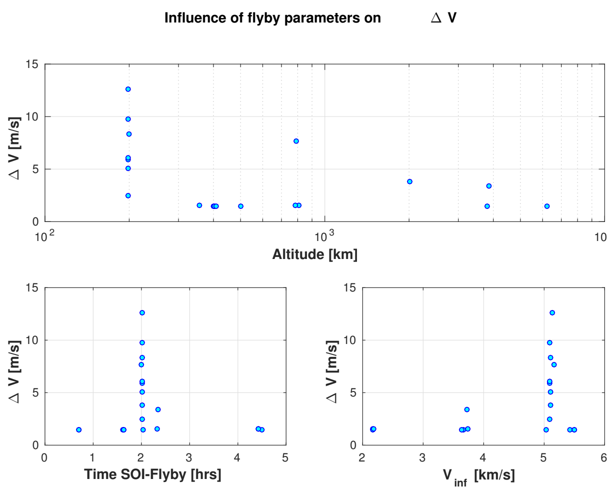

(a) Correlations for the three moons

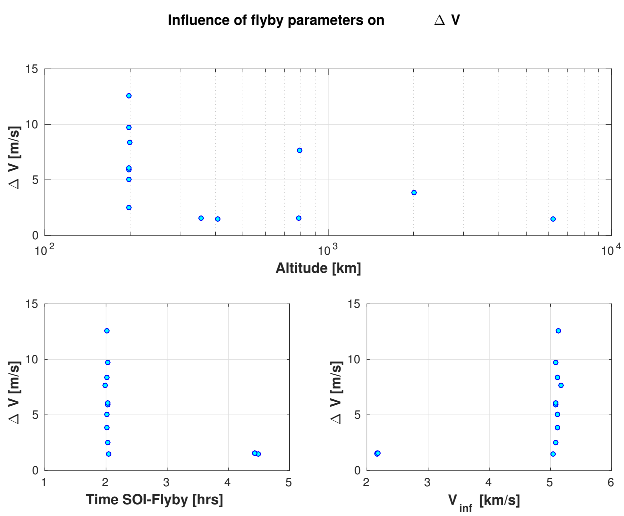

(b) Correlations for Callisto

Figure 8.8: Correlations ΔV - flyby parameters (altitude, V_∞, flyby duration)

8.2.2. Results for Strategy 3

The results for the Strategy 3 are presented here. The ΔV and the correspondent uncertainty (the sum of the 3 dimensional uncertainties of JUICE and the flyby moon) at the time of maneuver are shown in Figure 8.9.

These plots, contrarily to the ones of the previous Subsection, are in a semi-logarithmic scale because the improvement obtained along the Tour changes the order of magnitude of the uncertainties determined by the CA and the ΔV of the TCMs. Regarding the pre-flyby maneuver, in Figure 8.9a it is seen that the ΔV generally decreases along the Tour but not in a monotonic way. The decrease from the 1st flyby of Ganymede to the 3rd is of about 1 order of magnitude (corresponding to a decrease of one order of magnitude of the uncertainty).

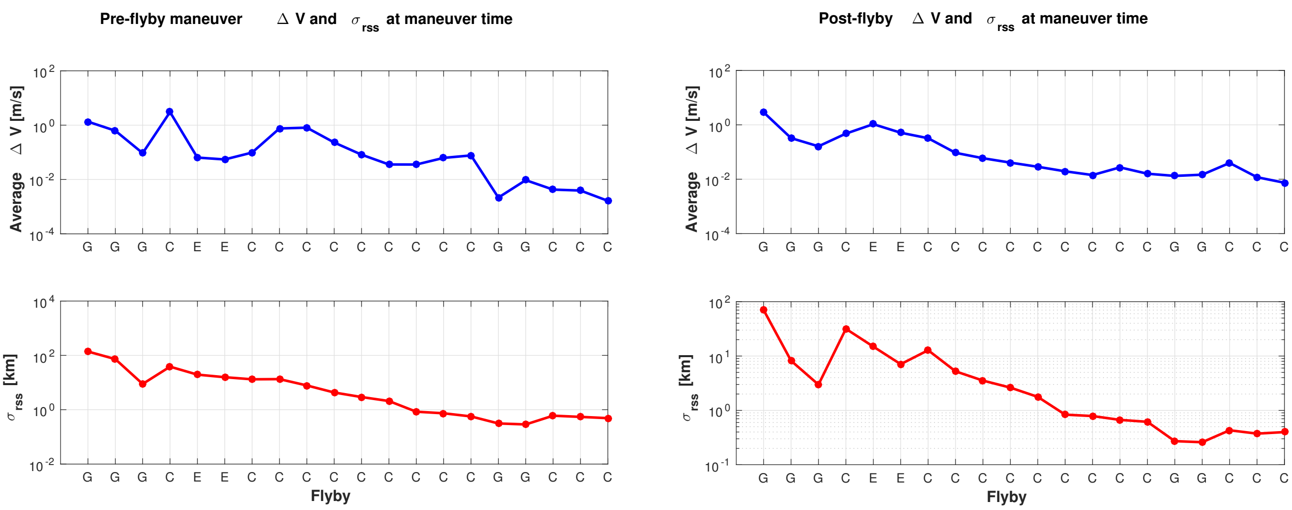

(a) Pre-flyby maneuver

(b) Post-flyby maneuver

Figure 8.9: Uncertainties at maneuver time and ΔV - Strategy 3

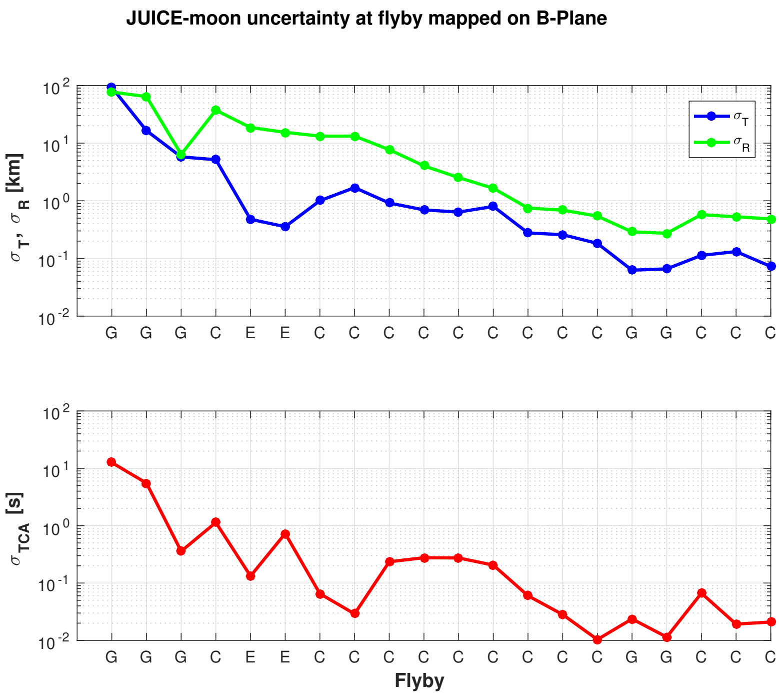

Figure 8.10: Uncertainties mapped in the B-Plane - Strategy 3

The first flyby of Callisto instead requires a higher ΔV than the previous three flybys; this is due to the fact that, even if data from those flybys are used to estimate the uncertainty for this flyby, Callisto is not included in the Laplace resonance and thus its position knowledge is not improved considerably from other moons flybys. The first flyby of Europa instead shows a ΔV comparable to the 3rd flyby of Ganymede and a very similar uncertainty. This because the uncertainty of Europa is improved considerably with just flybys of Ganymede. The rest of the Tour shows a strange increase of ΔV in the central part of the flyby Tour, corresponding to the series of central flybys of Callisto; this increase is however not due to an higher uncertainty, since this decreases steadily from the first flyby. The reason is that every flyby has a different sensitivity to the TCMs depending upon its characteristics. At the end of the Tour the ΔV is really small, around 1 mm/s, corresponding to a very low uncertainty (around 500 m). The considerations for the post-flyby maneuvers are similar; the ΔV decreases during the tour. However in the last part a plateau is reached and the values are similar to the middle part of the tour. The uncertainties instead decrease also in the final part but of a very small amount; this behavior can depend from the fact that the geometry of the last three flybys of Callisto is different from the one of the central series of resonant flybys. This is found also in [43], where a similar analysis is conducted for a series of flybys of Europa.
It is concluded that for the Strategy that implements the data accumulation version of the CA, the total ΔV budget depends mainly from the first 10-12 flybys, while the contribution of the flybys in the second part of the tour is much smaller. This was expected from the results of the CA (Section 7.2). The main difference of the results of Strategy 3 with respect to the results of Strategy 1 is that for the latter the contribution of the TCM of each flyby to the total budget is similar, while for the former the contribution decreases along the Tour; this is expected and is a direct consequence of the different CA strategies. The standard deviations mapped in the B-Plane for each flyby are shown in Figure 8.10; similar considerations of above can be done for this plot. It is noticed how the uncertainty in the out-of-plane direction (R) is always higher than the one for the in-plane direction (T). The uncertainty for the time of flight is of around 20 s for the first flyby but it decreases to under 1 s already after two flybys. At the end of the Tour these values arrive to under 0.1 km; they are indicative of the decrease. A very similar decrease for the uncertainties mapped in the B-Plane is presented also in [43].

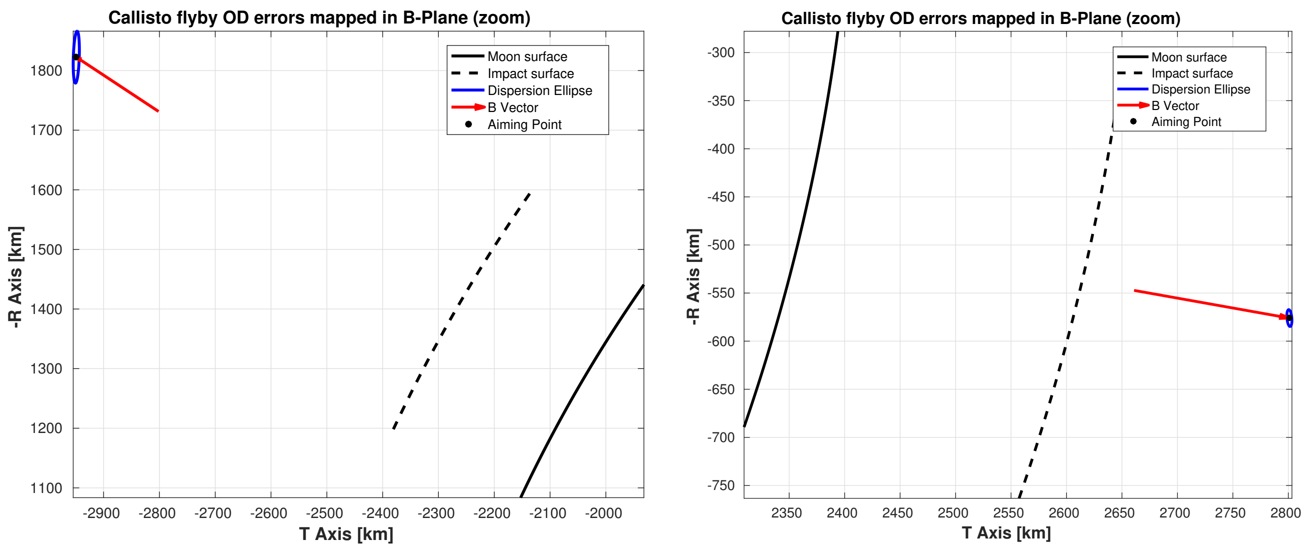

(a) 4^{th} **flyby (Callisto)**

(b) 15^{th} **flyby of (Callisto)**

Figure 8.11: Reduction of uncertainty ellipses along the flyby tour

The reduction of the size of the uncertainty ellipses on the B-Plane obtained along the Tour is shown in Figure 8.11 (for the 4^{th} and 15^{th} flybys of the tour only, both of Callisto). It is clearly visible the reduction of size of the ellipse at the 15^{th} flyby, when data from 14 previous flybys are included (the semi-major axis is 7.4 km while for the 4^{th} flyby is 46.2 km). From the complete series of uncertainty ellipses, not reported here, the progressive improvement obtained is immediately visible.

8.3. EXTENDED SENSITIVITY ANALYSIS FOR THE ΔV

In this Section the influence of two parameters of the Guidance algorithms is analyzed; these parameters are the maneuver time and the maneuver execution error model. This Section addresses the research question 3, since these two parameters are peculiar to the guidance only and not to the CA.
These are the main parameters that influence the guidance, for all the three version of the targeting algorithms (4.3); for specific targeting algorithms different parameters could be analyzed (e.g. the influence of the tolerance for the optimized targeting).

8.3.1. INFLUENCE OF THE MANEUVER TIME

The influence of the maneuver time has already been partly analyzed in Section 8.1; as seen from the results of the Monte Carlo analysis, the maneuver time is fundamental for ΔV saving; however, due to the fact that just a limited number of times were tried, it was not possible to capture the complete behavior of the ΔV with respect to this variable. The apparent behavior observed in Section 8.1 is that until the time of 24 hours before the flyby the ΔV decreases with increasing time, while between 24 hours and 72 hours there is a minimum, meaning that that the ΔV is not always decreasing. To characterize completely this behavior an analysis focused on the time of maneuver has been conducted.
This analysis is performed for the Strategy 1 only; the optimized targeting algorithm is used instead than the approximated, in order to have a more accurate ΔV computation (since the ΔV differences between different times can be quite small). The analysis is thus performed for the pre-flyby maneuver only, since it is the only maneuver for which the use of the optimized algorithm is possible (see 5.3).
This analysis consisted in running Monte Carlo simulations for 71 different maneuver times in the interval [1-73] hours before the flyby. To reduce the computational time (required for the optimized targeting), 100 samples have been used; a higher number should be used to have more confidence in the results but due to computational constraints this was not possible. The configuration used for the covariance analysis is fixed.

The first observation is that for two maneuver times (55-56 hours before the flyby) the Monte Carlo simulations were failing due to a wrong eccentricity of the perturbed orbit (smaller than one, hence transforming the flyby hyperbola into an ellipse). To avoid this issue, these times were excluded. All the other times gave positive results.

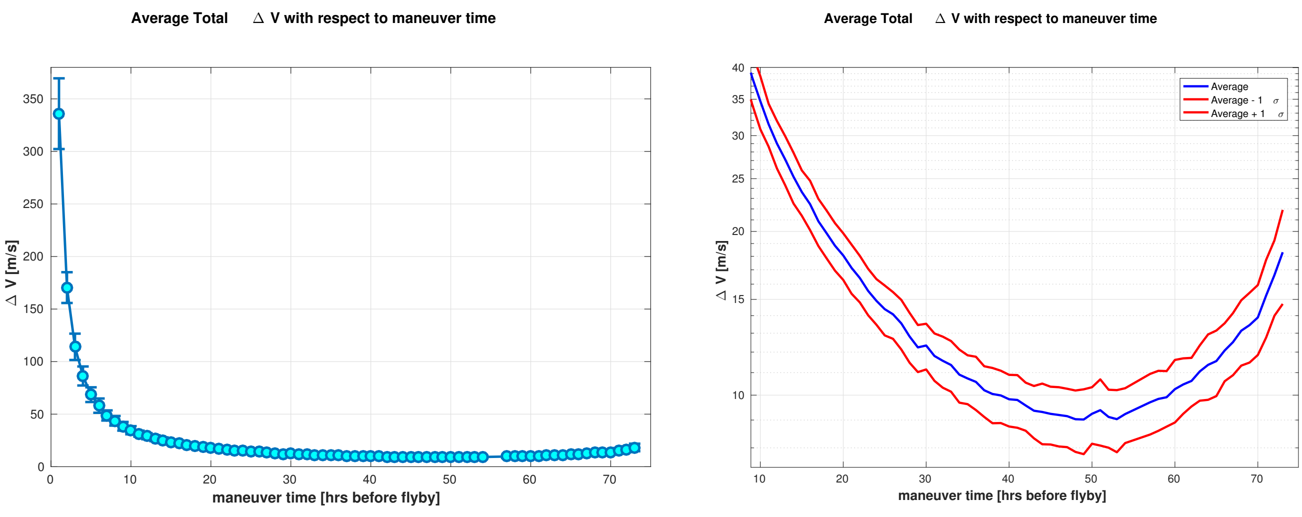

(a) Full interval (b) Zoom on minimum's region

Figure 8.12: Total ΔV behavior with respect to the maneuver time

In Figure 8.12 the results obtained are shown, as average total mission ΔV for the 100 runs. It is immediate to notice three things; first of all, the ΔV required in the interval [1-6] hours before flyby is noticeably higher than the one required the rest of the time. Indeed in the interval [7-71] hours the plot is quite flat compared

to the other interval. The second observation is that in this interval there is a minimum, located at 49 hours before the flyby. The last observation is that also at a local level the plot is not always monotonic; for example also at [29-30] hours and [50-54] hours there in an inversion of tendency.
Regarding the values at the end of the interval ([72-73] hours before flyby), these are at the level of [20-22] hours before flyby; in particular, the value at 72 hours is slightly higher (17.1 m/s respect to 16.62 m/s) than the value at 24 hours. In the preceding simulations it was observed that sometimes the ΔV was higher at 72 respect to 24 hours and some other times the opposite situation was happening. This depends from the particular configuration of the CA.
The error bars (1σ) on the ΔV computed from the Monte Carlo simulations are shown in the same Figure, to see the level of accuracy of the results obtained. In Figure 8.12a it is visible the relative size of the error bars; coherently with what seen until now, they increase in size when the ΔV is higher. In Figure 8.12b, plotted in logarithmic scale, is shown a zoom on the interval of interest, which shows quite limited bands around the average value (the blue line). Considering that the ΔV can fall inside the two red bands with a probability of 68.27 %, it is clear that there is an uncertainty also on the minimum found, which could be located anywhere in the range [35-65] hours. This explains also why sometimes the behavior between 24 and 72 hours is inverted.

Table 8.5: Time investigation results for every flyby

Flyby	Globally monotonic	Minimum Location
-	[Y-N]	hrs before flyby
1-G	Y	-
2-G	Y	-
3-G	Y	-
4-C	N	46
5-E	Y	-
6-E	Y	-
7-C	Y	-
8-C	N	47
9-C	N	40
10-C	N	44
11-C	N	47
12-C	Y	-
13-C	N	49
14-C	N	46
15-C	N	48
16-G	Y	-
17-G	N	33
18-C	Y	-
19-C	Y	-
20-C	Y	-

A very important thing to remember when evaluating these results is that this behavior does not depend exclusively upon the time itself, but also upon the results of the covariance analysis. Indeed, for each flyby the results are different (although for the single arc version always of the same magnitude) and moreover there is a propagation of the covariance matrix to different times that can introduce differences (see 7.2). The results for a different configuration of the CA would be slightly different. Hence, since for each flyby the behavior respect to time can be different, in Table 8.5 is reported the behavior with respect to time for each single flyby, extracted from the plots. With "globally monotonic" it is indicated that the behavior of the function overall is monotonic, thus without minima inside the interval of interest; very often the behavior is not strictly monotonic everywhere, but there are local areas where the tendency is inverted. These inversions are most probably due to the small number of Monte Carlo samples and thus not considered. It is noticed that just 9 flybys show a minimum, while the rest are globally monotonic, meaning that the global minimum for the interval considered is the right end of the interval, thus 73 hours from flyby. However the last portion of the plot is quite flat, indicating that the difference in ΔV between the different times is quite small. Most of the flybys that have a temporal minimum are of Callisto, especially the central series of flybys. From this analysis it is concluded that

the selection of the ideal maneuver time has to be performed separately for each flyby, because the ΔV sensitivity with respect to the time of maneuver depends upon the moon in consideration and the particular flyby geometry. However, it is clear that the location of these minima is around 40-50 hours before the flyby time, if present; if not the minimum is located at the end of the interval (73 hours). Performing more accurate analysis in a similar fashion to the one conducted here can give more accurate indications on the optimal maneuver time.
Some considerations have to be done from an operational point of view; the times ranging from [1-6] hours before a flyby have been tried for the sake of completeness, but it is very unlikely that a maneuver would be placed in that interval. This because as seen the ΔV would be prohibitively high and because, in case of failure of the engine, there would not be enough time to design and perform a new maneuver. A maneuver could be performed in this interval only as backup, if the preceding maneuver failed and little time is available. The standard placement of the targeting maneuver as found in literature [52] is of 3 days; this is almost always a good choice because it requires a low ΔV and because is quite far away from the flyby, allowing more time for emergency operations (in [42] is stated that usually backup maneuvers are performed 24 hours after the primary maneuvers). For the tour in consideration it may not always be possible to perform the maneuver 3 days before the flyby since some of the flybys are very close in time; for example the central series of flybys of Callisto are spaced by 16 days while other 2 flybys are spaced by 11 and 12 days. Considering that after a flyby at least 2-3 days are required to perform the OD in support to the cleanup maneuver, then only 8 days are left to the next flyby. If the maneuver has to be done 3 days before the flyby, 5 days remain to perform these operations again in support to the targeting maneuver. They should be sufficient but anyway they can pose operational difficulties. Moreover an apoapsis maneuver is often necessary (which can be deterministic). This would further decrease the time available for the next maneuver.
In the next paragraph, some further considerations on the optimal maneuver time for a Keplerian orbit are exposed in order to try to understand the physical reason behind the presence of minima for these TCMs.

Influence of maneuver time for a Keplerian orbit
It is now clear that the optimal maneuver time depends from the dynamics of a flyby; however the exact set of variables that determine the location of this optimum is not known. In order to get some more insight on this phenomenon, two different investigations have been performed using the B-Plane targeting algorithm applied to a Keplerian orbit.

In the first investigation the classic B-Plane targeting with numerical derivatives for the Jacobian matrix has been used (see 4.3.2). For each maneuver time, a different random perturbation has been applied to the orbit; the ΔV is then computed. An indicator defined as the normalized scalar product between the $\mathbf{\Delta V}$ and the velocity has been defined as

$$d_{norm} = \frac{\mathbf{\Delta V} \cdot \mathbf{V}}{\| \mathbf{\Delta V} \| \ \| \mathbf{V} \|}$$

This represent the relative geometry between the velocity vector and the maneuver ($\mathbf{\Delta V}$) vector; this value approaches zero when the two vectors are perpendicular while it approaches one when the two vectors are parallel (and minus one when anti parallel). This is chosen because according to classic astrodynamics the efficiency (measured as change of energy) of a maneuver is maximized when the $\mathbf{\Delta V}$ is parallel to $\mathbf{V}$ [44].
In Figure 8.13a this indicator and the ΔV with respect to the time of closest approach are plotted. It is noted how this time interval is really small; this is due to the fact that it was quite difficult to find a set of values of perturbations and tolerances valid for a large interval (the targeting algorithm did not converge). Thus to prevent the algorithm from any failure a small interval has been used. In Figure 8.13b the true anomaly and the ΔV respect to the normalized scalar product are plotted. Among these four plots, the strongest correlation that is observed is between the scalar product and the ΔV (8.13b); in particular the ΔV reaches the highest values when the two vectors are almost perpendicular, while in the other cases it is considerably lower. The conclusion is that, due to the geometry of the orbit, to correct a certain perturbation sometimes the maneuver has to be parallel to the velocity and some other times perpendicular; this will strongly influence the magnitude of the impulse necessary for the maneuver. In the same Figure it is observed that the distribution of this scalar product is quite independent upon the geometrical position in the orbit, represented by θ.
From Figure 8.13a it is interesting to observe the influence of time: while the distribution of the scalar product apparently do not show strong correlation, the ΔV has a peak in correspondence of $t_{TCA} = 0.38$ hours. This means that the "worst" geometries are concentrated around that time, while the "good" geometries are spread

evenly across the interval.
This analysis has been partly extended to more maneuver times (far away from the flyby); this is done by modifying the tolerances and the perturbation values. For the time interval [8-22] hours before flyby a small decrease of ΔV when increasing the maneuver time has been found, with no dependence upon the scalar product result. This indicate that not always the direction of the ΔV is the origin of the high magnitude. This could be valid for certain time intervals but not for long ones.

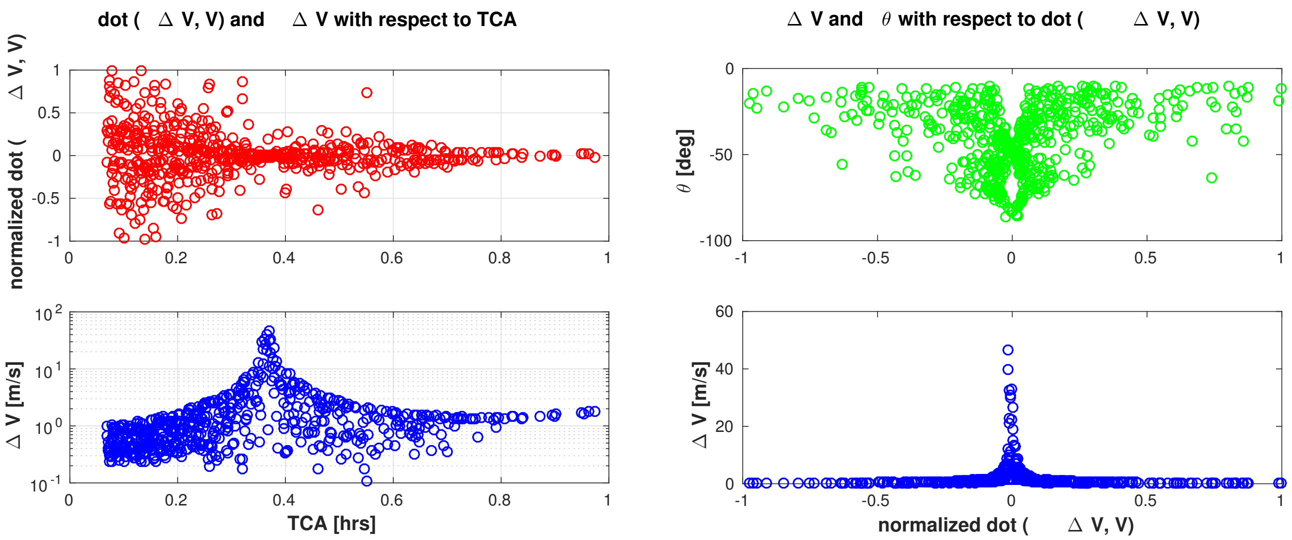

(a) Behavior respect to TCA

(b) Behavior respect to $\Delta V \cdot V$

Figure 8.13: Maneuver time investigation for Keplerian orbit - Numerical derivatives

In the second investigation a different logic has been used; always for a Keplerian hyperbola, the $\Delta\mathbf{V}$ correspondent to a fixed $\Delta\mathbf{B}$ perturbation has been computed using the matrix inversion

$$\Delta\mathbf{V} = J^{-1}\Delta\mathbf{B} \tag{8.1}$$

where J is the Jacobian matrix. In this case analytic derivatives of the B-Plane parameters with respect to the velocity vector have been used (deriving from [46] and briefly described in 4.3.2). Thus to compute the jacobian matrix only the keplerian elements are needed. In this way, varying the true anomaly only, it is possible to analyze the influence of time on the maneuver. Another option would be to write explicitly the ΔV and compute its derivative with respect to θ; this was not done because it entails very long algebraic manipulations and it is outside the scope of this investigation.
In Figure 8.14 the results are shown; it is noted that the times investigated are smaller than the ones analyzed for JUICE due to the choice of the minimum true anomaly of the hyperbola, θ_{min}; this is chosen higher than the angle corresponding to the asymptote, θ_{lim}, because this angle would lead to an infinite distance and infinite time to closest approach. In Figure 8.14b is observed again that the highest ΔV are in correspondence of a null scalar product, while for the rest of the cases the scalar product is always negative, meaning that a deceleration is always required to correct for that particular perturbation. This peak, as visible in Figure 8.14a, is located in a precise location along the orbit; moreover the ΔV reaches a minimum after the peak but then increases again. This maximum is quite strange because is much higher than the average ΔV values, which are in the interval [1-10] m/s, while the maximum is around 600 m/s. The presence of this maximum is explained by the fact that the matrix J becomes rank deficient (this is observed by the very high condition number correspondent to that maneuver time), hence the linear system solved in Eq. 8.1 becomes undetermined and more solutions are possible. The solver selects a high ΔV; the matrix becomes rank deficient because that particular true anomaly gives an almost linearly dependent combination of the partial derivatives. This is however specific for this particular Keplerian orbit; when trying other sets of parameters, different behaviors are observed, for example the presence of two or more peaks and a decrease of ΔV with time after the peaks. What is found always is the maximum in correspondence of null scalar product.

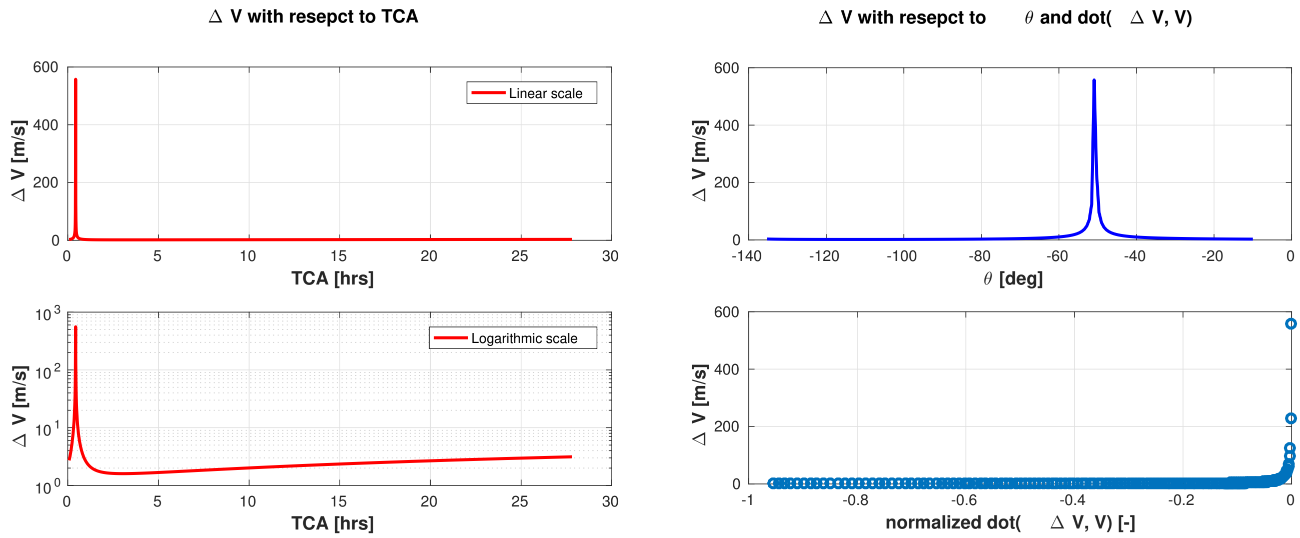

(a) Behavior respect to TCA

(b) Behavior respect to θ and $\Delta V \cdot V$

Figure 8.14: Maneuver time investigation for Keplerian orbit - Analytic derivatives

Different conclusions are drawn from this analysis; first of all, contrarily to what initially assumed, the ΔV does not always decrease monotonically with time, neither for a Keplerian orbit nor for a strongly perturbed orbit such as JUICE. There are however areas where the difference in magnitude is noticeable: it is clear that generally performing the maneuver a few hours before the flyby will require much more ΔV than performing it some days before. The behavior inside these two intervals is however not always the same.
At the present time, no analytic solutions for the determination of the optimal maneuver time have been found; only with numerical analysis is possible to determine this time. It is difficult to predict a priori if a minimum exists and if so where it is located, due to the strong dependence upon the trajectory geometry.

8.3.2. INFLUENCE OF THE MANEUVER EXECUTION ERROR MODEL

The maneuver execution error model (explained in 4.3.5) is applied to the computed ΔV with any targeting algorithm to modify the nominal value computed and simulate the effect of the errors in the pointing of the engine and/or in the magnitude of the thrust force. These errors depend essentially upon three elements: the ΔV itself, the parameters of the model (e.g. accuracy in the pointing), and a random factor.
In the two following paragraphs the effects of this error model are discussed; in the first paragraph its influence on the magnitude of the maneuver is analyzed. In the second paragraph its influence on the final position error (miss distance) at flyby is analyzed.
In both cases the Strategy 1 has been used for the CA, with $\sigma_r = 1$ m and the tracking schedule of Table 7.2. The targeting used is the optimized (see 4.3.3), because it is the only one that provides information on the miss distance at flyby since a full propagation is performed.

Influence on the magnitude of the total ΔV

The influence of the maneuver execution error model on the magnitude of the ΔV is shown in Figure 8.15. The ΔV and ΔV error magnitudes are shown with respect to 7 different simulations (corresponding to 7 different maneuver times, from 1 to 72 hours before the flyby). The 95 % percentiles of a Monte Carlo simulation with 100 samples are shown.
A comparison of the upper plot with the correspondent plot in the case of no maneuver error reveals that the total value of ΔV for the two cases are almost identical; in the lower plot is shown the magnitude of these errors, which is much smaller compared to the total ΔV (for example is of about 2 m/s for the first case, being 0.2 % of the total ΔV). The error increases of magnitude when the ΔV is higher; this is in accordance with the error model. This error is in the interval [0.2-2] m/s; its relative influence is slightly higher when the maneuver is smaller, thus more far away from the flyby. It is noted that this is the magnitude of the ΔV error only; the error is a vector that can be in the same or opposite direction of the ΔV.

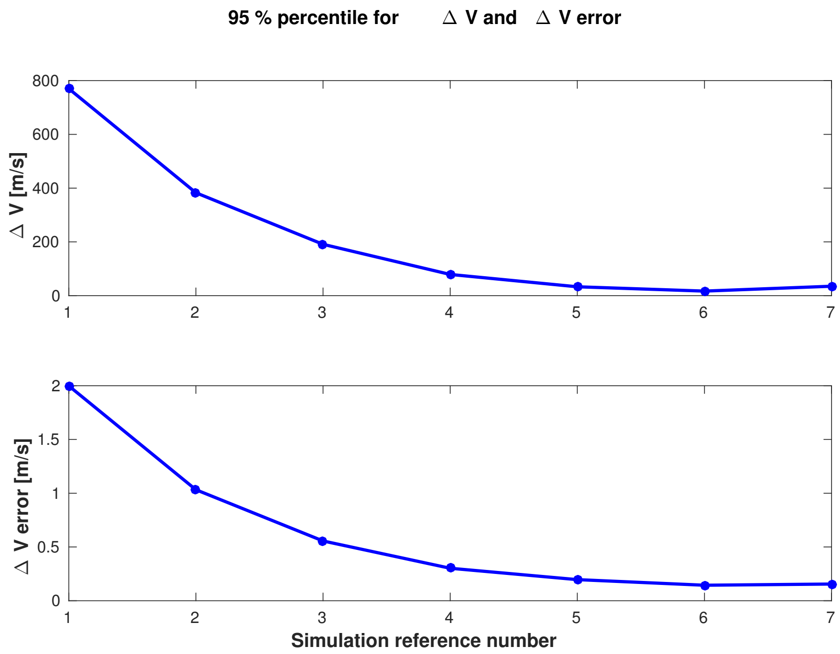

Figure 8.15: Influence of the maneuver execution error model on the magnitude of the ΔV

The results in term of total ΔV magnitude obtained in this case do not show a big difference with the case of no maneuver error for the following reason. The simulated error on the ΔV is a vector in an arbitrary direction (because a multiplication for a random number is done); this means that this error sometimes represent an over thrusting and sometimes an under thrusting. In a Monte Carlo simulation with a high number of samples the net effect on the ΔV magnitude will be zero, because the ΔV in excess for some samples will compensate the ΔV in defect for the other samples. This happens for both the total and single-flyby ΔV. The total cost of the mission remains practically unchanged.

Effect of the maneuver execution error on the flyby miss distance

With the optimized algorithm (4.3.3) the miss distance at flyby is corrected; this has to satisfy a tolerance in order to consider the targeting successful. This is expressed by Eq. 4.38, reported here for clarity

$$\parallel \Delta \mathbf{x}_{flyby} \parallel = \parallel \mathbf{x}_{corr}(t_{flyby}) - \mathbf{x}_{nom}(t_{flyby}) \parallel$$

which represents the difference between the corrected trajectory and the nominal trajectory at the time of flyby. At this stage it is interesting to analyze also the effect of maneuver errors on the propagation of the trajectory; since the application of the ΔV error is performed outside the optimizer, this could cause a failure in the targeting, because the state vector is corrected with the wrong ΔV and hence it is not guaranteed that the trajectory will converge to the nominal flyby conditions. For this reason a final propagation after the application of the ΔV error is performed, to check the final state vector at the time of flyby.
It is observed that this happens very rarely, because the magnitude of the ΔV error is very small compared to the ΔV itself; the maneuver computed is thus perturbed only slightly and can still bring back the spacecraft at the desired location at the time of flyby satisfying the required tolerance.
The effect of the maneuver error could be a decrease of the precision of the correction, increasing the miss distance at flyby; this is not always necessarily true, because the convergence is defined by a tolerance, and it could happen that the application of the ΔV error is seen just as another step of the Newton-Raphson algorithm, hence increasing the accuracy of the final miss-distance.

The influence of the maneuver error on the flyby miss distance is shown in Figure 8.16, where the average error of the corrected trajectory at flyby is shown ($\parallel \Delta \mathbf{x}_{flyby} \parallel$) for all the 20 flybys of the Tour; this average is computed for a Monte Carlo simulation with 100 samples. The maximum error allowed (the tolerance of the optimizer) is of 10 km. These plots are for a maneuver time of 72 hours before the flyby. The parameters used

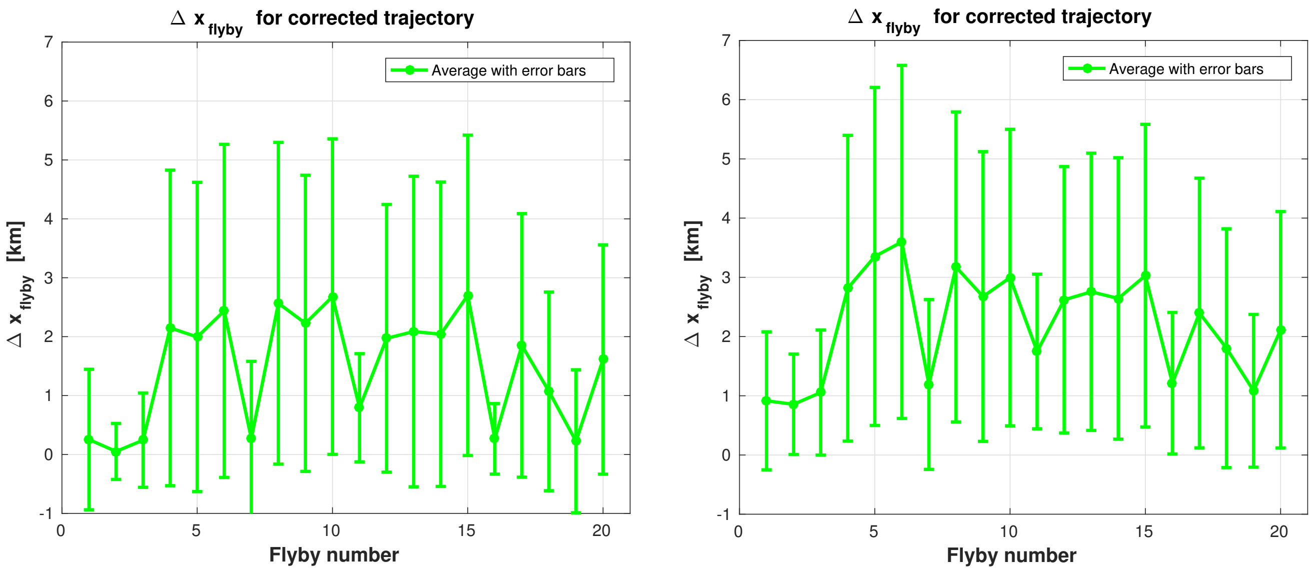

(a) Without maneuver execution error

(b) With maneuver execution error

Figure 8.16: Influence of the maneuver execution error on the flyby position error

for the maneuver execution error model are the ones from the Cassini mission (from [52], reported in 4.3.5). In Figure 8.16a is presented the case without the application of the maneuver error, while in Figure 8.16b is shown the case with the application of the maneuver error. The first observation is that for both cases the Monte Carlo simulations were successful (for all the samples). This is particularly meaningful for the case with maneuver error, indicating that the influence of this error is quite limited and does not prevent a successful flyby targeting; however, as seen from 8.16b, the miss distance at flyby for this case is slightly higher than for the case of no error (8.16a). This increase is of around 1 km per flyby, being different for each flyby.
This influence depends also from the time of propagation; it has been observed that when being closer to a flyby the influence of this maneuver error is much smaller, since the miss distance at flyby remains almost identical to the one computed without the application of this error. The plots presented here are for a maneuver time of 72 hours before the flyby; the maneuver error has thus time available to propagate its effects into a worst flyby miss distance.

The conclusion of this Section is that the research question 3 has been answered partly, since the effects of the maneuver time and the maneuver execution errors have been widely analyzed and understood. For each flyby the interval of time during which is better to perform the maneuver has been found. The maneuver error does not influence noticeably the overall ΔV budget, but it can decrease the accuracy of the targeting of a few km. The research question has been answered only partly because the effect of many other parameters shall be investigated too, as for example the optimizer tolerance and the effect of a non-zero thrusting time.

8.4. Impact Analysis Results

As seen in Chapter 2 due to the Planetary Protection requirements it is necessary to guarantee that no impacts with the Galilean moons, especially Europa, are likely. The navigation analysis provides information about the possibility of impacts of the spacecraft with the flyby moon; this information derives essentially from the propagation of the covariance analysis uncertainties to the time of flyby. This analysis thus links the covariance analysis to possible mission risks. Two methods have been used; the first uses the results of the covariance analysis only, computing analytically the probability from the uncertainties in the spacecraft and moon positions and the nominal flyby conditions. The second uses the results of the covariance analysis and the full numerical propagation performed in the navigation analysis (with the optimized targeting only) to derive such probabilities. These methods are exposed here and the results obtained with them are analyzed.
This Section, although it does not answer directly to any research question, contributes to describe the effect of the OD uncertainties (see Chapter 7) on the overall mission performance.

Method 1 - Integration of probability density function
Using the uncertainties from the covariance analysis it is possible to define a function that represents the relative probability of a trajectory to be located at a certain point in space. Since one of the components of the 3-D spatial uncertainties can be transformed in time uncertainty, this function has been defined on the remaining 2-D spatial directions; these are the direction $\hat{T}$ and $\hat{R}$ of the B-Plane.
Thus the statistical distribution used is the *bivariate normal distribution*, for which the probability density function is

$$p(x_T, x_R) = \frac{1}{2\pi\sigma_T\sigma_R\sqrt{1-\rho^2}} \exp\left(-\frac{1}{2(1-\rho^2)}\left[\frac{(x_T - B_T)^2}{\sigma_T^2} + \frac{(x_R - B_R)^2}{\sigma_R^2} - \frac{2\rho(x_T - B_T)(x_R - B_R)}{\sigma_T\sigma_R}\right]\right)$$

where σ_T, σ_R are the uncertainties in the $\hat{T}$ and $\hat{R}$ directions, ρ their correlation and B_T, B_R the components of the B-vectors in those directions. The independent variables are x_R, x_T and they represent the coordinates on the B-Plane. This distribution is centered at the aiming point.

To proceed it necessary to define the *capture radius* (or *impact B-vector*) as the minimum value required to the B-vector to avoid an impact during the flyby. It can be derived from the condition that the pericenter radius of the flyby hyperbola must be bigger than the radius of the moon [44]; its formula is

$$B_i = \sqrt{R_{moon}^2\left(1 + \frac{2\mu}{R_{moon}V_\infty^2}\right)}$$

It is bigger than the radius of the moon due to the gravitational focusing effect of the central body on the trajectory. If the B-vector is larger than this value then the periapsis of the hyperbola will be higher than the planet radius.

The probability of impact is then computed by integrating the probability density function over the moon capture circle ([53], [61]). The parametric equation for this circle is

$$x_T^2 + x_R^2 = B_i^2$$

from which the functions for the upper and lower boundaries can be derived (writing x_R as function of x_T)

$$\begin{aligned} x_R^{sup} &= \sqrt{B_i^2 - x_T^2} \\ x_R^{inf} &= -\sqrt{B_i^2 - x_T^2} \end{aligned}$$

The integration over this domain is thus

$$\begin{aligned} P &= \int_{x_{T_{min}}}^{x_{T_{max}}} \int_{x_{R_{min}}}^{x_{R_{max}}} p(x_T, x_R)\, dx_T\, dx_R \\ &= \int_{-B_i}^{B_i} \int_{-\sqrt{B_i^2 - x_T^2}}^{\sqrt{B_i^2 - x_T^2}} p(x_T, x_R)\, dx_T\, dx_R \end{aligned} \tag{8.2}$$

This integration is performed in Matlab with the function *integral2*.

Method 2 - Numerical propagation of trajectories until flyby
In this case the probability is computed using information already available from the optimization process (hence it can be computed only when using the optimized version). Two conditions are evaluated to define an impact.
Using the state vector of the spacecraft when it pierces the sphere of influence of the moon, the B-Plane parameters are computed for that specific trajectory. The computed B-vector is then compared with the *capture radius*; the first condition for impact is then simply

$$\begin{cases} |\mathbf{B}| \leq B_{impact} \rightarrow \text{ impact} \\ |\mathbf{B}| > B_{impact} \rightarrow \text{ no impact} \end{cases}$$

However, since for a non Keplerian orbit this computation is not always very accurate, a second condition was deemed necessary; this is an evaluation of the position of the spacecraft at the time of flyby ($\mathbf{x}^{fb}$) with respect to the radius of the moon

$$\begin{cases} |\mathbf{x}^{fb}| \leq R_{moon} \rightarrow \text{ impact} \\ |\mathbf{x}^{fb}| > R_{moon} \rightarrow \text{ no impact} \end{cases}$$

The meaning is that at the flyby time the state vector of the spacecraft with respect to the moon must be bigger than the radius of the moon (the limit case would be a flyby at zero altitude).
The probability of impact is then computed as

$$P = \frac{N_{impact}}{N_{tot}}$$

where N_{impact} is the number of trajectories that impact on the moon and N_{tot} is the total number of trajectories (the number of samples of the Monte Carlo). Contrarily to the previous case, the probability computed in this way depends upon time, because the effects of a perturbation are different upon the time of its application.
This computation is done for both the perturbed and corrected trajectory. The expected results are that there could be some impacts on the moons for the perturbed trajectories (depending upon the magnitude and the time of application of the perturbations) but there shall not be impacts for the corrected trajectory (after the execution of the TCM). In particular, if the optimization cycle has converged successfully, then an impact for the corrected trajectory is impossible because the corrected trajectory has been taken back to the nominal one at flyby time.
This analysis however has a limited scope due to the limitations of the dynamical model; since the propagation errors close to a flyby can be quite high, these results can be biased from this fact (it is difficult to say if the cause of the impact is the application of the perturbation or the numerical propagation errors only). Thus it is applied only when using a complex dynamical model with a smaller time step, to guarantee small propagation errors.

Results for method 1
Figure 8.17 shows a graphical representation of the probability density function over the integration domain, the capture circle of the moon; is it immediate to see how the function is flat inside this circle while it has its maximum at the center of the uncertainty ellipse.

In Table 8.6 the results for the first method for Strategy 1 and Strategy 3 are shown. Two different data accuracies have been used. From this Table it is immediate to see that, using current level data accuracies and assuming the estimated trajectory to be coincident to the nominal one, the risk of impacts is quite low for almost all the flybys.
The first flyby of the tour is the one with the highest impact probability; this is expected since for that flyby there are not yet data available, hence the a priori uncertainty on the moon position has to be used. The difference between the two strategies is due to the influence of the determination of JUICE.
For Strategy 1, when using data with high accuracy, only the first flyby of Europa has a non-zero impact probability; this is due to the very low altitude of the first Europa flyby (400 km) and to the fact that in this version the a priori uncertainty is used for the fist flyby of each different moon. The first flyby of Callisto has a zero probability because it is at a much higher altitude. When using worst data accuracies, also the central series of Callisto flybys present a nonzero impact probability, but always under the level of 10^{-4}; this is justified by the low altitude of these flybys (around 200 km).
For Strategy 3 the probabilities of impact are zero for almost all the flybys; only for the case of worst data accuracies there is a non-zero probability for the first low altitude flyby of Callisto. The next low altitude flybys instead have a zero impact probability; this is the effect of the data accumulation algorithm.
These results satisfy the planetary protection requirements (which set a limit of the probability to 10^{-4}), if current level accuracies are used for the tracking data.

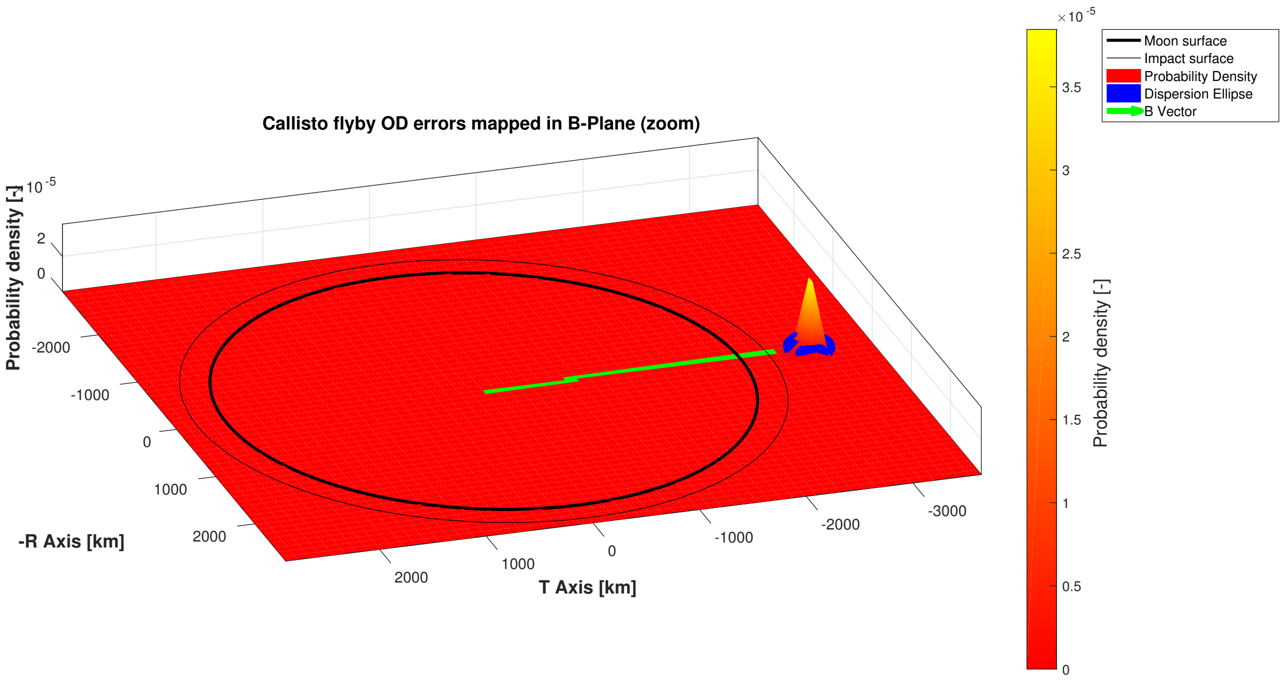

Figure 8.17: Representation of the probability density function over the integration domain

Table 8.6: Impact analysis results for method 1 (Zero indicates a probability smaller than machine precision, $\approx 10^{-16}$)

Flyby	Probability of impact			
	Strategy 1		Strategy 3	
	σ_r m 0.2, σ_v nrad 0.1	σ_r m 10, σ_v nrad 10	σ_r m 0.2, σ_v nrad 0.1	σ_r m 10, σ_v nrad 10
1-G	$0.77 \cdot 10^{-5}$	$0.77 \cdot 10^{-5}$	$0.99 \cdot 10^{-5}$	$0.99 \cdot 10^{-5}$
2-G	0	0	0	0
3-G	0	0	0	0
4-C	0	0	0	0
5-E	$0.19 \cdot 10^{-6}$	$0.19 \cdot 10^{-6}$	0	0
6-E	0	0	0	0
7-C	0	0	0	0
8-C	0	$0.12 \cdot 10^{-13}$	0	$0.91 \cdot 10^{-5}$
9-C	0	$0.10 \cdot 10^{-4}$	0	0
10-C	0	$0.20 \cdot 10^{-7}$	0	0
11-C	0	0	0	0
12-C	0	$0.60 \cdot 10^{-14}$	0	0
13-C	0	0	0	0
14-C	0	$0.15 \cdot 10^{-5}$	0	0
15-C	0	0	0	0
16-G	0	0	0	0
17-G	0	0	0	0
18-C	0	0	0	0
19-C	0	0	0	0
20-C	0	0	0	0

Results for method 2

In order to evaluate the results obtained with this method, at first the propagation errors with respect to the nominal trajectory at the time of flyby have to be computed; it was observed that for most of the cases they are quite limited, being under 20 km. However, in 9 cases on 80 they are higher than 50 km. Considering that the lowest flybys altitudes are of 200 km, in this cases the results of the impact analysis will not be reliable because they are biased by the high propagation error. The results can be considered valid only when the propagation error remains under the arbitrary value of 50 km.

An analysis has been performed using range and VLBI data with accuracies of $\sigma_r = 1$ m and $\sigma_v = 1$ nrad. The results obtained are unluckily not useful due to the very low number of samples; indeed, no impacts are observed for any of the cases where the error remains under 20 km. The probability is thus zero for all the cases. This for both the single-arc and data accumulation versions of the CA.

Observing the probabilities obtained with the first method, it is possible to conclude that to obtain those values with a sampling method, a number of samples of at least $N = 1/P$ is necessary to represent accurately those probabilities. This is well outside the computational capabilities of the computer used, thus a more powerful system shall be used to obtain results about impacts with this method.

9

Conclusions and Recommendations

In this Chapter the conclusions on the work performed are presented in Section 9.1 and recommendations on possible future improvements are given in Section 9.2.

9.1. Conclusions

With respect to the research objective and the research questions posed at the start of the project (see Chapter 1), the following comments can be formulated. They are separated in two paragraphs, corresponding to the main results of this Thesis.

Covariance Analysis

The *research question* answered is

> *How do the different parameters that play a role in the orbit determination strategy influence the determination of the spacecraft position and Galilean moons ephemerides?*

From the sensitivity analysis conducted in Section 7.2 it is clear that the main parameters that influence the spacecraft and moons uncertainties are the data types and their weights. Moreover these uncertainties depend highly upon the strategy used (the differences are in the tracking interval and in the amount of data used for a flyby).

In relation to JUICE, as seen in Subsection 7.2.3, it is concluded that range data alone are not enough because they do not allow a very accurate determination of its orbit; this is especially true if current level accuracy ($\sigma_r = 1$ m) is used, in which case the uncertainty can arrive to the level of few tens of km. This level is far too high for a mission that requires very precise targeting of low-altitude flybys (with lowest altitudes of 200 km). Increasing the accuracy to $\sigma_r = 0.2$ m (possible with a technology update, using Ka-band, see [14]) allows an improvement, but a reduction under the level of few km is not possible (see Figures 7.8 and 7.9a).
The reason for this is that range data alone do not provide very accurate information on the out-of-plane position of the spacecraft. A further mathematical explanation of this fact is that the problem of spacecraft orbit determination during short arcs using range (and Doppler) data only is an ill-posed problem.
To improve the quality of the determination, the inclusion of Doppler data shall be done to have information on the out-of-plane position; however, for what described in Section 5.2, the inclusion of Doppler data has not been done in this project. Since Doppler is still a fundamental data type for spacecraft OD, it is concluded that the current modeling of the OD of JUICE is not very accurate but just indicative. To compensate for the absence of Doppler data, use of VLBI is made (see 3.1); using range and VLBI together is a possible operational alternative to the use of Doppler data. VLBI is fundamental for JUICE, especially to improve its out-of-plane position. Current level accuracies of VLBI ($\sigma_v = 1$ nrad) appear enough for an uncertainty reduction to the level of a few hundred meters (using range data with $\sigma_r = 1$ m), which are enough for a precise flyby targeting. With a technology update ($\sigma_v = 0.1$ nrad and with range data with $\sigma_r = 1$ m) a reduction to the level of a few tens of meters would be possible (see Figures 7.8 and 7.9b). The improvement of the out-of-plane and in-plane positions with VLBI data is of around 2 and 1 orders of magnitude, respectively.
The tracking schedule is also important; the measurements have to be performed regularly and often enough

to allows a precise orbit reconstruction along all the mission.

Regarding the Galilean moons ephemerides, the determination of their uncertainties (standard deviations) depends upon the strategy used.
The uncertainties obtained when using data from a single flyby only, even if during the flyby arc and without interrupting the tracking before the flyby, are relatively high (see Section 7.2.1 and Table 7.3). With current level accuracies they can arrive to the level of 10-30 km (in the presence of VLBI data); with better accuracies they can decrease to the level of 5-15 km. The influence of VLBI data for this Strategy is quite visible on the in-plane and out-of-plane uncertainties; they are reducedup to 30 % with respect to the case of range data only. No evident correlation between the geometry of a flyby and its computed standard deviations are found (see Figure 7.6); perhaps because there are not enough flybys to compute such statistics.
The following two strategies use the data accumulation; if tracking data are gathered for every flyby and the necessary software is implemented, the data accumulation procedure would be the logical choice, since it allows to exploit all the past flybys.
The uncertainties obtained when adding all the data from the previous flybys for the estimation are instead much lower than the previous case. If the tracking is performed during the flyby arc (see Section 7.2.2 and Table 7.4) the uncertainties reach the level of 0.5 m (for Callisto and for good data accuracies). This case is considered too optimistic since such levels do not even have a physical meaning for a planetary body with a size of thousands of km. However it is confirmed from literature that such very optimistic results can be obtained from the covariance analysis.
The most interesting and realistic case is the last, the data accumulation with tracking performed just before the flyby (Section 7.2.3); this because during a real mission the tracking can be interrupted during the flyby. The results obtained using the tracking schedule in Table 7.5 show a consistent reduction of the uncertainties (see Table 7.6). The decrease of the uncertainties along the tour when adding continuously flybys data is clearly visible, for example in Figure 7.10; during the Tour they are around the level of few km, arriving to the level of tens of meters at the end of the Tour. In particular the improvement of Callisto is significant only in correspondence of its flybys while for the other three moons the improvement is significant after each flyby of them. This is explained by the Laplace resonance, explained in 2.1.2.
The improvement noticed is highest for Callisto, followed by Ganymede, Europa and Io; this is explained since is also the order of the number of flybys. However it has to be noticed that this does not happen for all the configurations of the CA used. The uncertainties obtained at the end of the Tour are of the level of 0.2 km for Callisto and Ganymede, 0.25 km for Europa and 0.30 km for Io (with current data accuracies for range and VLBI). The impact of VLBI data is less visible than for Strategy 1, especially when high accuracy range data are used. This can be explained by the fact that if already a lot of range data are used (which are in number much more than the VLBI data) the few VLBI data have overall a smaller influence. This is true especially when very good range and bad VLBI data are used; increasing the VLBI accuracy their impact increases. It is remembered that just one day of VLBI per week is scheduled.
Using optical data for the determination of the moons ephemerides will be fundamental, since it allows an uncertainty reduction up to a few tens of meters at the end of the Tour (in particular 0.07 km for Callisto, 0.08 for Ganymede, 0.09 for Europa and 0.11 for Io). This is also quite optimistic but is confirmed again by similar analysis. Their impact on the moons ephemerides is higher with respect to the VLBI data. Moreover they help to stabilize the performance of the Covariance Analysis algorithms.

A last note is on the accuracy of the results obtained, using as indicator the condition number (see 6.2.1 and 7.1); for the last case they are quite accurate since the condition number is always quite low. Instead for the first two cases they are less accurate since the condition number has much higher values, very often close to the limit of 10^{16}.

Regarding the ephemerides improvement (Section 7.3), it is difficult to evaluate the contribution of JUICE to the long term ephemerides update since use of past data shall be done. Using only JUICE tracking data this improvement is not stable for a long time duration (outside the boundaries of the mission, see Figure 7.14). This is in accordance with [36]. However, the short term improvement (during the mission duration, see Figure 7.13) is stable since it is done during a period for which data are gathered regularly; the ephemerides uncertainties show a periodic behavior with periodicity equal to half the orbital period.

Flyby Tour Navigation
The *research questions* answered are

> *How much do the size of the TCMs decrease thanks to the ephemerides update performed during the flyby tour?*
>
> *How do the different parameters that play a role in the Guidance influence the design of the TCMs?*

Before answering the two questions, it has to be highlighted once again the difference between the three targeting algorithms. The B-Plane targeting (4.3.2) performs well only inside the SOI of a Galilean moon; the optimized targeting (4.3.3) performs well everywhere, even days before the maneuver, but at the cost of high computational time. The approximated targeting (4.3.4) has the great advantage of a computational effort practically null, however its accuracy is limited. The results exposed in Chapter 8 are almost all obtained with the approximated targeting to reduce the computational times, hence they all present some errors; the ΔV during the real mission has to be computed with an algorithm similar to the optimized one.

The answer to the first research question comes from a comparison between the results obtained when considering the a priori value of the uncertainty, which represents the current knowledge (Section 8.1.1) and when considering the ephemerides improvement obtained with the estimation (Sections 8.1.3 and 8.1.4). First of all it is concluded that, as expected, there is always a reduction of ΔV when the moons positions are estimated; it is not possible to provide a single value for this decrease because it depends upon the configuration of the simulation chosen (see Table 8.1, 8.3 and 8.4 for all the different cases). Moreover the reduction reflects directly the results of the covariance analysis (see previous Paragraph).
For the case of single-arc estimation only this reduction is of the order of 70 % (with accuracies of $\sigma_r = 1$ m and $\sigma_v = 1$ nrad and maneuver time of 3 days before the flyby). For the data accumulation case the reduction, for the same configuration, is of 90 %; this translates directly in propellant savings.
The total ΔV budget for the flyby tour for this configuration is of 35.1 m/s (an average of 1.76 m/s per flyby) for Strategy 1 and of 13.5 m/s (average of 0.67 m/s per flyby) for Strategy 3. These values are easily obtained by the propulsion system. With a technology update (using accuracies of $\sigma_r = 0.2$ m and $\sigma_v = 0.1$ nrad and maneuver time of 3 days before the flyby) those two values become 16.9 m/s and 6 m/s for the whole Tour.
It is however highlighted again how these $\Delta V s$ represent only the effort required to correct for the spacecraft and moons positions uncertainties and do not take into account other effects that can displace the spacecraft from its nominal trajectory (for example non-gravitational forces). Thus the real ΔV required would probably be higher.
The values for the pre-flyby maneuver are very often higher than those for the post-flyby maneuver since in the latter the uncertainties are further reduced; however the targeting logic used for the cleanup maneuver (see 5.3.1) is not formally correct, unlike for the targeting maneuver. The results for that maneuver are thus only indicative.
The results for the single flybys reveal that, at least for Strategy 3, the ΔV decreases steadily along the Tour; the sensitivity of the ΔV with respect to the perturbation is different for each moon. It appears that, for a same perturbation, Callisto is the moon that requires the highest ΔV. This can be due to the geometrical characteristics of the flybys (see Figure 8.8b); for example the highest ΔV are observed for the lowest altitude flybys. However a clear correlation was not found, also due to the low number of flybys.

The second research question has been answered with a detailed investigation on the influence of the maneuver time (for the pre-flyby maneuver only) and on the effects of the maneuver execution error model (in Section 8.3).
The time of the maneuver is the parameter that has the greatest influence on the ΔV magnitude; as explained in Subsection 8.3.1, the ΔV does not decrease monotonically with time as initially thought. A minimum for the total Tour ΔV has been found around the time of 48 hours before the flybys (see Figure 8.12). However it has been observed that for every flyby the location of the minimum is different; some flybys do not have a minimum inside the interval analyzed, hence for them the optimum maneuver time is at the right end of the interval (3 days before the flyby). The flybys that present a minimum are 9 on 20; this is located around the time of 45 hours before flyby. This phenomenon has been partly explained due to the geometry of the trajectory, in particular the angle between the current velocity vector and the ΔV vector. It is clear anyway that performing the maneuver at least 24 hours before the flybys entails an important ΔV saving with respect to the cases of 2-10 hours before the flyby, where the cost is prohibitive. This because not enough time is available until the

flyby and the gravitational pull of the celestial body makes it difficult to control the spacecraft trajectory. The maneuver execution error (Subsection 8.3.2) does not influence heavily the overall ΔV budget as observed in Figure 8.15; this because the error is sometimes an over-thrusting and sometimes an under-thrusting of the engine (no bias is applied), hence in a statistical analysis these two effects are compensated. From the navigation analysis with the optimized targeting it can be seen that the maneuver error influences very slightly the targeting accuracy at flyby (see Figure 8.16), increasing the error of the corrected trajectory. This worsening depend also upon the maneuver time; it is anyway limited to a few kilometers. The final spacecraft state is well below the required tolerance (10 km); it appears that this effect is not such to cause a mission failure.

The *research objective* of this Thesis is

> *Determine the impact and mitigation of the Galilean moons ephemerides improvement obtained during the flyby tour of JUICE on the trajectory correction maneuvers.*

It can be considered accomplished, since a complete characterization of the uncertainties and their impact on the Flyby Tour ΔV budget has been performed. As it will be exposed in the next Section there are wide margins of improvements for a more realistic and detailed navigation analysis.

9.2. Recommendations

Recommendations for future work are given for each working package of this Thesis. Many different improvements and variations are possible.

Data

Regarding the data on the trajectory of JUICE received by ESA, as exposed in Section 6.1, there were different problems due to their incompleteness. Thus, for a more complete analysis, two extra information are required.

- complete dynamical model. To model accurately the dynamics of all the bodies, all the forces and physical parameters shall be provided. Also information on the number of bodies considered, the numerical integrator and the time step used could be useful.
- maneuver epochs and $\Delta \mathbf{V}$ (magnitude and direction). With these complete information the deterministic maneuvers can be taken into account in the analysis, improving the fidelity of the navigation analysis. For example further considerations on the distance deterministic-statistical maneuvers can be done.

In this way, provided that the software has the capabilities of implementing the same dynamical model and including the effect of the maneuvers in the numerical propagation, the trajectory of JUICE can be recreated accurately. This would avoid spending time in analyzing the effect of the propagation errors.

Orbit Determination

The observations about the Orbit Determination are perhaps the most influent for a fruitful continuation of this project.

- use a LSQ rather than just the Covariance Analysis (see the difference in 3.3 and 5.1). In the analysis performed only the uncertainties of the parameters have been computed, but not the parameters themselves. If the LSQ is used the real trajectory can be estimated allowing a more realistic simulation of the maneuvers.
  It would then be possible to analyze the influence of a different number of parameters (dynamical model and observations) on the deviation of the real trajectory from the nominal. For example, using a different truth and estimation dynamical model would allow to analyze the influence of the uncertain dynamics of the spacecraft and the moons. This will have an immediate effect on the maneuvers design, which would be more realistic. Moreover, the influence of different parameters uncertainties (and not only the spacecraft and Galilean moons positions) on the maneuvers can be analyzed.
- use Doppler data to track the spacecraft. Due to software and timing limitations, the Doppler data could not be used in this project (see 5.2). However, they are fundamental for interplanetary spacecraft tracking, hence they shall also be included to determine accurately the spacecraft state and its uncertainties.

- add the effect of the measurement errors (as station location errors, media errors, spacecraft and ground station instrumentation errors). The inclusion of these errors would increase the fidelity of the orbit determination modeling. Another option is to investigate the impact of non-Gaussian and time-correlated accuracies on the results of the OD.

- improve the computation of the tracking schedule tacking into account the eclipses periods. In the current version of the software, the observables are generated following a temporal discretization. However, geometrical effects like eclipses of the spacecraft from Jupiter or any moon are not taken into account; during this period the tracking may not be available or highly degraded. This should be taken into account, modifying the number of observables and/or their accuracy. Also the use of different accuracies for the observables of a same tracking type should be investigated.

- explore different tracking schedule and strategies. The software allows high flexibility in selecting the arcs lengths and the tracking times; however plenty of time is required to analyze different configurations.

- regarding the ephemerides improvement (see 7.3), it would be of high interest to analyze the impact of the JUICE data in a long-term epehemrides update for the Jovian System. To do so, real historical data shall be used, augmented by the JUICE data. The improvement obtained in the current project is indeed just a short term one because the data available are quite limited for a complete description of the Jovian System over time span of decades.

- include the estimation of extra parameters like the masses of the moons and the spherical harmonics coefficients. This functionalities are available in the code but could not be used due to the lack of time and problems in obtaining feasible solutions when their estimation was included. An investigation is necessary.

Guidance
From the point of view of the Guidance (see 4, 5.3), the following aspects can be improved.

- once an accurate trajectory propagation is available different improvements to the TCM scheme can be implemented. The first would be to include the apoapsis maneuver, not included in this project due to these limitations. The second would be to perform the optimization also for the cleanup maneuver, for now just computed with the B-Plane targeting.
  Another interesting follow up could be a re-optimization of the trajectory after the orbit determination; in [51] a more complex scheme which entails an optimization of more maneuvers (for different flybys) together is presented.

- explore different targeting strategies as performing two or more maneuvers before a flyby (which could bring to a reduced cost). Another option can be to implement different targeting algorithms (for example targeting the complete state vector at flyby rather than the position vector only).

- analyze the influence of the finite thrusting time of the engine on the performance of the maneuvers; in this work the maneuvers are modeled as instantaneous.

- implement the guidance for a low-thrust engine. The guidance scheme implemented here is for an high-thrust engine since such is the one of JUICE. Performing the TCMs with a low-thrust engine requires completely different algorithms and control logic.
  In [46] are provided some suggestions on this topic; it would be very interesting to model a closed-loop GNC system for a low-thrust engine, with the thrust changing continuously in reaction to external disturbances.

- compute the mass from the ΔV. When the engine characteristics will be available, it would be immediate to convert the ΔV estimates in propellant mass estimates.

Monte Carlo analysis
The final recommendations for the Monte Carlo analysis are the following (see 5.4) that stem from the results (8.1, 8.2)

- continue the analysis on the maneuver time influence to try to understand the exact set of parameters that rule this phenomenon.
- following the observation that for every flyby the location of the ΔV minimum (in term of time) is different, it would be required to include in the software the capability of performing the maneuver at a different time for every flyby.
- for the optimized version of the navigation analysis, increase the number of samples to get more accurate results.
- for the approximated version of the navigation analysis, even though the Jacobian matrices computed showed a good accuracy in the ΔV computation, improvements are possible. This require an optimization to find the best perturbation to be used for their computation (eventually using a different one for every time of maneuver, which was not done).
- for the impact analysis, increase the number of samples to get more accurate results. Moreover perform again this analysis when the complete dynamical model and maneuver information are available.

A

Influence of other parameters on the Covariance Analysis

In Section 7.2 a sensitivity analysis for the Covariance Analysis with respect to the tracking data accuracies and schedule has been performed, to analyze the influence of those parameters on the computed uncertainties of the Galilean moons ephemerides.
In this Appendix the influence of other parameters that play a role in the CA is analyzed; these parameters have a minor influence respect to the data types and accuracies, but nonetheless they modify the results of the simulations. These parameters are: the arcs initial and end times (A.1), the a priori weights (A.2) and the dynamical model (A.3).

A.1. Influence of the arcs subdivision

The results of the Covariance Analysis depend also upon the multi-arc division (Section 5.2). This is particularly important for the moons, since this division determines the duration of the arcs during which the estimation of the moons takes place (see Figure 5.8). This has a direct consequence on the amount of observations collected and used to determine the moons uncertainties. For the same tracking schedule, the amount of observations increase if the arc duration is increased.
If the estimation is performed before the flyby (see Figure 5.7) then it is of high importance the distance of the final time of the estimation arc to the time of flyby. This distance has a very high impact on the results because the gravitational attraction of a moon on JUICE increases when the distance is smaller; hence when the spacecraft is far away from a moon the determination of the moon can be difficult because the gravitational attraction of Jupiter is the predominant acceleration. Thus interrupting the tracking of JUICE when far away from the moon can give bad or not reliable results. A typical flyby duration is of around a few hours (where the distance of JUICE from the moon goes from around 30,000 km to 2,500 km); thus a few days before flyby the distance JUICE-moon is of the order of magnitude of 10^5 km.
In the sensitivity analysis performed in Section 7.2.3 the pre-flyby arc is interrupted 3 hours before the flyby, hence quite close to the time of flyby. For almost all the flybys the spacecraft is already inside the sphere of influence of the moon with respect to Jupiter, hence the gravitational pull of the moon is higher. The determination is so quite accurate.
In Table A.1 are compared the results for different arc divisions (keeping the tracking data accuracies and schedule constants; only range has been used). Strategy 3 is used for this analysis.

It is possible to see that the behavior of the estimation is different. There is a general increase of the uncertainties when reducing the arc duration (t_{nom}) and when moving the end of the pre-flyby arc away from the flyby (t_{int} where int stands for interruption).
An interesting phenomenon is that the final uncertainties vary for the four moons depending upon these parameters; in particular, for the case of t_{int} = 3 hours, the sequence of best accuracies for the moons is C-G-E-I. This sequence represents also the decrease of number of flybys per moon (13 for C, 5 for E, 2 for E, 0 for I). This means that all the flybys of Callisto are exploited to determine its position uncertainty with the best accuracies. In other cases the sequence is different, showing that even if Callisto has most of the flybys, it is not determined better than the other moons. In particular, when setting t_{int} to 3 days (last row of the Table), the

Table A.1: Comparison of different multi-arc divisions

Variables			Results											
Times			Io			Europa			Ganymede			Callisto		
t_{int}	t_{nom}	t_{min}	σ_{IP}	σ_{OP}	σ_{avg}	σ_{IP}	σ_{OP}	σ_{avg}	σ_{IP}	σ_{OP}	σ_{avg}	σ_{IP}	σ_{OP}	σ_{avg}
hrs	$days$	$days$	km	km	km	km	km	km	km	km	km	km	km	km
3	10	6	0.02	0.39	0.30	0.03	0.39	0.25	0.03	0.25	0.17	0.07	0.10	0.17
3	4	3	0.04	0.96	0.78	0.13	0.83	0.78	0.05	0.87	0.72	0.34	1.32	1.46
6	10	6	0.02	0.33	0.31	0.03	0.34	0.23	0.03	0.32	0.21	0.06	0.29	0.29
24	6	6	0.01	0.16	0.13	0.06	0.60	0.44	0.06	0.18	0.19	0.02	0.05	0.21
72	6	4	0.05	1.23	1.06	0.14	2.37	2.90	0.21	1.15	1.23	0.61	6.07	8.22

sequence of best uncertainties is I-G-E-C. It is interesting to notice that in this case the best uncertainty is for Io, even though there are no flyby for this moon. This can be explained by the Laplace resonance (2.1.2) that relates the positions of Io, Europa, Ganymede but not Callisto. When interrupting the arc quite far away from the flyby, the strong gravitational attraction during the flyby is not exploited completely; hence, especially for Callisto, the position is not so well determined due to this fact. For the other moons instead the resonance has the effect of improving the situation with respect to Callisto.
It is noted that the optimal situation would be to track the spacecraft or during the flyby or as close as possible to it.

A.2. Influence of the a priori weights for JUICE and the moons

The a priori uncertainties for JUICE and the Galilean moons are used to provide information about the initial knowledge of their positions; however their choice is not very strict since they have also the function to help the algorithm to converge. They can have an influence on the results too. For JUICE, its computed uncertainty is quite insensitive to the a priori uncertainty, since the tracking data weights have the highest influence; hence, using a value of $\overline{\sigma}_J$ = 100 m or $\overline{\sigma}_J$ = 1000 km has a small influence on the results. In both cases the final uncertainty arrives to levels of the tens of m. However, since the post-fit uncertainty is often found to be smaller than the a priori uncertainty, when using $\overline{\sigma}_J$ = 100 m then the post-fit uncertainty is often smaller than 100 m, instead when using $\overline{\sigma}_J$ = 1000 km the uncertainty can reach sometimes the level of a few km.

Table A.2: Comparison of different a priori standard deviations for the moons

σ $[km]$	$\overline{\sigma}_m$ = 10 km				$\overline{\sigma}_m$ = 80 km				$\overline{\sigma}_m$ = 150 km			
	I	E	G	C	I	E	G	C	I	E	G	C
σ_{rss}	1.229	2.318	1.158	5.206	1.239	2.378	1.172	6.136	1.239	2.379	1.172	6.149
σ_{avg}	1.057	2.868	1.221	7.705	1.066	2.910	1.230	8.238	1.066	2.910	1.230	8.246

Also the moons are not very sensitive to the a priori uncertainty on their position, at least in the data accumulation algorithm. In the single-arc algorithm the a priori standard deviation is quite important, because due to the limited amount of data the post-fit uncertainty depends quite a lot from the a priori one. Instead, as is visible in Table A.2 (obtained using the Strategy 3 for the CA, with an interruption time of 3 days before flyby), in the data accumulation version the final standard deviation is quite insensitive to the a priori value, meaning that overall the data have much more influence in the determination of the final standard deviations.

A.3. Influence of the dynamical model

A small number of simulations has been performed using the complex dynamical model (including the spherical harmonics of Jupiter and the moons and the perturbations due to the Sun and Saturn). The description of the difference between simple and complex dynamical model is presented in Subsection 3.2.1, where a selection of the forces to include in the complex dynamical model is done. As explained in Subsection 5.3.4, when the complex dynamical model is used the time step has to be reduced to 600 s to prevent the propagation errors from crashing the spacecraft into the moons.
In Table A.3 (obtained using the Strategy 3 for the CA, with an interruption time of 3 days before flyby) are shown the results for one simulation (using range and VLBI data with accuracies of σ_r = 1 m, σ_v = 1 nrad). The

results for the case of complex dynamical model show higher uncertainties than the case of simple dynamical model for every moon, showing the highest influence on Europa and Callisto and the lowest influence on Ganymede and Io.

Table A.3: Comparison of simple and complex dynamical model

σ $[km]$	Simple dynamical model				Complex dynamical model			
	Io	Europa	Ganymede	Callisto	Io	Europa	Ganymede	Callisto
σ_{IP}	0.055	0.149	0.211	0.615	0.059	0.204	0.244	0.747
σ_{OP}	1.238	2.372	1.152	6.075	1.443	4.865	1.275	8.156
σ_{rss}	1.239	2.376	1.172	6.106	1.445	4.869	1.298	8.191
σ_{avg}	1.066	2.909	1.229	8.221	1.525	5.610	1.443	11.198

The order of magnitude of the uncertainty does not change; the influence on the navigation analysis (and thus on the ΔV) will be small but present.
The plots of the propagation of the standard deviations, not reported here, show an identical behavior; the only difference is that for the case of complex dynamics they are shifted up by a factor $\sigma^c_{avg} - \sigma^s_{avg}$, where the apexes c and s stand for complex and simple.
Regarding the results for JUICE instead, the post-fit uncertainty is practically identical for the two cases, indicating that while these perturbations may have a significant effect on the motion of JUICE, they do not influence substantially the accuracy of the orbit determination for JUICE.
The other simulations performed show a similar behavior; it is not immediately clear why the effect is most noticeable on the Galilean moons and not on JUICE. It is important to keep in mind that this perturbations act not only on the spacecraft, but also reciprocally among the celestial bodies (since they are all of gravitational nature). For example, the J_2 effect of Jupiter has an influence also on Ganymede, and so on.
For JUICE the great amount of data allows to determine in a good way its position even if the dynamics of the spacecraft is more complex; however for the moons, since no direct data are available (unless optical data are used), adding new forces increases somehow the norm of the state transition matrix, responsible for degrading the accuracies. It is possible that new terms appear in this matrix such that they give a constant offset. If optical data are used the results are still worst in the case of complex dynamics but the difference is smaller.
Further investigations, which could not be performed with the scope of this Thesis, are required to understand better this phenomenon.

B

Monte Carlo Analysis Simulations using the Optimized targeting

The results of the Monte Carlo analysis for the optimized version of the targeting algorithm are shown here. Due to constraints of computational nature (see Chapter 8) a lower number of samples has been used (250 instead of 2000); since extensive results covering a wide range of data weights and maneuver times have already been obtained for the approximated targeting, a small number of simulations has been performed for this version of the Monte Carlo navigation analysis.
Section B.1 presents the results for the single arc version, while Section B.2 presents the results for the data accumulation version. These results are not comparable with the ones of Section 7.2 because different assumptions and parameter values are used here; in particular the a priori uncertainty of the moons positions is set to 50 km (per axis), the confidence level is set to 1 (and not to 3) and the arcs division is different. Due to these differences it is normal to obtain quite different results. The reason is that these simulation have been performed before the finding of the optimal parameters for the analysis in Section 7.2; there was no time available to perform new simulations for the optimized version of the targeting with those optimal parameters.

B.1. Optimized targeting, single-arc data

Due to the different settings, the CA failed quite often for this case. The percentage of success is 33 % when using only range data and when using range and VLBI; it increases to 50 % when adding optical data. The feasible combinations have been found using the grid search (see 6.2.1) on the covariance analysis only, before performing the Monte Carlo analysis. Only one tracking schedule has been tried; if different tracking schedule are tried, more feasible results would be obtained. In these simulations it is assumed that the spacecraft can be tracked also during the flyby arcs; the information from this tracking are used to design the cleanup maneuver.
In Table B.1 (part of) the results obtained are shown. For the no ephemerides improvement case, regarding the difference between the pre-flyby and the post-flyby ΔV, they are quite similar because they are always placed symmetrically with respect to the flyby (for example, if the targeting maneuver is 4 hours before the flyby, then the cleanup maneuver will be 4 hours after the flyby). This is not necessarily true for the real mission, but is more convenient for results analysis (because in the simulation the two maneuvers are independently computed). The second reason is that the same a priori uncertainty for the moon is used for both the maneuvers; hence the cleanup maneuver is not affected by the greater improvement in the uncertainty obtained during the flyby arc. The differences can be explained by the uncertainties used for JUICE, which are not the same for the two maneuvers since they come from different arc. Another difference comes from the computation method: while for the targeting maneuver the accurate, optimized version is used, for the cleanup maneuver the B-Plane targeting is used which introduces often an error (see 6.3.1).
For the case of range and VLBI only, the combinations that converge successfully have quite high weights for the range measurements (10 m), while the weights for the VLBI are quite different (from 10^{-8} rad to 10^{-10} rad). It is immediate to see the decrease of ΔV with respect to the case of no ephemerides improvement. The decrease is significant especially for the cleanup maneuver, because in this case the observations are gathered during the flyby, hence the uncertainty of the moon position decreases greatly (only for a limited amount of time during the flyby). The decrease in ΔV of the pre-flyby maneuver is not very significant in the case of only

range, due to the very low accuracy used; it is only of 7.2 m/s (5 %) and 1.6 m/s (7 %) for the cases of 4 and 24 hours, decreasing to only 0.89 m/s (6 %) for the case of 48 hours. When adding VLBI data with better accuracy the situation improves, reducing the size of the ΔV up to 46.1 m/s (32 %) and 7 m/s (30 %) for the cases of 4 and 24 hours. For the post-flyby maneuver the decrease is even more significant, arriving to 101 m/s (86 %) and 14.2 m/s (83 %) for the cases of 4 and 72 hours; due to the tracking interval, this was expected.
When optical data are used the success percentage of the covariance analysis for this case is of 50 % (4 combinations out of 8 converge successfully). The inclusion of optical data helps to stabilize the covariance analysis, increasing slightly the number of feasible combinations. The Galilean moon target of the flyby is observed optically in both the pre-flyby and flyby arc; in the flyby arc there is however an interruption of 3 days around the flyby time. It is not possible to get accurate optical data for the navigation when very close to a moon due to difficulties in data processing (3.1.2). The improvement is indeed quite significant with respect to the case of radiometric data only. For the targeting maneuver, when adding optical data with accuracy of 10 μrad the decrease of ΔV is of 62.2 m/s (62 %) and 5.66 (54 %) for the cases of 4 and 48 hours. For the cleanup maneuver, the decrease is of 21.5 m/s (67 %) and 2.9 m/s (62 %) for the same two times, showing a greater impact. The conclusion is the same as for the approximated version: optical data are necessary to improve the navigation of the spacecraft in the flyby tour and to reduce the total ΔV.

Table B.1: Monte Carlo Analysis results - Optimized, single arc

	Pre-flyby ΔV			Post-flyby ΔV			Parameters			
N	mean	1σ	95%	mean	1σ	95%	σ_r	σ_v	σ_o	t_{man}
	m/s	m/s	m/s	m/s	m/s	m/s	m	$nrad$	μrad	$hrs(fb)$
No ephemerides improvement										
1	142.72	15.64	168.85	116.89	11.48	137.84	-	-	-	4
2	24.08	2.38	27.59	24.12	2.43	28.39	-	-	-	24
3	14.27	1.59	17.14	15.76	1.75	18.74	-	-	-	48
4	21.25	3.14	26.57	17.07	2.70	21.67	-	-	-	72
Range only										
5	135.49	16.07	162.13	60.43	8.69	74.41	10	-	-	4
6	22.54	2.33	26.50	13.15	1.83	15.95	10	-	-	24
7	13.38	1.57	16.07	8.68	1.19	10.54	10	-	-	48
8	20.69	3.15	26.05	9.14	1.36	11.45	10	-	-	72
Range and VLBI										
9	96.56	9.37	111.48	15.97	2.05	19.44	10	1.0E-10	-	4
10	17.11	1.56	19.86	3.53	0.46	4.34	10	1.0E-10	-	24
11	10.21	1.27	12.34	2.40	0.33	2.93	10	1.0E-10	-	48
12	18.00	2.86	22.74	2.81	0.57	3.83	10	1.0E-10	-	72
13	99.48	9.58	115.20	31.99	3.99	38.96	10	1.0E-9	-	4
14	17.62	1.59	20.27	7.06	0.85	8.50	10	1.0E-9	-	24
15	10.52	1.29	12.62	4.74	0.60	5.79	10	1.0E-9	-	48
16	16.11	2.21	19.66	5.25	0.96	6.92	10	1.0E-9	-	72
Range, VLBI and optical										
17	37.27	4.35	44.73	10.45	1.25	12.58	10	1.0E-9	1.0E-5	4
18	7.71	0.89	9.24	2.52	0.33	3.06	10	1.0E-9	1.0E-5	24
19	4.84	0.57	5.76	1.78	0.25	2.21	10	1.0E-9	1.0E-5	48
20	7.25	1.22	9.39	2.22	0.49	3.12	10	1.0E-9	1.0E-5	72
21	66.84	6.95	77.14	23.03	2.64	27.41	10	1.0E-9	5.0E-5	4
22	12.66	1.29	14.67	5.33	0.65	6.44	10	1.0E-9	5.0E-5	24
23	8.09	0.95	9.79	3.67	0.49	4.53	10	1.0E-9	5.0E-5	48
24	10.87	1.47	13.35	4.29	0.88	5.84	10	1.0E-9	5.0E-5	72

B.2. Optimized targeting, data accumulation

A few simulations for the optimized targeting have been run also with the data accumulation version of the CA; this is the most complete and realistic version of the navigation analysis implemented, however also the most computationally expensive. Since the purpose of the approximated version was to have extensive results varying the parameters, only four simulations (per maneuver time) have been performed with this version. The maneuver error is also included. As for the approximated case, comparing these results with the single-arc version shows a decrease in ΔV for the targeting maneuver; for the cleanup maneuver instead there is not a decrease in ΔV. This is due to the different tracking period used used; in the single arc this is during the flyby arc while for the data accumulation the tracking period is interrupted 3 days before the flyby, which gives quite high uncertainties. There is then a propagation of the covariance matrix to the maneuver time. In the Figures below are shown the ΔV and combined JUICE-flyby moon uncertainty mapped at the time of maneuver, for all the 20 flybys of the tour. These results are for the combination σ_r = 1 m, σ_v = 1 nrad.

Table B.2: Monte Carlo Analysis results - Optimized, data accumulation

	Pre-flyby ΔV			Post-flyby ΔV			Parameters			
N	mean	1σ	95%	mean	1σ	95%	σ_r	σ_v	σ_o	t_{man}
	m/s	m/s	m/s	m/s	m/s	m/s	m	$nrad$	μrad	$hrs(fb)$
1	44.36	10.40	62.80	35.29	10.16	53.95	1	-	-	4
2	8.72	1.76	11.97	8.93	2.26	12.85	1	-	-	24
3	5.12	1.14	7.28	6.51	1.84	9.40	1	-	-	48
4	9.26	1.99	12.52	6.73	1.95	10.06	1	-	-	72
5	33.09	8.45	48.25	32.79	8.75	47.86	1	1.0E-9	-	4
6	6.61	1.52	9.17	7.94	1.87	10.93	1	1.0E-9	-	24
7	4.24	0.99	6.03	5.94	1.59	8.68	1	1.0E-9	-	48
8	7.43	1.59	10.08	6.37	1.69	9.26	1	1.0E-9	-	72
9	68.99	11.26	88.19	69.16	12.88	90.04	10	1.0E-9	-	4
10	13.07	1.92	16.27	16.20	2.76	20.97	10	1.0E-9	-	24
11	7.91	1.32	10.14	11.54	2.30	15.49	10	1.0E-9	-	48
12	16.21	3.08	21.50	11.60	2.15	15.43	10	1.0E-9	-	72
13	24.45	5.83	35.45	13.18	6.38	26.10	1	1.0E-9	1.0E-05	4
14	4.58	1.00	6.37	2.93	1.09	5.01	1	1.0E-9	1.0E-05	24
15	2.52	0.54	3.48	2.26	1.00	4.28	1	1.0E-9	1.0E-05	48
16	4.02	0.93	5.86	2.69	1.07	4.67	1	1.0E-9	1.0E-05	72

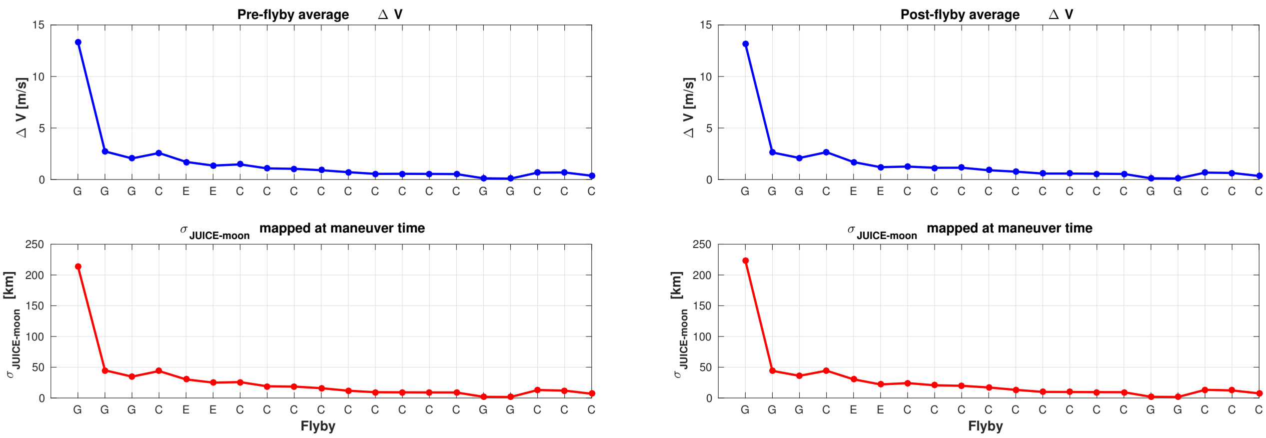

(a) Pre-flyby maneuver **(b) Post-flyby maneuver**

Figure B.1: Flybys ΔV and σ_{rss} - Maneuver time: 4 hours before flyby

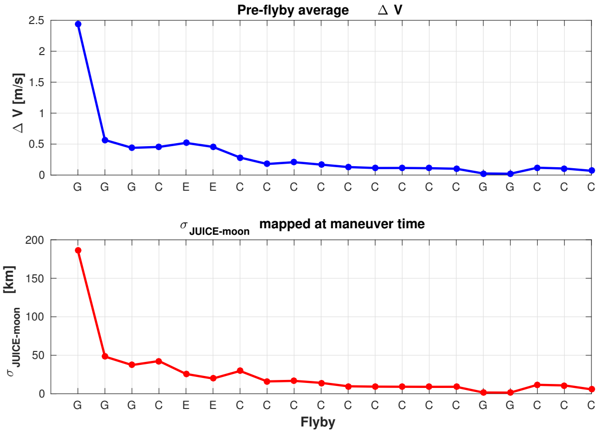

(a) Pre-flyby maneuver

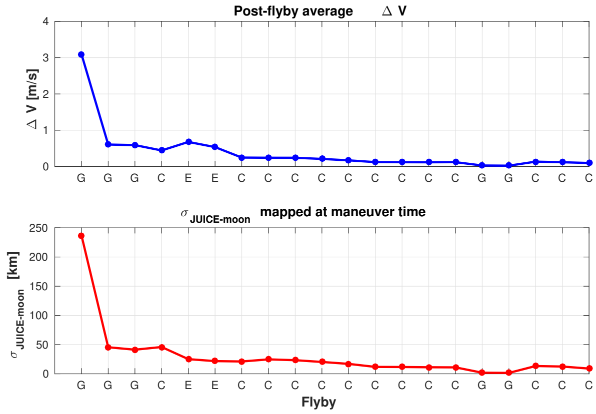

(b) Post-flyby maneuver

Figure B.2: Flybys ΔV and σ_{rss} - Maneuver time: 24 hours before flyby

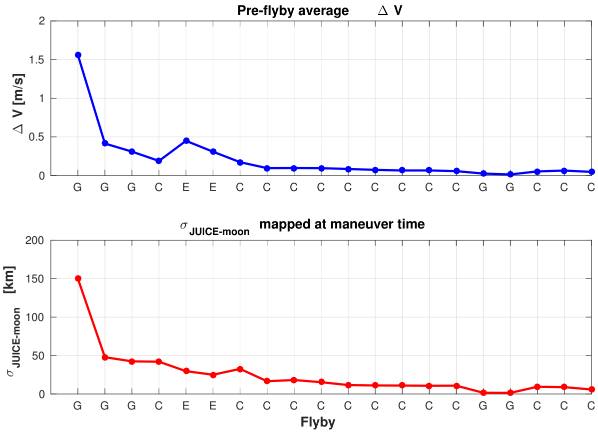

(a) Pre-flyby maneuver

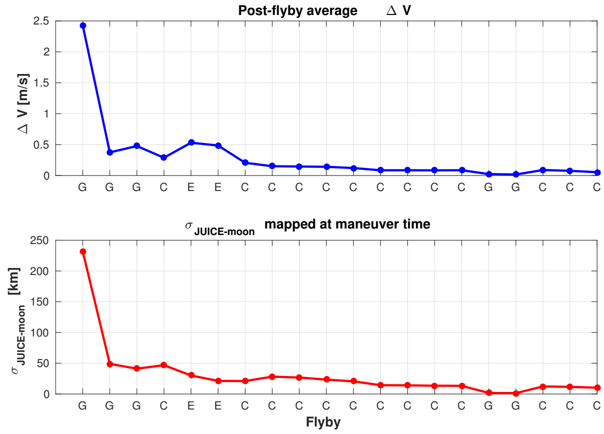

(b) Post-flyby maneuver

Figure B.3: Flybys ΔV and σ_{rss} - Maneuver time: 48 hours before flyby

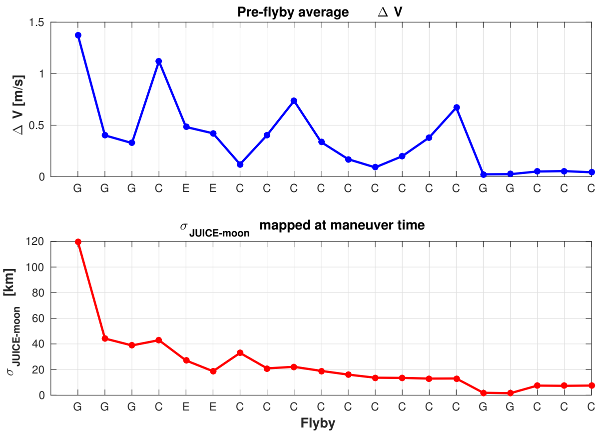

(a) Pre-flyby maneuver

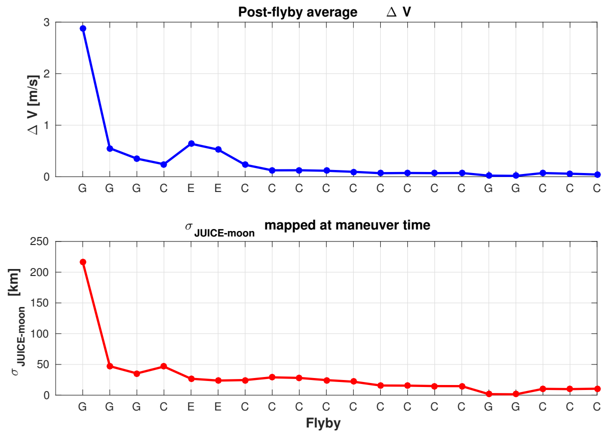

(b) Post-flyby maneuver

Figure B.4: Flybys ΔV and σ_{rss} - Maneuver time: 72 hours before flyby

Bibliography

[1] ESA, *JUpiter ICy moons Explorer - Definition Study Report (JUICE Red Book)*, Tech. Rep. (ESA, 2014).

[2] Lissauer and De Pater, *Fundamental Planetary Science: Physics, Chemistry and Habitability* (Cambridge University Press, 2013).

[3] O. Grasset, M. Dougherty, A. Coustenis, E. Bunce, C. Erd, D. Titov, M. Blanc, A. Coates, P. Drossart, L. Fletcher, H. Hussmann, R. Jaumann, N. Krupp, J. Lebreton, O. Prieto-Ballesteros, P. Tortora, F. Tosi, and T. Van Hoolst, JUpiter ICy moons Explorer (JUICE): An ESA mission to orbit Ganymede and to characterise the Jupiter system, Planetary and Space Science (2013).

[4] S. Musotto, F. Varadi, W. Moore, and G. Schubert, Numerical Simulations of the Orbits of the Galilean Satellites, Icarus (2002).

[5] R. Greenberg, The icy Jovian satellites after the Galileo mission, Reports on Progress in Physics (2010).

[6] J. Campbell and S. Synnott, Gravity field of the Jovian system from Pioneer and Voyager tracking data, The Astronomical Journal (1984).

[7] B. Moultrie, P. Kenyon, J. Kechichian, R. Davis, and F. Nicholson, Galilean satellite tour orbit determination assessment, in *AIAA 25th Aerospace Sciences Meeting, Nevada* (1987).

[8] S. Finocchiaro, *Numerical Simulations of the Juno Gravity Experiment*, Ph.D. thesis, Università di Roma - La Sapienza (2012).

[9] L. Iess, 3GM: Gravity and Geophysics of Jupiter and the Galilean Moons, in *European Planetary Science Congress* (2013).

[10] M. Parisi, L. Iess, and S. Finocchiaro, The gravity fields of Ganymede, Callisto and Europa: how well can JUICE do?, Geophysical Research Abstracts (2014).

[11] A. E. Lynam and J. M. Longuski, Preliminary analysis for the navigation of multiple-satellite-aided capture sequences at Jupiter, Acta Astronautica (2012).

[12] C. L. Thornton and J. S. Border, *Radiometric Tracking Techniques for Deep-Space Navigation* (JPL, NASA, 2000).

[13] Schutz, Tapley, and Born, *Statistical Orbit Determination* (Academic Press, 2004).

[14] L. Iess, M. Di Benedetto, N. James, M. Mercolino, L. Simone, and P. Tortora, Astra: Interdisciplinary study on enhancement of the end-to-end accuracy for spacecraft tracking techniques, Acta Astronautica (2013).

[15] T. D. Moyer, *Mathematical Formulation of the Double-Precision Orbit Determination Program*, Tech. Rep. (JPL, NASA, 1971).

[16] T. Hamilton and W. Melbourne, *Information content of a single pass of doppler data from a distant spacecraft*, Tech. Rep. (JPL, NASA, 1966).

[17] D. W. Curkendall and J. S. Border, *Delta-DOR: The One-Nanoradian Navigation Measurement System of the Deep Space Network - History, Architecture, and Componentry*, Tech. Rep. (IPN Progress Report, 2013).

[18] N. James, R. Abello, M.Lanucara, M. Mercolino, and R. Madde, Implementation of an ESA delta-DOR capability, Acta Astronautica (2009).

[19] H. Hussmann, K. Lingenauber, J. Oberst, M. Kobayashi, N. Namiki, J. Kimura, N. Thomas, L. Lara, and G. Steinbrugge, The Ganymede Laser Altimeter (GALA), in *European Planetary Science Congress* (2014).

[20] L. Gurvits, T. Bocanegra Bahamon, G. Cimo, D. Duev, G. Molera Calves, S. Pogrebenko, I. De Pater, L. Vermeersen, P. Rosenblatt, J. Oberst, P. Charlot, S. Frey, and V. Tudose, Planetary Radio Interferometry and Doppler Experiment (PRIDE) for the JUICE mission, in *European Planetary Science Congress* (2013).

[21] D. Dirkx, V. Lainey, L. Gurvits, and P. Visser, Dynamical Modelling of the Galilean Moons for the JUICE Mission, Planetary and Space Science (2016).

[22] G. Lanyi, D. S. Bagri, and J. S. Border, Angular Position Determination of Spacecraft by Radio Interferometry, Proceedings of the IEEE (2007).

[23] T. Martin-Mur, P. Antreasian, J. Border, J. Benson, V. Dhawan, E. Fomalont, E. Graat, R. Jacobson, G. Lanyi, T. McElrath, J. Romney, and C. Walker, *Use of Very Long Baseline Array Interferometric Data for Spacecraft Navigation*, Tech. Rep. (JPL, NASA, 2006).

[24] J. Miller and K. H. Rourke, *The application of differential VLBI to planetary approach orbit determination*, Tech. Rep. (DNS Progress Report, 1977).

[25] D. A. Duev, G. Molera Calves, S. V. Pogrebenko, L. I. Gurvits, G. Cimo, and T. Bocanegra Bahamon, Spacecraft VLBI and Doppler tracking: algorithms and implementation, Astronomy and Astrophysics (2013).

[26] D. Dirkx, L. Gurvits, V. Lainey, G. Cimo, T. Bocanegra-Bahamon, and P. Visser, On the contribution of JUICE-PRIDE to Jovian system ephemerides, Planetary and Space Science (2016).

[27] T. Martin-Mur, S. Bhaskaran, R. J. Cesarone, and T. McElrath, *The Next 25 Years of Deep Space Navigation*, Tech. Rep. (JPL, NASA, 2008).

[28] C. Jackman and P. Dumont, Optical Navigation Capabilities for Deep Space Missions, in *23rd AAS/AIAA Space Flight Mechanics Conference Hawaii* (2013).

[29] Y. Guo, B. Williams, F. Pelletier, J. McAdams, and W. Shyong, Trajectory Monitoring and Control of the New Horizons Pluto Flyby, 25th International Symposium on Space Flight Dynamics, Munich, Germany (2015).

[30] V. Lainey, L. Duriez, and A. Vienne, New accurate ephemerides for the Galilean satellites of Jupiter - Part I, Astronomy and Astrophysics (2004).

[31] V. Lainey, L. Duriez, and A. Vienne, New estimation of usually neglected forces acting on Galilean system, Celestial Mechanics and Dynamical Astronomy (2001).

[32] Montenbruck and Gill, *Satellite Orbits - Models, Methods and Applications* (Springer, 2000).

[33] P. Argentiero and J. Lynn, *Estimation Strategies for Orbit Determination of Application Satellites*, Tech. Rep. (Goddard Space Flight Center, NASA, 1974).

[34] A. Verma, *Improvement of the planetary ephemerides using spacecraft navigation data and its application to fundamental physics*, Ph.D. thesis, Universite de Franche-Comte (2013).

[35] E. Pitjeva, Modern Numerical Ephemerides of Planets and the importance of Ranging Observations for their creation, Celestial Mechanics and Dynamical Astronomy (2001).

[36] D. W. Murrow and R. A. Jacobson, Galilean Satellite Ephemeris Improvement Using Galileo Tour Encounter Information, in *AIAA/AAS Astrodynamics Conference, Minneapolis, 1988* (1988).

[37] J. Lieske, Theory of Motion of Jupiter Galilean Satellite, Astronomy and Astrophysics (1976).

[38] G. A. Kosmodamianskii, Numerical Theory of the Motion of Jupiter Galilean Satellites, Solar System Research (2009).

[39] J. Lieske, Improved Ephemeris of the Galilean Satellites, Astronomy and Astrophysics (1979).

[40] J. Lieske, Galilean satellite ephemerides E5, Astronomy and Astrophysics (1998).

[41] X. Newhall, E. Standish, and J. Williams, DE-102 - A nunumerical integrated ephemeris of the Moon and planets spanning forty-four centuries, Astronomy and Astrophysics (1983).

[42] P. N. Valerino, B. Buffington, Y. Criddle, K.and Hahn, R. Ionasescu, J. A. Kangas, T. Martin-Mur, R. B. Roncoli, and J. Sim, Preliminary Maneuver Analysis for the Europa Clipper Multiple-Flyby Mission, in *AIAA/AAS Astrodynamics Specialist Conference* (2014).

[43] T. J. Martin-Mur, R. Ionasescu, P. Valerino, K. Criddle, and R. Roncoli, Navigation Challenges for a Europa Flyby Mission, in *24th International Symposium on Space Flight Dynamics* (2014).

[44] K. F. Wakker, *Fundamentals of Astrodynamics* (Faculty of Aerospace Engineering - Delft University of Technology, 2015).

[45] M. Jah, Derivation of the B-plane (Body Plane) and Its Associated Parameters, in *A Lecture Series on Orbit Mechanics and Interplanetary Mission Design, University of Colorado* (2002).

[46] D. Cho, Y. Chung, and H. Bang, Trajectory correction maneuver design using an improved B-plane targeting method, Acta Astronautica (2012).

[47] P. Kenyon, J. Kechichian, B. Moultrie, and F. Nicholson, Galileo Probe Delivery and Orbiter Approach Orbit Determination, in *AlAA 25th Aerospace Sciences Meeting, Nevada* (1987).

[48] R. Haw, P. Antreasian, T. McElrath, E. Graat, and F. Nicholson, Navigating Galileo at Jupiter Arrival, Journal of spacecraft and rockets (1997).

[49] R. Ionasescu, Orbit Determination Covariance Analysis for the Cassini Solstice Mission, in *AIAA/AAS Astrodynamics Specialist Conference, Toronto, Canada* (2010).

[50] M. Wilson, C. L. Potts, R. A. Mase, C. Allen Halsell, and D. V. Byrnes, Maneuver design for Galileo Jupiter approach & orbital operations, in *Space Flight Dynamics* (1997).

[51] D. Roth, V. Alwar, J. Bordi, T. Goodson, Y. Hahn, R. Ionasescu, J. Jones, W. Owen, J. Pojman, I. Roundhill, S. Santos, N. Strange, S. Wagner, and M. Wong, *Cassini Tour Navigation Strategy*, Tech. Rep. (JPL, NASA, 2003).

[52] T. Goodson, Y. Hahn, N. Strange, S. Wagner, and M. Wong, Maneuver-Targeting Strategies and Results for the Cassini-Huygens Mission, in *Book of Abstracts* (2005).

[53] L. Miller, D. Sonnabend, C. Chadwick, and J. Michel, Galileo Satellite Tour Maneuver Strategies-Preliminary Results, in *AIAA/AAS Astrodynamics Conference, Palo Alto, California* (1978).

[54] W. Kizner, *A Method of Descriving Miss Distances for Lunar and Interplanetary Trajectories*, Tech. Rep. (JPL, NASA, 1959).

[55] R. Groves, *Injection and Midcourse Correction Analysis for the Galactic Probe*, Tech. Rep. (Goddard Space Flight Center, NASA, 1966).

[56] B. Raofi, M. D. Guman, and C. L. Potts, Preliminary statistical Delta V analysis for a representative Europa Orbiter Mission, in *AIAA/AAS Astrodynamics Specialist Conference, Denver, CO* (2000).

[57] C. J. Weeks, A Statistical Analysis of Spacecraft Maneuvers for a Deep Space Mission, in *AIAA/AAS Astrodynamics Specialist Conference and Exhibit* (2008).

[58] A. M. Didion and A. E. Lynam, Guidance and Capture of a Callisto-Io-Ganymede Triple Flyby Jovian Capture, Advances in the Astronautical Sciences Astrodynamics (2015).

[59] K. Kumar, Y. Abdulkadir, P. van Barneveld, F. Belien, S. Billemont, E. Brandon, M. Dijkstra, D. Dirkx, F. Engelen, D. Gondelach, *et al.*, Tudat: a modular and robust astrodynamics toolbox, in *Fifth ICATT, International Conference on Astrodynamics Tools and Techniques* (ESA Noordwijk, 2012).

[60] D. Dirkx and B. Vermeersen, *WP3: Laser Ranging - Selected Software modifications*, Tech. Rep. (ESPaCE Deliverable, 2014).

[61] Milani and Gronchi, *Theory of Orbit Determination* (Cambridge University Press, 2009).

[62] T. Lam, J. R. Johannesen, and T. D. Kowalkowski, Planetary protection trajectory analysis for the Juno mission, in *AIAA/AAS Astrodynamics Specialist Conference and Exhibit* (2008).